Universität Hamburg
DER FORSCHUNG | DER LEHRE | DER BILDUNG

BNITM
Bernhard-Nocht-Institut für Tropenmedizin

Analysis of the viral evolution of zoonotic RNA viruses in their natural host

Dissertation

Zur Erlangung des akademischen Grades
Doktorin der Naturwissenschaften (Dr. rer. nat.)

vorgelegt dem
Fachbereich Biologie der Universität Hamburg

angefertigt in der Abteilung Virologie am
Bernhard-Nocht-Institut für Tropenmedizin, Hamburg

von
Nele Marie Brinkmann, geb. Burckhardt

Hamburg, Mai 2024
Disputation abgehalten am 30.08.2024

Die vorliegende Arbeit wurde im Zeitraum von Januar 2021 bis Mai 2024 in der Abteilung Virologie des Bernhard-Nocht-Instituts für Tropenmedizin in Hamburg unter der Leitung von Dr. Lisa Oestereich angefertigt.

Erstgutachter:	Prof. Dr. med. Dr. med. habil. Jonas Schmidt-Chanasit Fachbereich Biologie Universität Hamburg
Zweitgutachter:	Prof. Dr. med. Stephan Günther Abteilung Virologie Bernhard-Nocht-Institut für Tropenmedizin, Hamburg

Table of contents

Zusammenfassung

Das Lassa-Virus (LASV) kann bei einer Infektion Lassafieber (LF) auslösen, eine schwerwiegende, fiebrige Erkrankung, die für 900.000 Infektionen und bis zu 18.000 Tote jährlich verantwortlich ist. LASV ist ein negativ-strängiges, zoonotisches RNA-Virus, das zur Familie der *Arenaviridae* gehört. Die Übertragung auf den Menschen geschieht hauptsächlich durch Körperflüssigkeiten und Ausscheidungen des primären Nagetierreservoirs, *Mastomys natalensis*. Kürzlichen Publikationen zufolge, wurden auch andere Nagetierarten identifiziert, die LASV in sich tragen. Infektionsexperimente mit verschiedenen LASV-Stämmen konnten zeigen, dass Stämme, die zuvor aus *M. natalensis* isoliert wurden (homologe Stämme) bei Infektion in *Mastomys* persistente Infektionen verursachen können. Hingegeben konnten Stämme, die aus anderen Tieren isoliert wurden (heterologe Stämme) keine Persistenz hervorrufen. Basierend auf diesen Erkenntnissen war es Ziel dieser Arbeit, Faktoren zu identifizieren, die das Wirtsspektrum von LASV limitieren. Um dies zu erreichen, wurde zu Beginn dieses Projektes ein *in vitro* System mit *Mastomys*-Zellen entwickelt und bezüglich der LASV-Rezeptorexpression und der Entstehung von infektiösen Viren charakterisiert. Dieses System erlaubte es, viele Untersuchungen zunächst *in vitro* durchzuführen und somit die Zahl der für diese Studien benutzten Tiere signifikant zu reduzieren. Die Wachstumskinetiken von LASV-Stämmen, die von verschiedenen Wirtstieren isoliert wurden, wurden auf zwei verschiedenen Zelllinien, *Mastomys* Nierenepithelzellen (MasKEC) und *Mastomys* embryonalen Fibroblasten (MasEF) charakterisiert. Der heterologe Kak428-Stamm war im Vergleich zum homologen, von *Mastomys* isolierten Ba366-Stamm in seinem Wachstum verlangsamt. Da dieses Wachstumsverhalten vorherigen *in vivo* Experimenten entsprach, wurde im nächsten Schritt untersucht, welchen Einfluss die einzelnen Virusproteine auf die Virus-Wirts-Barriere haben. Hierfür wurden chimäre Viren hergestellt und sowohl *in vitro* als auch *in vivo* charakterisiert. Wenn das Glykoprotein (GP), das L Protein (L) oder das Nukleoprotein (NP) des heterologen Stammes in den genetischen Hintergrund des homologen Stammes eingefügt wurde, war das Wachstum stark eingeschränkt and die Viren wurden schnell von den Tieren eliminiert. Darüber hinaus wurden Stämme, die in den vorherigen Analysen ein eingeschränktes Wachstum auf MasKEC zeigten, weiter charakterisiert. Mittels serieller Infektionsexperimente auf MasKEC wurden die Viren *in vitro* an *Mastomys natalensis* adaptiert und potentiell Wirts-adaptive Mutationen wurden mithilfe von *Next Generation*

Sequencing identifiziert. Die Adaption resultierte in einem beschleunigten Wachstumsverhalten und erhöhten Virustitern für den heterologen Stamm. Die während dieses Prozesses auftretenden Mutationen akkumulierten vor allem in den GP, L und NP Genen und wurden auch in der zugehörigen 3D Proteinstruktur lokalisiert. Zusätzlich wurden Virusvarianten, die durch die Adaption in den Zellkulturexperimenten entstanden sind, auch in *in vivo* Experimenten getestet und zeigten unterschiedliche Phänotypen.

Mithilfe von Virus-Lebenszyklus-Modellierungssystemen wurden die verschiedenen Prozesse des viralen Lebenszyklus weiter erforscht. Während des Eintrittsprozesses wurde eine Beeinträchtigung des heterologen Stammes festgestellt und in Replikon-Assays, die die Virusreplikation und -transkription näher untersuchen, hat das NP des heterologen Kak428-Stammes stärker zur Beeinträchtigung der Prozesse beigetragen als das L Protein. Der Replikon-Assay wurde zudem benutzt, um Mutationen im NP, die während der Adaptionsexperimente auftraten, weiter zu untersuchen.

In dieser Arbeit wurde ein *in vitro* Modell für die Infektion von LASV in den Zellen des natürlichen Wirtstiers entwickelt, das die Beobachtungen aus *in vivo* Experimenten nachstellen kann. Darüber hinaus konnte gezeigt werden, dass LASV sich schnell an neue Wirtszellen anpassen kann. Potenziell Wirts-adaptive Mutationen im Virusgenom wurden zudem in Replikon-Assays und in *in vivo* Experimenten weiter charakterisiert.

Abstract

Lassa virus (LASV) can cause Lassa fever (LF), a severe febrile illness which is responsible for 900,000 infections and 18,000 deaths annually. LASV is a the negative-sense RNA virus, which belongs to the family of *Arenaviridae*, and is a zoonotic pathogen. Transmission of LASV to humans occurs through the body fluids and excretions of its primary rodent reservoir, *Mastomys natalensis*. Recent findings indicate that additional rodent species also carry LASV and infection and transmission experiments involving different LASV strains in *M. natalensis* revealed previously that strains originating from *M. natalensis* (homologous strains) establish persistent infections, while those from other sources (heterologous strains) are cleared rapidly. The objective of this project was to pinpoint viral factors that limit the host range of LASV. To achieve this, an *in vitro* system with *M. natalensis* cells was established in the beginning of this project and characterized regarding the expression of receptors required for LASV cell entry and the release of infectious progeny viruses. This system allowed to study host barriers *in vitro* and thus reduced the number of animals used during these studies significantly. The growth kinetics of LASV strains originating from different rodents were assessed on two cell lines derived from *M. natalensis*, namely *Mastomys* kidney epithelial cells (MasKEC) and *Mastomys* embryonal fibroblasts (MasEF). The growth of the heterologous Kak428 strain was attenuated compared to the *Mastomys*-derived Ba366 strain. As these growth kinetics resembled the growth of previous *in vivo* experiments, the next step was to assess the role of each viral protein on the virus-host barrier. Therefore, chimeric viruses were generated and used both for *in vitro* and *in vivo* experiments. When the glycoprotein (GP), L protein (L) or nucleoprotein (NP) of a heterologous strain was inserted into the genetic background of a homologous strain, the growth was strongly impaired, and the virus was cleared rapidly from the animals. The strains exhibiting attenuated growth on MasKEC cells were further characterized. Serial *in vitro* infection experiments on MasKEC were employed to adapt the heterologous LASV strain *to Mastomys* natalensis, and potential host-adaptive mutations were identified by Next Generation Sequencing. Following serial passaging on MasKEC, rapid adaptation occurred, resulting in accelerated replication and elevated peak titers for the heterologous strain. The mutations occurring during this process were accumulating in the GP, L and NP genes and mapped to their respective 3D protein structures. Additionally, some virus variants after ten passages of adaptation in cell culture, were used for *in vivo* experiments and revealed varying levels of adaptation.

By using virus-life cycle modelling systems, the different life cycle steps were elucidated further. During entry, an impairment of the heterologous strain was noted and in replicon assays to assess the replication and transcription, the NP of this strain seemed to be more restricting than the L protein. The latter assay was also used to characterize the NP mutations identified during the adaptation experiments further.

In summary, an *in vitro* model for LASV infection of natural host cells was established, and it closely mirrors the *in vivo* observations. Moreover, LASV demonstrated the ability to adapt to new host cells quickly, and potential host-adaptive mutations within the virus genome were characterized in replicon assays, entry assays and in *in vivo* experiments.

1. Introduction

1.1. Lassa fever

Lassa fever (LF) is a severe febrile illness which affects up 900,000 persons annually and causes up to 18,000 deaths per year [1]. It is a zoonotic disease which mainly occurs in West African countries such as Nigeria [2-6], Guinea [7-10], Sierra Leone [11, 12], Benin [13, 14], Liberia [15-20], Côte d´Ivoire [21, 22] and Togo [23, 24] in seasonal epidemics with the highest incidence between December and April [25]. The causative agent of LF is Lassa virus (LASV), which is mostly transmitted from the main rodent host *Mastomys natalensis* to humans [26]. As *M. natalensis* shed LASV in their urine and feces, consumption of contaminated food is thought to be the predominant route of infection [9, 11, 27]. In addition, also nosocomial transmissions have been observed [28]. LF also has been seen in sporadic imported infections among others to the United Kingdom, the United States of America and Germany, which poses a threat also on non-endemic countries [29-33].

1.1.1. Symptoms and diagnostics

Symptoms of LF are ranging from mild and flu-like to severe hemorrhagic fevers, with estimated 80 % of infections being mild or asymptomatic [32]. Case fatality rates in hospitalized patients vary based on the country, ranging from 15 % in Nigeria to 69 % in Sierra Leone [34-36]. A recent study, however, suggests that the case fatality rates are highly underestimated, as surveillance is not routinely performed in all countries affected and access to diagnostics is often limited [37]. Importantly, pregnant women are at particularly high risk to die from the infection and to lose their fetuses [38-40]. The onset of symptoms usually ranges from 7 to 21 days post infection (d. p. i.) and after a few days of mild illness with fever, general malaise, weakness and headaches, 20 % of the patients develop more severe symptoms such as hemorrhage, respiratory distress, vomiting, generalized body pain, shock and multi systems organ failure [18, 41-43]. High viral load and upregulated liver enzymes such as aspartate and alanine transamidases and kidney creatinine are associated with poor outcome [35, 37, 44, 45] Furthermore, neurological problems such as tremors, encephalitis, and hearing loss have been reported [46-48]. The hearing loss can be temporary, but in some cases also lead to permanent deafness [18, 49, 50].

As most of the early symptoms of LF are rather unspecific and similar to other febrile illnesses such as malaria, Dengue fever and typhoid fever that are co-circulating in the respective areas [41, 51, 52], LF diagnosis is often challenging. For imported cases of LF, diagnosis might also be delayed when the travelers did not stay in known endemic regions or show atypical LF symptoms [29-31]. As for many viruses, virus isolation or direct detection of virions with electron microscopy has long been a standard method to confirm virus infections. However, this is challenging for LF as the causative agent LASV is a biosafety level 4 (BSL-4) pathogen and those facilities are rare and not available in the endemic areas. In the early 1990s, conventional polymerase chain reaction (PCR) was used to detect LASV [53, 54]. Nowadays, reverse transcription polymerase chain reaction (RT-PCR) is used as a standard tool for the detection of LASV RNA [55-57]. Additionally, Next Generation Sequencing (NGS) is becoming used more frequently to identify new LASV strains and to follow up on LF outbreaks in a timely manner as e.g. done in the 2018 LF outbreak [58, 59]. Nonetheless, the capacity to perform NGS analysis in the affected countries is often limited [60].

Additionally, serological assays such as lateral flow immunoassays and Enzyme-linked Immunosorbent Assays (ELISA) can be used in the absence of RT-PCR capacity to directly detect the viral proteins, but these assays have limited sensitivity [56, 61, 62]. The combination of RT-PCRs with ELISA detecting virus-specific IgG and IgM increases sensitivity [63]. However, detecting IgG does not allow to identify acute infections and IgM ELISA have a tendency for false positives [64]. Also, potential ELISA cross-reactivity between related arenaviruses such as Lujo virus, Mobala virus and Mopeia virus needs to be taken into consideration [65-67]. The same is true for diagnostics with immunofluorescence assays to detect LASV antibodies [68]

1.1.2. Immune reactions to LASV

Studies on the immune response to LASV have found dendritic cells and macrophages among the main target cells of LASV, which could potentially facilitate the spread of the virus by migrating into secondary lymphoid organs and carrying the virus along with them [27, 69-71]. Infected macrophages and dendritic cells show a lack of activation marker upregulation and cytokine expression, which are important as co-stimulatory molecules for T cells. This results in a reduced T cell proliferation [27, 69, 71]. In human patients and non-human primate models, an early and strong immune reaction is important for survival, whereas weak immune

responses as well as uncontrolled viral replication are characteristic of a fatal outcome [72]. High viral load and high levels of pro-inflammatory cytokines such as interferon-γ (IFN-γ) and tumor necrosis factor-α (TNF-α), which might have contributed to multi-organ failure and shock, have also been observed in fatal LF cases in humans [73]. In non-human primates, surviving animals gained rapid control over the infection with a moderate inflammatory response and a balanced innate and T-cell response, whereas in fatal cases systemic dissemination led to massive replication and a subsequent cytokine/chemokine storm, defective T-cell responses and multi-organ failure [74, 75]. In mice however, T cells are not always protective but can also enhance the pathogenesis of LF [76].

The role of LASV neutralizing antibodies is still insufficiently understood. LF-survivors can recover without neutralizing antibodies and LASV-specific antibodies develop late and sometimes only during the convalescence phase of the disease, indicating a minor role of antibodies for the viral clearance [77-79]. A recent study indicated, that like other viral hemorrhagic fever viruses such as Ebola virus and Marburg virus, LASV is able to evade the immune system and persist in different body fluids of survivors such as urine, vaginal fluids and seminal fluids for up to nine months [80, 81].

1.1.3. Treatment, vaccines and preventive measures

So far, no approved treatment and vaccines are available for LASV. Aside from supportive care such as monitoring of fluid and electrolyte balance as well as oxygenation, ribavirin has been used to treat LF patients [43]. Ribavirin is a guanosine nucleoside analogue which has been approved by the Food and drug administration (FDA) for the treatment of Respiratory Syncytial virus and hepatitis C virus and is regularly used off-label for LF patients in outbreak settings as well as for imported LF cases [41, 82, 83]. However, it is not completely understood how ribavirin is acting against LASV, and concerns have been raised regarding efficacy and safety [84]. In addition to ribavirin, the purine nucleoside analogue favipiravir is currently examined in a phase II efficacy trail [85]. Apart from nucleoside analogues, plasma of convalescent individuals has also sporadically been used for treatment. Further treatment options have only been evaluated in non-human primates or other animal models and include human-monoclonal antibodies [86-88] as well as entry inhibitors [89].

Until 2022, four LASV vaccine candidates were tested or are currently undergoing assessment during clinical trials [90] including one DNA-based vaccine candidate (INO-4500), a live-

attenuated Schwarz strain measles virus vector (MV-LASV; [91]) that express the LASV glycoprotein (GP) and nucleoprotein (NP) genes and two viral vector-based candidates. These vector-based candidates (namely rVSVΔG-LASV-GPC; [92] and Emergent Biosolution-LASV (EBS-LASV) [93]) both encode the LASV (Josiah strain) GPC gene and have been developed in analogy to the already FDA-approved ERVEBO® Ebola virus vaccine. The MV-LASV vaccine showed acceptable safety and tolerability already during a first phase I clinical trial [91]. The rVSVΔG-LASV-GPC vaccine candidate has been found to induce rapid activation of the adaptive immune system and protects non-human primates from severe disease outcome [94]. In a phase I clinical trial, the vaccine was well tolerated and immunogenic in a wide dose range with induction of broadly cross-reactive antibodies [95]. Since March 2024, the rVSVΔG-LASV-GPC vaccine candidate is now in the first phase II clinical trial as LASV vaccine in Nigeria [96].

A different approach to lower the number of human LF cases is to reduce the contact between humans and potentially infected rodents. Beyond educating the population at risk about the disease, the reservoir and transmission routes, rodent control has been evaluated in the fight against LASV. Trapping of rodents and using rodenticides were tested in Guinea over a time period of four years within the dry season from December to April. A significant reduction of animals was observed, but the rodent populations grew back to their original size quickly after the measures were stopped. Nonetheless, the prevalence of LASV in the rodent population was negatively affected by trapping. However, the authors did not investigate the effect of the diminished rodent populations on human LF cases [97, 98].

1.2. The family of *Arenaviridae*

The causative agent of LF is Lassa virus (LASV, species name: *Mammarenavirus lassaense*) which belongs to the order of *Bunyavirales* and the family of *Arenaviridae.* The *Arenaviridae* family has five genera namely *Antennavirus*, *Hartmanivirus, Reptarenavirus*, *Innmovirus*, and *Mammarenavirus*, which infect different vertebrate host species including fish, reptiles and mammals. The most recently identified genus is the *Innmoviruses* which have been found in hedgehogs [99]. The viruses that pose a major risk for human health all belong to the genus of *Mammarenavirus.* This genus can be sub-divided into two groups based on their antigenic, phylogenic and geographical characteristics, namely the Old World and New World arenaviruses. The Old World arenaviruses include viruses such as LASV, Lujo virus, and the

lymphocytic choriomeningitis virus and are geographically located in Europe and Africa. In addition, some Old World viruses have been found in Asia, such as Wenzhou Virus and Plateau Pika Virus [100]. In contrast, the New World arenaviruses are mainly found in the Americas and include both nonpathogenic viruses such as Tacaribe virus as well as hemorrhagic fever viruses like Junín virus, Guanarito virus, Sabiá virus and Machupo virus [101].

1.2.1. Virion structure and genome organization

The spherical LASV particles range from 70 to 150 nm in size [102]. LASV is a single-stranded negative-sense RNA virus carrying a bi-segmented genome with an ambisense coding strategy that enables the independent regulation of the viral genes [103]. The two segments are the small segment (S) and large segment (L) and have sizes of 3.7 and 7.2 kb, respectively. The ends of the viral genome segments contain highly conserved untranslated regions (UTRs), with the terminal 19 nucleotides acting as a promoter for the viral polymerase [104, 105]. The S segment encodes for the viral glycoprotein precursor complex (GPC) and the nucleoprotein (NP), while the L segment encodes the matrix protein (Z) as well as the L protein (L). The genes on both segments are separated by a stable secondary structure, called the intergenic region, which is important for the termination of transcription [106, 107] (see Figure 1A).

Figure 1B shows a schematic overview of the LASV virion. The heterodimeric trimers of the GPC are located on the outside of the virion surface which mediates the virus binding to its receptors and virus entry into host cells. The virion envelope is lined on the inside by the matrix protein Z, which is acquired during virus budding. The NP is covering the viral RNA to protect it from recognition of innate immune sensors and is one of the minimal components for viral transcription and replication, which is facilitated by the viral L protein. Together these three components are considered the ribonucleoprotein complex (RNP) and are sufficient for virus replication. As the LASV genome is organized in an ambisense manner (Figure 1C), an intermediate anti-genomic viral RNA is needed for viral transcription and replication of the GP and Z genes. In contrast, the NP and L genes can be transcribed directly from the viral RNA.

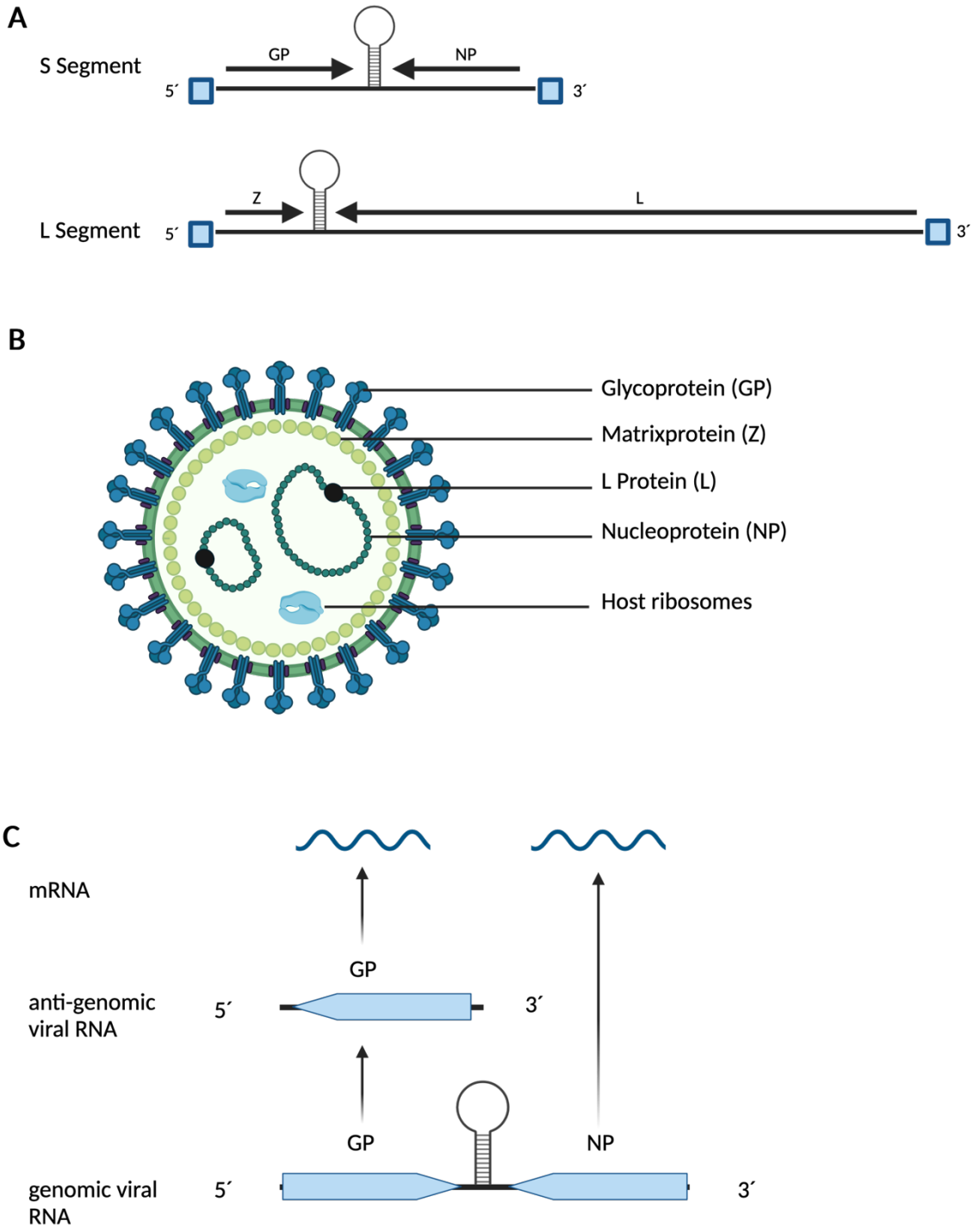

Figure 1: LASV virion and genome structure. **A** LASV virions consist of the nucleocapsid, which is covered with the GP on the surface and the Z protein on the inside. Inside the particles, the NP, the viral RNA and the L protein form the ribonucleoprotein complex. **B** The two genome segments encode both for two proteins each. The S segment encodes the GP and NP genes, whereas the L and Z proteins are encoded on the L segment. **C** The ambisense coding strategy of arenaviruses is depicted with the LASV S segment as an example. While the NP can directly be transcribed into mRNA, the GP needs to be transcribed into a complementary, antigenomic RNA intermediate before it can serve as a template for transcription. This figure was created with BioRender.com and modified according to [29].

1.2.2. Viral life cycle

1.2.2.1. Virus entry is facilitated by the glycoprotein

The primary receptor for LASV is α-dystroglycan (αDG) [108, 109], which is a matriglycan found on the surface of a wide range of different cell types [110, 111]. Together with the transmembrane β-dystroglycan subunit, αDG interacts both with the cytoplasm of the cell and the extracellular matrix [110, 111]. αDG can interact with LASV GP1 on the virus surface, but to do so it requires a specific type of glycosylation, called O-mannosylation [112]. These glycosylations are attached to αDG by enzymes of the like-acetylglucosaminyltransferase (LARGE) family. In the absence of αDG or if it is inadequately glycosylated, alternative receptors can mediate LASV entry such as the Tyro3/Axl/Mer (TAM) receptor tyrosine kinases [113-115] and other phosphatidylserine-binding receptors and C-type lectin receptors such as dendritic cell-specific intercellular adhesion molecule-3-grabbing non-integrin (DC-SIGN) [115, 116]. After the binding of the LASV GP1 subunit to α-DG, the virions are internalized via receptor-mediated clathrin-independent endocytosis [117]. In the endosomes, acidification leads to conformational changes of the GP1 and its dissociation from αDG. Meanwhile, the GP2 starts to interact with the lysosomal-associated membrane protein 1 (LAMP1) and facilitates membrane fusion and the release of the LASV genome segments into the cytoplasm [118, 119].

1.2.2.2. Viral replication by the L protein and the nucleoprotein NP

After the virus segments have been released into the cytoplasm, viral transcription and replication are performed by the RNPs, which consist of L, NP and viral RNA [120]. First, the endonuclease domain of the L protein cleaves off the 5´cap of the mRNAs to serve as a primer [121] and initiates viral replication of both viral RNA (vRNA) and complementary vRNA as well as transcription of capped, non-methylated viral mRNA [122]. As the L and NP are encoded in 3´to 5´direction, they are synthesized first, and thus easily available for further replication and transcription processes. The structural proteins GP and Z that are needed for the virions, are produced later during the viral life cycle via an intermediate complementary RNA. The mRNAs are translated at the ribosomes, and the translation of the GPC is taking place at the endoplasmic reticulum, where it is directly glycosylated. The GPC is further processed by the cellular signal peptidase (SPase) or the subtilase/kexin isozyme-1 (SKI-1/S1P) in the trans-Golgi network. This results in three proteins, the stable signal peptide (SSP), the receptor-binding

subunit GP1 and the transmembrane domain GP2 [123-125]. Thereafter, the GPC is transported to the cell membrane, where it forms the final glycoprotein complex. The synthesis of Z proteins additionally controls the transcription and replication process [126, 127].

1.2.2.3. Virus assembly by zinc binding protein Z

LASV budding is mainly driven by the matrix protein Z. The matrix protein interacts with the viral L protein through its Really Interesting New Gene (RING) domain to inhibit viral RNA synthesis and initiate the budding process [126-128]. It controls packaging of the virus particles as well as budding from the plasma membrane [129, 130]. For this, the new RNPs are recruited to the plasma membrane by the Z protein interacting with the endosomal sorting complexes required for transport (ESCRT) machinery of the host together with the viral NP [131]. Budding is finally initiated through accumulation of viral Z protein at the cell membrane, resulting in the assembly of the NP, Z and L protein together with the viral RNA segments and the release of new virus particles [132].

1.2.2.4. Life cycle modelling systems for individual steps

Since LASV is a BSL-4 pathogen, working with the full virus requires a high containment laboratory and trained personnel to conduct the often time-consuming and very complex experiments. Virus life cycle modelling systems allow the study of individual processes of the viral life cycle independent from one another under BSL-2 conditions.

For studying virus entry, often so-called pseudotyped viruses with the Vesicular Stomatitis Virus (VSV) as the genetic background are used [133, 134]. While the replication and transcription machinery are derived from VSV, in this system the surface glycoprotein (G) of VSV is exchanged with the LASV GP. This enables the study of viral entry, independent of LASV-specific transcription and replication. The system can be employed to monitor the early infection kinetics over time, for single-round infections or simply to determine if a specific glycoprotein can efficiently mediate entry into different host cells e.g. via immunofluorescence approaches. Similarly, lentivirus-based systems are often employed. Shimojima et al., used a pseudotyped system based on a lentiviral vector with the LASV Josiah strain GPC on the virus surface and identified receptors from the TAM family and from the C-type lectin family to serve as alternative entry receptors for LASV [115].

The viral transcription and replication can be studied by using a replicon system [135]. Figure *2* schematically shows the workflow of the LASV replicon assay. Here, a T7-polymerase-based minigenome (MG) was generated for LASV, which consists of the 5´ and 3´ UTRs and the intergenic region of the LASV S segment as well as two reporter genes, which replace the open reading frames of the viral RNA. The reporter genes are the chloramphenicol acetyltransferase (CAT) and the Renilla luciferase which are encoded in an ambisense manner. This plasmid is co-transfected into BSR-T7/5 cells stably expressing the T7-polymerase, together with expression plasmids encoding for the LASV L and NP gene. In the cells, the L, NP and MG are expressed, leading to the formation of RNPs. Those RNPs facilitate the replication and transcription of reporter genes encoded by the LASV MG like the replication of the viral segments in the full virus context. The Renilla luciferase enables easy monitoring of the MG replication and transcription via luminescence read outs (RLU). This means, a high signal in RLU corresponds to a high RNP activity and subsequently high transcription and replication efficiency. As a transfection control, a Firefly luciferase-encoding plasmid is co-transfected.

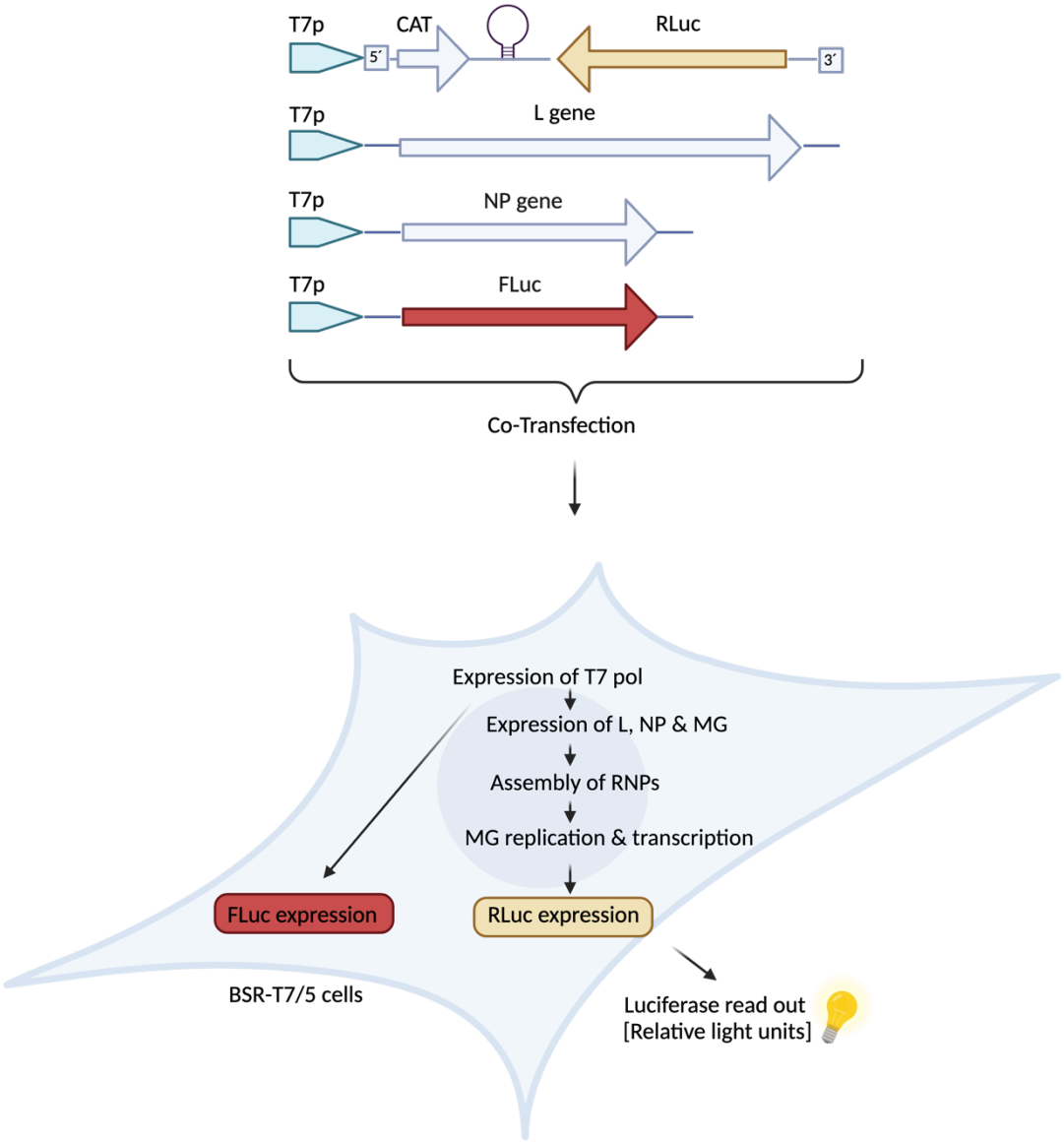

Figure 2: Schematic of the LASV replicon assay. Plasmids encoding the LASV minigenome (MG) with the Renilla luciferase (RLuc) and the chloramphenicol acetyltransferase (CAT) as well as expression plasmids for the NP or the L protein of LASV are co-transfected into BSR-T7/5 cells with a Firefly luciferase (FLuc) expression plasmid which serves as transfection control. All plasmids are under control of the T7-promotor (T7p). After co-transfection, the L, NP and MG are expressed, leading to the assembly of ribonucleoparticles (RNPs), which facilitate replication and transcription of the MG. This leads to the expression of RLuc and FLuc, which can be tracked with a luminometer and is a measure for transcription and replication on the one hand and on the other hand indicate the transfection efficiency. This figure was created with BioRender.com.

To study viral budding, virus-like particle (VLP)-based systems are widely used. As it is known for LASV, the Z protein alone is sufficient to initiate virus budding [136] and *in vitro* expression of the Z protein leads to the formation of VLPs, that are released into the cell culture supernatant. To characterize LASV budding, often HEK293-T cells are used as these are easy

to transfect. After the transfection, VLPs in the cell culture supernatant can be harvested 24 h post transfection and purified via a sucrose gradient ultracentrifugation. The VLPs as well as the lysate from the transfected cells are used for Western Blotting and analyzed regarding size and amount of released vesicles. Budding defects can be identified by Western Blotting e.g., if there is a more intense chemiluminescence signal for the Z protein in the cell lysate compared to the released VLPs in the cell culture supernatant.

1.2.3. Geographical distribution and phylogeny of LASV

LASV is endemic in several West African countries, mainly Nigeria, Guinea, Sierra Leone and Liberia and to a lesser extent Mali [22], Benin [13, 14], Côte d´Ivoire [21, 22] and Togo [23, 24]. LASV has a very diverse genome with variations at the nucleotide level of up to 32 % for the L segment [137, 138]. There are currently seven known LASV lineages, which geographically cluster together (see Figure 3). The lineages I, II, III and VI are circulating in Nigeria, while lineage VII is found in Togo. Lineage V is found in Mali and Côte d´Ivoire, and lineage IV is mostly present in Guinea, Sierra Leone and Liberia [137].

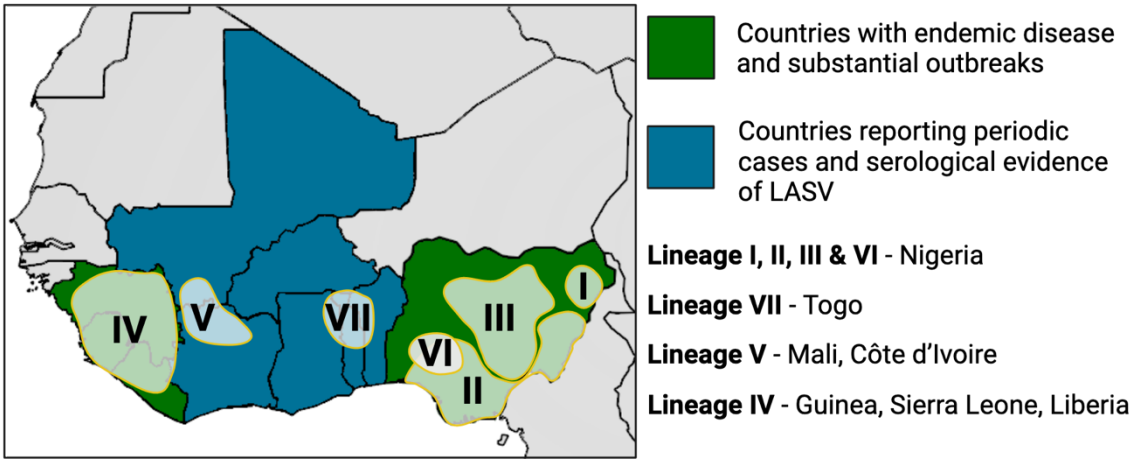

Figure 3: Distribution of different LASV lineages in West Africa. Countries in which LF is endemic are shown in green and countries reporting periodic cases of LF or have serological evidence of LASV are colored in blue. Depicted in shaded color are the distributions of the different LASV lineages. The figure was created with Biorender.com and kindly provided by Dr. Chris Hoffmann. It is based on data presented by the CDC and [137].

1.2.4. Hosts of LASV

For many years, the multimammate mouse, *Mastomys natalensis,* has been known as the natural host for LASV [26]. *Mastomys* often live close to human households, and they can shed LASV in their urine or other body excretions. Hence, human infections mainly occur due to

direct contact to the animals, rodent excreta or by consumption of the animals or contaminated food [11, 27]. In endemic regions, studies found 50-100 % of all rodents in human households to be *Mastomys* of which a substantial fraction is seropositive for LASV [11, 27, 139, 140]. When taking the vast geographical distribution of *Mastomys* over the whole Sub-Saharan continent [141] into consideration, large human populations are potentially at risk for contracting LF. Up to now, it is not clear, why LASV is only found in a few West African countries although the main rodent reservoir is found more broadly distributed. Apart from geographical barriers, the sub-division of *M. natalensis* into two major lineages, based on their mitochondrial DNA has been discussed [142, 143]. As shown in Figure 4, clade A is mainly distributed over West and Central Africa, whereas clade B is found in Eastern and Southern Africa. Both clades can be sub-divided into three phylogroups, which likewise correspond to geographical locations and have been suggested to be important for the distribution of arenaviruses that infect *Mastomys*.

Furthermore, recent field studies indicate an even broader host range for LASV. As shown in Figure 4, new LASV strains were isolated from other rodent species including the Kak428 strain from the African wood mouse *Hylomyscus pamfi* in Nigeria [144, 145], the Madina strain (MAD39) from the Guinea multimammate mouse *Mastomys erythroleucus* in Nigeria and Guinea [144] as well as the D96 strain carried by the striped grass mouse *Lemniscomys striatus* in Benin (Fichet-Calvet, personal communication, 2019). However, to this date factors enabling or preventing host switches of LASV remain to be elucidated. Furthermore, *M. natalensis* has been found to carry several other arenaviruses such as the closely related Morogoro virus (MORV) [146, 147], Gairo virus (GAIV) found in Tanzania [148], and Mopeia virus (MOPV) in South-East Africa [148, 149]. For the arenaviruses found in East Africa, a strong correlation between geographical occurrence and *M. natalensis* matrilineage presence has been observed [143].

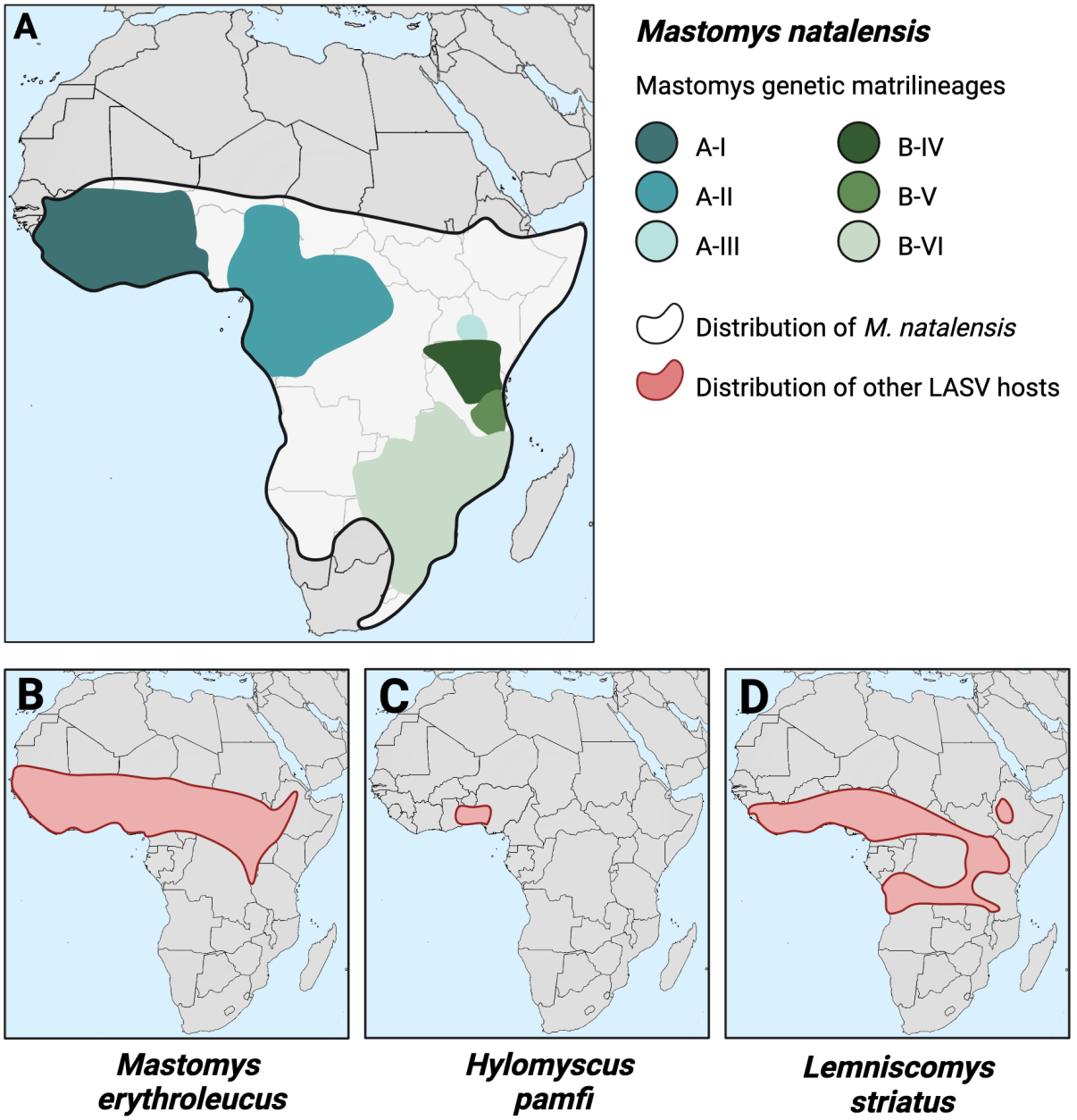

Figure 4: Overview of LASV reservoir hosts distribution. A shows the widespread distribution of the main host *M. natalensis* on the Sub-Saharan African continent. *M. natalensis* can subsequently be divided into six matrilineages, which are shown in blue (A-I to A-III) and green (B-IV and B-VI). In addition to *M. natalensis*, other rodent hosts have been identified such as **B** *M. erythroleucus*, **C** *Hylomyscus pamfi*, and **D** *Lemniscomys striatus*. This figure was adapted from Dr. Chris Hoffmann (created with BioRender.com) and is based on [142] and the IUCN Red List.

1.2.5. LASV in its natural host *M. natalensis*

Since studies on the interplay of LASV and its natural host are sparse, groups in the USA and Canada established a colony of *Mastomys natalensis*, that were initially caught in Mali [150]. In addition, secondary breeding colonies were established at the Bernhard Nocht Institute for Tropical Medicine (BNITM) in Hamburg and at the Robert Koch Institute (RKI) in Berlin. For the

first time, hematology and clinical chemistry parameters of *M. natalensis* were characterized at RKI in 2021 setting a reference range for this not-well studied model organism in comparison to mice and *Mastomys coucha* [151]. In addition, infection experiments with *M. natalensis* were conducted to gain insights into the infection dynamics of LASV in its natural host [27]. As an example, different infection routes of LASV were compared, namely intraperitoneal (i. p.), intranasal (i. n.), intramuscular (i. m.), subcutaneous (s. c.) and oral gavage during infection of adult *M. natalensis*. All infection routes led to subclinical disease with systemic infection, inflammatory changes and widespread virus dissemination in the organs [27]. However, the i. n. infection route was found to most likely mimic the natural route of infection with a longer time till viral clearance, whereas the s. c. and i. p. routes lead to lower virus titers and less pronounced histological changes [152, 153]. Additionally, the ability of geographically non-matched LASV strains to infect *M. natalensis* was determined. For this, the LASV Sorombra-R strain was used, which is an isolate from *M. natalensis* in Mali, and compared it to the geographically non-matched Z132 and Josiah strains, which are both human isolates from Libera and Sierra Leone, respectively. All LASV isolates were able to infect *M. natalensis* originating from Mali irrespectively of their geographic origin and were cleared in most organs within 40 d. p. i.. Here, lung and spleen were the exception as those remained virus positive up to 60 d. p. i.. Furthermore, horizontal transmission to cage mates was observed in up to 23.3 % of the cases [153].

Among these studies, only adult animals from 6 - 16 weeks of age were used for the infection experiments, but the authors of both beforementioned studies argued, that *M. natalensis* which mainly come into contact with humans are younger [152, 154] and viral persistence in nature may rely on vertical transmission and chronically infected offspring, hence, infection experiments with younger animals are needed [153]. Therefore, the immunology and virology of LASV and related arenaviruses in its natural host *M. natalensis* was further characterized [155, 156]. An age-dependent clearance of arenaviruses in infected *M. natalensis* was observed, as contact with the LASV strain Ba366 strain at a young age led to viral persistence, whereas infections of adult animals were rapidly cleared. In more detail, the age of two weeks at the time of infection was most critical. Infection of younger animals resulted in life-long persistence, whereas viral clearance within several weeks was observed when animals were two weeks or older at the time of infection. Virus clearance was even further accelerated with increasing age at the time of infection. LASV was shown to persist up to 15 months with a

ubiquitous virus presence in blood, urine, feces, saliva and various organs. The virus titers in non-persistently infected individuals declined over time, which was less pronounced in kidney, lungs and gonads, but for animals with persistent infections, virus titers were relatively stable over time. Additionally, no correlation between antibody response and virus clearance was found [156]. Characterization of the transmission dynamics showed that both persistently infected as well as transiently infected animals were able to transmit the virus to cage mates via horizontal transmission, most likely by their body fluids and excretions.

Furthermore, it was assessed, how host-species barriers between *M. natalensis* and recently identified new LASV strains affect the infection dynamics and transmission patterns. Importantly, for the above-mentioned experiments, the Ba366 strain was used exclusively, which resembles a homologous strain as it was initially isolated from *Mastomys natalensis*. For the last experiments, LASV strains isolated from other rodent hosts (heterologous strains) were used, namely the D96 strain (isolated from *Lemniscomys striatus* (Fichet-Calvet, personal communication, 2019)) and the Kak428 strain (isolated from *Hylomyscus pamfi* [145]). Infection experiments with the heterologous strains resulted only in transient infections and a higher infectious dose of the Kak428 strain led to even faster clearance. Additionally, no horizontal transmission was found after infection with heterologous strains. The author argues that the innate immune system could be triggered by the NP and Z proteins of the heterologous Kak428 strain which might be less efficient in immune evasion than the homologous NP and Z from the homologous Ba366 strain [157]. To address this question, a RT-PCR assay to detect changes in type I interferon (IFN)-induced immune response on the level of interferon-stimulated genes (ISGs) was previously developed. When bone marrow-derived macrophages (Mθ) or *Mastomys* kidney epithelial cells (MasKEC) were infected with the homologous Ba366 strain or one of the heterologous strains, the heterologous Kak428 induced the weakest ISG response. *In vivo* experiments showed, the LASV strains Ba366, Kak428 and D96 induced a strong and, in some cases, long-lasting ISG response with a trend towards physiological levels when the virus was cleared by the animals [158]. These results indicate that contrary to previous theories, the innate immune evasion is not the major factor responsible for the accelerated clearance seen for the heterologous LASV strains in comparison to the homologous strain, but other mechanisms are likely to be key. Thus, the question was raised, what other factors influence the ability of heterologous strains to infect *M. natalensis* and overcome potential virus-host barriers.

1.3. Virus host barriers and host-switching

A recent study showed that spillover events of zoonotic pathogens into human are becoming more likely with an increase of almost 5 % annually [159]. Additionally, it was estimated that there will be more than 15,000 interspecies transmission events between mammals by 2040 [160]. This poses the question, which factors enable and restrict viruses from spillover into new hosts in general. Figure 5 depicts the different steps for cross-species transmission. At first, a single transmission event into a new host is needed. The likelihood of this first infection is influenced by different factors such as the distribution and ecology of the initial and the new recipient host species, their behavior and frequency of contacts. Additionally, those factors can be influenced by climate change (including altered temperatures and precipitation) as well as habitat changes. Both, climate change-related weather alternations as well as human-driven habitat changes such as deforestation are getting more and more frequent, thus host distributions as well as their behavior might change, leading to more spillover events into new host species [161].

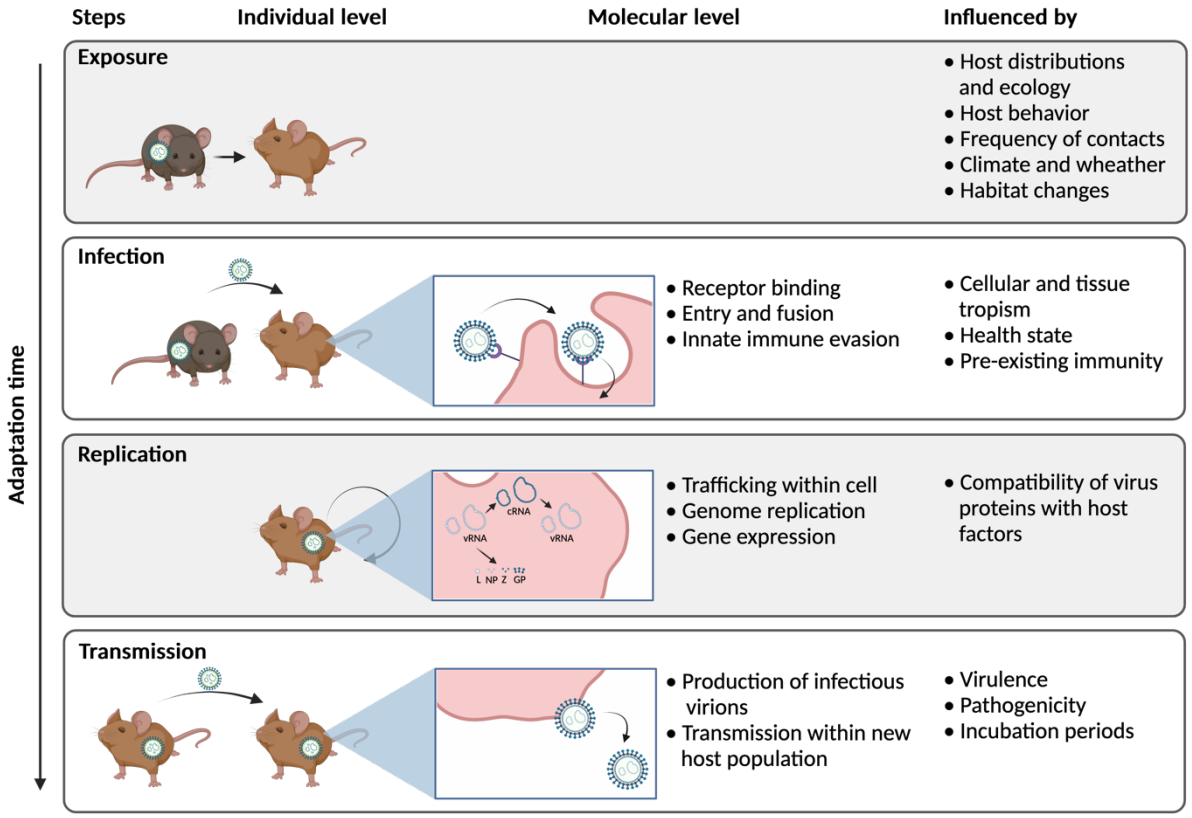

Figure 5: Overview of essential steps for cross-species transmission of viruses. This figure shows the necessary steps for successful spillover of viruses into a new host population, namely exposure, infection, replication and transmission. Shown are the individual level, the molecular level and influencing factors. This figure is based on [161-163] and was created with BioRender.com.

The infection of a new host is restricted by successful receptor binding of the virus to surface proteins, followed by entry and fusion. In the case of New World arenaviruses, all five hemorrhagic fever viruses (Machupo virus, Junín virus, Guaranito virus, Sabia virus and Chapare virus) are able to infect human cells by using the human transferrin receptor 1 (hTFR1). In contrast, closely related non-pathogenic arenaviruses can enter host cells by interaction with their respective transferrin receptor orthologs. It has been shown, that changing only one amino acid in the virus glycoprotein of the non-pathogenic Tacaribe virus renders it able to infect human cells and switches its receptor from a rodent transferrin receptor towards hTFR1 [164]. Recently, also a potentially pathogenic virus strain of the *Tamiami mammarenavirus* has been discovered in Florida (TAMV-FL), which can use the hTFR1. Additional mutations occurred during the isolation process via serial passaging, which increased the strains dependence on hTFR1 [165]. Knowing about the restrictions, entry receptors might pose for adaptation of potentially zoonotic viruses also helps to implement surveillance systems. For influenza A virus (IAV), years of research helped to unravel, which genetic changes are needed to overcome the species barriers between birds, and mammals. There are 18 subtypes of the IAV surface glycoprotein [166], namely hemagglutinin (HA), which enable binding to the host cell´s glycan structures. These terminate in N-acetylneuraminic acid (Neu5Ac) linked to galactose (Gal) in a β1-4 linkage to glucosamine (GlcNAc). This linkage is a predictor of species specificity as avian IAV strains bind to α2,3 sialic acid (SIA), whereas mammalian strains are known to bind α2,6 SIA. Regarding HA, position 226 determines to which SIA to bind to. When glutamine is inserted at position 226 as seen for avian species, HA preferably binds to α2,3 SIA and if glutamine is exchanged to leucine at this position as seen for the human strains, HA mostly binds to α2,6 SIA. Thus, the HA of IAV is an important factor for the species barrier [167]. Also, the site of infection plays an important role, as the local environment such as tissue barriers, temperature and pH can affect the outcome of an infection. Systemic infection of IAV for example is facilitated by a polybasic insertion in the HA, leading to higher pathogenicity [167].

Once the virus successfully entered a cell, the release of the virus genome can pose another barrier to propagation in a new host. As shown for TAMV-FL, mutations in the virus GP can influence the release from the endosomes. Here, it was shown, that the two mutations identified led to virus fusion at a lower pH and therefore later escape from the endosomal

compartment. This could be beneficial for the virus as it facilitates viral genome delivery to perinuclear structures which shield the virus from the innate immune system during replication [165]. Evading the innate immune system is likewise important for viruses to infect new host species. There are several intracellular factors which can restrict the host range of a virus. For retroviruses the cytidine deaminase apolipoprotein B mRNA editing enzyme, catalytic polypeptide (APOBEC) and tripartite motif-containing protein 5α (TRIM5α) have been shown to block infection. In turn, the human immunodeficiency virus (HIV) actively inhibits these processes with its p17 Gag protein, which has been seen in the adaptation process of HIV to humans. For influenza virus, the non-structural protein 1 (NS1) has been shown to impede the interferon signaling [162]. For LASV, the NP and Z protein have been shown to efficiently antagonize the innate immune response [168-175]. The exonuclease domain of the LASV NP efficiently inhibits the recognition of viral RNA by the retinoic acid-inducible gene I (RIG-I) [168] and the translocation of the IFN regulatory factor 3 (IRF3) to prevent downstream signaling and induction of ISGs [170]. Direct interactions of the LASV Z protein with the N-terminal domains of RIG-I [173] and melanoma differentiation-associated protein 5 (MDA5) additionally contribute to immune evasion [175].

For the amplification within the new host, it is crucial for the virus to successfully replicate to high titers. This might require the interaction of the viral proteins with host cell factors. As an example, for efficient virus replication in human cells, the Influenza virus polymerase needs to interact with the acidic nuclear phosphoprotein 32 family members (ANP32A and ANP32B) host proteins [176, 177]. The replication of RNA viruses is error prone as there is no proofreading mechanism and can lead to mutations both in promotors as well as in coding regions. For Old World Arenaviruses, substitution rates are comparable to other RNA viruses with 10^{-3} - 10^{-4} substitutions per site and year [178, 179]. Taken together with the other factors identified to allow cross-species transmission such as a rapid replication, short virus generation times and large virus populations, arenaviruses are likely to be able to spill over to new host species.

Finally, to establish continuous transmission chains, infectious progeny virus needs to be produced and passed to animals of the new host species. Taking IAV as an example, the neuraminidase (NA) is needed to cleave sialic acids on the cell surface to facilitate efficient

budding. There are 11 different NAs in IAV and those underly a strict HA-NA receptor balance, which requires adaptations for cross-species transmission [166].

Factors affecting efficient transmission are virulence, pathogenicity and incubation periods. According to the tradeoff hypothesis, transmission rate and virulence trade-off each other. Thus, fast replicating pathogens might generate larger population sizes and have high transmission rates, but at the same time induce more damage to the host. This damage could increase the mortality and subsequently negatively affect the infectious period, rendering infection of more individuals less likely [180].

Overall, several transmission chains could be needed as one single introduction into a new host species might not be sufficient. Additionally, it is important to note that the ability to infect new host will likely reduce fitness in the original host and that full adaptation to a new host species likely takes several months or even years [162].

1.4. Surveillance strategies for LASV

To monitor the LASV prevalence in the wildlife population and asses the risk of spill over events into new host populations, surveillance is needed. For other zoonotic pathogens, such as avian influenza virus, wildlife monitoring systems are in place, that enable the surveillance of circulating variants and selection of suitable vaccines [181]. This pathogen is known to bring forth virus variants capable of infecting large populations and being able to induce pandemics. For influenza virus, as early as 1952, the Global Influenza Surveillance Network (GISN) was founded, which was later renamed into Global Influenza Surveillance and Response System (GISRS) in 2011. The GISRS currently includes 129 World Health Organization (WHO) member states. Its main function is to provide resources for the prevention and control of seasonal human influenza and avian influenza, including the recommendation of vaccine strains, serving as a reference for antiviral resistance treatment and conducting risk assessment. Surveillance methods for avian influenza virus (AIV) include the monitoring of wild birds, which are the primary reservoir of AIV, along with the most important flyways of migratory birds. Sampling of birds includes cloacal swabs, fecal specimens, oropharyngeal swabs as well as environmental samples from water and soil. Additionally, domestic birds are monitored regarding clinical infection signs such as rhinorrhea, sneezing, coughing and diarrhea by analyzing the same sample types. Beyond the sampling of birds, also human cases and the environment are subject of surveillance to obtain a comprehensive picture of the disease

spread. Especially people at high risk of AIV infection such as poultry farmers, traders or slaughters are monitored for symptoms and e. g. in China environmental samples are analyzed from live poultry markets and major poultry farms [182, 183].

For avian influenza virus, several factors are known to be important for spillover from birds to mammals. This includes the binding of HA to receptors, where human influenza viruses can use α2,6-SA as a receptor and avian influenza viruses are restricted to α2,3-SA [184, 185]. Also, single mutations have been identified to be important to overcome species-specific restrictions. Among them is the Thr552Ser mutation of the avian influenza polymerase PA-subunit, which both increased its activity as well as pathogenicity in human cells [186]. Including these findings into the readily surveillance systems enable the prediction of an altered host range of avian influenza virus.

In contrast to the efforts in AIV surveillance, there is no supra-regional surveillance program which includes wildlife sampling for LASV. Surveillance of human infection is done regularly and improved over the last decades [187], however, further improvement still is needed as stated in the Research and Development Blueprint by the WHO [188]. Moreover, a One Health approach is needed for LASV monitoring and control, due to its zoonotic origin [187]. So far, only limited wildlife surveillance studies on rodents have been performed, for example in Guinea, Nigeria and Sierra Leone [1, 189-194]. Important to note, most of these studies on LASV are performed either with rapid diagnostic tests, ELISAs or RT-PCR assays and that NGS approaches are very rarely used due to limited local capacities and lack of funding. However, these approaches are needed to ensure timely monitoring of spillover events to humans or new hosts.

2. Research questions

The aim of this project was to identify the underlying mechanisms of viral clearance and if there are virus-host barriers that restrict LASV strains to their respective hosts. Given the fact that to this date, no relevant variations on the host side of this virus-host interaction have been identified to be responsible for restricting LASV infection of heterologous viruses in *M. natalensis*, the different virus strains must be better characterized. This is especially required for implementation in surveillance systems, so that potential spillover events into new host species can be predicted in a timely manner.

2.1. Can LASV infection be modelled *in vitro*?

To better characterize the course of LASV infection, usually an animal model is used. However, during this project, the aim was to develop an *in vitro* model for LASV infections to reduce the use of animals. During the model characterization, first the receptor expression in different *M. natalensis* organs as well as *M. natalensis*-derived immortal cell lines was examined. Thereafter, the infection kinetics of different homologous and heterologous LASV strains were investigated and finally, the production of infectious virus particles was confirmed by means of electron microscopy.

2.2. Which viral proteins are responsible for the observed virus-host-barrier?

Within the second objective of this project, it was determined, which viral proteins are of importance for the observed virus-host barrier. For this, chimeric viruses with viral proteins from heterologous virus strains inserted into the backbone of a homologous strain were created by reverse genetics approaches. The growth of those viruses was characterized *in vitro* as well as *in vivo* during infection experiments with *M. natalensis.* This approach allowed us to narrow down which viral protein plays a major role in host restrictions. Additionally, single steps of the virus life cycle were assessed with life cycle modelling systems. To test, if an insufficient interaction of the GP of heterologous viruses with receptors on the surface of *M. natalensis* is the reason for the observed *in vivo* infection patterns, a Vesicular Stomatitis virus-based system has been applied in a complementary manner to full virus infections. Also, a replicon system was used to determine, if the capacity of the LASV NP and L proteins of

homologous and heterologous strains to replicate and transcribe the minigenome might differ [135].

2.3. Which mutations are required for LASV host switching?

Several new LASV hosts have been recently identified, but none of them live as close to human dwellings as the main rodent host, *M. natalensis*. This raises the question, what mutations are necessary for heterologous LASV to overcome the virus-host barrier and infect this broadly distributed host.

The third objective was to describe and characterize the mutations found during virus adaptation processes. The viral evolution of LASV was analyzed in a new *in vitro* system. By serial passaging, a heterologous LASV strain was adapted to MasKEC, and the growth kinetics of the adapted virus variants were compared to the original, non-adapted virus strain. The mutations occurred during the adaptation process were identified by subsequent NGS analysis and further characterized by using the above-mentioned virus-life cycle modelling systems.

3. Materials

3.1. Virus strains and cell lines

Table 1: Overview of virus strains, virus origins, GenBank number and reference.

Virus strain	Isolated from	Origin	GenBank No.	Reference
Ba366	*M. natalensis*	External laboratory	GU830839	doi:10.1038/srep25280
D96	*L. striatus*	BNITM, Virology	Unpublished	Personal communication, Elisabeth Fichet-Calvet, 2019
Kak428	*H. pampfi*	BNITM, Virology	KT992425.1	doi:10.3201/eid1212.060812.

Table 2: Overview of mammalian cell lines used during this project and their respective supplier.

Cell line	Full name	Supplier
BHK-21	ATCC® CCL-10™	American Type Culture Collection, Manassas, VA, USA
BSR-T7/5		kindly provided by Ursula Buchholz and Karl-Klaus Conzelmann at University Munich
HEK293-T	ATCC® CRL-3216™	American Type Culture Collection, Manassas, VA, USA
MasEF	*Mastomys* embryonal fibroblasts	Kindly provided by Eleonore Ostermann and Wolfram Brune at Leibniz Institute of Virology
MasKEC	*Mastomys* kidney epithelial cells (D-valine selected)	Kindly provided by Eleonore Ostermann and Wolfram Brune at Leibniz Institute of Virology
Vero76	ATCC® CRL-1587™	American Type Culture Collection, Manassas, VA, USA
VeroE6	ATCC® CRL-1586™	American Type Culture Collection, Manassas, VA, USA

Table 3: Overview of bacteria used during this project, their specifications and supplier.

Cells	Specifications	Supplier
DH5α	F$^-$ Φ80*lac*ZΔM15 Δ(*lac*ZYA-*arg*F) U169 *rec*A1 *end*A1 *hsd*R17(r_k^-, m_k^+) *pho*A *sup*E44 *thi*-1 *gyr*A96 *rel*A1 λ^-	Thermo Fisher
One Shot™ TOP10	F-*mcrA* Δ(*mrr-hsd*RMS-*mcr*BC) Φ80*Lac*ZΔM15 Δ *Lac*X74 *rec*A1 *ara*D139 Δ(*araleu*) 7697 *gal*U *gal*K *rps*L (StrR) *end*A1 *nup*G	Thermo Fisher
SureII	*McrA-, McrCB-, McrF-, Mrr-, HsdR- endA-, recB-, recJ-*	Agilent

3.2. Media and supplements

Table 4: Overview of media and supplements including their ingredients and their respective supplier.

Medium	Ingredients	Volumes / Weight	Supplier
Cell culture medium Dulbecco´s Modified Eagle´s Medium (DMEM) with 3 % FCS	DMEM	470 mL	PAN™ Biotech
	Fetal calf serum (FCS) – heat inactivated	15 mL	Gibco
	Penicillin/Streptomycin/Glutamine (10.000 U/mL; 10 mg/mL; 200 mM)	5 mL	PAN™ Biotech
	Non-essential amino acids (100 x)	5 mL	PAN™ Biotech
	Sodium pyruvate (100 mM)	5 mL	PAN™ Biotech
Cell culture medium Dulbecco´s Modified Eagle´s Medium (DMEM) with 5 % FCS	DMEM	460 mL	PAN™ Biotech
	Fetal calf serum (FCS) – heat inactivated	25 mL	Gibco
	Penicillin/Streptomycin/Glutamine (10.000 U/mL; 10 mg/mL; 200 mM)	5 mL	PAN™ Biotech
	Non-essential amino acids (100 x)	5 mL	PAN™ Biotech
	Sodium pyruvate (100 mM)	5 mL	PAN™ Biotech
Cell culture medium Glasgow's Minimum	GMEM	460 mL	PAN™ Biotech
	Fetal calf serum (FCS) – heat inactivated	25 mL	PAN™ Biotech
	Non-essential amino acids (100 x)	5 mL	PAN™ Biotech

Essential Medium (GMEM) with 5 % FCS	Tryptose-phosphate buffer solution	20 mL	Gibco
	Geneticine G418 (50 mg/mL), freshly added to the cell while splitting	260 µL/T75 -> 13 mL	Gibco
Primary cell culture medium RPMI-1640 with 10 % FCS	RPMI-1640	435 mL	PAN™ Biotech
	Fetal calf serum (FCS) – heat inactivated	50 mL	Gibco
	Penicillin/Streptomycin/Glutamine (10.000 U/mL; 10 mg/mL; 200 mM)	5 mL	PAN™ Biotech
	Non-essential amino acids (100 x)	5 mL	PAN™ Biotech
	Sodium pyruvate (100 mM)	5 mL	PAN™ Biotech
Overlay medium: DMEM with 3 % FCS and 1 % Methylcellulose	DMEM	174 mL	PAN™ Biotech
	Fetal calf serum (FCS) – heat inactivated	20 mL	Gibco
	Penicillin/Streptomycin/Glutamine (10.000 U/mL; 10 mg/mL; 200 mM)	2 mL	PAN™ Biotech
	Non-essential amino acids (100 x)	2 mL	PAN™ Biotech
	Sodium pyruvate (100 mM)	2 mL	PAN™ Biotech
	3 % Methylcellulose solution	100 mL	Sigma Aldrich
OptiMEM™	Ready-to use for transfections		Thermo Fisher
LB Medium	Peptone	10 g	Carl Roth
	Yeast extract	5 g	Carl Roth
	Sodium chloride	10 g	Carl Roth
	Deionized water	1 L	
SOC Medium	Outgrowth medium (ready-to-use)		New England Biolabs

3.3. Growth factors

Table 5: Overview of growth factors, their final concentration used as well as supplier.

Growth factor	**Final concentration**	**Supplier**
Recombinant Mouse M-CSF (carrier-free)	50 ng/mL	BioLegend®

3.4. Buffers and other reagents

Table 6: Overview of buffers and other reagent with the respective ingredients, quantity and supplier.

Name	Ingredients	Quantity	Supplier
Blocking Buffer with 5 % FCS	FCS	5 mL	Gibco
	1x PBS	95 mL	
Ethanol (EtOH) ROTIPURAN® ≥99.8 %, p.a.	-	-	Carl Roth
Formaldehyde solution, 4.5 %	-	-	SAV Liquid Production GMBH
Methylcellulose solution	Methylcellulose	16.8 g	Sigma-Aldrich
	Distilled water	600 mL	
Tetramethylbenzidine (TMB) solution	Tetramethylbenzidine (TMB) – immunoblot substrate	40 mL	MIKROGEN Diagnostik
	1x PBS	80 mL	
Trypsin/EDTA	-	-	PAN™ BIOTECH
Permeabilization Buffer with 0.5 % Triton X-100	Triton X-100	2.5 mL	Carl Roth
	1x PBS	497.5 mL	
Phosphate-Buffered Saline (PBS)	NaCl	80.06 g	Carl Roth
	Na_2HPO_4	14.20 g	Carl Roth
	KCl	2.24 g	Carl Roth
	KH_2PO_4	2.31 g	Carl Roth
	Distilled water	1 L	
Coal and formvar-coated copper grids (300mesh)	-	-	Science Services
2 % Uranyl acetate solution	-	-	Science Services

Fluoroshield	-	-	Merck
Tween-80	-	-	Carl Roth
BD Pharm Lysis buffer	BD Pharm Lysis buffer	10 mL	BD Biosciences
	Distilled water	90 mL	
Passive lysis buffer	Passive lysis buffer	1 mL	Promega
	Distilled water	4 mL	
Dual-Luciferase® Reporter Assay System			Promega

3.5. Molecular biology kits and reagents

Table 7: Overview of molecular biology kits and reagents with their respective suppliers.

Name	**Supplier**
1% ethidium bromide solution	Carl Roth
Antarctic Phosphatase	New England Biolabs
AvaI	New England Biolabs
AvrII	New England Biolabs
BsaI	New England Biolabs
Gel Loading Dye, Purple (6X)	New England Biolabs
High-Capacity RNA-to-cDNA™ Kit	Applied Biosystems
HindIII	New England Biolabs
Lipofectamine 2000™	Themo Fisher
NdeI	New England Biolabs
NEBuilder® HiFi DNA Assembly Mastermix	New England Biolabs
NextSeq 1000/2000 P2 reagents	QIAGEN
Nucleo® Gel and PCR Clean up	Macherey and Nagel
NucleoBond® Xtra Midi Plus	Macherey and Nagel
NucleoBond® Xtra Midi Plus EF	Macherey and Nagel
NucleoSpin® Plasmid	Macherey and Nagel
Panadea LASV IgG ELISA Kit	Panadea Diagnostics
PCR Mycoplasma Test Kit I/C	Promo Cell
Phusion DNA Polymerase	New England Biolabs

PstI	New England Biolabs
PvuII	New England Biolabs
Q5 HiFi DNA polymerase	New England Biolabs
QIAamp viral RNA Mini kit	QIAGEN
QIAseq FX DNA Library UDI-A Kit	QIAGEN
Quick-Load 1 kb DNA Ladder	New England Biolabs
Quick-Load 100 bp DNA Ladder	New England Biolabs
RealStar® Lassa Virus RT-PCR Kit 2.0	Altona Diagnostics
RealStar® LASV RT-PCR kit 2.0	Altona Diagnostics
SacI	New England Biolabs
SapI	New England Biolabs
SpeI	New England Biolabs
SuperScript™ One-Step RT-PCR System with Platinum™ Taq DNA Polymerase	Thermo Fisher
SYBR green Master 1 mix	Roche
SYBR green solution	Thermo Fisher
T4 DNA Ligase	New England Biolabs
Turbo DNase™	Themo Fisher

3.6. Primers and plasmids

Table 8: Overview of primer sequences for the determination of LASV receptor expression.

Primer	**Sequence (5´→ 3´)**
αDG_fwd	GGCACATTGCCAATAAGAAG
αDG_rev	TGCAATGGCTGGAGATG
LARGE_1_fwd	TGGACAAGCTTCGGAAGA
LARGE_1_rev	GAAGCAGGGAAGCTGATACA
LARGE_2_fwd	TCCTGCCTCTCAGCCTG
LARGE_2_rev	TTGCCCAGGTACCAGTC
Tyro3_fwd	CGTGGGCAGACGCCATAT
Tyro3_fwd	CCCGCCGATGAGGTAGTTGT
βactin_fwd	TCCGTAAAGACCTCTATGCCAA

βactin_rev	CAGAGTACTTGCGCTCAG
60S_fwd	GATGAATACCAACCCCTCTCG
60S_rev	CTCAAGGTGTTGGATGGGAT

Table 9: Overview of primer sequences used for cloning the pDP_AG_Ba366_S_Kak428_NP plasmid.

Primer	**Sequence (5´→ 3´)**
Kak428_HindIII_Infusion_fwd	CACCAACATAAAGCTTCAAG
Kak428_HindIII_Infusion_rev	GTGAGTCCAAAAGCTTTCTA
Kak428_HindIII_NEB_fwd	TATTGCACCAACATAAAGCTTCAAG
Kak428_HindIII_NEB_rev	GTGAGTCCAAAAGCTTTCTAATGTC
Kak428_MscI_Infusion_rev	TATGGCCACCCATTCCCTGA
Kak428_SacI_Infusion_fwd	ACTGAAAGGCCTCTGAGCTC
Kak428_MscI_NEB_rev	TATGGCCACCCATTCCCTGAAAGAC
Kak428_SacI_NEB_fwd	TTAGAACTGAAAGGCCTCTGAGCTC
Kak428_NdeI_Infusion_rev	ATCCCGGTGTGCATATGGCA
Kak428_SacI_Infusion_fwd	ACTGAAAGGCCTCTGAGCTC
Kak428_NdeI_NEB_rev	CAACTATCCCGGTGTGCATATGGCA
Kak428_SacI_NEB_fwd	TTAGAACTGAAAGGCCTCTGAGCTC

Table 10: Overview of sequencing primers to confirm plasmid sequences derived from the Kak428 strain during the generation of the pDP_AG plasmids for the rescue of chimeric viruses.

Primer	**Sequence (5´→ 3´)**
KAK-GP_5-24	GTCAAATAGTGACCTTCTTC
KAK-GP_501-520	CAGTCACTCCTACGCTGGTG
KAK-GP_581-600	CAGATAACTACCTCCCCAAG
KAK-GP_891-910	CGCTAAGTGTAATGAGAAAC
KAK-GP_972-990	CTGGGCCTCTGCTTTGAGC
KAK-GP_1454-1473	TCATCTCTTCCATCGTACTG
KAK_L_3562-3579	CATGTTTCATACAGTATG
KAK_L_4241-4260	GCAAGGAACCCCATCAACTG
KAK_L_4951-4969	GCAGAGCTTAAAGGTGTTG

KAK_L_5431-5450	CACTATATAGTGTTGTCATC
KAK_L_5992-6012	GTCCTTGAAACAAAGGTCATG
KAK_L_6313-6332	GTGCAGGATCAAGACCTAGAG
KAK_L_6571-689	CACTTGACTGTATCATCAC
Kak428_L_37-56	AAGGTTGGTATTTGGGTGTC
Kak428_L_628-647	CTACAACCTCAAGCAGACTG
Kak428_L_748-727	GCTGTTAGTTTGTTGTCCACTC
Kak428_L_1379-1360	CACACCAACATCTTTCAGGG
Kak428_L_1280-1299	TCCGACTCTCTCACCTTCAC
Kak428_L_1866-1884	TGGTTGGAAAACTGTGCTG
Kak428_L_1972-1953	TTTTGACTACGCTTACTGGG
Kak428_L-2561-2579	GTTTACAGATGGCACCAGG
Kak428_L_2628-2610	ACTGGGTTACAGCCAATGC
Kak428_L_3284-3301	AGAAAGCAACTCCGAAGC
Kak428_L_3319-3300	GACAGTGCTTTACTCAATGC
Kak428_L_3902-3930	AGTTGGTGTAGTGCCATCC
Kak428_L_4122-4103	ATTCTTCTGGGTCTCTTTGC
Kak428_L_4612-4632	CAAACTATCTGTCAGGTGAGC
Kak428_L_4704-4685	GGTATTGAAGGTCTGTTGGC
Kak428_L_5266-5284	TGCTTGAGGATAGAGTGGG
Kak428_L_5449-5430	GACAATGCTTCACAGTTGAC
Kak428_L_5961-5980	GTAAAGAGTCAGGACACTGC
Kak428_L_6093-6075	CACATTGGTTGACTGACCC
Kak428_L_6500-6519	AGTATTGGTCCTCAGCAAAC
Kak428_L_6656-6638	TAGTTTGCCCCCACTTGAC
Kak428_L_6714-6696	TATCCTCCACACAAACCGC
Kak428_L_6903-6883	CGCTTCCCACCAAAATAAAGG
KAK-NP_1-18	ATGAGCAACTCAAAGGAG
KAK-NP_493-511	GATGTCAAAAATGCAGACC
KAK-NP_561-580	CAACTTGGCCCTGCTTTGTC
KAK-NP_921-940	GTATAAGGTATGTCTTTCAG

KAK-NP_974-99	CATGCTCTCCCAACAATTG
KAK-NP_1414-1433	GACTCACAGGACAGGAAAGA
KAK-NP_1691-1710	TTACAGGACGACTTTGGTTG

Table 11: Overview of sequencing primers to confirm plasmid sequences derived from the Ba366 strain during the generation of the pDP_AG plasmids for the rescue of chimeric viruses.

Primer	**Sequence (5´→ 3´)**
LV_Ba_L_1190+	GATGCATTGATTCTCCTTGCCAGT
LV_Ba_S_219-	GTTGTTGTACAGGATCTGCCACA
Ba_L_2023+	GCTCACCCTAGTAAACGCTC
LV_Ba_S_813-	AATGTCCAGGTGAATGTGCCTAACA
LV_Ba_S_1105-	GTATGGTATTCCCATGATGTCACGC
LV_Ba_S_1105+	GCGTGACATCATGGGAATACCATAC
LV_Ba_L_400+	CTGATGGTTACAAACTGACAGGCAA
LV_Ba_L_3442+	TAGTCAAGAGTCACCACAGTCTTACAGTTC
LV_Ba_L_4410+	ATCATTGATCAATCGGTTGCGAATG
366_L_601-	CTACTCCTGACAACCTCCCTGATG
366_L_263+	CTGATGGTTACAAACTGACAGGCAA
366_L_601+	CATCAGGGAGGTTGTCAGGAGTAG
366_L_1048+	GATGCATTGATTCTCCTTGCCAGT
366_L_1536+	CACTGTGAAGTTGAGGCAGA
366_L_2328+	GCCTGGTGTTTCAAAGAGG
366_L_4317-	CAGGTTGCATAAATGGACAG
366_L_3876+	CAGCTCCATACTTGACATG
366_L_5877-	CTGACTCAGTTTTGCAGACC
366_L_5794+	TTGGTTGGCCCCAGGTTTGATTCATTAGA

Table 12: Overview of cloning primers for the mutagenesis of the Kak428 NP used in the replicon assay.

Primer	**Sequence (5´→ 3´)**
M13 fwd	GTAAAACGACGGCCAGT
M13 rev	CAGGAAACAGCTATGAC

Ser473Leu_fwd	GCAATTCAGACAGGATGCAA
Ser473Leu_rev	TTGCATCCTGTCTGAATTGC
Leu569Met_fwd	CTTTTGGACTTACAGGACAG
Leu569Met_rev	CTGTCCTGTAAGTCCAAAAG
Lys424Arg_fwd	CAAAGTCGTCATGTAAAGTG
Lys424Arg_rev	CACTTTACATGACGACTTTG

Table 13: Overview of original plasmids used as templates for cloning of the recombinant, chimeric virus segments.

Plasmid	**Origin**
pX12_Ba366_L_Kak428_Z	Cloned by Selina Krüger
pX12_Ba366_S_Kak428_GP	Cloned by Selina Krüger
pDP_AG_Ba366_S_Segment	Cloned by Dr. Lisa Oestereich
pDP_AG_Ba366_L_Segment	Cloned by Dr. Lisa Oestereich
PUC_57_Kak428_L	Synthesized by GenScript

3.7. Antibodies

Table 14: Overview of antibodies used during this project and their respective supplier.

Name	**Supplier**
4',6-Diamidino-2-phenylindole (DAPI)	Thermo Fisher
DyLight™ 488 Donkey anti-rabbit IgG	BioLegend®
Evans Blue	Sigma Aldrich
Fluoroshield medium	Sigma Aldrich
LASV NP-specific monoclonal antibody 2B5	BNITM, Virology
Monoclonal human α-GP-2 "37.7H"	absolute antibody
Peroxidase-conjugated AffiniPure Sheep Anti-Mouse IgG (H+L)	Jackson Immuno Research
Phalloidin	Thermo Fisher
Polyclonal chicken α-rabbit-AlexaFluor 488	Molecular Probes
Polyclonal rabbit α-GP-2 "gp4"	Prof. Dr. Wolfgang Garten, Institute for Virology, Marburg

Polyclonal rabbit α-VSV	Prof. Dr. Wolfgang Garten, Institute for Virology, Marburg
Polyclonal rabbit α-human-FITC secondary antibody	Dako
Polyclonal Rabbit-LASV Nucleoprotein antibody (GTX134884)	GeneTex, Inc.
Polyclonal α-rabbit-HRP secondary antibody	Agilent

3.8. Technical devices

Table 15: Overview of technical devices.

Name	**Supplier**
Animal Clipper GT415	Aesculap Suhl GmbH
Centrifuge 5415 R	Eppendorf
Confocal Laser Scanning Microscope TCS SP5 II	Leica
FastPrep-24™ 5G tissue lysis system with Lysing matrix D	MP Biomedicals
Gel imaging system	INTAS science Imaging
iSPOT ELISpot Reader	AID
LUNA II Automated Cell Counter	Logos Biosystems
Nanodrop2000 spectrophotometer	Thermo Fisher
NextSeq2000	Illumina
PowerPac™ Basic Power Supply	Bio-Rad
Rotor-Gene Q 5 plex Platform	QIAGEN
School balance EMB 1200-1	KERN & SOHN GmbH
Spectrophotometer Junior LB 9509	Berthold Technologies
Thermal Cycler T100	Bio-Rad
Thermo Mixer C	Eppendorf
ThermoLux® heating mat	Witte + Sutor GmbH
Transmission electron microscope	Fei Electron Optics
Univentor 410 Anesthesia Unit	Univentor Limited

3.9. Reagents and consumables for animal experiments

Table 16: Overview of reagents and consumables for animal experiments.

Name	Supplier
Anesthesia induction chamber	UNO
Cut resistant gloves, ActivArmr®	Carl Roth
EDTA tubes Microvette® 500 K3E S-Monovette® 2.7 mL K3E	Sarstedt
100 % Isoflurane-Piramal	Piramal Critical Care B.V.
Lysing Matrix D	MPBio
Nylon-tipped swab IMPROSWAB® Microbiological Transport Swab	IMPROVE Medical
ROTI®Cell PBS CELLPURE® ready to use	Carl Roth
Safety-Lancet Normal 21G / Penetration Depth 1.8 mm	Sarstedt
Syringes and Needles of varying sizes	BRAUN BD Biosciences TERUMO

3.10. General consumables

General consumables were purchased from Sarstedt, Eppendorf, Greiner, BioOne, Merck, Marienfeld and Qiagen.

3.11. Computer tools and programs

Table 17: Overview of computer tools and programs used during this study.

Name	Supplier
AlphaFold2 (www.alphafold.ebi.ac.uk)	Deepmind
BioRender (www.biorender.com)	Science Suite Inc.
DeepL (www.deepl.com)	DeepL SE
ELISpot Reader (Version 7.0)	AID GmbH

EndNote (Version X9.3.3)	Clarivate Analytics
Galaxy EU server (www.usegalaxy.eu)	Galaxy Project
GraphPad Prism (Version 10.0.2)	GraphPad Software
ImageJ 2 (Version 2.9.0)	National Institute of Health
Integrative Genomics Viewer (Version 13.1.2)	Broad Institute, UC San Diego
MacVector (Version 18.2.0)	MacVector Inc.
National Library of Medicine Server (www.ncbi.nlm.nih.gov)	National Institutes of Health
Pymol (Version 2.5.5)	DeLano Scientific LLC, Schrödinger Inc.
RCSB Protein Database (www.rcsb.org)	State University of New Jersey and University of California

4. Methods

4.1. Molecular biological methods

4.1.1. Nucleic acid isolation

Virus RNA from cell culture supernatants was extracted by using the QIAamp viral RNA kit (QIAGEN, Venlo, Netherlands) according to the manufacturer´s instructions and performing a second elution step. The first elution was split into two different tubes to reduce the number of freeze-thaw cycles during subsequent experiments. All RNA samples were stored at -80 °C.

4.1.2. Library preparation for Illumina sequencing

Library preparation was done according to the protocol described by [195], by using the QIAseq FX DNA Library UDI-A kit (QIAGEN, Venlo, Netherlands). The libraries were sequenced on a NextSeq2000 with the NextSeq 1000/2000 P2 reagents (Illumina, San Diego, USA).

4.1.3. NGS data analysis

The *fasta* datasets generated by Illumina sequencing were uploaded to the Galaxy EU server (www.usegalaxy.eu) as well as the following reference genomes from National Center for Biotechnology Information (NCBI): i) LASV Ba366 strain GU830839.1 and GU979513.1, ii) LASV Kak428 KT992435.1 and KT992425.1 as well as iii) chimeric reference genomes for the chimeric viruses. Those chimeric genomes were generated manually by exchanging the genes of Ba366 with the Kak428 genes. The workflow for NGS data analysis on the Galaxy EU server is displayed in Figure 6.

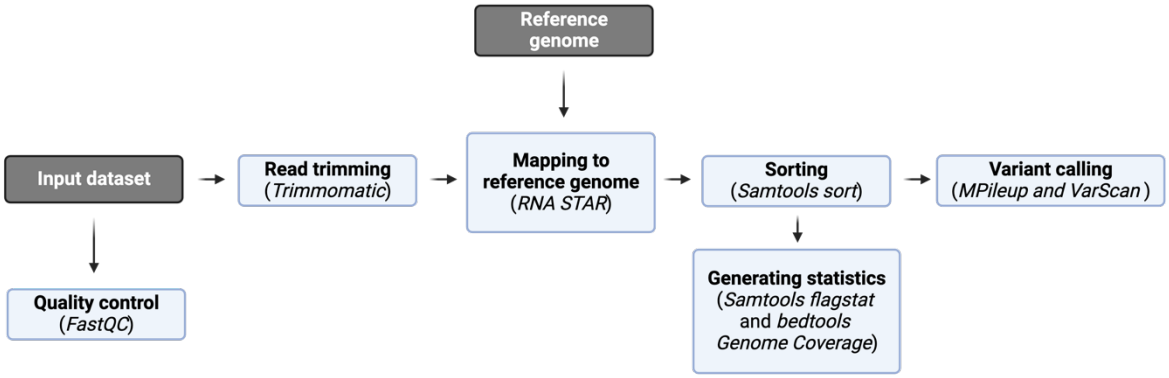

Figure 6: Workflow for NGS data analysis on the Galaxy EU Server. The input dataset as well as the corresponding reference genome were uploaded to the server. The input dataset underwent quality control (*Fast QC*) and trimming (*Trimmomatic*) before it was mapped to the reference genome with *RNA STAR*. Then, the reads were sorted (*Samtools sort*) and general statistics were generated (*Samtools flagstat* and *bedtools Genome Coverage*). In the final step, variants were called with *MPileup* and *VarScan*. This figure was created with BioRender.com.

The initial quality control was done with *FastQC* followed by trimming of the adapter sequences by using the *Trimmomatic* function. Thereafter, the reads were mapped against the corresponding reference genome by using the splice-aware *RNA Star* algorithm. The mapped reads were sorted by using *Samtools sort* and variant calling was done with *MPileup* and *VarScan*. In parallel, the *Samtools* tool *flagstat* and *bedtools Genome Coverage* were used to get more detailed statistics about the data generated. In the last step, the bam files containing the alignments were loaded into the *Integrative Genomics Viewer* (IGV) for visualization and all sequencing runs with an average coverage >1000 reads were used for screening for potential host-adaptive mutations. Variants displaying >10 % of a single nucleotide polymorphism (SNP) were considered relevant for the corresponding growth characterization.

4.1.4. RT-PCR to detect the LASV L gene

To detect the LASV L gene in cell culture supernatants and quantify the RNA copy numbers, an RT-PCR with the RealStar® Lassa Virus RT-PCR Kit 2.0 (Altona Diagnostics, Hamburg, Germany) was performed according to the manufacturer´s instructions. The internal control for the subsequent qPCR was added before inactivation. As an extraction control, nuclease-free H_2O was included in the inactivation process in the BSL4.

4.1.5. Cloning of plasmids for the rescue of chimeric viruses

Cloning was done to generate the plasmids needed to rescue the four chimeric viruses as shown in Table 18 either by restriction cloning or by using the NEBuilder HiFi DNA Mix (New England Biolabs, Ipswich, USA).

Table 18: Overview of plasmids generated by cloning to rescue the chimeric viruses.

Chimeric virus	Plasmid generated
GPC chimera	pDP_AG_Ba366_S_Kak428_GPC
NP chimera	pDP_AG_Ba366_S_Kak428_NP
L chimera	pDP_AG_Ba366_L_Kak428_L
Z chimera	pDP_AG_Ba366_L_Kak428_Z

Figure 7 shows the cloning strategy for the different plasmids. For all plasmids, the pre-existing pDP_AG-plasmids served as a backbone in which the Kak428 genes were inserted. Those were cut with the indicated restriction enzyme for 2-8 h at 37 °C and extracted from an agarose gel with the PCR and Gel Clean up kit (Macherey and Nagel, Düren, Germany) by following the manufacturer's instructions. The 0.8 % agarose gel was previously run for 60 min at 100 V and stained with SYBR green solution for a minimum of 45 min. The Kak428-derived inserts were either extracted from a pre-existing plasmid (pX12-based) or a commercially synthesized plasmid with the restriction enzymes indicated in Figure 7. The exemption was the Kak428 NP gene, which was directly amplified from the viral RNA by RT-PCR with the primers listed in Table 9. For all plasmids except for the pDP_AG_Ba366_S_Kak428_NP construct, the plasmid backbones were dephosphorylated with the antarctic phosphatase (New England Biolabs, Ipswich, USA) for 1 h at 37 °C. Afterwards, the ligation was done with the T4 DNA polymerase (New England Biolabs, Ipswich, USA) overnight at 16 °C by using a total amount of 50 ng plasmid DNA and varying amounts of DNA insert (ranging from 1:2 to 1:7). To generate the pDP_AG_Ba366_S_Kak428_NP construct, the restricted plasmid backbone and the PCR-derived insert were used for NEBuilder assembly with a total of 50 ng of plasmid DNA and varying ratios of plasmid and insert DNA (1:2 or 1:3). The reactions were incubated for 1 h at 50 °C. Then, the ligation reactions were transformed into chemically competent bacteria (SureII (Agilent, Santa Clara, USA) or DH5α OneShot™ (Thermo Fisher, Waltham, USA)) according to the respective manufacturer´s instructions and incubated overnight at 37 °C on LB agar plates with 1 mg/mL carbenicillin.

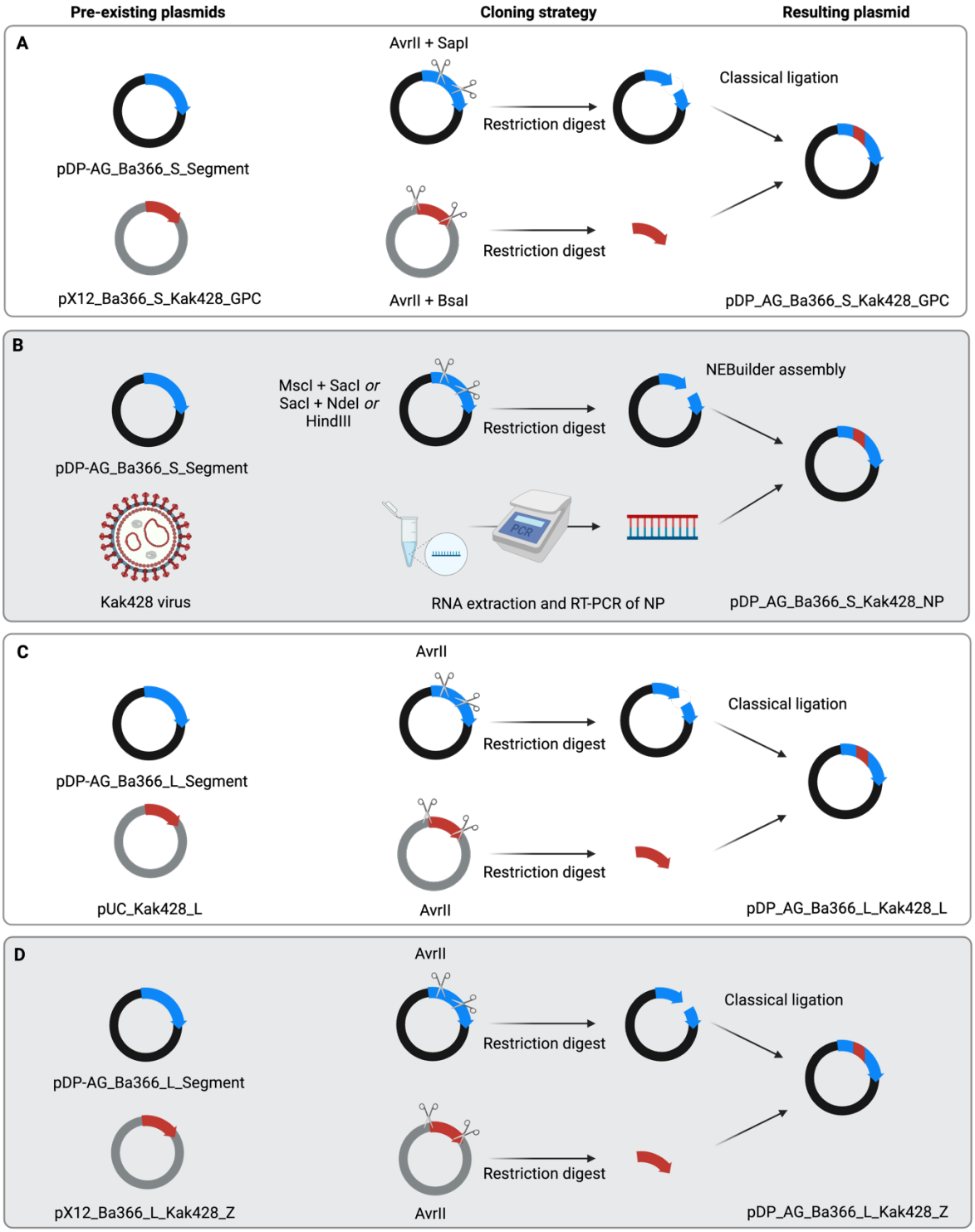

Figure 7: Cloning strategy to generate the pDP plasmids required for generating recombinant viruses with exchanged viral proteins. The figure shows how the plasmids were generated to rescue the chimeric viruses **A** GPC chimera, **B** NP chimera, **C** L chimera, and **D** chimera.

On the next day, single colonies were picked and used for inoculating 5 mL LB cultures with 1 mg/mL of carbenicillin. These cultures were incubated overnight at 30 °C while shaking at 250 rpm and used afterwards for Miniprep with the NucleoSpin Plasmid kit (Macherey and

Nagel, Düren, Germany). The plasmids were restricted with the same restriction enzymes that were used for restricting the corresponding plasmid backbone before and incubated for 1 h at 37 °C. Their restriction pattern was checked on an agarose gel as described above. If the band pattern was correct, the plasmid was re-transformed into SureII competent bacteria and used for inoculating 200 mL LB cultures with 1 mg/mL of carbenicillin. The cultures were incubated overnight at 30 °C while shaking at 250 rpm and used for plasmid isolation with the NucleoBond Midi kit (Macherey and Nagel, Düren, Germany) according to the manufacturer's instructions for NucleoBond Finalizers the with an elution volume of 200-300 µL. In case the following test digest looked as expected, 1400 ng of the plasmids were sent to sequencing at LGC Genomics with gene-specific primers. The sequencing results were analyzed with MacVector.

4.1.6. Mutagenesis of the Kak428 NP gene for replicon assays

During this project, mutations in the NP were identified. Those required further characterization in the minreplicon system. Therefore, the Kak428 NP needed to be modified by site-directed mutagenesis. For this, modified primers, which carry the mutations identified during the adaptation experiments were designed (see Table 12) and synthesized by Integrated DNA Technologies (IDT). Plasmid-specific forward or reverse primers were used together with one of the modified primers to get two overlapping fragments (forward piece and reverse piece) by PCR with the Q5 polymerase (New England Biolabs, Ipswich USA). Afterwards, these fragments were separated on a 2 % agarose gel for 60 min at 100 V and the bands were visualized by applying a SYBR green solution (Thermo Fisher, Waltham, USA) in TAE buffer for 1 h at room temperature. The desired bands were excised and purified with the PCR and Gel Clean-up kit (Machery and Nagel, Düren, Germany). Those purified bands were used as templates (10 ng template DNA) to perform a fusion PCR with the Q5 polymerase, which results in a PCR fragment carrying the desired point mutation. The DNA concentration was determined with a Nanodrop2000 spectrophotometer, and the PCR product was sent to sequencing with the flanking forward and reverse primers at LGC Genomics.

4.2. Cultivation of mammalian cells

All *Mastomys*-derived cell lines used for this project were kindly provided by the group of Dr. Wolfram Brune (Leibniz institute of Virology (LIV), Hamburg). To ensure reproducibility of all data obtained, cells with a rather low passage (<60) were used for experiments.

4.2.1. Mycoplasma testing

All cell lines were regularly tested for contamination by mycoplasma by using the PCR Mycoplasma Test Kit I/C (Promo Cell, Heidelberg, Germany) according to the manufacturer`s instructions.

4.2.2. Cell lines

All cell lines were cultured at 37 °C and 5 % CO_2 in their respective growth media as shown in Table 19. They were regularly split before they reached confluency.

Table 19: Overview of growth media and supplements used per cell line.

Cell line	Growth media	Supplements
BHK-J	DMEM with 5 % FCS	1 % Penicillin/Streptomycin/Glutamine and 2 % non-essential amino acids/ sodium pyruvate
BSR-T7/5	GMEM with 5 % FCS	2 % non-essential amino acids/sodium pyruvate 1.3 mg/mL Geneticine G418 4 % Tryptose-phosphate
Mastomys embryonal fibroblasts (MasEF)	DMEM with 5 % FCS	1 % Penicillin/Streptomycin/Glutamine and 2 % non-essential amino acids/ sodium pyruvate
Mastomys kidney epithelial cells (MasKEC)	DMEM with 5 % FCS	1 % Penicillin/Streptomycin/Glutamine and 2 % non-essential amino acids/ sodium pyruvate
Vero76	DMEM with 3 % FCS	1 % Penicillin/Streptomycin/Glutamine and 2 % non-essential amino acids/ sodium pyruvate

4.2.3. Primary cells

4.2.3.1. Isolation of primary cells from Mastomys natalensis

Four adult *M. natalensis* were euthanized by isoflurane overdose and decapitation by trained personnel. After dislocating the hindlimbs, muscles and skin were removed from femur and tibia, which were afterwards stored in ice cold phosphate buffered saline (PBS). To sterilize the surfaces, bones were rinsed with 70 % ethanol. Thereafter, the bones were cut open at the ends and transferred into a 0.25 mL Eppendorf tube with two holes in the bottom, which was placed into a 1.5 mL Eppendorf tube. Bone marrow was harvested by centrifugation at $800 \times g$ for 30 s. This procedure was repeated until most of the bone marrow was removed and finalized by flushing the bone with a 22 G cannula attached to a 20 mL syringe filled with PBS under sterile conditions. Single cells were prepared by resuspending the cells with a 10 mL serological pipette and passing the suspension through a 70 µm cell strainer. Thereafter, cells were pelleted by centrifugation at $500 \times g$ for 7 min and resuspended in 20 mL of the BD Pharm Lyse™ red blood cell lysis buffer (diluted 1:10 in ddH_2O, BD Biosciences, Franklin, USA). The lysis was performed for 10 min at room temperature, followed by adding 50 mL of PBS to stop the reaction and another filtration with a 70 µm cell strainer to remove all clotted cells and bone fragments. Cells were pelleted again by centrifugation at $500 \times g$ for 7 min and resuspended in fresh cell culture medium for cell number determination with a Neubauer counting chamber. Cells used for subsequent experiments were directly seeded in six-well plates at 1×10^6 cells/well in RPMI-1640 supplied with 10 % FCS, 1 % Penicillin/Streptomycin/Glutamine, 2 % non-essential amino acids and pyruvate and cultured at 37 °C and 5 % CO_2. Excess of isolated cells were aliquoted in 10×10^6 cells/vial and frozen in FCS with 10 % dimethyl sulfoxide (DMSO) in a slow freezing device at -80 °C. For long-term storage, cells were transferred to a liquid nitrogen tank on the next day.

4.2.3.2. Differentiation of the primary bone marrow-derived cells into macrophages

The differentiation of the bone marrow-derived cells into macrophages was initiated directly after seeding. For this, growth media were supplied with 50 ng/µL of murine macrophage colony- stimulating factor (M-CSF; BioLegend®, San Diego, USA) at the time of cell seeding and when exchanging media on day three post seeding. The cells were completely differentiated six days after seeding and were used for experiments in the following two weeks.

4.3. Virological methods

4.3.1. Safety and security

All work with full LASV virus strains was performed under BSL-4 conditions at the BNITM. All other work, including handling of the recombinant pseudotyped Vesicular Stomatitis virus, was performed under BSL-2 conditions at the BNITM and the Philipps University of Marburg.

4.3.2. Virus amplification, harvest and concentration

To amplify virus stocks, 1×10^6 cells of Vero76 cells were seeded in a T75 flask one day prior to infection. Cells were infected with a multiplicity of infection (MOI) of 0.01 in an inoculum diluted in DMEM without additives. After incubation for 1 h at 37 °C and 5 % CO_2, the inoculum was replaced by 20 mL of fresh growth medium containing 3 % FCS. The cells were further incubated at 37 °C and 5 % CO_2 for 3-4 days. The cell culture supernatants were harvested and centrifuged for 5 min at 4000 × g to pellet the cell debris. Thereafter, the supernatant was routinely filtered by a 0.1 µm filter and an aliquot to determine the viral titer by immunofocus assay at a later time was kept seperately.

If the expected viral titer was $<1 \times 10^4$ FFU/mL, up to 100 mL of the virus containing supernatant were concentrated by 100 kDa Amicon tubes (Merck, Darmstadt, Germany) by adding up to 15 mL of the supernatant to the filter and centrifugation at 4000 × g until the supernatant was reduced to 3-5 mL. Both, the unfiltered, virus-containing supernatants as well as the flow through were stored at -80 °C until used for immunofocus assay to determine the viral titers.

4.3.3. Immunofocus assay

As standard method for virus titer determination in focus forming units per mL (FFU/mL), an immunofocus assay was established in a 96-well format. One day before the titer determination, 1.5×10^3 Vero76 cells/well of were seeded in 96-well Nunclon-Delta coated plates with a white bottom (Thermo Fisher, Waltham, USA). The virus-containing supernatants were diluted in a half-logarithmic dilution series (undiluted, 10^{-1}, 10^{-2}, 10^{-3}, 10^{-4}, 10^{-5}). The medium was discarded and replaced with 100 µL/well of the diluted virus as an inoculum. After incubation for 1 h at 37 °C and 5 % CO_2, the inoculum was replaced by 100 µL/well overlay medium, which prevents the spread of viral particles through the medium so that only neighboring cells can get infected. The plates were further incubated for 23-25 h at the same

conditions. After discarding the overlay medium, the titration plates were inactivated by incubation in 4 % formaldehyde in PBS for 30 min at room temperature. Thereafter, the plates were washed 3 x with tap water, and cells were permeabilized by 0.5 % triton-X solution in PBS with 50 µL/well. The plates were incubated for 30 min at room temperature. This and all subsequent steps were performed on a rocking table to allow even distribution of the fluid in the wells. The plates were washed again 3 x with tap water and 50 µL/well of the blocking solution was applied for 1 h at room temperature or 4 °C overnight. After discarding the blocking solution, the specific antibody staining was commenced by adding 50 µL/well of the primary "2B5" LASV-specific antibody in a 1:5000 dilution in 2.5 % FCS in PBS and incubating for 1 h at room temperature or at 4 °C overnight. The plates were washed again 3 x to ensure complete removal of the primary antibody. Then, 50 µL/well of the secondary, peroxidase-coupled Affini Pure sheep anti-mouse antibody (Jackson Immuno Research, Baltimore, USA) was added in a 1:1000 dilution in 2.5 % FCS in PBS and incubated again for 1 h at room temperature. Before adding 50 µL/well of the substrate solution (1:3 diluted tetramethylbenzidine (MIKROGEN Diagostik, Neuried, Germany) in PBS) for 45 min, the plates were washed again. After the final incubation time, the plates were washed 1 x with tap water and dried either under a running flow hood for 1-2 h or overnight in a dark drawer. Counting of the foci was done by using the iSPOT ELISpot Reader (AID, Straßberg, Germany) and the respective ELISpot reader software (AID, Straßberg, Germany) with settings displayed in Table 20.

Table 20: Count settings for viral foci on the ELISpot reader.

	Ba366	**D96**	**Kak428**
Intensity	50	30	30
Size	60	60	60
Gradient	Not specified	Not specified	Not specified
Algorithm	C	C	C
Size	Big	Small	Tiny

Settings were slightly adjusted if the background differed extensively to the usual measurements. Viral titers were then calculated by using the following equation:

$$\text{Focus forming units/milliliter} = \text{counted foci} \times \text{dilution factor (per well)} \times \text{dilution factor (to 1 mL)}$$

The same assay was applied in 24-well plates when the virus titer was determined in organ samples from animal experiments. Here, the incubation time was prolonged to 5 days at 37 °C and foci were counted manually.

4.3.4. Immune fluorescence staining

After inactivation of the slides, these were either directly stained or kept at -20 °C for up to two weeks. For the specific staining, 10 µL of the primary GTX134884 polyclonal rabbit IgG (GeneTex, Inc., Alkon Pwky, USA) was applied in a 1:1000 dilution in PBS with 5 % FCS for 1 h at room temperature. After washing 1 x for 15 min in PBS on a rocking table, 10 µL of the secondary DyLight488 donkey anti-rabbit IgG (BioLegend®, San Diego, USA) was applied in a 1:300 dilution together with Evans Blue (Sigma Aldrich, St. Louis, USA) in a 1:200 dilution in PBS with 5 % FCS for 1 h at 37 °C. The slide was washed 1 x with PBS and analyzed under the fluorescence microscope.

4.3.5. Limiting dilution assays

Since the original virus stocks used during this project are isolates directly from wild rodents, they contain the viral quasispecies naturally found in the host animal, which might complicate subsequent analysis with NGS. Therefore, a limiting dilution assay was established to generate single virus variants from the initial virus mixture. One day before the experiment, 1×10^4 cells/well of Vero76 were seeded in 96-well Nunclon-Delta coated plates (Thermo Fisher, Waltham, USA). As virus titer determination always has a standard error of up to 36 % [196], different calculated amounts (e. g. 2.5, 1, 0.5, 0.25, 0.1) of virions/well were used as inoculum for the plates, which were incubated for 5 days at 37 °C and 5 % CO_2. Thereafter, the supernatant was transferred into a clean 96-well plate and stored at -80 °C until the staining of the initial plate was complete, and we determined which wells contained a single virus variant to proceed with. The initial plates were inactivated and stained as described in 4.3.3, but no analysis with the ELISpot Reader was performed. Wells were considered virus-positive, when a blue staining was visible. Suitable plates for the isolation and amplification of the

obtained single variants were selected based on the total amount of infected wells per plate. When ten or less wells were infected in a 96-well plate, this plate was used for virus isolation, as it was highly likely an infected well resulted only from one initial virus particle ($P(X \geq 2) = 0.00499$). The virus variants were used for amplification on Vero76 cells (see 4.3.2) and their titers were determined as described above.

4.3.6. Growth kinetics

4.3.6.1. Growth kinetics on standard cell lines

Growth kinetics of the initial virus stocks, the virus variants before adaptation as well as the chimeras have been performed with three technical replicates. All other growth kinetics were performed in three technical replicates and were repeated three times.

To compare the growth kinetics on different cell lines, one day prior to infection 1×10^4 cells/well of the cell lines used (either Vero76, MasKEC, or MasEF) were seeded in 96-well Nunclon-Delta coated plates (Thermo Fisher, Waltham, USA). The plates were infected with a multiplicity of infection (MOI) of 0.001, 0.01 or 0.1. The virus stocks to be investigated were diluted in DMEM without the addition of FCS and the plates were incubated for 1 h at 37 °C and 5 % CO_2. After removing the inoculum, 200 µL/well of fresh DMEM with 3 % FCS for Vero76 or 5 % FCS for the *Mastomys*-derived cell lines were applied. For each time point, three replicate wells of the 96-well plate were harvested and transferred to a new 96-well plate, which was stored at -80 °C until titration.

4.3.6.2. Growth kinetics on primary cells

The growth kinetics on the primary cells were done with three biological replicated but without independent repetitions.

In contrast to the growth kinetics with the standard cell lines (Vero76, MasKEC and MasEF), growth kinetics with primary cells were not done in a 96-well format but in 6-well plates. This simplified seeding and differentiation of the primary bone marrow cells to macrophage-like cells. Also, the 6-well plate format allowed keeping the cells alive for a longer time than in the 96-well plates when multiple wells were harvested.

After the differentiation to macrophage-like cells, the primary cells were infected with an MOI of 0.01 by using 500 µL/well inoculum. During infection, RPMI-1640 without the addition of FCS was used and the cells were incubated for 1 h at 37 °C and 5 % CO_2. The inoculum was

removed, and the cells were provided with a mixture of 1 mL old, murine M-CSF (BioLegend®, San Diego, USA) containing RPMI-1640 and 1 mL fresh 10 % FCS containing RPMI-1640. The old medium was re-applied to further stimulate the cells. Of this fresh supernatant, 1 mL of was harvested as a day 0 sample and stored at –80 °C until virus titer determination. The cells were supplied with 1 mL of fresh RPMI with 10 % FCS. This procedure was repeated on seven subsequent days. Thereafter, all supernatants were used for titer determination by immunofocus assay (see 4.3.3).

4.3.7. Adaptation of LASV variants to MasKEC

The adaptation of the LASV variants previously generated by limiting dilution assay to MasKEC was done by serial passaging of the single variants obtained after isolation by the limiting dilution assays and subsequent amplification. For this, three variants, namely A11, C2 and E8 were used.

Always one day prior to infection, 1×10^6 MasKEC were seeded in T25 flasks with DMEM containing 3 % FCS. For the first passage (VP1), the infection was done with an MOI of 0.01 in a total volume of 2 mL virus-containing, serum-free DMEM. After 1 h incubation at 37 °C and 5 % CO_2, the inoculum was replaced by 7 mL of fresh DMEM supplied with 5 % FCS. On day 3 post infection, the supernatant was harvested, centrifuged for 5 min at 4000 × g and after shortly freezing it at -80 °C to ensure same sample treatment for all passages, 0.5 or 1 mL were used for subsequent infection of fresh cells to generate the next virus passage. To check for virus in the supernatant, an aliquot of the supernatant was always used for RNA extraction and consecutive RT-PCR (see 4.1.1 and 4.1.4). Additionally, an aliquot of each passage was stored at -80 °C for later titration (see 4.3.3). To ensure the presence of viral proteins inside the previously infected cells, also slides for immunostaining (see 4.3.4) were prepared. For this, the cells were detached with trypsin and 10 % of the cells in the T25 flask were harvested by centrifugation for 5 min at 500 × g. The pellet was resuspended in the backflow and used for the preparation of the slides, which were left for drying under the flow hood and inactivated in ice-cold acetone for 20 min.

4.3.8. Rescue of chimeric viruses

Viruses can be generated by reverse genetics via transfection of plasmids into cells that induce the formation of RNPs and subsequently result in the production of infectious virus particles.

This process is named virus rescue and is used in this project to generate chimeric viruses with Kak428-derived proteins in the genetic background of the Ba366 strain.

For this, one day prior to transfection, three 6-well plates with 3×10^5 BHK-J cells/well were seeded in 2 ml DMEM with 3 % FCS. Immediately before transfection, the DNA components indicated in Table 21 were diluted to 100 ng/µL in OptiMEM (Thermo Fisher, Waltham, USA) and used for the preparation of the DNA mastermixes.

Table 21: DNA master mix set up for transfection of plasmids used during a virus rescue. Shown here is the rescue of the GPC chimera exemplarily. Conc. = Concentration, Tm= Dead mutant, wt = wildtype.

	Amount [ng]	**Conc. [ng/µl]**	**Tm 3 x (+10 %)**	**Chimera 3 x (+10 %)**	**wt control 3 x (+10 %)**
LASV Pol II L (pCAGGS)	1500	100.0	49.5 µL	49.5 µL	49.5 µL
LASV Pol II NP (pCAGGS)	750	100.0	24.75 µL	24.75 µL	24.75 µL
Modified LASV Pol I S-Segment	750	100.0	-	24.75 µL	-
LASV Pol I S-Segment (1) control (pDP AG)	750	100.0	24.75 µL	-	24.75 µL
LASV Pol I L AG #1 (A) (pDP AG)	1500	100.0	-	49.5 µL	49.5 µL
pCITE 2a(+)	1500	100.0	49.5 µL	-	-

The Lipofectamine2000™ (Thermo Fisher, Waltham, USA) was shortly vortexed and a mastermix with Lipofectamine2000™ and OptiMEM was prepared in a 5 mL Eppendorf tube with a ratio of 300 ng DNA per 1 µL Lipofectamine2000™ and incubated for 5 min at room temperature (see Table 22).

Table 22: Lipofectamine master mix set up for transfection of plasmids used during a virus rescue.

	1x	**10x**
DNA	**4.5 µg**	**45 µg**
Lipofectamine 2000	15.0 µl	150 µL
OptiMEM (300 µl – DNA – LF)	240 µl	2400 µL

Per construct, 841.5 µL of the Lipofectamine200™ mastermix were added to each DNA mastermix and shortly vortexed followed by 20 min of incubation at room temperature started. Thereafter, the medium was removed from the BHK-J cells and 450 µL of fresh OptiMEM was added per well. The DNA-lipofectamine2000™ mastermix was carefully mixed by pipetting and 300 µL were added per well. The cells were incubated for 4 h at 37 °C and 5 % CO_2 before the medium was exchanged with fresh DMEM with 5 % FCS.

The cells were transferred into a T75 flask and expanded to a T175 flask, when they reached confluency. For the rescue of the NP chimera, a co-culture with Vero76 was started during the second passage post transfection. For this, 1×10^6 Vero76 were seeded in a T175 flask, and the BHK-J cells were added during passaging. During each passage, the cells were split depending on their density, and 2/3 of the supernatant as well as 1 mL of the supernatant for titration were kept in case of a high virus titer. Additionally, slides were stained to detect the viral NP antigen with specific antibodies (see 4.3.4).

4.4. Functional assays

4.4.1. Determination of LASV receptor expression with a qPCR assay

To evaluate, if *Mastomys* cells might be a suitable *in vitro* model for LASV infections, their expression pattern for typical LASV receptors was analyzed.

The LASV entry receptor expression for αDG, which is found on the cell surface, as well as the expression of the LARGE1 and LARGE2 enzymes, that are important for αDG posttranslational modifications, were determined by a qPCR assay, which was initially described by [197]. Additionally, primer pairs for the Tyro3 gene (kindly provided by Dr. Thomas Strecker´s lab at the Philipps University Marburg) and the 60S ribosomal protein L13a as a second reference gene were included according to [198]. Organs from uninfected, two-month-old *M. natalensis* (one male and one female) were sampled including brain, liver, kidney, lungs, eyes, thymus, ovaries/testis/seminal tracts and lymph nodes. The organs were homogenized with a tissue lyser and RNA was isolated according to the RNeasy Mini kit (QIAGEN, Venlo, Netherlands). RNA was also isolated from the *Mastomys*-derived cell lines MasKEC and MasEF. cDNA was synthesized with the High-Capacity RNA-to-cDNA™ kit (Applied Biosystems, Waltham, USA) according to the manufacturer´s instructions and stored at -20 °C until further use. The qPCR was performed with the SYBR green Master 1 mix and the fold change of expression was

calculated in relation to the reference genes β-actin and 60S according to the following equation (adapted by [199]):

$$\text{Expression level (gene)} = 2^{-\Delta(\text{Ct(gene)} - \text{Ct(average of reference gene)}}$$

4.4.2. Entry assays

4.4.2.1. Immune fluorescence staining of slides for confocal laser scanning microscopy

Cells were seeded on coverslips and infected with a MOI of 1 of the pseudotyped VSV/LASV_GP_LinIV_Josiah or VSV/LASV_GP_LinVI_Kak428 for 1 h at 37 °C and 5 % CO_2. The infected cells were incubated 18-24 h post infection at 37 °C and 5 % CO_2. Thereafter, the coverslips were inactivated by adding 4 % formaldehyde. Then, they were washed 2 x with PBS and to stop the crosslinking reaction of the formaldehyde, 300 µL/well of 0.1 M glycine was added for 10 min at room temperature, followed by another washing step. The cells were permeabilized with 0.1 % triton in PBS for 10 min at room temperature and blocked with 0.2 % BSA in PBS after another wash step with PBS. Staining with the primary antibodies α-VSV (Institute for Virology, Marburg), α-GP-2 ((gp4), Institute for Virology, Marburg), or α-GP-2 ((37.7H), absolute antibody, Oxford, UK) was performed by adding 20 µL of the 1:100 diluted antibodies for 1 h at room temperature in a moist chamber. The slides were washed again before adding the secondary antibodies chicken α-rabbit-488 (Molecular Probes, Eugene, USA) or chicken α-human-488 (Dako, Denmark) in a 1:200 dilution in PBS. At the same time, DAPI (Thermo Fisher, Waltham, USA) was applied in a 1:10,000 dilution as well as 1:200 diluted phalloidin (Thermo Fisher, Waltham, USA). Before mounting the slides with Fluoroshield medium (Sigma Aldrich, St. Louis, USA), two washing steps in PBS and one final wash in water were conducted. The slides kept overnight in the dark before visualization at the confocal laser scanning microscope.

4.4.2.2. Entry assays

In 96-well plates, 2.5×10^4 cells/well of either MasEF, MasKEC, or Vero76 were seeded one day before infection. Then, the medium was replaced by 100 µL/well of medium that contained different amounts of virions (200, 100, 50 or 25 FFU/well) of the Ba366 strain or the Kak428 strain for 1 h at 37 °C and 5 % CO_2. Subsequently, the inoculum was discarded, and

the cells were supplied with 100 µL/well of overlay medium. After 16 h of infection, cells were inactivated by adding 100 µL of 4 % formaldehyde per well for 30 min at room temperature. The cells were permeabilized with permeabilization buffer for 30 min at room temperature. After washing the plates three times with tap water, the blocking solution was applied for 1 h at room temperature. Then, immunostaining was performed for 1 h at room temperature with 50 µL/well of the primary 2B5 antibody in a 1:000 dilution in blocking buffer. The plates were washed 3 x with tap water and 50 µL/well of the secondary AffiniPure sheep anti-mouse peroxidase-coupled antibody (Jackson ImmunoResearch, Baltimore Pike, USA) was applied in in a 1:1000 dilution was applied for 1 h at room temperature. Staining with TMB (diluted 1:3 in PBS, MIKROGEN Diagnistik, Neuried, Germany) was performed for 45 min at room temperature till foci became visible. Plates were washed 1 x with tap water and left for drying for 1 h under a running flow hood or overnight in a dark drawer. Then, images were taken at the iSPOT ELISpot Reader (AID, Straßberg, Germany) and spots were manually counted.

4.4.3. Replicon assays

To assess the replication and transcription performance of the Kak428 L and NP proteins in combination with the Ba366 proteins, replicon assays were performed as described in [135]. For replicon assays, 0.85×10^5 cells/well of BSR-T7 cells were seeded in 24-well plates in 500 µL GMEM one day before the experiment started. Then, a DNA mastermix with 250 ng of the pCITE_Ba366_minigenome and 250 ng of the pCITTE_Ba366_NP plasmids as well as 10 ng of the pCITE_Firefly plasmids was prepared. The mastermix was distributed to 250 ng of the respective pCITE_L plasmids or mutant plasmids, and 50 µL of the Lipofectamine2000™ (Thermo Fisher, Waltham, USA) mastermix were added and vortexed shortly. The mixture was incubated for 15 min at room temperature and in the meantime, the medium was removed from the cells and replaced with 20 µL of OptiMEM (Thermo Fisher, Waltham, USA) per well. After the incubation time, 100 µL of the transfection mix was added per well. The cells were further incubated for 4-5 h at 37 °C before the medium was exchanged with 500 µL/well of GMEM with 5 % FCS. Readout was performed at least 24 h post-transfection. For this, the medium was discarded, and the cells were washed with PBS. The cells were lysed by adding 100 µL/well of the passive lysis buffer (Promega, Madison, USA) and a 20 min incubation time at room temperature on a shaker. The cells were scraped off from the cell culture plate and the lysate was mixed by pipetting. Thereafter, cell debris was collected at the bottom of the

plate and 10 µL of the lysate was used for the measurement. At first, 10 µL of the lysate was mixed with 60 µL of the LARII reagent (Promega, Madison, USA) and the relative light units (RLU) for the Firefly luciferase were determined in a Junior LB 9509 spectrophotometer (Berthold Technologies, Bad Wildbad, Germany). Then, 50 µL of the 1:50 diluted Stop and Glow substrate (Promega, Madison, USA) was added and the Renilla luciferase values were measured. The percentage of activity compared to the Ba366 wt L was calculated by dividing the Renilla luciferase RLU by the square root of the Firefly luciferase RLU normalized to the average of the Ba366 wt L.

$$\text{Proportion of Renilla and Firefly Luciferase } = \left(\frac{\text{Renilla luciferase [RLU]}}{\sqrt{\text{Firefly luciferase [RLU]}}}\right)$$

4.5. Transmission electron microscopy

In order to assess if all cell lines used regularly for infection experiments in this study (Vero76, MasKEC and MasEF) can efficiently release progeny viruses, transmission electron microscopy approaches were applied. For the transmission electron microscopy experiments, 0.5×10^6 cells of Vero76, MasKEC or MasEF were seeded in 10 cm dishes and infected one day later with a MOI of 0.5 with the Ba366 or the Kak428 strain. Supernatants were harvested 3 and 4 d. p. i. respectively and concentrated with a 100 kDa Amicon filtering unit by centrifugation at 4000 x g for 10 min. Afterwards, the supernatants were inactivated by adding formaldehyde to a final concentration of 4 % for 30 min at room temperature. The samples were further processed by the EM core facility by Dr. Katharina Höhn for the negative staining described in the following. The virus particles were directly spun onto glow-discharged formvar coated cupper grids for 20 minutes. Then, the grids were washed with water for 5 s and shortly blotted with Whatman paper. After a 15 s incubation in 2 % uranyl acetate, the grids were dried at room temperature and analyzed with a Tecnai Spirit transmission electron microscope (TEM), equipped with a LaB6 filament and operated at an acceleration voltage of 80 kV.

The pictures taken with the TEM were analyzed with the Fiji ImageJ2 *measure* software tool to determine the diameter of the particles at two distinct locations, with one measurement in a horizontal and the other in a vertical orientation.

4.6. Creation of amino acid alignments in MacVector

To compare the amino acid sequences of the Kak428 strain with isolates from *M. natalensis*, the sequences for the Ba366 strain, the MAD39 strain and isolates from *Mastomys* caught in the houses of LASV-infected individuals were downloaded from the NCBI server. Table 23 shows the GenBank reference numbers used.

Table 23: Overview of GenBank reference numbers used for the creation of amino acid alignments.

	Gene		
Isolate	**GP**	**NP**	**L**
Kak428	ANH09740.1	ANH08741.1	ANH09760.1
Ba366	ADI39451.1	ADI39452.1	ADU56645.1
MAD39	ANH09722.1	ANH09723.1	ANH09742.1
LM774-SLE-2012	AIT17820.1	AIT17821.1	AIT17819.1
LM886-SLE-2012	AIT17824.1	AIT17825.1	AIT17823.1
LM778-SLE-2012	AIT17828.1	AIT17829.1	AIT17826.1
LM7749SLE-2012	AIT17832.1	AIT17833.1	AIT17831.1
Z0947-SLE-2011	AIT17840.1	AIT17841.1	AIT17839.1
Z0948-SLE-2011	AIT17844.1	AIT17845.1	AIT17843.1

Those sequences were loaded into MacVector and aligned by using the Clustal W algorithm. Then, we analyzed the residues that showed mutations in our NGS dataset regarding their conservation.

4.7. Mapping of mutations to the proteins 3D structures

To facilitate the structural mapping of the mutations identified in our NGS datasets, 3D protein models were generated for the Kak428 proteins by using the artificial intelligence tool AlphaFold2. The sequences for the Kak428 proteins were downloaded from the National Center for Biotechnology Information (NCBI) Protein databank with the following accession numbers: GP ANH09740.1, L ANH09760.1 and NP ANH09741.1. The amino acid sequences were inserted in the Colab notebook (https://colab.research.google.com/github/deepmind/alphafold/blob/main/notebooks/AlphaFold.ipynb) and the modelling

process was executed with standard parameters. The predicted protein structures as well as the corresponding protein quality measurements were downloaded. As the Kak428 GPC model did not meet the expectations when compared to GPC models experimentally determined, we decided to use the LASV Josiah GPC structure 8ejd instead and downloaded it from the protein database. Thereafter, the structures were locally loaded into Pymol for visualization. The structures were colored, and the mutations found during the adaptation process were displayed as sticks in either red or yellow, depending on the time of first identification during the NGS analysis.

4.8. Animal experiments

All experiments involving *in vivo* inoculation with LASV were performed in the BSL-4 laboratory of the BNITM by trained personnel.

4.8.1. Ethics statement

This study was strictly carried out in accordance with the recommendations of the German Society for Laboratory Animal Science under supervision of a veterinarian. All protocols have been approved by the Committee on the Ethics of Animal Experiments of the City of Hamburg with the permit no. N 028/2018, N 050/2021, and O 42/2018. To minimize the number of animals used and to mitigate suffering during experimental procedures, all efforts were made. All staff members involved in animal experiments and handling underwent the necessary education and training according to the category B or C of the Federation of European Laboratory Animal Science Associations (FELASA). Additionally, personnel responsible for animal sample handling was trained in good scientific practice and good laboratory practice. For more details about personnel, who performed the animal experiments, see Supplementary Table 10.

4.8.2. Breeding, housing and origin of the animals

The non-domesticated *M. natalensis* used during this study were bred in the animal facility of the BNITM. The breeding colony descends from animals kindly provided by Heinz Feldmann from the Rocky Mountain Laboratories, Montana, USA, who initialized their colony with wild-caught, arenavirus-free animals from Mali. Animals are housed in small groups of 3-4 sex-matched individuals using open cage rearing (ca. 1200 cm^2) with access to sterilized water and

food (Altromin International, Lage, Germany) *ad libitum* according to FELASA guidelines. The colony is kept outbred with 1:1 mating. Our experiments were performed with whole litters regardless of sex. In total, 82 animals were used during this study. Per group, 8 to 13 animals were used with 2-6 animals per timepoint.

4.8.3. Handling of animals during experiments, monitoring, and scoring

The breeding pairs were put together in the breeding facilities of the BNI and the parents were moved together with the new litter the BSL4 at least three days before the start of the experiment so that they could acclimate to the new surroundings. They were housed in small groups in individually ventilated cages (1500 cm^2) with food and water provided *ad libitum*.
All animals were monitored at regular intervals and scoring for general well-being, bodyweight, and clinical signs of disease. Animals were sacrificed for terminal sampling, at the end of the experiments or if any of the termination criteria were fulfilled. Humane endpoint criteria included, among others body weight loss of more than 10 % and reduced growth in juveniles (see Supplementary Table 1 for more detail).

4.8.4. *In vivo* inoculation

During this study, all animals were inoculated subcutaneously (s . c.) at an age of 7-9 days post birth with either 1,000 focus forming units (FFU) for the chimeric viruses (GP, L, NP and Z chimera) or 10,000 FFU for the adapted Kak428 variants (Kak428 A11, C2 and E8). The inoculum was prepared in 50 µL of PBS. As juveniles younger than two weeks showed a strong pinch-induced behavioral inhibition when retained in the neck with a forceps, the inoculations did not require anesthesia. After inoculation, potential excess droplets on the fur were removed with a tissue and the animals were placed back into the cage for monitoring. To prevent potential aggression from the parents, inoculated juveniles were kept separated for a minimum of 20 min before returning the parents into the cage.

4.8.5. Euthanasia

Animals were euthanized for terminal sampling at the end of the experiments. Euthanasia was performed with an initial dose of 3.5 % isoflurane (Piramal Critical Care B.V. Bethlehem, USA) until loss of consciousness, followed by an overdose, heart puncture and finally cervical dislocation.

4.8.6. Sampling during animal experiments

4.8.6.1. Sampling schedules

At weekly intervals, blood and urine, as well as organs were sampled. For later analysis, sampling periods were rounded to the week level, in case sampling was not performed on day 7 post inoculation, but e. g. at day 8 or 9 post inoculation.

4.8.6.2. Blood and plasma samples

During these experiments, only terminal blood sampling was performed. For this, cardiac puncture was done after euthanasia. The blood was collected in 0.5 mL EDTA tubes and plasma was obtained by centrifugation at 5000 × g for 10 min.

4.8.6.3. Other body fluids and excretions

Urine was collected via bladder puncture or after voiding following euthanasia with tissue paper. By vigorous agitating in 0.2 mL PBS, the urine was removed from the filter paper. Alternatively, urine was collected via bladder puncture after euthanasia.

4.8.6.4. Organ samples

The following organs were sampled at all time points: liver, spleen, kidney, heart, lung, brain, salivary gland, and eyes. Additionally, gonads were sampled from animals starting from animals older than one week, while the thymus was mostly sampled from animals younger than two weeks.

4.8.7. Processing of collected samples

4.8.7.1. Extraction and detection of viral RNA

To analyze the viral RNA levels in the whole blood and urine, qRT-PCR assays were performed. For this, RNA was extracted by using the QIAmp Viral RNA Mini Kit by adhering to the manufacturer's instructions. Afterwards, the L gene of LASV was detected with the RealStar® LASV RPCR kit 2.0 according to the manufacturer's protocol. For the creation of standard curves, *in vitro* transcripts were used, which were based on the LASV Ba366, Kak428 or D96 strain.

4.8.7.2. Serological analysis

For serological analysis, plasma samples were inactivated by adding the same volume of PBS with 2 % Triton X-100 and subsequent mixing. By using the Panadea LASV IgG ELISA Kit the presence of virus-specific IgG antibodies was investigated according to the manufacturer's instructions.

4.8.7.3. Viral titers in organs

The sampled organs were weight and homogenized in 1 mL of DMEM with 3 % FCS by using the FastPrep-24™ 5G tissue lysis system (MPBio, Irvine, USA) with the lysing matrix D (MPBio, Irvine, USA) for 3 x 30 s. To collect debris, the samples were centrifuged for 5 min at 3,000 × g and 200 µL of the supernatant were transferred to 96-well plates, which were stored at -80 °C until they were used for the immunofocus assay as described in 4.3.3.

4.8.8. Waste disposal

All consumables and reagents used during animal experiments were strictly regulated, collected and disposed according to the biorisk management of BNITM. Infectious waste such as bedding, remaining food and cadavers, that were generated during this study, were autoclaved and disposed professionally by the company AGS Nord GmbH. The release of murine genetic material into the environment was prevented by strict barrier and hygiene measures.

4.9. Sample storage

All samples were stored at -80 °C for long-term storage, while for short-term storage for up to four weeks storage at -20 °C was sufficient.

4.10. Statistics and data presentation

Data presentation and plot preparation were performed in GraphPad Prism. Statistical differences were determined by Mann-Whitney test. All overview figures were created with BioRender.com.

5. Results

Little is known about the virus-host barriers, that might restrict the spillover from new LASV strains into the widely distributed and peri-domestic rodent host, *Mastomys natalensis*. To predict these potential risk factors and implement them into surveillance systems, the new LASV strains need to be better characterized. Therefore, in the first step, an *in vitro* system to model LASV infection in *M. natalensis* cells was established and used to characterize the infection dynamics of different LASV strains. Next, it was examined which viral proteins are responsible for the observed virus-host barrier by creating recombinant, chimeric viruses. Here, the viral proteins of a strain that was previously isolated from *M. natalensis* (homologous strain) were exchanged with proteins of a virus strain isolated from a different rodent host (heterologous strain) and the growth behavior of the different viruses were analyzed both *in vitro* as well as *in vivo*. Additionally, life cycle modelling systems were used to assess the contribution of each viral protein to the virus-host barriers. Lastly, a homologous and a heterologous strain were used for *in vitro* adaptation by serial passaging on *Mastomys* kidney epithelial cells and assessed how their infection dynamics change over time. During these experiments, NGS approaches were applied to identify potential host-adaptive mutations, that were later characterized further.

5.1. Can heterologous LASV strains infect *Mastomys natalensis* cells *in vitro*?

Previous *in vivo* experiments have shown that LASV strains, which have been isolated from different rodent hosts than *Mastomys natalensis* (heterologous strains) fail to establish long-lasting persistent infections in *M. natalensis* [157]. This abbreviated virus presence indicates that virus-host barriers might constrain heterologous viruses from spillover into *M. natalensis* [157]. We developed a RT-PCR assay, which allows the detection of changes in the interferon-stimulated gene (ISG) expression to investigate their contribution within the innate immune response to this barrier. The ISG expression upon infection with either homologous or heterologous LASV strains did not significantly differ, hinting towards a rather unlikely contribution of the innate immune system to the faster viral clearance of heterologous strains [158, 198]. In this study, the question of what restricts viruses from spilling over into new hosts was addressed. Classically, *in vivo* studies are used to assess the mechanisms relevant for virus-host barriers, but this project particularly aimed to adhere to the 3R´s rule “reduce,

replace, refine". Therefore, an *in vitro* model was established to mimic virus growth kinetics and adaptation processes in *M. natalensis* cells *in vitro* first. This newly developed model was proven relevant by complementing *in vivo* experiments later during this study.

5.1.1. Are the most important LASV entry receptors and the enzymes required for their functional modification expressed on the *Mastomys natalensis´* cells and organs?

Virus entry is the first step of the virus life cycle. Thus, to establish a reliable *in vitro* model for LASV infections, at first, the expression of the most important LASV receptors on the immortalized *Mastomys* cell lines needed to be ensured. Among those are the primary receptor for LASV entry α-dystroglycan (αDG) and the alternative receptor tyrosine-protein kinase receptor (Tyro3). Additionally, the glycosyltransferase-like protein 1 (LARGE1) and glycosyltransferase-like protein 2 (LARGE2) were included in this experiment, as they facilitate O-mannosylation of the αDG. This O-mannosylation is essential for the expression of functional αDG [108, 109, 112, 200]. A qPCR assay by Tayeh et al. (2010) was used and complemented by the Tryo3 primers kindly provided by the research group of Dr. Thomas Strecker, Philipps University Marburg [197]. Initially, the qPCR assay was tested on uninfected organs from *M. natalensis* (namely liver, kidney, lung, heart, testis, prostate, ovaries, salivary gland, eyes, brain, spleen, thymus and lymph nodes) to ensure the assays´ ability to reliably detect the gene expression in various tissues. Subsequently, the expression on the *Mastomys* cell lines MasKEC and MasEF was assessed. All receptors were found to be expressed in all organs tested (see Supplementary Figure 1). In the MasKEC and MasEF cells, all receptors were expressed with the exemption of LARGE2, which was not detectable (see Supplementary Figure 2). These data indicate the presence of the most important LASV-receptors also in immortalized cells. These cell lines are therefore a potential model system for LASV infections.

5.1.2. Do the growth kinetics *in vitro* resemble the previous observations in animal experiments?

To evaluate, if infection of the different *Mastomys* cell lines with the different LASV strains results in the same infection kinetics as has been seen by our group in previous animal experiments, growth kinetics were performed on MasKEC and MasEF. Additionally, Vero76 cells were included as a control because these are regularly used for amplification of LASV.

Also, the growth of LASV on bone marrow-derived macrophage-like cells (MΦ) was assessed to see if the immortalized cell lines could be used as a surrogate model for these primary cells. The infection was done with LASV strains originating from various rodents (Ba366 from *M. natalensis*, D96 from *Lemniscomys striatus*, Kak428 from *Hylomyscus pamfi*). Figure 8 shows the viral titers in focus forming units per mL on day three post infection of all four cell lines with either the homologous strain Ba366 (blue) or the heterologous strains D96 (pink) or Kak428 (red).

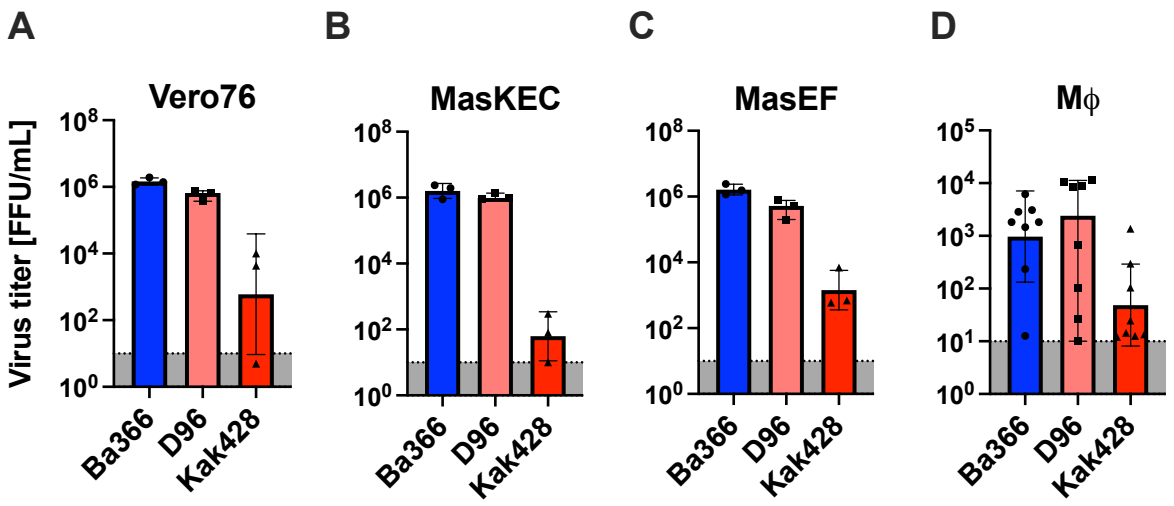

Figure 8: Growth kinetics of homologous and heterologous LASV strains on different cells. Three different stable cell lines **A** Vero76 **B** MasKEC **C** MasEF and **D** bone marrow-derived macrophage-like cells (MΦ) were infected with a MOI of 0.01 for eight days with Ba366 (blue), D96 (pink) or Kak428 (red). Virus supernatant was harvested on days 0, 1, 2, 3, 4, 5, 6, 7, and 8 post infection, depicted here is exemplarily data from day 3 post infection only. Viral titers in focus forming units per mL (FFU/mL) were determined by immunofocus assay. The shaded area indicates the limit of detection. Negative samples have been assigned a default value below the limit of detection. Experiments were done with three technical replicates per experiment. Depicted are median titers with a 95 % confidence interval and standard deviation.

The infection with the Ba366 strain resulted in the highest titers on all cell lines with titers up to 1×10^6 FFU/mL, followed by the D96 strain which reached slightly lower titers. In contrast, the Kak428 strain never reached more than 1×10^4 FFU/mL. Especially in the MasKEC and the MΦ, the virus titer of the Kak428 strain was less than 1×10^3 FFU/mL (see Figure 8). Interestingly, infection with none of the viruses led to titers more than 1×10^4 FFU/mL on the primary MΦ, but the trends with the Ba366 strain reaching the highest and the Kak428 strain having the lowest titers were maintained. Comparing the overall growth profile over time, the Kak428 strain grew slower and had reduced titers in comparison to the homologous Ba366 strain and the D96 strain in all cell lines (see Supplementary Figure 3). Previous animal

experiments have shown, that the Ba366 strain leads to persistent infection in *M. natalensis* when the animals were infected at a young age, whereas the D96 and Kak428 strains were cleared. Especially the Kak428 strain was cleared rapidly from the animals [157]. Taking these results together, the LASV growth characteristics on the *M. natalensis* cells mirrored their observed *in vivo* patterns. The heterologous Kak428 strain was attenuated compared to the *Mastomys*-derived Ba366 strain. The D96 strain was excluded from further experiments, as it showed similar growth patterns as the homologous Ba366 strain. For future adaptation experiments, the MasKEC were used because of the strong attenuation of the Kak428 strain, which indicates a high genetic pressure to acquire mutations (see chapter 5.3). In addition, using these immortalized cells substantially reduces the number of animals needed to generate the MΦ, as those always would have to be freshly prepared from bone marrow.

5.1.3. Do *Mastomys* cells efficiently release progeny viruses and are heterologous viruses morphologically different from homologous viruses?

The first set of growth kinetics led to the question, whether infection of *Mastomys* cells results in an efficient production of progeny virus and if these progeny viruses are morphologically similar or distinct between homologous and heterologous LASV strains. Therefore, transmission electron microscope approaches were used to generate representative images of the released viruses.

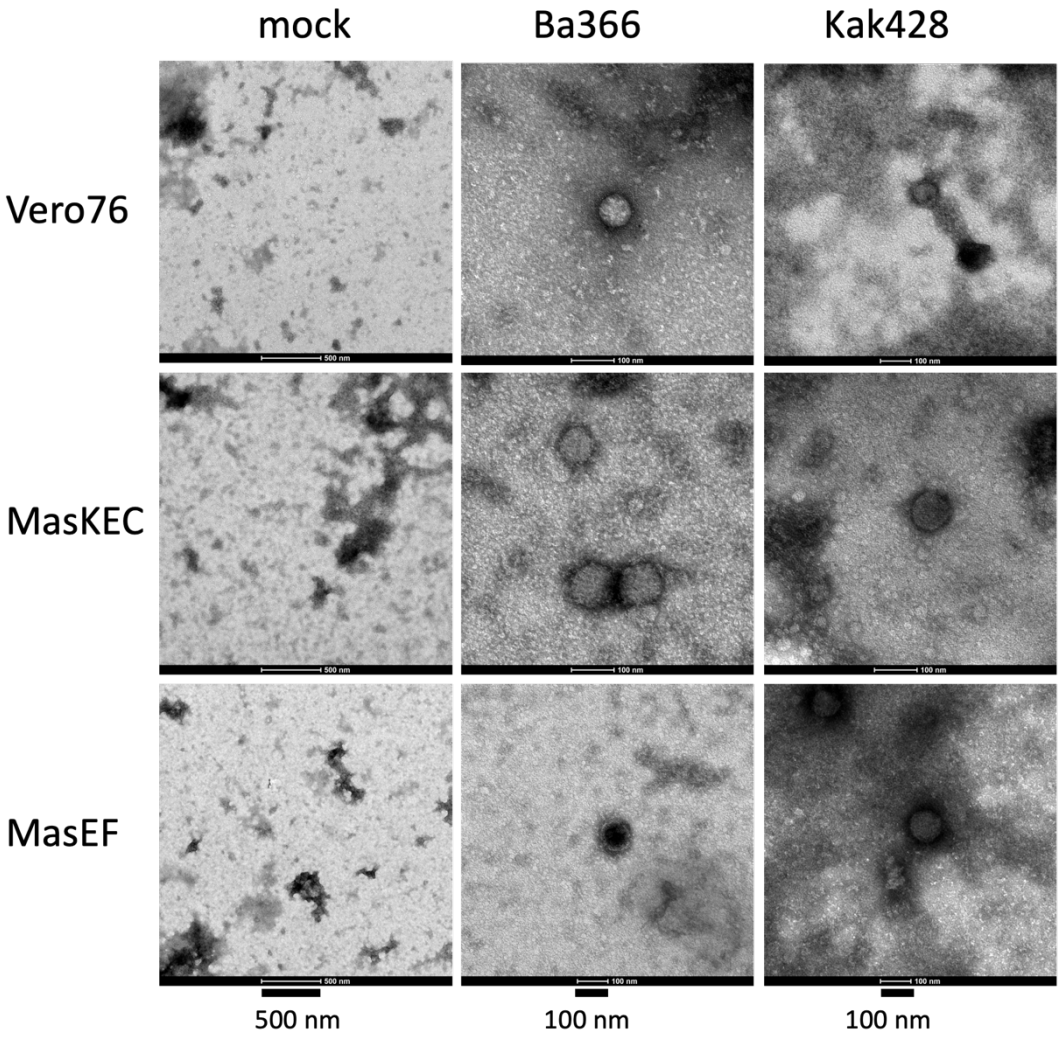

Figure 9: Negative stained electron microscopic pictures of LASV particles released from different cell lines infected with Ba366 or Kak428. Three different cell lines (Vero76, MasKEC or MasEF) were infected with a MOI of 0.5 of Ba366 or Kak428 or mock-infected. Virus supernatants were harvested 3 d. p. i. (Ba366) or 4 d. p. i. (Kak428). A negative stain was applied in the EM facility of the BNITM, and pictures were taken with a transmission electron microscope (TEM). The scale bar is 100 nm for the infected cells and 500 nm for the mock-infected controls. d. p. i. = days post infection. The pictures were kindly taken by Dr. Katharina Höhn, BNITM.

As shown in Figure 9, both virus strains were efficiently released by all the cell lines tested in this experiment. Additionally, their particle size was determined by using the *Measure* tool of ImageJ2, and the mean diameter was calculated with GraphPad prism. The Figure 10 shows the particle sizes of this experiment.

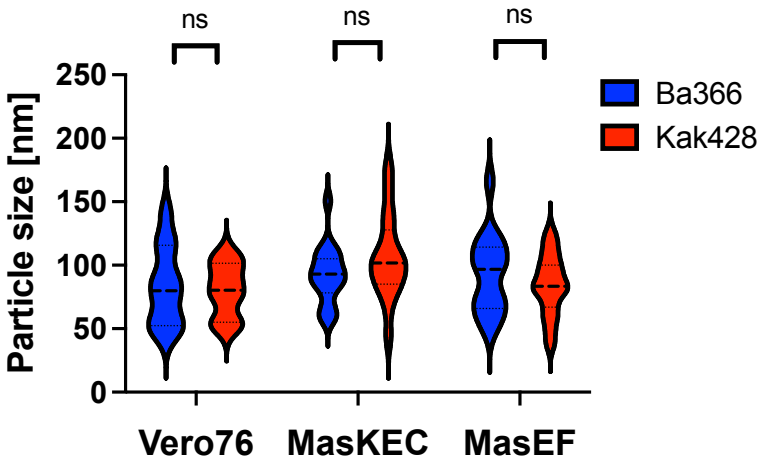

Figure 10: Particle size of different LASV strains determined by TEM. Three different cell lines (Vero76, MasKEC or MasEF) were infected with a MOI of 0.5 of Ba366 or Kak428. Virus supernatants were harvested 3 or 4 d. p. i., respectively. A negative stain was applied in the EM facility of the BNITM and pictures were taken with a transmission electron microscope. The particle sizes were determined with ImageJ2 and the data was further processed with GraphPad Prism. Depicted is the median of the LASV particle diameters. ns = non-significant.

Table 24: Median particle size, number of counted particles and standard deviation of LASV particles determined by TEM. N = number of counted particles, STD = standard deviation.

	Virus					
	Ba366			Kak428		
Cell line	Median Size [nm]	N	STD	Median Size [nm]	N	STD
Vero76	79.87	11	31.18	80.39	7	21.71
MasKEC	93.03	19	22.56	101.87	17	33.56
MasEF	96.75	16	30.80	83.52	28	50.67

The median particle diameters are listed in Table 24 and they ranged from 79.87 nm to 101.87 nm. This finding matches observations from others, that LASV particles range from 70 to 150 nm in size [102]. Neither between the two viruses nor based on the cells they were grown on a statistically significant difference in the particle size could be found. For testing this, the non-parametric Mann-Whitney test was applied to the data. In conclusion, the size of the viral particles was not considerably different, meaning that probably, functional particles can be produced by all the cell lines. Furthermore, the homologous and heterologous strain showed no obvious morphological difference.

5.2. Which impact do individual viral proteins have on the ability to establish persistent infection in *M. natalensis*?

To assess the contribution of each LASV protein to the observed virus-host barrier during previous animal experiments [157] and subsequently their ability to maintain stable virus titers in *M. natalensis* over the course of the experiment, chimeric recombinant viruses were created. Those had the genetic background of the Ba366 strain with one protein exchanged with the corresponding Kak428 protein, resulting in four chimeras, namely the GPC, L, NP and Z chimera (Figure 11). This approach allowed us to assess the relevance for the virus-host barrier of each LASV protein individually.

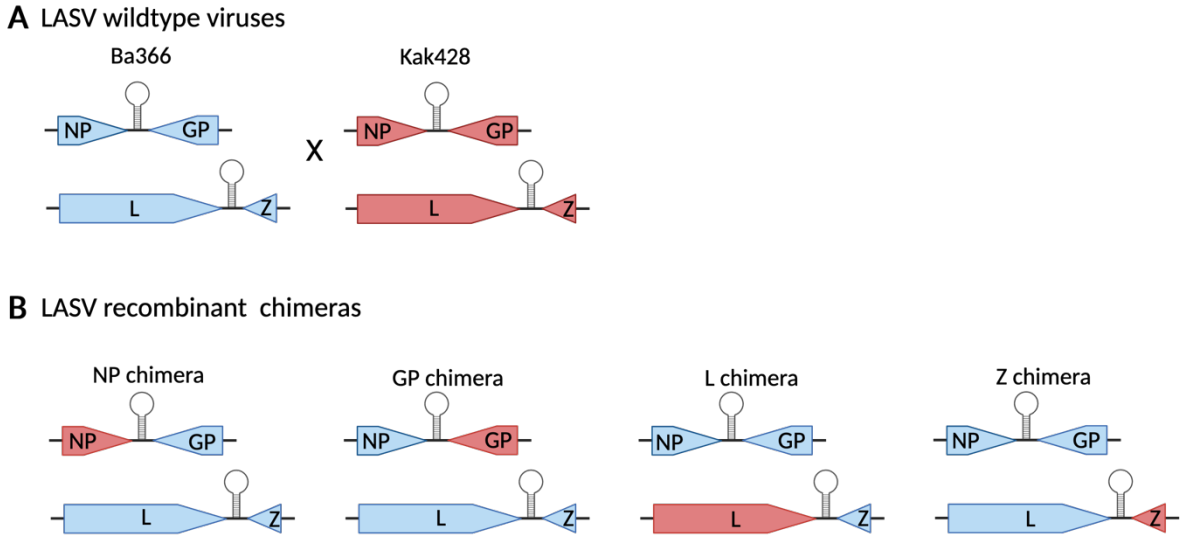

Figure 11: Schematic structures of recombinant, chimeric LASV. **A** shows the S- and L-segment of the wildtype LASV strains Ba366 (blue) and Kak428 (red). **B** Viral proteins, which have been exchanged (red) for the generation of the NP chimera, GP chimera, L chimera and Z chimera. This figure was created with BioRender.com.

5.2.1. Can viral proteins between homologous and heterologous LASV strains be exchanged?

Initially, it was not clear, if it is possible to rescue viruses with interchanged proteins between heterologous and homologous viruses. Cloning of virus segments has been proven challenging in the past, but all plasmids needed for virus rescue (namely pDP_AG_Ba366_S_Kak428_GP, pDP_AG_Ba366_S_Kak428_NP, pDP_AG_Ba366_Kak428_L and pDP_AG_Ba366_L_Kak428_Z) have been successfully generated by either restriction cloning or assembly with the NEBuilder kit. Since it was not possible, to generate the latter plasmid with restriction cloning as done for the other plasmids, another approach with the NEBuilder kit was applied. Sequencing

confirmed the correct nucleotide sequences for each plasmid. The rescue difficulty of the different chimeras depended on the gene which was exchanged. With only one attempt, the Z chimera was generated very quickly. For the L and GP chimeras, two and four attempts were needed, respectively and it was sufficient to follow the readily established protocols for the rescue of recombinant LASV. For the rescue of these recombinant viruses, BHK-J cells were transfected, and the infectious viruses were harvested at latest 15 d. p. i.. Most challenging to rescue was the NP chimera, for which five attempts were required. In contrast, the protocol for rescuing the NP chimera needed major adaptations such as co-culturing the BHK-J cells with Vero76 from passage two onwards. Also, the highest titers for the NP chimera were reached 21 d. p. i., which is remarkedly later than for the other chimeras (7-15 days). All chimeras were sequenced by both, Sanger as well as NGS to ensure the rescued viruses were correct. In summary, the generation of the NP chimera was more challenging and time-consuming than the other chimeras, but finally all four chimeras were rescued successfully.

5.2.2. How do the LASV chimeras grow on *M. natalensis* cells *in vitro*?

After all chimeric viruses were successfully generated, their growth was characterized on *Mastomys* and Vero cells. The kinetics of all four chimeras were done on Vero76, MasKEC and MasEF cells for four days after an infection with MOI 0.001.

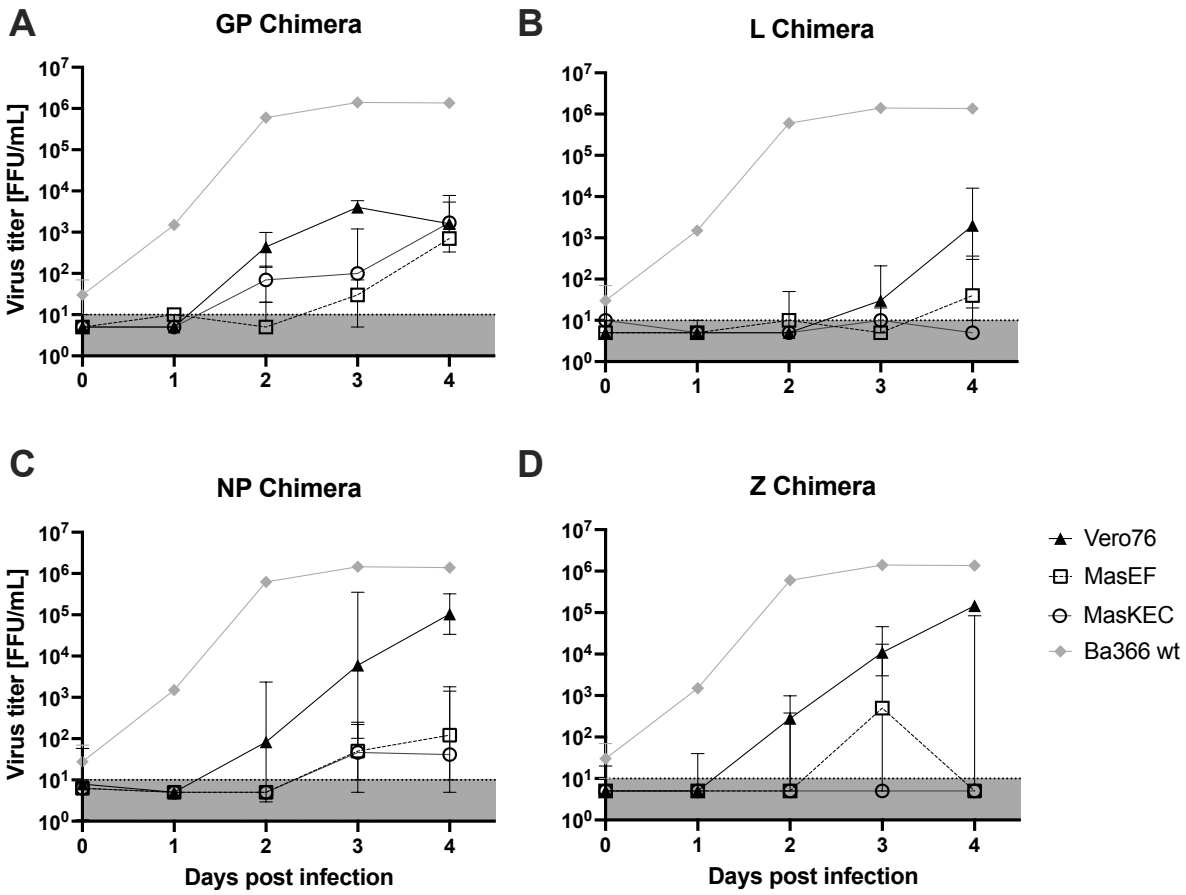

Figure 12: Growth kinetics of chimeric LASV. Three different cell lines, Vero76, MasEF, and MasKEC, were infected with an MOI of 0.001 with **A** GP chimera, **B** L chimera, **C** NP chimera, and **D** Z chimera. Virus supernatant was harvested on days 0, 1, 2, 3, 4 post infection each. Viral titers in focus forming units per mL (FFU/mL) were determined by immunofocus assay. The shaded area indicates the limit of detection (LoD). Negative samples have been assigned a default value below the LoD. Experiments were done with three technical replicates per experiment. Vero76: filled triangles, solid line; MasEF: rectangles, dashed line; MasKEC: circles, grey line. The grey diamonds indicate the growth of the LASV Ba366 strain on Vero76 as a reference. This data was previously generated as shown in Supplementary Figure 3. Depicted are median titers with a 95 % confidence interval and standard deviation for the different time points.

Overall, none of the chimeric viruses reached peak titers compared to the Ba366 wt at 3 d. p. i., (Figure 12, grey diamonds). The Ba366 wt strain usually grows to titers around 1×10^6 FFU/mL, while the chimeric viruses had a 1,000-fold lower titer even 4 d. p. i. All chimeric viruses grew the fastest on Vero76. The GP chimera showed delayed virus growth on the *Mastomys* cells but reached similar titers on 4 d. p. i. on all cell lines, indicating that initial virus entry might be affected but the effect becomes less distinct in multicycle infections. On the *Mastomys*-derived cell lines, especially the L and NP chimeras showed a delayed growth compared to the Ba366 wt. These findings suggest that replication and transcription might be relevant processes for the virus-host barrier. The exchange of the Z protein had the least impact on virus growth in all cell lines. However, the data generated need to be confirmed as

MasKEC cell viability was impaired, and experiments were only performed once. Altogether, all chimeras seem to be impaired in growth compared to the wildtype viruses, with varying levels of deficits depending on the cell line.

5.2.3. Can the LASV chimeras establish long-lasting infection in *M. natalensis*?

In addition to the *in vitro* experiments on the *M. natalensis* cells*, in vivo* infection experiments with *M. natalensis* were performed to gain insights into the infection dynamics. Especially the question if these chimeric viruses were still able to establish long-lasting infection needed to be clarified as the *in vitro* model from the previous section does not allow to gain insight into the long-term infection dynamics in the host organism. Moreover, these experiments were performed to verify the results from the *in vitro* system.

M. natalensis were experimentally infected one week after birth with 1,000 FFU of the different chimeras or the Ba366 and Kak428 wt strains and 2–6 individuals were sacrificed every week for up to four weeks post-infection to check for virus presence in blood and organ samples. The infection with the Ba366 and Kak428 wt strain was performed earlier, and data shown here are historical controls [157]. The virus titers in the organs (see Figure 13, Supplementary Table 2, Supplementary Table 3 and Supplementary Table 4) as well as the RNA copy numbers (see Figure 14) in the blood and urine were determined. The heterologous Kak428 wt (**A**) only reached low titers up to 1×10^4 FFU/g and was cleared within 2 weeks post infection (w. p. i.) from all organs except for the lung and salivary gland. In contrast, infectious virus of the homologous Ba366 strain (**B**) could still be found in all organs after 2 w. p. i. with titers up to 1×10^6 FFU/g. Similarly, the GP chimera (**C**) caused a transient infection and was only detected for up to 3 w. p. i.. However, the virus presence was limited to the lungs, brain and spleen with titers of max. 7×10^3 FFU/g. The L chimera (**D**) resembled the infection pattern of the Kak428 wt strain, although virus titers in the lung and heart were slightly higher compared to the Kak428 wt strain during the first week post infection. The L chimera was completely cleared from most organs within 2 w. p. i., except for the brain, which tested positive (10 FFU/g) up to 3 w. p. i.. A fast clearance was also observed for the NP chimera (**E**), which was only detected during the first week post infection. The highest virus titers for the NP chimera were observed in the spleen with 1×10^3 FFU/g. The NP and the L protein are known to be important to act complementary, so exchanging one of the proteins might render them incompatible for transcription and replication. The course of infection following the

inoculation with the Z Chimera (**F**), showed a strong resemblance to the infection pattern observed with the Ba366 wt experiments. Infectious virus could be detected throughout all tested organs for up to 2 w. p. i. Virus titers reached similar levels to the Ba366 wt control with 1×10^4 FFUg - 8×10^7 FFU/g FFU/g. The overall highest virus levels were detected in the lungs which reached peak titers of up to 1×10^8 FFU/g during the first w. p. i., as well as the testes (1×10^8 FFU/g) at 2 w. p. i. [156]. Important to note here is, that the eye was among the organs which retained high titers of infectious virus of the Z chimera infected animals 2 w. p. i. infection. However, the eye was not sampled in the Kak428 wt and Ba366 wt infected animals in previous experiments.

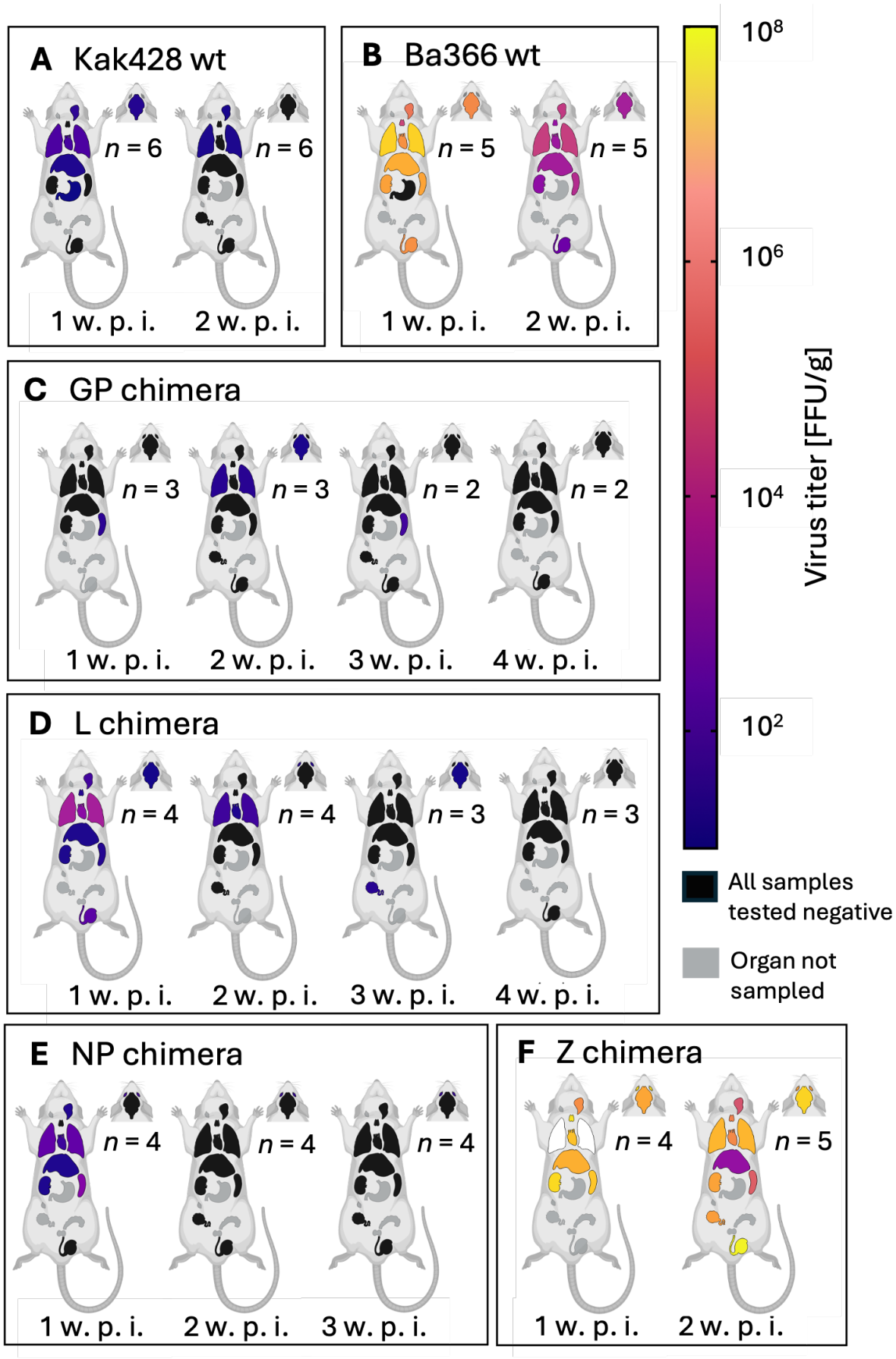

Figure 13: Virus titers in organs of *M. natalensis* infected with the LASV chimeras. *M. natalensis* were infected s. c. at day 7-9 post birth with 1,000 FFU of **A** Kak428 wt, **B** Ba366 wt, **C** GP chimera, **D** L chimera, **E** NP chimera,

and **F** Z chimera. The number of animals euthanized (n) at each time point (w. p. i., weeks post infection) is shown. Organs are shown as schematic: eyes, brain, salivary glands, thymus, lung, heart, liver, spleen, kidneys, ovaries and testes. Viral titers in focus forming units per gram tissue (FFU/g) of *M. natalensis* organs were determined by immunofocus assay. Geometric means of LASV-titers are depicted as spectral heat map with blue as limit of detection. Negative samples have been assigned a default value at the limit of detection: 10^1 FFU/g; max. value yellow: 10^8 FFU/g; orange: 10^6 FFU/g; pink: 10^4 FFU/g; purple: 10^2 FFU/g; black: all samples tested negative at that timepoint, grey: organs not sampled. Data from **A** and **B** are historical controls of [157] and shown here for reference purposes. This figure was created with BioRender.com.

Virus RNA levels in the blood resembled the infection patterns observed in the organs. The blood from the animals infected with the GP, L or NP chimeras only tested positive for viral RNA up to one week post infection, and most animals had antibodies present from week 2 onwards. Following the inoculation with the L chimera, antibodies were detected at 2 w. p. i., however, animals sacrificed at later time points no longer showed a detectable antibody response. Urine samples from infected animals could only be collected for the groups infected with the GP chimera and the L chimera and were positive at these time points. Interestingly, the *Mastomys* infected with the L chimera, had PCR-positive urine at a time when the blood tested negative, and no infectious virus was found in the kidneys. In concordance with the high virus titers in organs, animals infected with the Z chimera had high RNA copy numbers in their blood for 2 w. p. i. with up to 1×10^{10} RNA copies/mL, which is comparable to what has been observed for the Ba366 infected *M. natalensis* [156].

In summary, these results indicate that the Z protein does not contribute substantially to the virus-host restrictions for LASV. However, the GP, as well as the NP and L seem to significantly influence the infection outcome, indicating that entry similar to replication and transcription would be promising processes for future investigations.

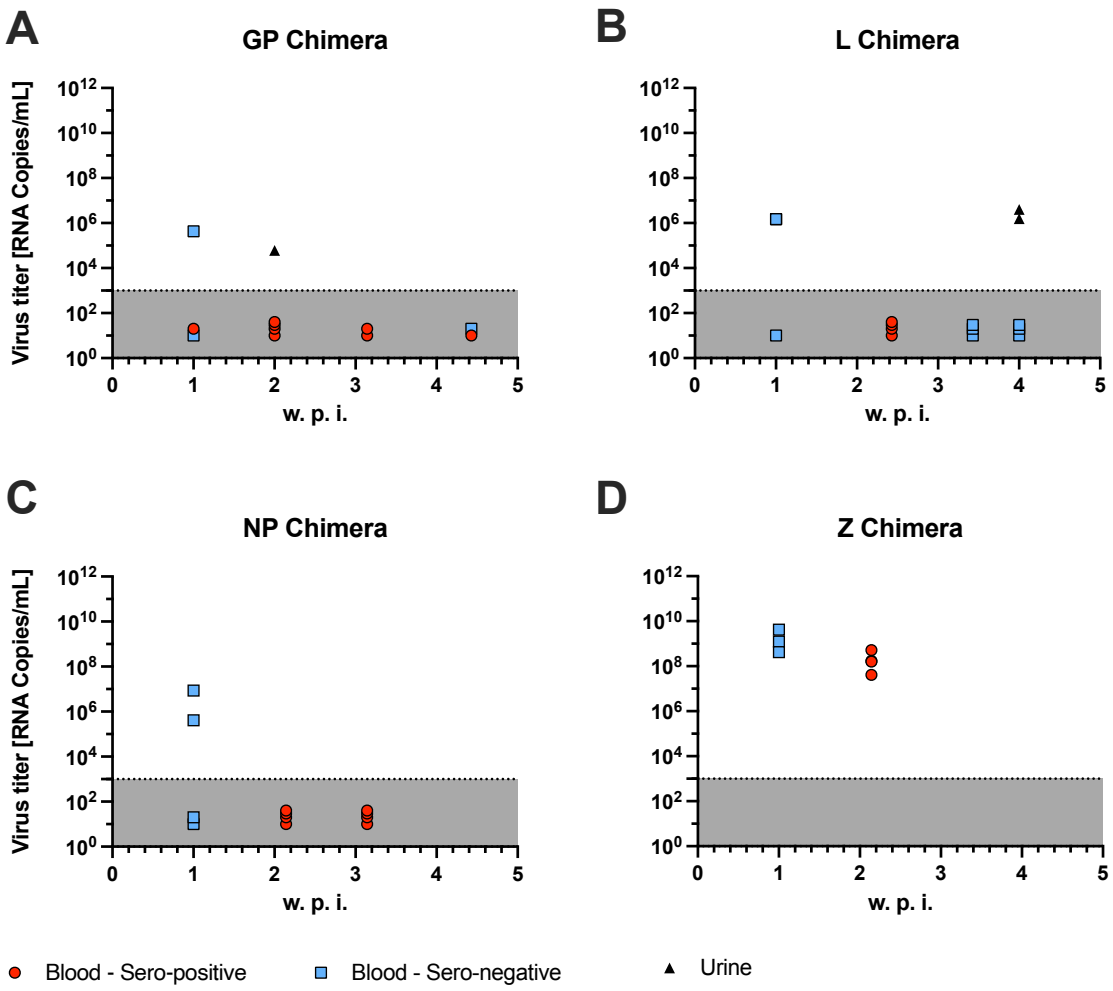

Figure 14: Longitudinal analysis of blood and urine samples from LASV-infected *M. natalensis* experimentally infected with the LASV chimeras. Virus titers in blood (RNA copies/mL; red circles for sero-positive individuals and blue squares for sero-negative individuals) and urine (RNA copies/mL; black triangles) are shown over time. Animals were inoculated at day 7-9 post birth with 1,000 FFU of **A** GP chimera, **B** L chimera, **C** NP chimera, and **D** Z chimera. The blood was sampled at weekly intervals and tested for the presence of LASV RNA via qRT-PCR with the Altona RealStar 2.0 PCR for the LASV L gene. The ct values were converted into copy numbers by using a standard curve. The shaded area indicates the limit of detection (LoD) of the qRT-PCR assay. PCR-negative samples were assigned a default value below the LoD. w. p. i. = weeks post infection.

5.3. Is *in vitro* adaptation of heterologous LASV strains possible to *M. natalensis* cells and do host-adaptive mutations occur?

After having looked at the role of each LASV protein for the establishment of long-lasting *in vivo* infections and their contribution to restrict spillover events, the question arose, if adaptation of heterologous LASV strains to *M. natalensis* cells is possible *in vitro*. The workflow to answer this question is depicted in Figure 15. First, clonal selection was done followed by *in vitro* adaptation experiments for ten consecutive passages on *M. natalensis* cells. Here, MasKEC were selected for the adaptation of Kak428, because this strain exhibited strongly

attenuated growth in MasKEC. (see 5.1.2). In the next step, a characterization of the adapted viruses *in vitro* was done (see Figure 15B). To follow up on potential host-adaptive mutations, NGS approaches were employed either directly (see Figure 15C) or after another clonal selection and subsequent growth characterization (see Figure 15D). The latter approach was used in case, the direct sequencing of the adapted variants after ten passages (VP10 variants) proved challenging. The effect of the mutations acquired during the adaptation process was also assessed during further *in vivo* studies with *M. natalensis* (see Figure 15C) to see if the observations from the *in vitro* studies could be replicated *in vivo*.

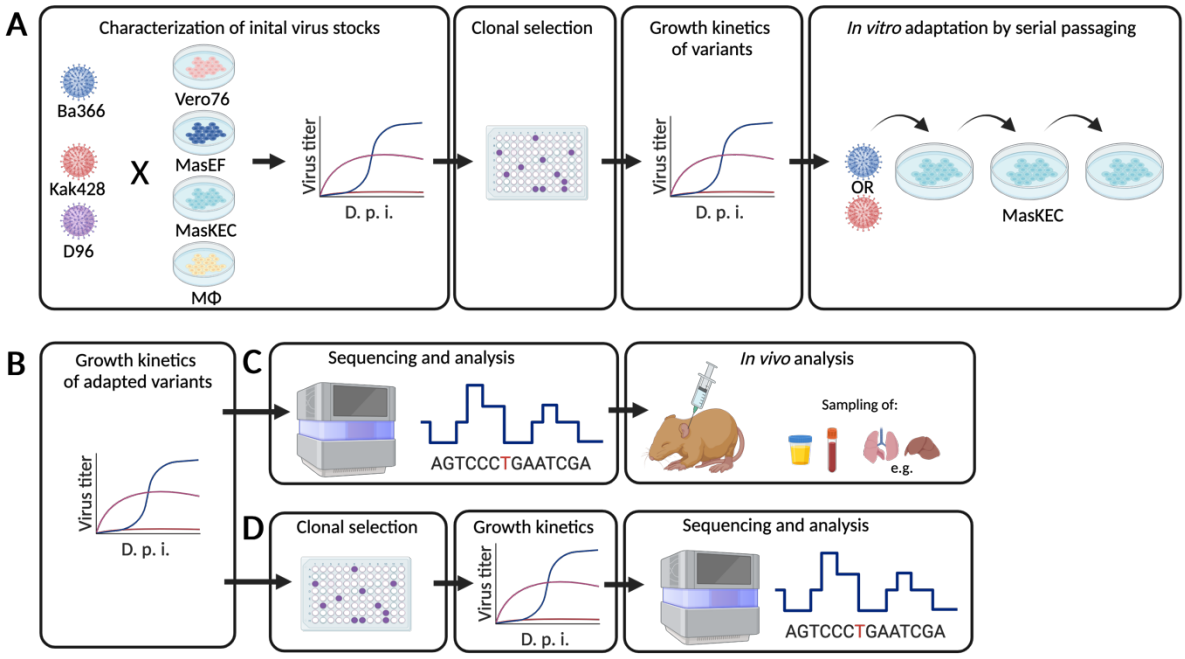

Figure 15: Workflow of the in vitro adaptation experiments with Kak428 on MasKEC and subsequent characterization of the adapted variants. **A** Characterization of the initial virus stocks, the clonal selection and following growth characterization as well as the *in vitro* adaptation on MasKEC. **B** shows the *in vitro* characterization of the adapted variants. Thereafter, **C** the VP10 variants were either sequenced directly and used for confirmation of the *in vitro* experiments by *in vivo* infections or **D** used for clonal selection followed by growth characterization on MasKEC and subsequent sequencing. MasEF: *Mastomys* embryonal fibroblasts, MasKEC: *Mastomys* kidney epithelial cells, MΦ: bone marrow-derived macrophage-like cells, d. p. i.: days post infection. This figure was created with BioRender.com.

5.3.1. What are the characteristics of single LASV variants after limiting dilution assay?

The Kak428 strain used for this study has been isolated from animals caught in Nigeria. These animals are very likely to carry virus quasispecies, meaning they harbor different virus variants with genetic variations within the same host. To reduce the genetic variation at the start of the experiment, virus variants needed to be isolated and propagated. This procedure enabled

the identification of possible host-adaptive mutations. As these LASV strains do not readily show cytopathic effect, the often-used approach of plaque purification was not suitable in this project to generate single virus variants. Instead, virus variants were generated by implementing a newly developed limiting dilution assay followed by virus amplification. This assay is based on the statistical observation that in a 96 well plate, it is unlikely that more than one virus caused the infection per well if, in total, not more than 10 wells per plate were infected ($P \geq 0.00499$). The generated variants of the Kak428 were named A11, C2 and E8 based on their well origin in a 96-well plate, respectively. Differences in the growth patterns of the Kak428 variants were observed during growth characterization (see Figure 16).

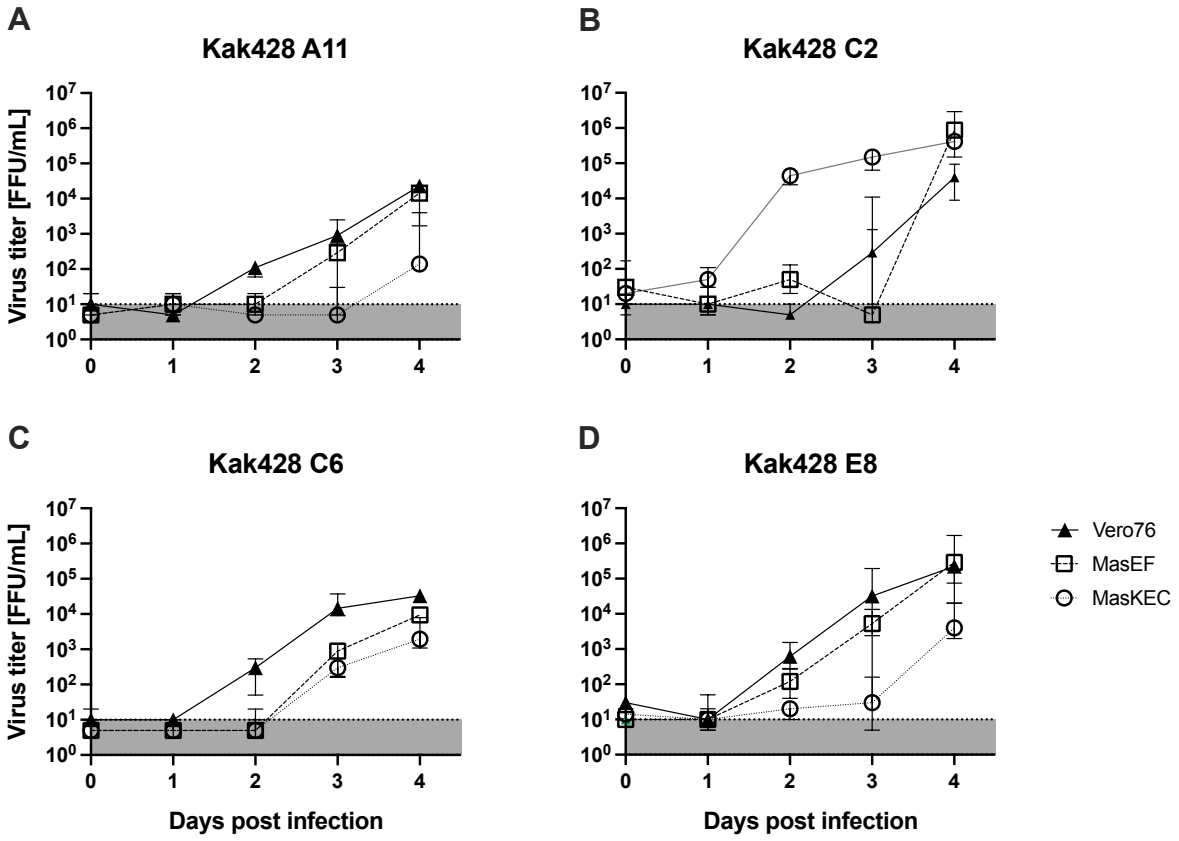

Figure 16: Growth kinetics of single LASV Kak428 variants. Three different cell lines, Vero76, MasEF, and MasKEC, were infected with an MOI of 0.01 with the **A** Kak428 A11, **B** Kak428 C2, **C** Kak428 C6, and **D** Kak428 E8 variants. Virus supernatant was harvested on days 0, 1, 2, 3, 4 post infection. Viral titers in focus forming units per mL (FFU/mL) were determined by immunofocus assay. The shaded area indicates the limit of detection. Negative samples have been assigned a default value below the limit of detection. Three independent experiments were done for each virus and cell line; Vero76: filled triangles, solid line; MasEF: rectangles, dashed line; MasKEC: circles, grey line. Depicted are median titers with a 95 % confidence interval and standard deviation for the different time points.

The Kak428 A11 and C6 variants had an overall slow growth that resulted in low virus titers with a maximum of 1×10^4 FFU/mL on day 4 post infection on all cell lines. This implies a

general replication deficit, and as the A11 variant showed stronger growth impairment, this variant was selected for undergoing the following adaptation experiments as it might be strongly affected by selection pressure. The C2 variant was of particular interest because it grew well on Vero76 cells, whereas it selectively showed growth impairment on the *Mastomys* cells. Overall, the C2 variant reached titers up to 1×10^6 FFU/ml on day four post infection. In comparison to the C2 variant, did the E8 variant grow slower in Vero76 and MasKEC. This slower growth on MasKEC, but not on MasEF was of interest for the adaptation experiments, because it might indicate an epithelial cell-specific replication deficit.
In summary, the isolated variants had distinct growth characteristics and all clones except for the C6 clone were used for the adaptation experiments on MasKEC.

5.3.2. Is *in vitro* adaptation of heterologous viruses to *M. natalensis* possible?

Subsequently, the *in vitro* adaptation was conducted for ten consecutive passages on MasKEC with the A11, C2 and E8 variants. The virus growth was evaluated for each passage by qPCR, immune fluorescence (not shown) as well as immunofocus assay. This approach was used to verify not only the presence of viral RNA but also the presence of infectious virus particles. Fluctuations in the infectious virus titers as well as the viral RNA levels were observed in a periodical pattern (see Figure 17).

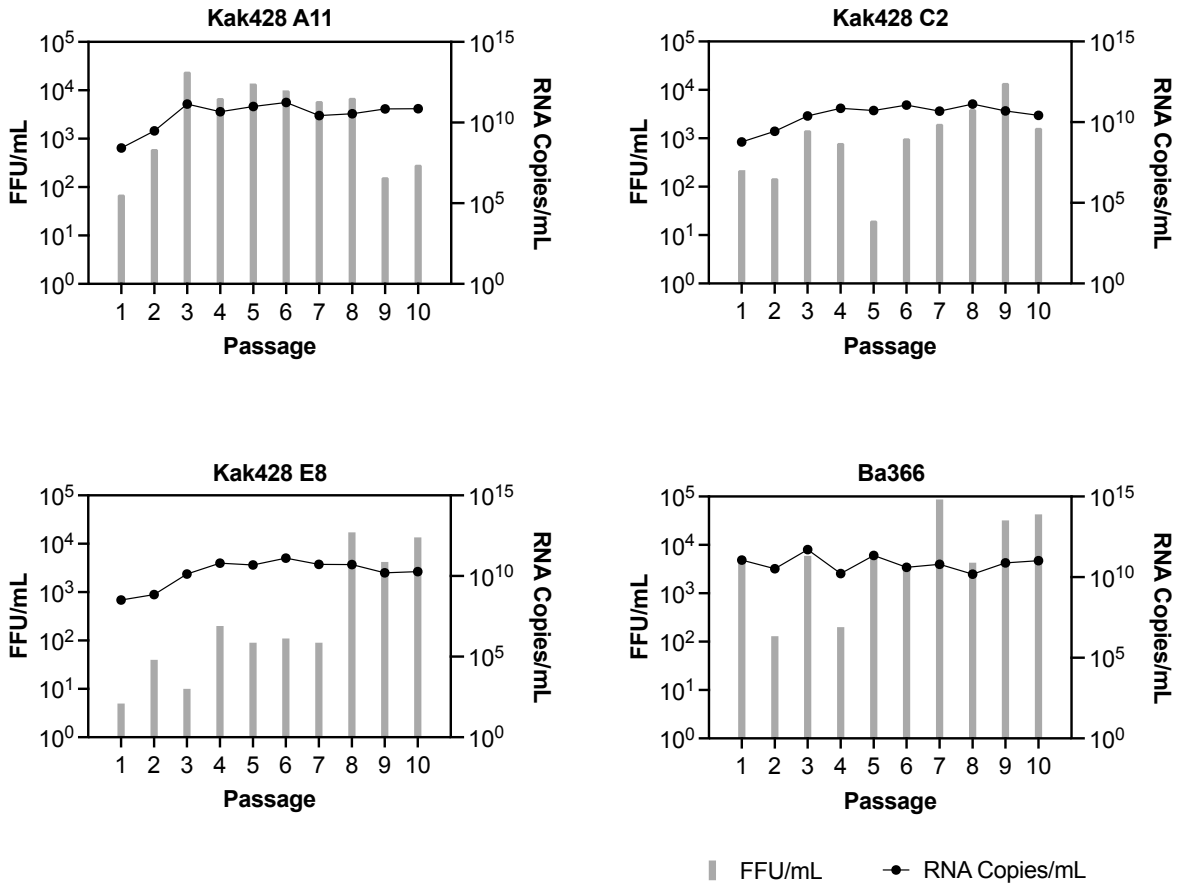

Figure 17: Viral load and copy numbers of the LASV single variants during *in vitro* adaptation experiments. Virus supernatant was harvested from each passage during the *in vitro* adaptation experiments. Viral titers in focus forming units per mL (FFU/mL) were determined by immunofocus assay and are depicted by the bars plotted on the left Y-axis. Viral RNA copies/mL were determined by the Altona 2.0 RealStar LASV L PCR and are shown by the black circles and connecting line plotted on the right Y-axis.

In contrast to the viral RNA copy numbers, which stayed relatively stable during the adaptation process with more than 1×10^{10} RNA copy numbers/mL most of the time, there were strong fluctuations seen for the infectious viral titers. Especially the C2 and E8 variants had viral titers with less than 1×10^3 FFU/mL for the first seven passages of the adaptation. In contrast, the A11 variant reached higher titers already after three passages. Interestingly, the homologous Ba366 strain, which served as a control during these experiments, showed most prominently the typical decrease of infectious virus titers after every other passage seen often for LASV. During all passages, high viral RNA copy numbers and high infectious virus titers were found in the supernatant, hence the *in vitro* adaption was successful. After ten passages on MasKEC, the virus variants were amplified and used for further characterization of the adapted variants *in vivo* and *in vitro*.

5.3.3. How do the growth kinetics of the adapted variants change *in vitro*?

To see if and how the growth kinetics changed after the adaptation process, the growth of the adapted variants was monitored over time (see Supplementary Figure 4). For this, the virus titers of the variants after ten passages (VP10) were compared to those of the initial virus stocks (VP0, see Figure 18).

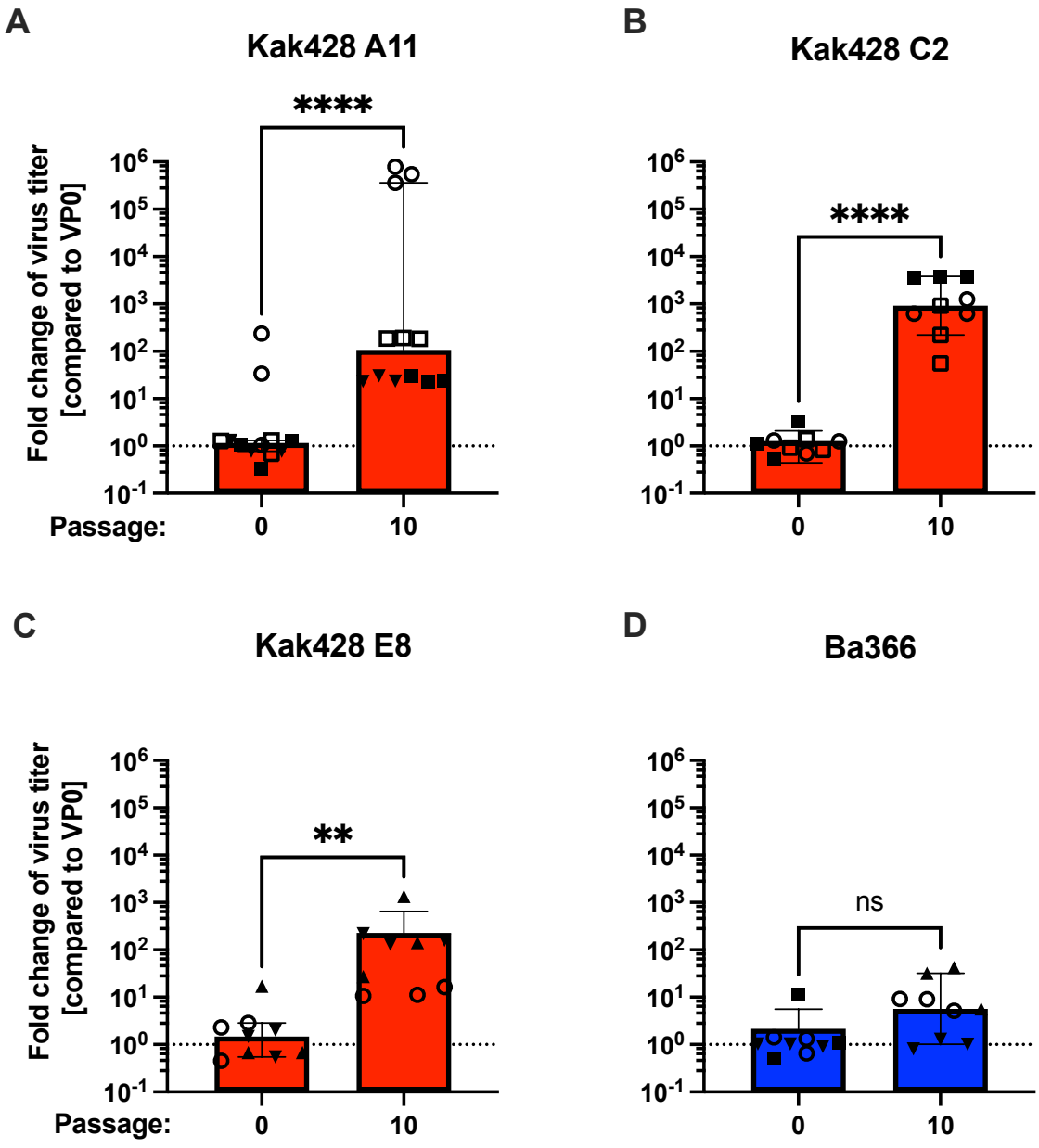

Figure 18: Growth behaviour before (VP0) and after adaptation (VP10) of LASV Kak428 (A-C) and Ba366 (D) on MasKEC. Three different LASV heterologous Kak428 variants (**A-C**) or **D** the homologous Ba366 strain (before the adaptation (VP0) and after passage 10 (VP10)) were used for infection of MasKEC with a MOI of 0.01 for 4 days. Virus supernatant was harvested on days 0, 1, 2, 3 and 4 post infection. Relative changes of the titers for the adapted variants on day 3 post infection compared to the titers of the initial stock are depicted. Viral titers in focus forming units per mL (FFU/mL) were determined by immunofocus assay and the fold change of infected cells compared to the VP0 was calculated. The dashed line indicates unchanged virus titers. The experiment was

repeated three times and experiments were done with three technical replicates per experiment. The data of the different experiments are represented by different symbols. The median with a confidence interval of 95 % and the standard deviation is indicated. A Kruskal-Wallis test was used to test for significant changes. VP = virus passage; ns = non-significant, P > 0.05; **P ≤ 0.01; **** P < 0.0001.

The homologous Ba366 strain served as a control in this experiment as further adaptation and increased virus growth was not expected for this strain. The Ba366 showed an 8-fold median increase of infected cells in the virus passage 10 (VP10) compared to the initial virus stocks (VP0), which was not statistically significant as confirmed with a Kruskal-Wallis test. In contrast, all Kak428 variants showed a more than 100-fold median change of infected cells. Especially the C2 variant seemed to have an accelerated growth characteristic with up to a median change of infected cells of more than 1,000-fold.

In the next step, sub-variants of these VP10 variants were generated via limiting dilution assay to simplify the subsequent correlation of host-adaptive mutations later identified with NGS with changes in growth kinetics. Those VP10 variants were named A11-C3, A11-C4, A11-F6, C2-B2, C2- E3, C2-H1, E8-B6, E8-D2 and E8-G5 respectively. All variants were characterized regarding their growth kinetics on MasKEC. Figure 19 shows the change of virus titers for the sub-variants of the adapted viruses and Supplementary Figure 4 shows the virus growth characteristics in FFU/mL over time. Here, it was observed that changes in the VP10 sub-variants were not always as pronounced as the VP10 variants. Nevertheless, all virus variants of the VP10 except for the A11-F6 variant showed significantly increased virus titers compared to their VP0 origin.

To conclude, *in vitro* adaptation of heterologous LASV strains to MasKEC is possible and results in accelerated growth kinetics.

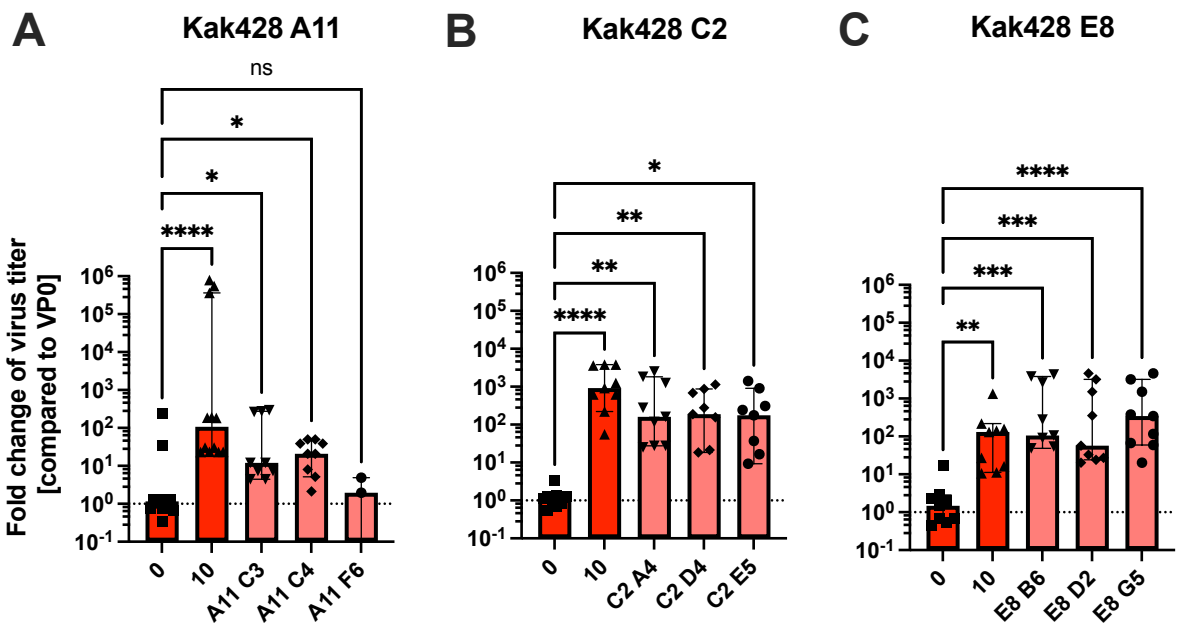

Figure 19: Growth kinetics before (VP0) and after adaptation (VP10) of LASV Kak428 variants (A-C) on MasKEC including the sub-variants after of the VP10 variants. Three different LASV heterologous Kak428 variants (**A-C**) and their subsequent sub-variants were used for a growth kinetic to compare viral titers before the adaptation (VP0) and after passage 10 (VP10). Infection was done on MasKEC with a MOI of 0.01 for 4 days. Virus supernatant was harvested on days 0, 1, 2, 3 and 4 post infection, depicted here is data from day 3 post infection only. Viral titers in focus forming units per mL (FFU/mL) were determined by immunofocus assay and the fold change of virus titers to the VP0 was calculated. The dashed line indicates unchanged viral titers. The experiment was repeated three times and experiments were done with three technical replicates per experiment each. The median with a confidence interval of 95 % and the standard deviation are shown. Data for the VP0 and VP10 was shown in Figure 18 already. A Kruskal-Wallis test was used to test for significant changes. ns = non-significant, $P > 0.05$; * $P \leq 0.05$; ** ≤ 0.01; *** $P \leq 0.001$; **** $P < 0.0001$.

5.3.4. Which genes accumulate potential host-adaptive mutations?

To identify potential host-adaptive mutations, the sequences of the adapted single virus variants and their sub-variants were determined with Illumina Next Generation Sequencing. All virus passages from 0 to 10 as well as the sub-variants of the VP10 were screened for potential host adaptive mutations by performing the following steps: (i) quality control, (ii) mapping and (iii) variant calling on the Galaxy EU server. The alignment (iv) was visualized in the integrative genomics viewer (IGV).

First, the data of the adaptation experiment was analyzed, which included samples of all passages ranging from the initial (VP0) viruses to VP10 adapted variants before the VP10 viruses were further separated by limiting dilution assays. Sequencing of the VP2 and VP3 variants was challenging as those had an average coverage of <1000 reads for almost all variants. This low coverage was problematic, as it was not possible in some regions to distinguish between SNPs and sequencing errors. The same was true for the VP10 of the C2,

the VP9 of the E8 and the VP7 of the Ba366 strain (see Supplementary Table 5 and Supplementary Table 6). The coverage plots for each variant and passage is shown in Supplementary Figure 5. Major variants, meaning mutations that occurred with a frequency of more than 10 %, were considered in this analysis. Interestingly, no dominant mutations were found throughout the adaptation of the homologous Ba366 strain. For all three Kak428 variants however, a total of ten major variants were identified during the ten passages on MasKEC.

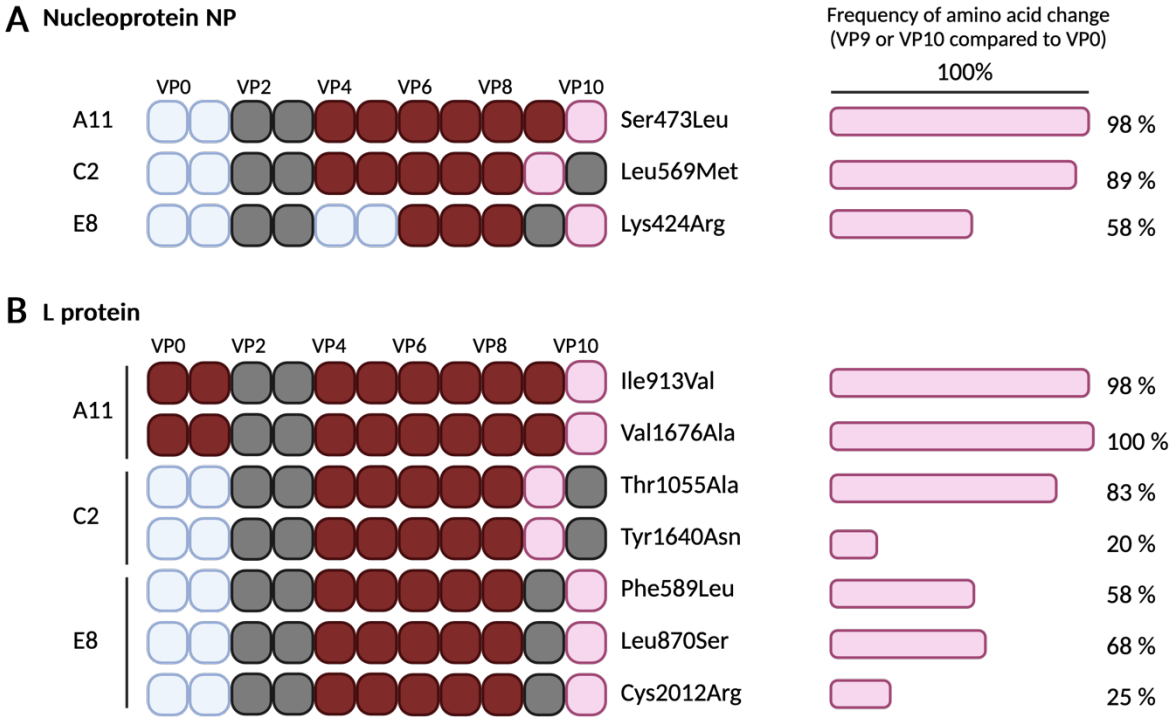

Figure 20: Overview of Kak428 variants' mutations during the *in vitro* adaptation experiments on MasKEC. The mutations in **A** the nucleoprotein, and **B** the L protein were identified in each virus passage. The first occurrence of this mutation in the different virus variants and following virus passages are shown in red rectangles. Blue rectangles indicate the presence of the original sequence, and grey rectangles indicate very low confident sequences due to low coverage. The frequency of the base exchanged at the last passage (VP9 or VP10, marked in pink) with a coverage >1000 depth is shown on the right. This figure was created with BioRender.com.

Figure 20 shows all mutations identified in the passages VP0-10 via NGS for the different genes. Three mutations were identified in the nucleoprotein, namely Ser473Leu, Leu569Met and Lys424Arg. The first two of them were found in high frequencies of 98 % and 89 % respectively in the A11 and C2 variants, whereas the Lys424Arg mutation was only found in 58 % of the sequences of the E8 variant. Moreover, seven mutations were mapped to the L gene. Two of them, the Ille913Val and Val1676Ala mutations, were identified in the A11

variant and were present already with frequencies of 98 % and 100 % before the adaptation process started, so the A11 variant was genetically different than the other variants from the beginning of the experiment. The C2 variant acquired a high frequency (83 %) of the Thr1055Ala mutation. The other mutations in the L gene occurred only in 20-68 % of the analyzed samples (Tyr1640Asn in C2 and Phe589Leu, Leu870Ser and Cys2012Arg in E8).

Overall, the experiment led to a quick adaptation of the virus to the heterologous host cells as all changes occurred within the first six virus passages and at high frequencies with more than 50 %. Notably, no mutations were mapped to the GP and Z genes in this first dataset.

After having analyzed the first dataset with all passages including the VP10 variants, the second dataset with the VP10 sub-variants generated through another limiting dilution assay was analyzed.

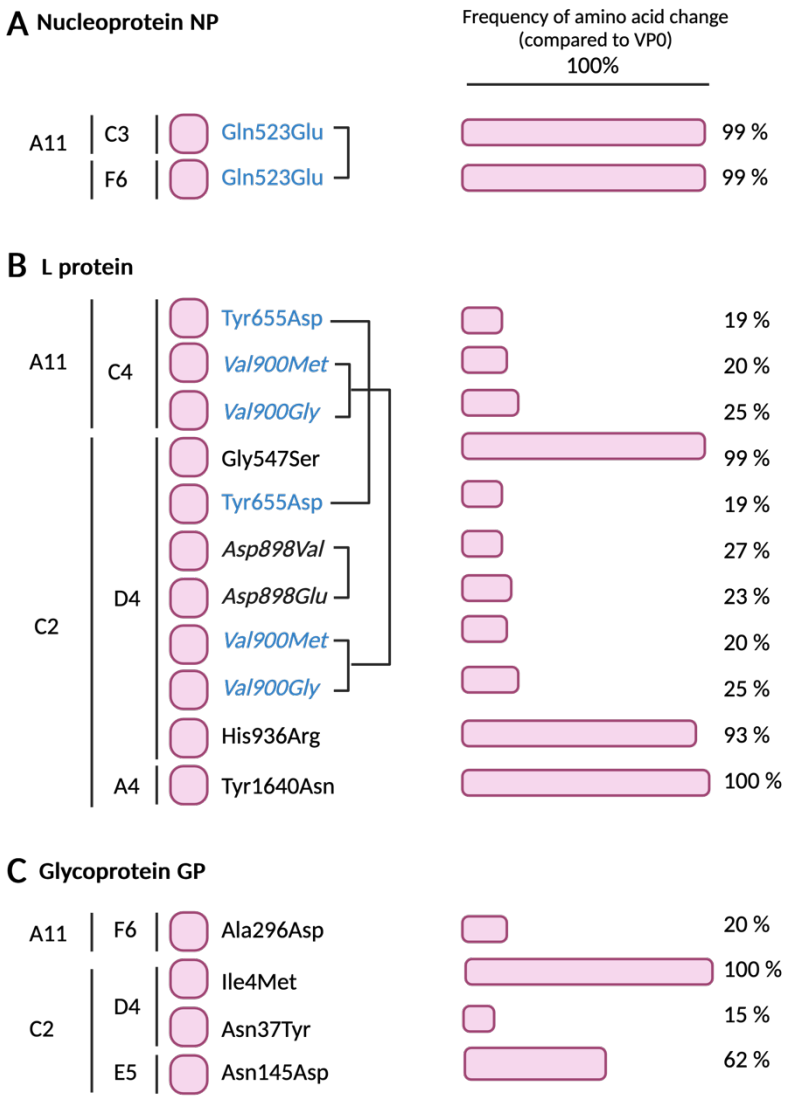

Figure 21: Overview of mutations identified in the Kak428 VP10 sub-variants after the *in vitro* adaptation experiments on MasKEC. After the adaptation experiments, sub-variants of the VP10 variants were generated by limiting dilution assay and analyzed by NGS. Identified mutations (red rectangles) in **A** the nucleoprotein, **B** the

L protein and **C** the glycoprotein are displayed with their frequency of occurrence. If a mutation was found in more than one sub-variant, blue font was used and the mutations were linked by brackets. If one gene locus showed two non-synonymous mutations, italics were used and they were linked with brackets. This figure was created with BioRender.com.

Here, it was noted that only the A11 and C2 sub-variants showed additional mutations compared to the consensus sequence of the VP10 variants, whereas the E8 sub-variants were identical to the E8 VP10 mixture. Only one additional mutation was mapped to the NP gene. However, seven positions were identified to have mutated in the L gene, and four mutations were mapped to the GP gene. The newly identified NP mutation Gln523Glu was found in two independent sub-variants of A11 (A11-C3 and A11-F6) with a frequency of up to 99 %. In the L gene, the Gly547Ser, His836Arg and Tyr640Asn mutations were the most abundant ranging from 93 - 100 %. The other mutations were only found in a maximum of 27 % of the sequenced reads. Interestingly, two loci were observed, in which a non-synonymous base exchange happened, resulting in viral quasispecies with two different mutations at the same time. One example is the C2-D4 variant at position 898, where an exchange from aspartic acid to valine occurred with a frequency of 17 %. Simultaneously, in the C2-D4 variant, a transition from aspartic acid to glutamine was seen with a frequency of 23 % in the same position. For the GP gene, dominant mutations were identified during our experiments for the first time. Here, the frequency of the observed mutations ranged from 15-100 %, with the Ille4Met and Asn145Asp mutations in the C2 variant being observed more frequently than the Ala296Asp and Asn145Asp mutations.

After having identified the mutated amino acids in both datasets of the adapted Kak428 variants and their sub-variants, these were mapped to their respective protein domains as shown in Figure 22 to evaluate their potential contribution to the changed growth phenotypes as described in 5.3.3.

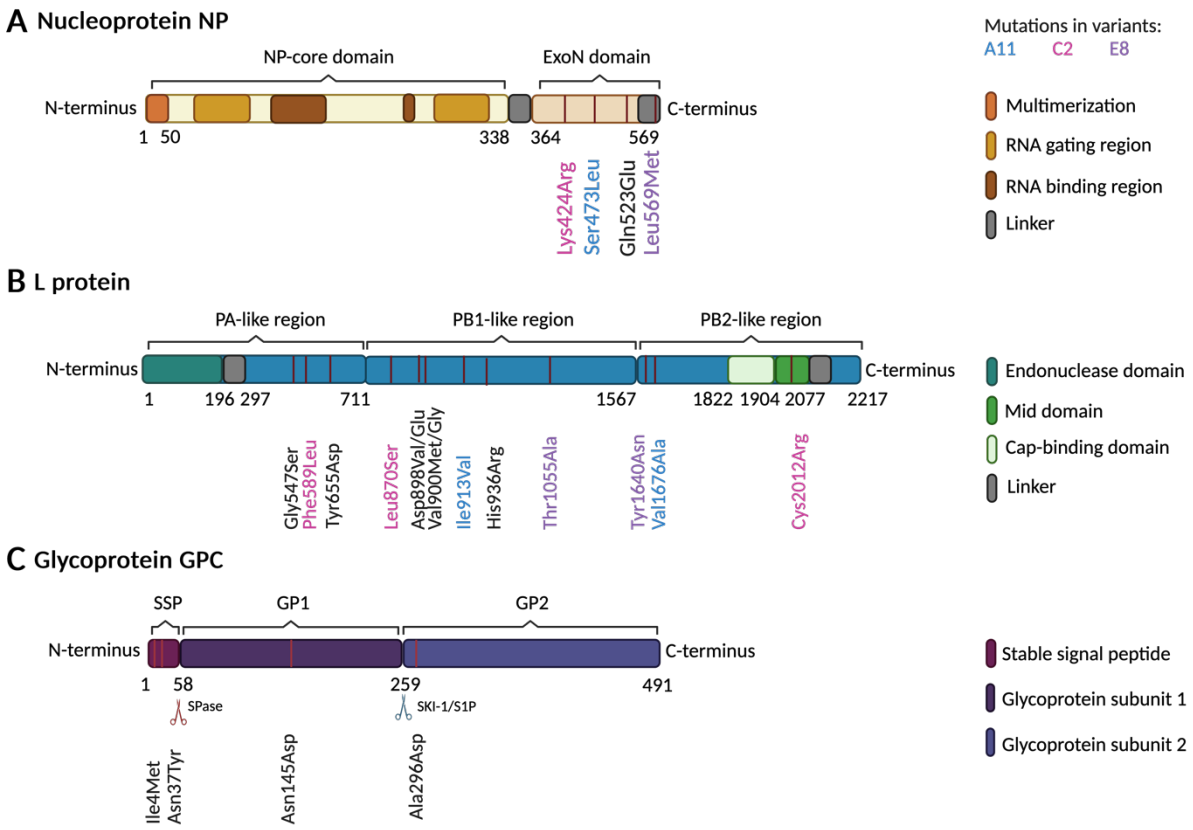

Figure 22: Mutations observed during *in vitro* adaptation experiments with potential influence on host adaptation. The occurring mutations in **A** the nucleoprotein, **B** the L protein and **C** the glycoprotein were mapped to their respective position in the protein domains. A11 variant mutations are shown in blue, C2 in purple and E8 in pink; the mutations of the VP10 sub-variants are shown in black. ExoN = Exonuclease domain, PA-like domain = polymerase acidic protein-like domain, PB1-like region = polymerase basic protein-like 1 region, PB2- like region = polymerase basic protein-like 2, SSP = stable signal peptide, GP1 = Glycoprotein subunit 1, GP2 = Glycoprotein subunit 2, SPase = cellular signal peptidase, SKI-1/S1P = subtilase/kexin isozyme-1. The scheme was adapted from [201] (NP), [202] (L), and [203] (GP). This figure was created with BioRender.com.

Also, amino acid alignments were generated in MacVector by using the Clustal W algorithm and aligning the Ba366 and Kak428 sequences to *Mastomys*-derived sequences such as the MAD39 strain and isolates from *Mastomys*, that were trapped in households of LASV-infected persons (named Z0947-SLE-2011 and Z0948-SLE-2011). The GP alignment revealed, that the Kak428 strain acquired mutations during the adaptation experiments only in conserved regions, in which all isolates initially had the same amino acids (see Supplementary Figure 10). The same was true for the NP alignment, with the exemption of the Gln523Glu mutation, where the other isolates all had a glutamic acid instead (see Supplementary Figure 8). For the L protein alignment (see Supplementary Figure 10), more mutations occurred in regions, where the Kak428 had a different amino acid initially than the other strains. Examples of this were the Val900Met or Val900/Gly mutation, as the *M. natalensis*-derived strains all had an

alanine or the His936Arg position, whereas the other strains presented a glycine. Most interesting was the Ille913Val mutation, because some of the other strains had a valine in this position as well as the Tyr1640Asn mutation, as in this position some of the *M. natalensis*-derived strains carried an asparagine as well. To conclude, most mutations occurred in rather conserved regions, but especially for one of the NP as well as two of the L mutations, a trend towards the amino acids carried by the other strains was observed.

In addition, 3D protein models for the Kak428 proteins were predicted with the artificial intelligence tool AlphaFold2 for the NP and L protein. For the Kak428 GP, the AlphaFold2 model was not reflecting the expected trimeric structure. Instead, the 8ejd structure of the LASV Josiah strain GP, which has been determined by electron microscopy, has been used for mapping the mutations [204]. The protein domains were colored in Pymol and the mutations found during the adaptation process were highlighted as sticks in either red or yellow, dependent on their identified origin, either VP10 variants (red) or the VP10 sub-variants (yellow). The protein models are depicted in Figure 23 to Figure 25, and the corresponding quality measures can be found in the Supplementary Figure 6 to Supplementary Figure 7.

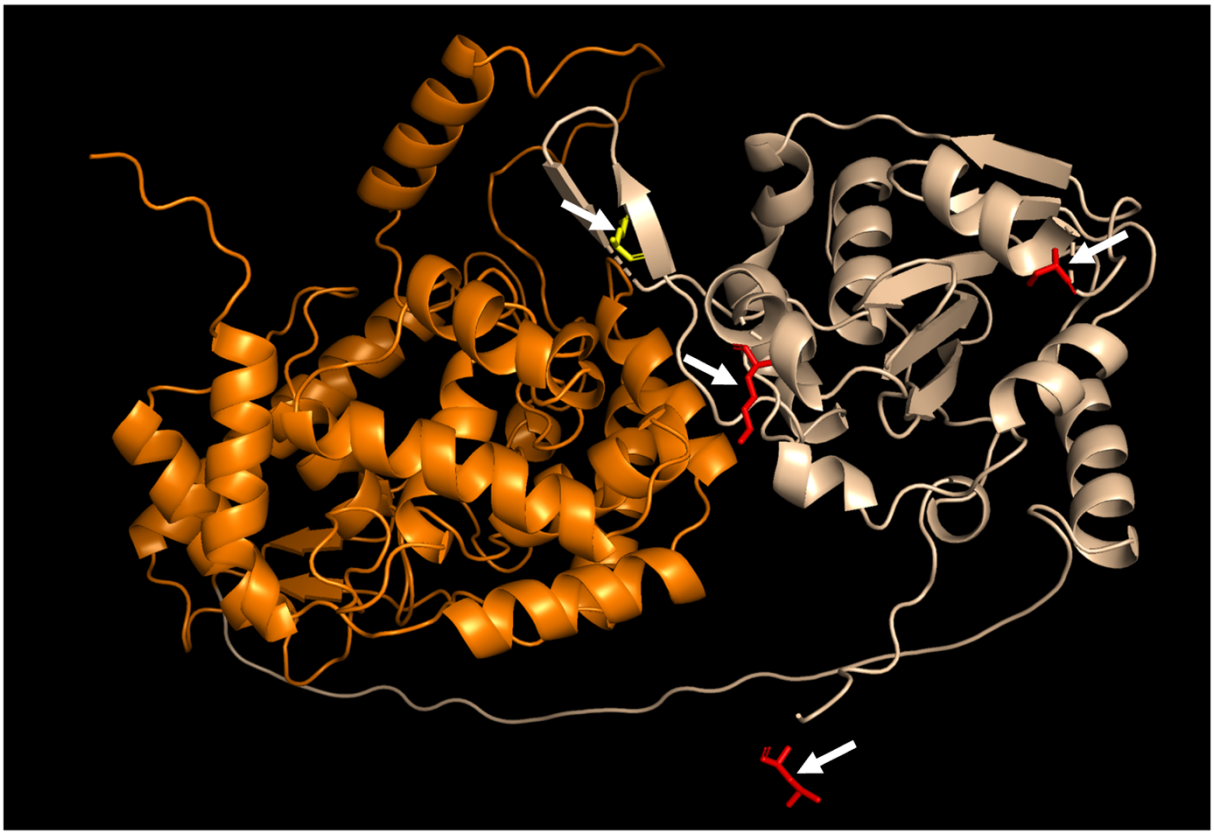

Figure 23: Model of the protein structure of the Kak428 NP generated with AlphaFold2. The NP-core domain is

colored in orange and the exonuclease domain in wheat. Marked in red are all mutations of the VP10 variants gained during the adaptation process and all mutations identified in the sub-variants are marked in yellow. The mutations are additionally highlighted with white arrows. The models were generated with AlphaFold2 and colored in Pymol.

All mutations found in the NP (Gln523Glu, Ser473Leu and Lys424Arg) were mapped to the exonuclease domain, with the Leu569Met mutation being located at the very end of the C-terminus (see Figure 23).

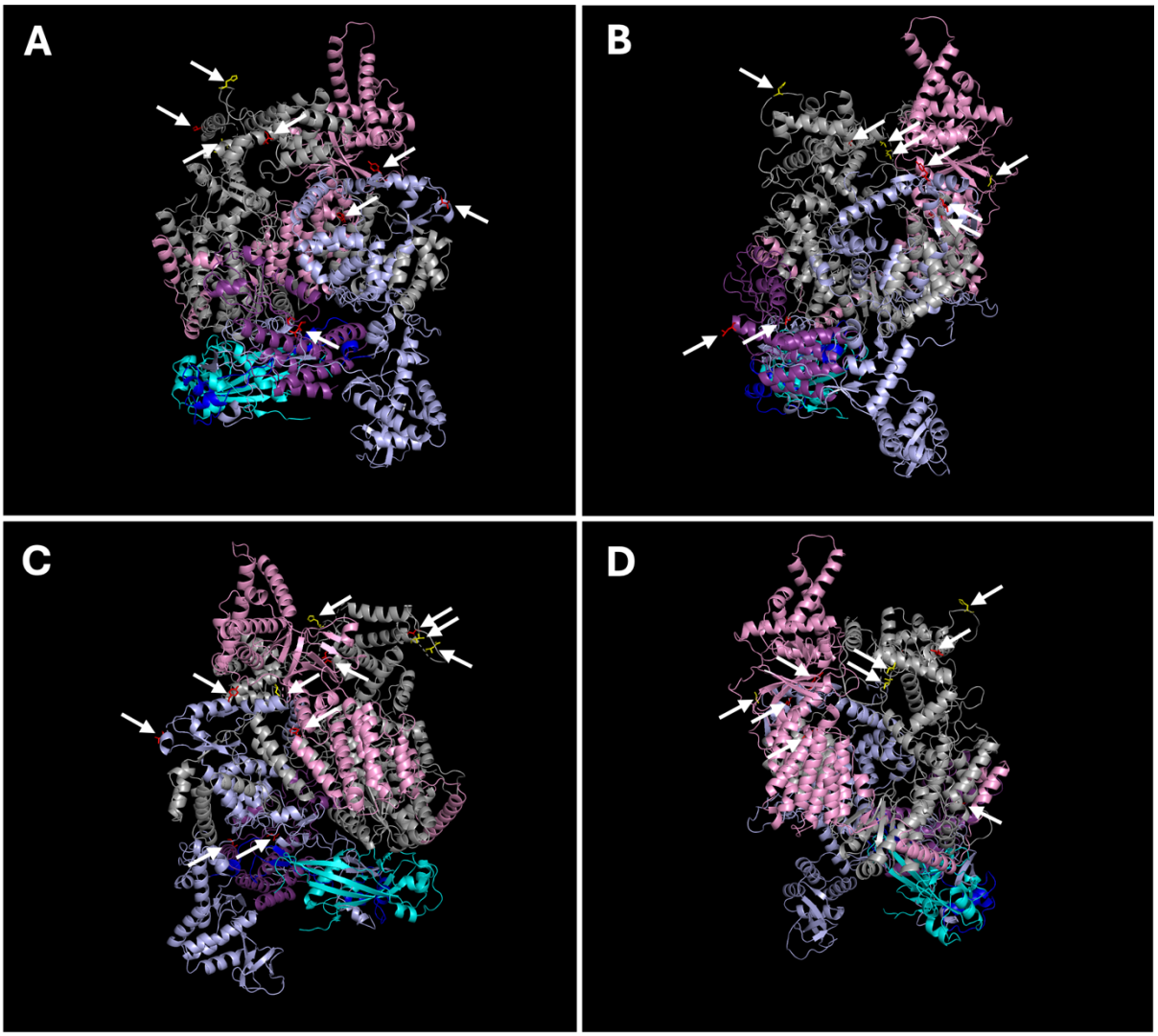

Figure 24: Protein structure model of the Kak428 L generated with AlphaFol2d. Shown in purple is the endonuclease domain, and the rest of the PA-like region in pink. The PB1-like region is colored in light grey, the PB2-like region in dark grey, the CBD in cyan and the mid domain in dark blue. Marked in red are all mutations of the VP10 variants gained during the adaptation process and marked in yellow are all mutations identified in the sub-variants. The mutations are additionally highlighted with white arrows. The models were generated with AlphaFold2 and colored in Pymol.

The mutations identified in the L protein were mapped to several domains. In the polymerase acidic (PA)-like region, three mutations, namely Gly547Ser, Phe589Leu and Tyr655Asp, were found. Six mutations were identified in the polymerase basic (PB1)-like region (Leu870Ser, Asp898Val/Glu, Val900Met/Glu, Ille913Val, His936Arg and Thr1055Ala) and three (Tyr1640Asn, Val1676Ala and Cys2012Arg) mapped to the PB2-like region (see Figure 24).

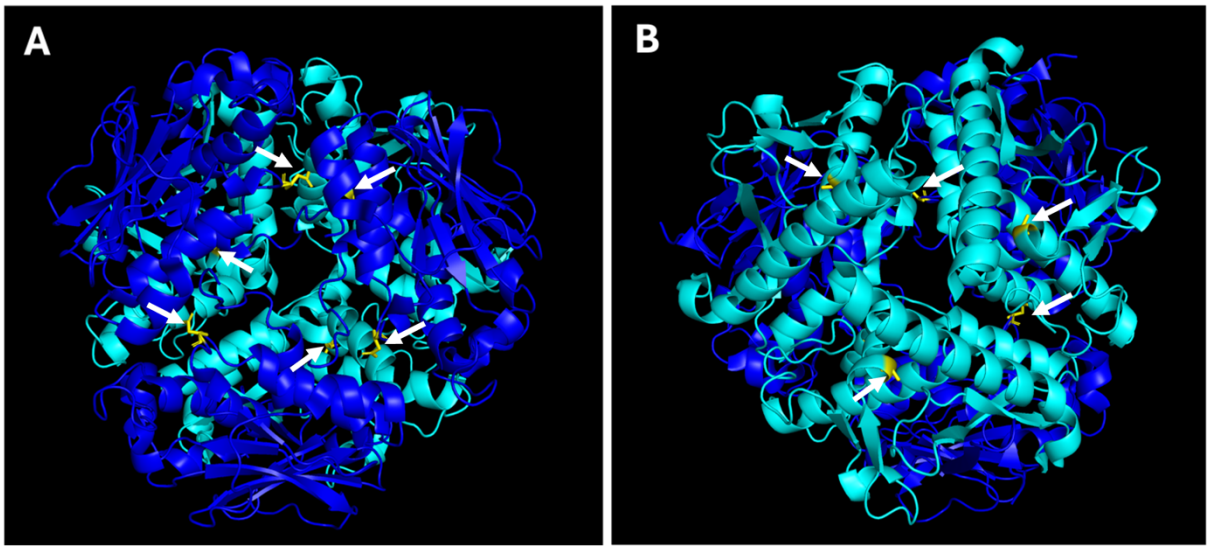

Figure 25: Model of the protein structure of the Josiah GP 8ejd. Shown here are the GP1 (dark blue) and GP2 (cyan) domains from amino acid 59 onwards. Marked in yellow are all mutations identified in the sub-variants. The mutations are additionally highlighted with white arrows. The model 8ejd was downloaded from the protein database and colored in Pymol.

Surprisingly, only four mutations identified in the GP gene were found in the VP10 sub-variants. Two of those (Ille4Met and Asn37Tyr) were found in the SSP, one on the GP1 subunit (Asn145Asp) and one at the beginning of the GP2 subunit (Ala296Asp). Shown in Figure 25 is the electron microscopy-derived structure of the Josiah GP. Since in this model the first 58 amino acids are missing, it was only possible to map the Asn145Asp and Ala296Asp mutations.

To summarize, major variants only occurred in the Kak428 variants after adaptation, whereas none were identified in the Ba366 strain. The GP, L and NP genes of the Kak428 accumulated mutations during the adaptation process. The frequency of the major variants ranged from 15-100 %. In the initial dataset, ten major variants were identified, which exclusively mapped to the NP and L genes, whereas four of the ten mutations found in the dataset of the sub-variants mapped to the GP. No mutations were observed for the Z gene.

5.3.5. Did the *in vitro* adaptation result in *Mastomys*-specific adaptations?

To confirm that the *in vitro* adaptation process resulted in *Mastomys*-specific adaptations and that those are not solely cell culture adaptation artefacts without major impact on the *in vivo* behavior of the virus, one week old *M. natalensis* were infected with the VP10 adapted viruses for four weeks, while monitoring the infection in the organs and blood. These *in vivo* experiments were required as cell culture experiments cannot mimic a complete organism including its immune system. *M. natalensis* were infected with 10,000 FFU of the VP10 variants as well as the Kak428 wt strain. Data for the latter strain was generated during previous experiments and included in this analysis are historical controls. During these experiments, 2-4 individuals were sacrificed every week for up to four weeks post infection to check for the presence of virus in the blood and various organs. Figure 26 shows the virus titers in the organs (for details of the organ titers see Supplementary Table 7, Supplementary Table 8, and Supplementary Table 9) and Figure 27 shows the virus RNA copy numbers in the blood and urine.

Previous experiments with the Kak428 wt strain showed viral clearance after 2 w. p. i. in all sampled organs (see Figure 26 A). During the first week post infection, virus was found in almost all organs, except ovaries, whereas the virus presence was limited to the salivary gland, lung and brain at 2 w. p. i.. For the A11 VP10 variant, the initial virus titers in the lung, heart, salivary gland, and testis were with up to 8×10^4 FFU/g strikingly higher than what was seen for the Kak428 wt, which had maximum titers of 7×10^3 FFU/g in the heart (see Figure 26 B). No infectious virus was present in any of the remaining organs from 2 w. p. i. onwards otherwise. The exemption were the thymus and the eyes, which were still positive 3 and 4 w. p. i. respectively in some animals, as well as the brain, which was still positive 4 w. p. i.. Infectious virus was only present in the thymus, eyes and salivary gland at 1 w. p. i.. No virus was found in any of the tested organs at later timepoints. The same was true for the C2 VP10 adapted Kak428 strain, as infectious virus particles were only found in very few organs already one week post infection (see Figure 26 C). The only organs that tested positive at any timepoint were the eyes, salivary gland and thymus with the highest titer being in the eye with 5×10^2 FFU/g. In contrast to the Kak428 wt control and the A11 VP10 variant, the C2 VP10 variant showed a weak virus presence and accelerated clearance. The Kak428 wt strain replicated in the lung, heart, spleen, salivary gland, brain, and testes in the first week post infection. Thus, an accelerated clearance of this C2 VP10 variant in *M. natalensis* was

observed. Similar to the Kak428 wt strain was the E8 VP10 variant cleared over the course of several weeks. The titers in the organs ranged from 4×10^1 FFU/g to 2×10^5 FFU/g with the lung having the highest titers (3×10^5 FFU/g). Furthermore, the salivary glands from the E8 VP10-infected *Mastomys* remain still virus-positive after 3 w. p. i. for the adapted strain compared to the Kak428 wt, which was already cleared at that time point. Most interesting was the apparent eye-tropism of the adapted A11 and E8 variants. The presence of virus in the eye for up to 4 w. p. i. for the A11 and E8 adapted variants demonstrated the virus´ ability to replicate and 'hide' in an immune-privileged site.

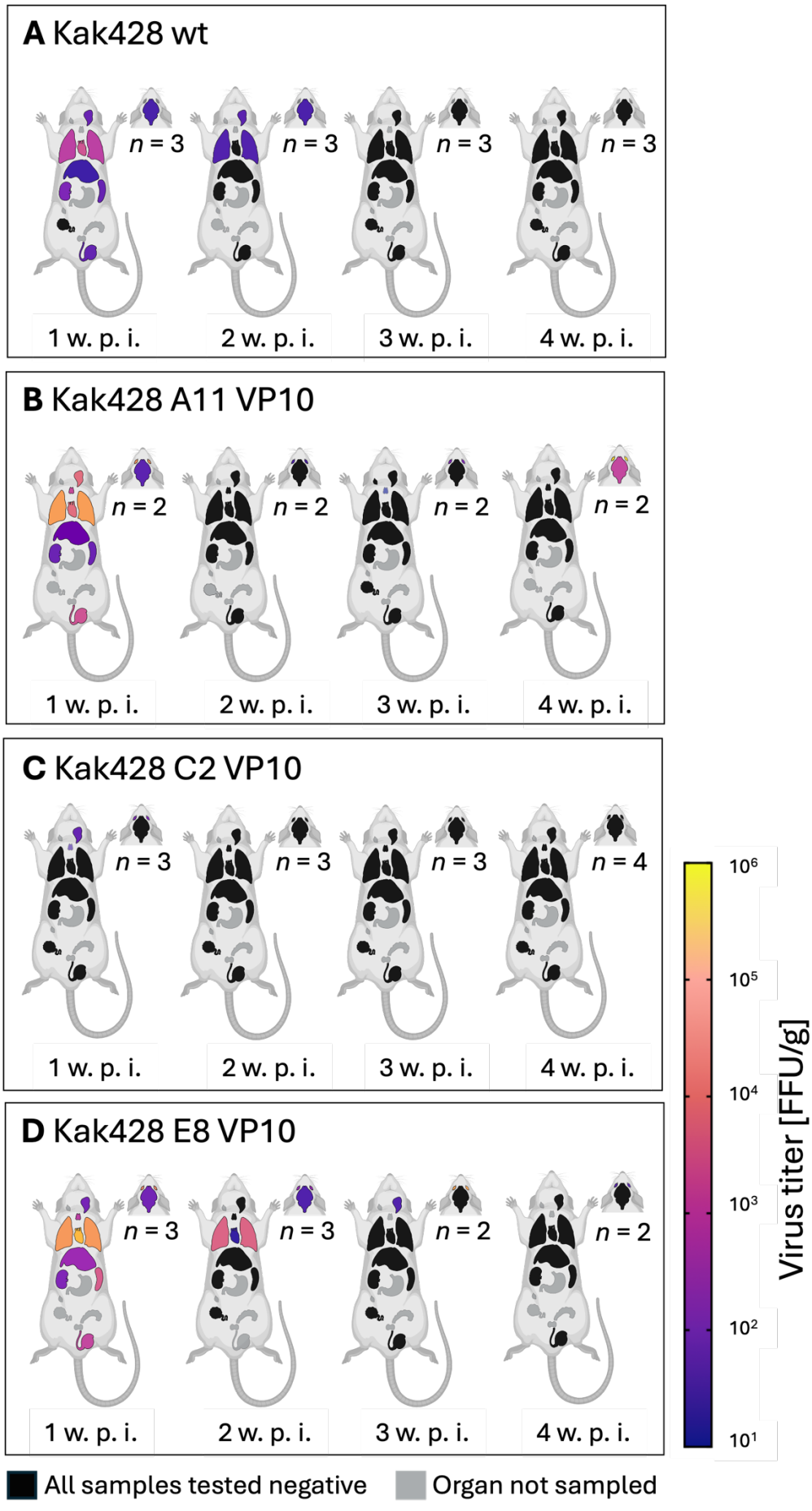
A Kak428 wt
n = 3
n = 3
n = 3
n = 3
1 w. p. i.
2 w. p. i.
3 w. p. i.
4 w. p. i.
B Kak428 A11 VP10
n = 2
n = 2
n = 2
n = 2
1 w. p. i.
2 w. p. i.
3 w. p. i.
4 w. p. i.
C Kak428 C2 VP10
n = 3
n = 3
n = 3
n = 4
1 w. p. i.
2 w. p. i.
3 w. p. i.
4 w. p. i.
D Kak428 E8 VP10
n = 3
n = 3
n = 2
n = 2
1 w. p. i.
2 w. p. i.
3 w. p. i.
4 w. p. i.
Virus titer [FFU/g]
10⁶
10⁵
10⁴
10³
10²
10¹
All samples tested negative
Organ not sampled

Figure 26: Virus titers of *M. natalensis* infected with adapted Kak428 strains. *M. natalensis* were s. c. infected at an age of day 7-9 post birth with 10,000 FFU of **A** Kak428 wt, or the VP10 variants of **B** Kak428 A11, **C** Kak428 C2, **D** Kak428 E8. The number of animals euthanized (*n)* at each time point (w. p. i., weeks post infection) is shown. Organs are shown as schematic: eyes, brain, salivary glands, cervical lymph nodes, thymus, lung, heart, liver, spleen, kidneys, ovaries and testes. Eyes have not been sampled of the Kak428 wt strain. Viral titers in focus forming units per gram tissue (FFU/g) of *M. natalensis* organs were determined by immunofocus assay. Geometric means of LASV-titers are depicted as spectral heat map with blue as limit of detection. Negative samples have been assigned a default value at the limit of detection: 10^1 FFU/g; max. value yellow: 10^6 FFU/g; orange: 10^4 FFU/g; pink: 10^3 FFU/g; purple: 10^2 FFU/g; black: all samples at that timepoint were tested negative, grey: organs not sampled. Data from **A** are historical controls of [157] and shown here for reference purposes. This figure was created with BioRender.com.

The course of infection in the blood resembled the observations in the organs (see Figure 27). Previous experiments with Kak428 wt infected *M. natalensis* proved the virus to be cleared from the blood within 2 w. p. i. after reaching a maximum virus titer with 1×10^7 RNA copies/mL. For the A11 VP10 variant, viremia was detected in all tested animals with up to 1×10^6 RNA copies/mL during the first week post infection. No virus RNA was present in blood at later time points. Similarly, for the C2 VP10 variant, low levels of viremia (1×10^4 RNA copies/mL) were only present during the first week, and only in one of three animals. The Kak428 E8 VP10 variant led to the highest virus titers in the blood with up to 1×10^8 RNA copies/mL and viremia could still be detected at 1×10^5 RNA copies/mL in a single individual at 2 w. p. i.. No viremia was detected at later time points. Antibodies were detected for the A11 and E8 VP10 variants from 2 w. p. i. onwards, whereas animals inoculated with the C2 VP10 variant already developed antibodies 1 w. p. i..

Taking these results together, the *in vivo* studies in *M. natalensis* with MasKEC-adapted virus variants did not in all variants result in *M. natalensis*-specific adaptations that increased virulence *in vivo*. While the A11 and E8 variants induced a longer viremia in the animals compared to the non-adapted Kak428 wt, the C2 variant was cleared even faster.

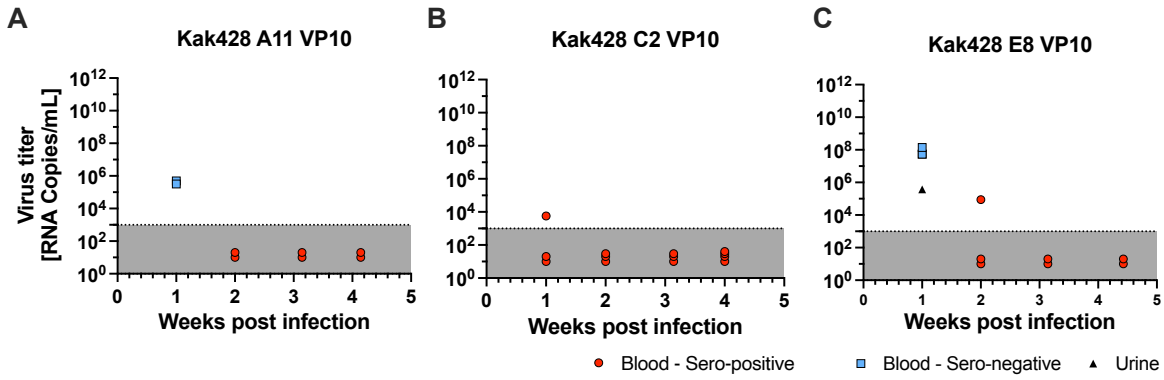

Figure 27: Longitudinal analysis of blood and urine samples from LASV-infected *M. natalensis* experimentally infected with the Kak428 VP10 adapted variants. Virus titers in blood (RNA copies/mL; red circles for sero-

positive individuals and blue squares for sero-negative individuals) and urine (RNA copies/mL; black triangles) are shown over time. Animals were inoculated at day 7-9 post birth with 1,000 FFU of the VP10 variants of **A** the Kak428 A11, **B** the Kak428 C2, **C** the Kak428 E8. The blood was sampled at weekly intervals and tested for the presence of LASV RNA via qRT-PCR with the Altona RealStar 2.0 PCR for the LASV L gene. The ct values were converted into copy numbers by using a standard curve. The shaded area indicates the limit of detection (LoD) of the qRT-PCR assay. PCR-negative samples were assigned a default value below the LoD.

5.4. Which step of the virus life cycle restricts LASV from spillover into new host species?

The findings of previous infection experiments with chimeric viruses indicated a major importance of the transcription and replication as well as the entry processes for LASV to overcome the virus-host barriers. These observations have been supported by the adaptation experiments, during which potential host-adaptive mutations only occurred in the L, NP and GP genes, which are known for their relevance in the named processes. The earlier experiments all focused on the production of progeny virus, making it impossible to strictly distinguish between the single life cycle steps of a virus, as these steps are closely interlinked in a full virus context. To be able to dissect the single life cycle steps further, during the last experiments of this study virus life cycle modelling systems were applied. These systems allow working under BSL-2 conditions and can e.g. help to gain insights into viral processes such as entry or transcription and replication independently of other the viral life cycle processes.

5.4.1. Virus entry

Virus entry is a complex process including attachment, internalization and viral release from the endosomes into the cytoplasm. Here, a pseudotyped, recombinant, and replication-competent Vesicular stomatitis virus system was used, which carried the LASV glycoproteins on its surface instead of its own GP, indicated by “VSVΔG”. It was developed by the group of Dr. Thomas Strecker (Philipps University Marburg) and allowed to analyze virus entry facilitated by the different LASV glycoproteins completely independent from e. g. transcription and replication or virus budding. As a surrogate for the Kak428 strain, a pseudotyped virus named as VSVΔG/LASVGP_LinVI was used. As the VSV system was not readily available with the Ba366 GP, the Josiah GP (human isolate; closely related to LASV strains isolated from *Mastomys* species) was used as a surrogate, later named as VSVΔG/LASVGP_LinIV. The Josiah strain belongs to lineage IV, the same as the Ba366 strain. Complementary experiments also

have been executed with authentic LASV Kak428, and Ba366 wt strains to validate the observations with the VSV system.

5.4.1.1. Does the LASV GP from heterologous viruses mediate efficient entry into M. natalensis cells?

As the glycoprotein of arenaviruses mediates cell attachment and entry, it was assessed if the GP of both virus strains, the surrogate homologous Josiah strain as well as the heterologous Kak428 strain, could efficiently mediate cell entry into VeroE6, MasKEC as well as MasEF. The cells were infected with recombinant and replication-competent VSVΔG/LASVGP_LinIV (Josiah) or VSVΔG/LASVGP_LinVI (Kak428). The replication and transcription machinery of these viruses originates from the same virus. Thus, the entry process in this system was only dependent on the virus glycoproteins. The cells were stained for LASV GP (green), actin (red) and the nucleus (blue). In contrast to uninfected control cells (mock), all tested cell lines were positively stained for the LASV GP indicating an efficient cell entry (see Figure 28).

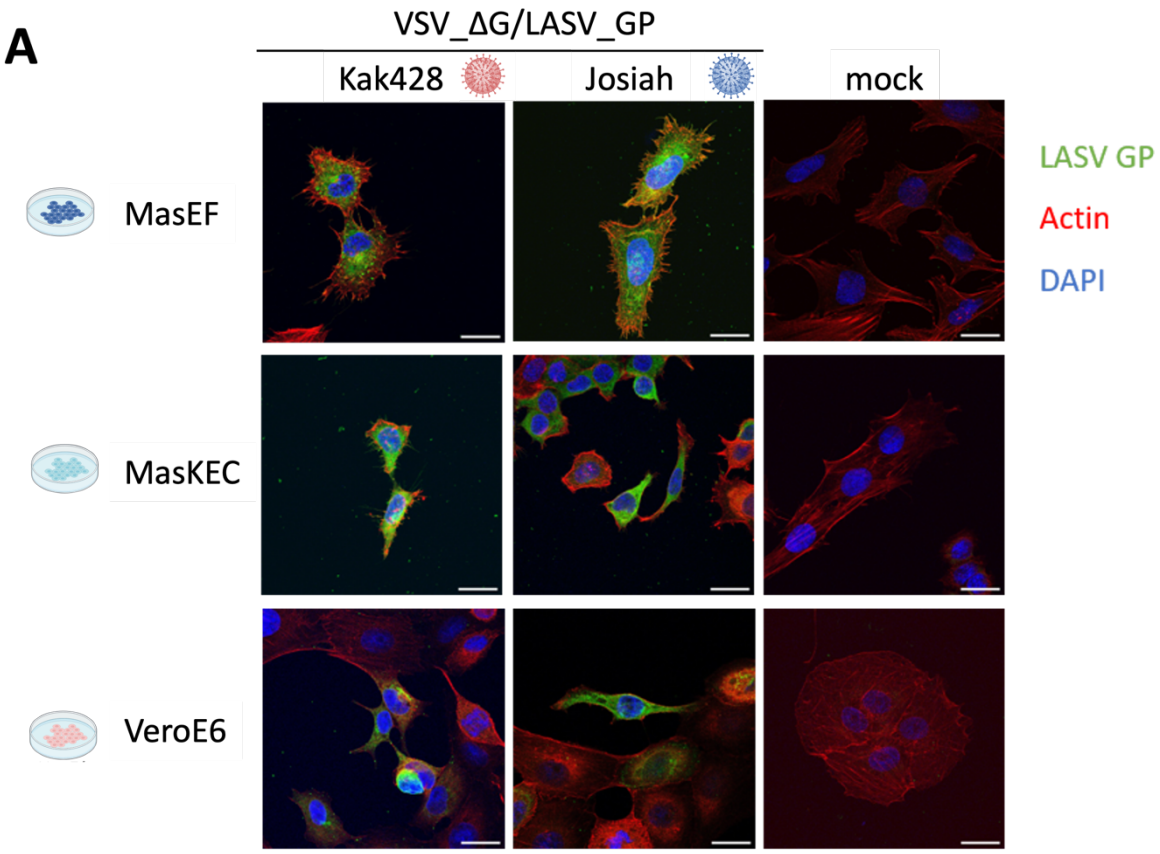

Figure 28: Pseudotyped LASV cell entry visualized by immunofluorescence confocal laser scanning microscopy. MasEF, MasKEC or VeroE6 cells were infected with recombinant and replication-competent VSVΔG/LASVGP_LinIV (Josiah) or VSVΔG/LASVGP_LinVI (Kak428) for 18 h with an MOI of 0.1. Staining was done with anti-LASV GP2 (human 37.7.H antibody; green), actin (red) and DAPI (blue), scale bar 20 µm. This figure was created with BioRender.com.

In addition, growth kinetics with the same viruses were performed (data not shown, data collected in collaboration with Sarah Müller-Aguirre, manuscript in preparation). Those data indicate no major impairment on the Kak428 GP in comparison to the Ba366 GP.

5.4.1.2. Is the entry of authentic LASV into M. natalensis cells restricted?

To confirm the efficient cell entry of the different LASV strains into *M. natalensis* in the full virus context, single-round infections of Vero76, MasKEC and MasEF with authentic LASV were performed under BSL-4 conditions. Here, the signals obtained resulted only from the initially infected cells, as the used overlay medium only allowed cell-to-cell spread, and prevented virus transmission via the medium. Figure 29 shows the infection rate changes for Kak428 normalized to Ba366 for the three cell lines. On Vero76 cells, the Kak428 strain showed no impairment but a trend towards slightly higher infection rates, which might be explained by the fact, that the virus titers of both viruses were always determined on Vero76 cells. In contrast to this observation were the findings on *Mastomys*-derived cells. On both *Mastomys* cell lines, MasKEC and MasEF, was the entry process about 50 % less efficient. This could imply a specific entry deficit of the Kak428 strain into *Mastomys* cells.

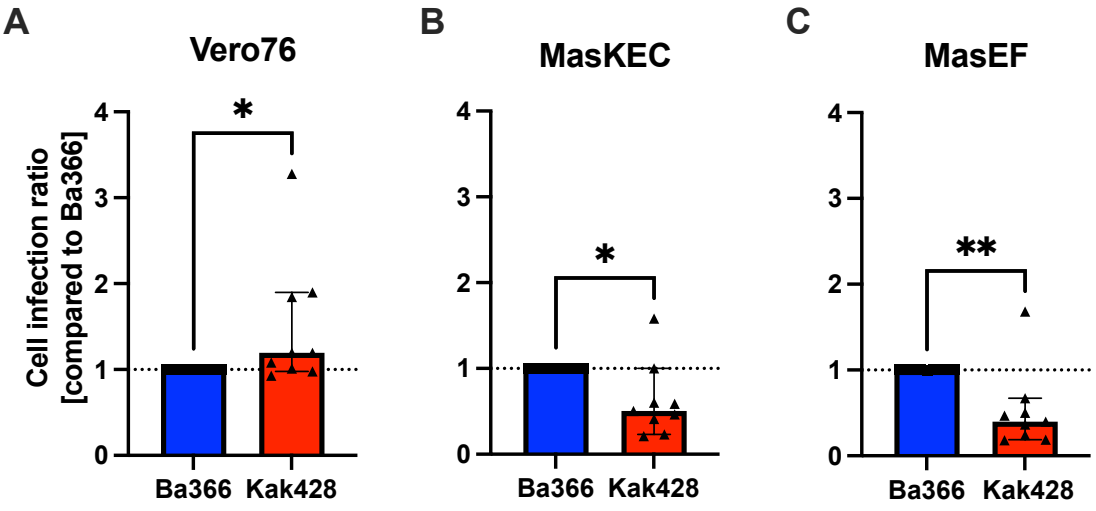

Figure 29: Cell entry efficiency of the two different LASV strains Ba366 and Kak428 tested on three cell lines. Three different cell lines **A** Vero76, **B** MasKEC and **C** MasEF were infected with 250, 125 or 62.5 focus forming units of Ba366 (blue) or Kak428 (red) for 1 h each, followed by 16 h incubation with overlay medium, that prevented the spread of viral particles in the supernatant. The infected cells were stained via immunofocus assay and counted manually. The number of Kak428-infected cells was normalized to Ba366 infection rates (=1; dashed line) in the respective cell lines and is displayed as cell infection ratio. Experiments were performed with three technical replicates per experiment. Nine independent experiments were done for each virus and cell line. Depicted are the median values of the triplicates for each independent experiment with a confidence interval of 95 % and the standard deviation. A Mann-Whitney test was used to test for significant changes. * $P \leq 0.05$; ** $P \leq 0.01$.

5.4.1.3. Do the adapted variants (VP10) show enhanced entry into M. natalensis cells in comparison to the non-adapted viruses (VP0)?

To assess the potential of the adapted variants to enter the cell more efficiently, as described above, entry assays have been performed by comparing infection characteristics of the viruses before (VP0) and after adaptation (VP10). First, it was noted that for the VP10 variants, the foci size changed when compared to the VP0 foci. Similarly, different foci sizes have been seen in earlier experiments for the different LASV strains. Figure 30 shows the different foci sizes of the LASV wt strains and the Kak428 A11 variant as an example. While cells infected with the Ba366 strain always resulted in bigger foci, the Kak428 strain initially had smaller foci. Interestingly, also the foci for the VP10 variants seemed bigger than seen for the initial VP0 variants. This could indicate a more efficient cell-to-cell spread of the VP10 variants in comparison to non-adapted VP0 strains.

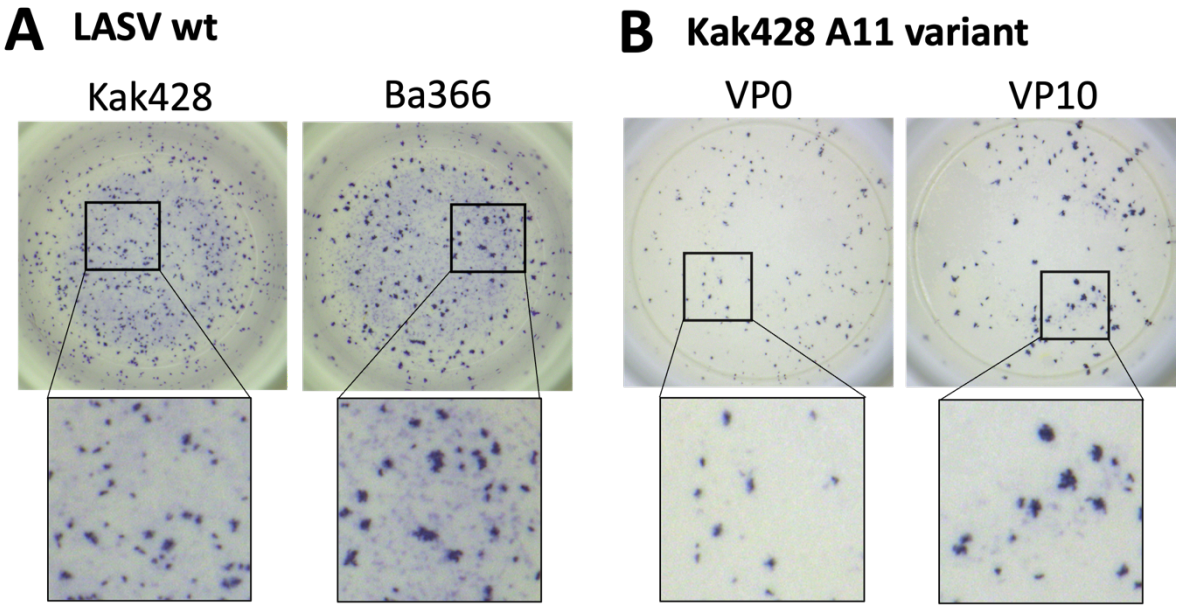

Figure 30: LASV wt viruses and Kak428 A11 variant foci size and appearance. Vero76 cells were infected with 125 FFU of **A** Kak428 wt or Ba366 wt and **B** the VP0 or VP10 Kak428 A11 variant in a 96-well format. The infected cells were stained via immunofocus assays. Exemplary pictures are shown.

In the next step, the fold change of infected cells of the Kak428 VP10 variants in comparison to the VP0 variant has been assessed (see Figure 31). The entry into Vero76 cells remained largely unchanged with a tendency for a less efficient cell entry of the C2 variant. The entry into the *Mastomys* cell lines was up to 100-fold more efficient for the A11 variant, whereas it remained rather stable for the C2 variant infected MasEF cells. Interestingly, the entry was up to 50 % less efficient in the MasKEC infected with the C2 variant. For the E8 variant, entry into

the MasKEC increased up to 10-fold, whereas it was approximately 2-fold as efficient in the MasEF cells.

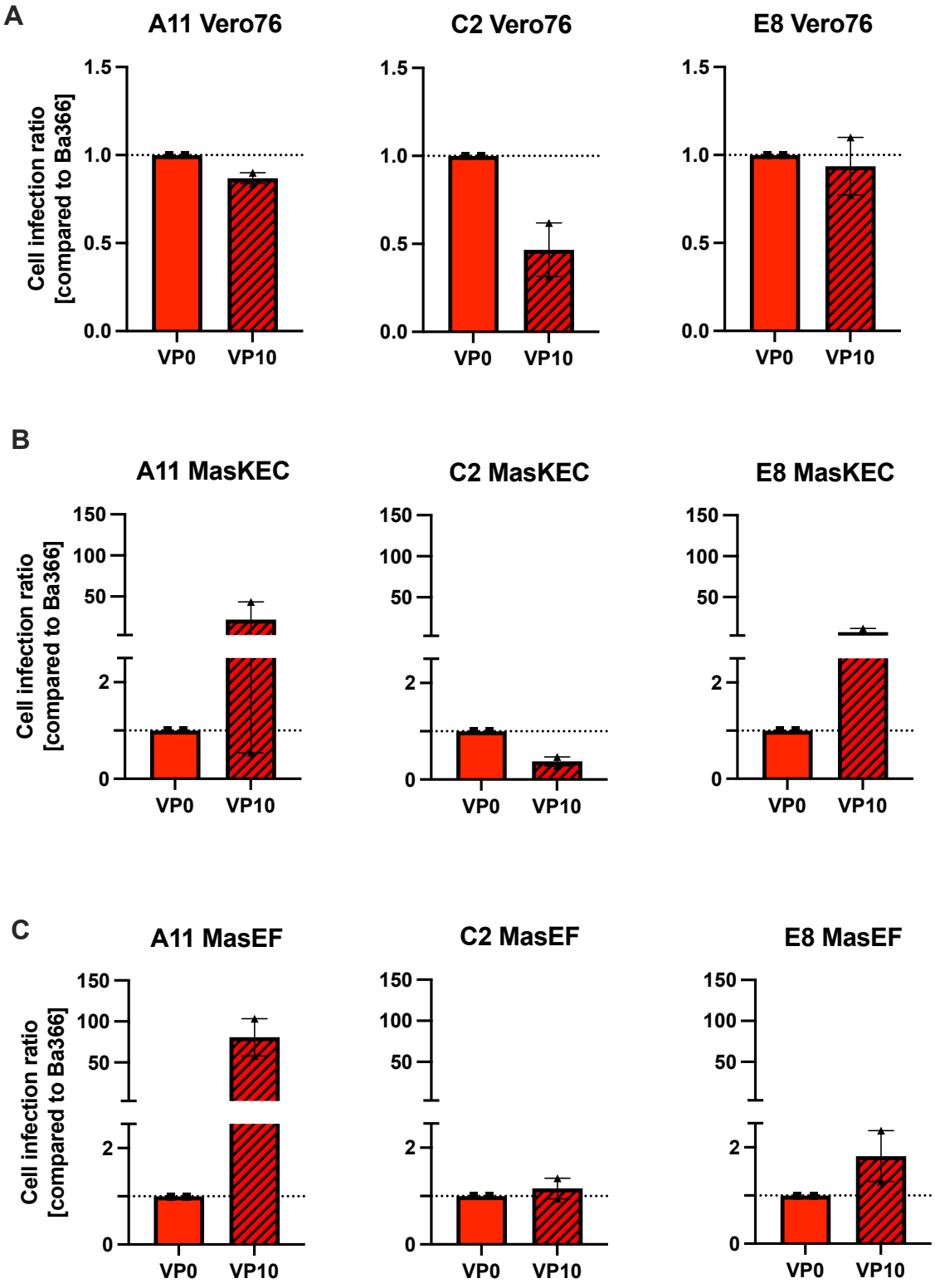

Figure 31: Cell entry efficiency comparison of native, non-adapted (VP0) and adapted (VP10) Kak428 LASV. Vero76, MasKEC or MasEF were infected with 250, 125 or 62.5 FFU/mL of the non-adapted (VP0, full red) or adapted (VP10, streaked red) Kak428 variants **A** A11, **B** C2 or **C** E8 for 1 h, followed by 16 h incubation with

overlay medium, that prevented the spread of viral particles in the supernatant. The focus forming units were determined by immunofocus assay. Shown here is the cell infection ratio of infected cells after normalization to VP0 (=1) infection rates (dashed line) in the respective cell lines. All experiments were performed in three technical replicates. Two independent experiments were conducted for each virus and cell line. Depicted is the median with a confidence interval of 95 % and the standard deviation.

5.4.2. Viral replication and transcription

In earlier experiments, two of the chimeric viruses, the NP chimera (Ba366 wt/Kak428 NP) and the L chimera (Ba366 wt/Kak428 L) showed major growth deficits compared to the Ba366 wt. Therefore, both NP and L proteins were further characterized in replicon assays. These assays are surrogate models for transcription and replication and allow studying these processes under BSL-2 conditions as it does not involve working with full viruses.

5.4.2.1. What happens to transcription and replication efficiency if the Ba366 and Kak428 L and NP proteins are exchanged?

During this study, the established Ba366 replicon system was used, which is regularly applied for testing mutations in the L and NP protein of the Ba366 strain. These assays were carried out with the Ba366 L and NP (Ba366 L/Ba366 NP) to perform the activity normalization (set to 1). In addition, a catalytically inactive mutant of the L protein with a Ala1331Asp amino acid change (neg. control) was used to determine the background activity in this assay. Figure 32 shows the normalized Renilla luciferase activity of different L and NP combinations for the Ba366 and Kak428 strains. Using the Kak428 L/Ba366 NP combination resulted in a up to 3.6-fold activity increase compared to the Ba366 L/Ba366 NP wt combination. This indicates that the Kak428 L is not generally less efficient in transcription and replication but had in contrast a higher activity. To assess the contribution of the Kak428 NP to this process, it was investigated in combination with i) the Ba366 L (Ba366 L/Kak428 NP) or ii) the Kak428 L (Kak428 L/Kak428 NP). When the Ba366L/Kak428 NP combination was tested, a major impairment in replication and transcription was observed as the Renilla luciferase activity remained less than 15 % compared to the Ba366 NP/Ba366 L combination. When the combination of Kak428 L/Kak428 NP was examined, the replication and transcription activities seem to have been partly restored and were comparable to the Ba366 NP/L combination.

These findings indicate a major contribution of the Kak428 NP in the observed growth impairments of this strain. The Kak428 L, however, seems to have a compensatory effect, when it was combined with the Ba366 L.

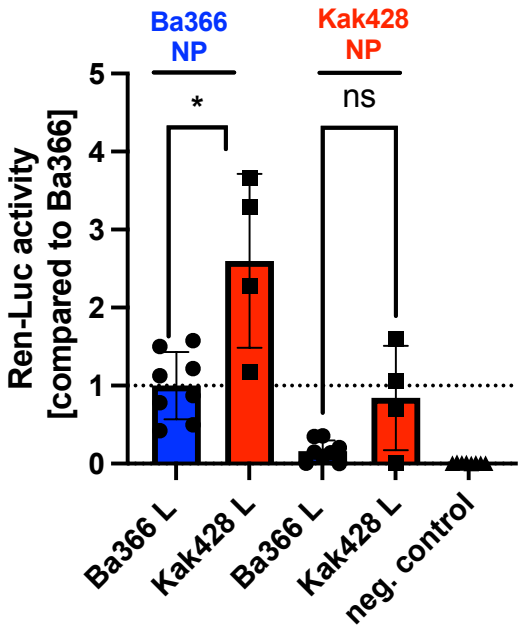

Figure 32: Replicon assay with interchanged viral proteins of the LASV strains Ba366 and Kak428. The Renilla (Ren-Luc) luciferase activity as indicator for replication and transcription was measured in a replicon assay with the Ba366 minigenome with either the Ba3656 NP (2 columns on the left) or the Kak428 NP (2 columns in the middle) in combination with the Ba366 L (blue) or the Kak428 L (red). Shown here is the Ren-Luc activity after normalization to Ba366 L and NP (= 1; dashed line). Three independent experiments were performed for each protein combination. Depicted is the median with a confidence interval of 95 % and the standard deviation. A Mann-Whitney test was used to test for significant changes. ns = non-significant, $P > 0.05$; * $P \leq 0.05$. neg. control = catalytically inactive L mutant (Ala1331Asp).

5.4.2.2. Do the potential host-adaptive mutations in the Kak428 NP enhance its function?

In the previous experiment (see 5.4.2.1) it has been experimentally demonstrated that the Kak428 NP seems to play a key role in restricting replication and transcription processes. Therefore, the further experiments focused on the characterization of the potentially host-adaptive mutations identified in the NP after the *in vitro* adaptation of Kak428 to MasKEC, namely Ser473Leu, Leu569Met and Lys424Arg. The Renilla luciferase activity was normalized to the Ba366 L/Ba366 NP combination (set to 1). The Ba366 L/Kak428 wt NP combination showed on average 9.0 % remaining activity compared to the Ba366 NP/L combination. In contrast, the insertion of the mutations into the NP enhanced their activity to an average of 16.8 %, 17.1 % and 14.7 %, respectively, which was not found to be significant in a Mann-Whitney test.

Taken together, the Kak428 mutations only had minor influence on the overall transcription and replication, but still show a slight enhancement on the Ren-Luc activity.

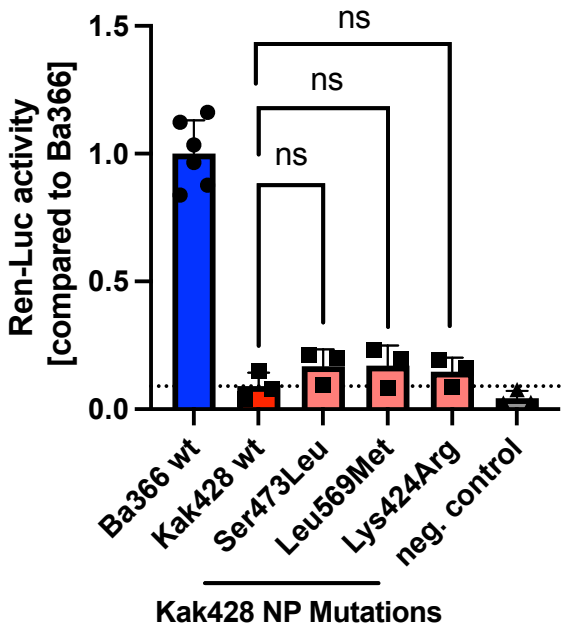

Figure 33: Influence of Kak428 NP mutations on viral replication and transcription tested in the LASV replicon system. The Renilla luciferase (Ren-Luc) activity was measured in a replicon assay with the Ba366 minigenome and L in combination with either the Kak428 wt NP (2 columns on the left) or three different mutations in the Kak428 NP (3 columns in the middle). Shown here is the fold change of Ren-Luc activity after normalization to Ba366 L and NP (=1). Three independent experiments were done for each combination. Depicted is the median with a confidence interval of 95 % and the standard deviation. The dashed line indicates the Ren-Luc activity of the Kak428 wt NP to which the Ren-Luc activity of the mutants was compared. A reaction without adding any NP but with the Ba366 L served as negative control. A Mann-Whitney test was used to test for significant changes. ns = non-significant, $P > 0.05$.

6. Discussion

Lassa virus, the causative agent of Lassa Fever, has long been known to be carried by *M. natalensis*. However, recently new LASV strains were isolated from different rodents, and little is known about the factors that restrict LASV from spillover into new hosts. Among the recently discovered LASV strains is the Kak428 strain, which was isolated from *H. pamfi* (heterologous strain) and had a reduced capacity to establish long-lasting infections in *in vivo* experiments with *M. natalensis* compared to the homologous Ba366 strain, which was isolated from *Mastomys*. A goal of this thesis was to further assess the virus-host barriers of LASV to gather information about possible mutations that facilitate or restrict viral spillover into new hosts and thus could be implemented in surveillance systems.

6.1. Can the heterologous LASV strain infect *M. natalensis* cells *in vitro?*

In the beginning of this project, a potential *in vitro* model was to be established to mimic LASV infection in cells of the main rodent reservoir host *M. natalensis*. As the expression of cellular receptors for the entry of LASV is crucial for an *in vitro* system, a previously developed qPCR assay was deployed to check for the expression of known LASV receptors such as αDG and Tyro3 as well as LARGE1 and LARGE2, which are important for the maturation of αDG [197]. We found αDG, Tyro3 and LARGE1 being expressed on both *Mastomys* cell lines, namely MasKEC and MasEF, used during this project. The expression of LARGE2 in those cells could not be confirmed with the applied assay. However, the assay including the LARGE2 primers principally worked, as the expression of LARGE2 in various organs from *M. natalensis* could be validated. LARGE2 has been found to be a gene duplicate of LARGE1 [205] with compensatory functions [206, 207] and has a more restricted tissue-specific expression profile than LARGE1 [205]. However, according to Grewal et al. (2005) [205] and observations made during this study, LARGE2 is expressed in the kidney of *M. natalensis*, which is contradictory to the findings with the immortalized *Mastomys* cells. One explanation for the changed expression patterns in MasKEC and MasEF compared to the qPCR data from the organs might be due to the immortalization of the cells with the SV40 antigen. It has been shown that alternations of the gene expression profile, e. g. an increase in IFN-related transcripts, can in some cases be seen due to the transformation [208]. Important to note here also is the lack of transcriptomic data of *M. natalensis*, which makes it impossible to design further primers and look into more

known LASV receptors such as DC-SIGN. However, αDG is the main receptor, which is most ubiquitously expressed and thus most important for this study.

After having proven, that the main receptor for LASV, αDG, is expressed on both *Mastomys* cell lines, growth kinetics with three LASV strains were performed. A partial correlation between the growth behavior previously seen during *in vivo* experiments with the growth observed *in vitro* was observed. Both the homologous Ba366 strain as well as the heterologous D96 strain replicated up to high titers in cell culture, whereas the heterologous Kak428 strain grew slower and never reached comparable titers. This growth impairment of the Kak428 strain was most pronounced on the MasKEC cells and the MΦ. During previous *in vivo* experiments with the same strains, similar observations were obtained. While the Ba366 strain was able to establish persistent infections in the animals when infected at a young age, the Kak428 was cleared rapidly. The D96 strain showed prolonged infection duration compared to the Kak428 strain but was not able to establish long-lasting infection as seen for the Ba366 strain [157]. Overall, the growth kinetics for the Ba366 and Kak428 strain seen during the *in vitro* experiments thus mimic the pattern seen during *in vivo* studies with *M. natalensis*. Taking a close look at the growth behavior of the D96 strain *in vivo* (initial high titers and clearance after two weeks) and combining it with the *in vitro* data, a defect in establishing persistent infection might be due to immune responses rather than a problem with replication itself. At this point, we decided to focus on the heterologous Kak428 strain in comparison to the homologous Ba366 strain because the D96 strain was not likely to be further adapted to *M. natalensis* as it was growing already to high titers in the *Mastomys*-derived cells. In the same line, we decided to use the MasKEC cells for further adaptation experiments, as those seemed to impose a greater selection pressure on the heterologous Kak428 strain than the MasEF. The primary MΦ are highly interesting, as they are among the first target cells during an infection [69, 209], and seemed to pose the highest selection pressure on the Kak428 to adapt to *M. natalensis*, indicated by the comparably lowest virus titers. However, they were not used in further experiments to adhere to the 3R rules and reduce the number of animals used during this study as the results with the immortalized MasKEC were comparably.

Finally, to answer the question, if heterologous strains can produce infectious virus particles in *M. natalensis* cells, the production of infectious progeny virus was investigated by means of electron microscopy. The virus production of either the homologous Ba366 or the

heterologous Kak428 strain was assessed on Vero76 as control cells, which are regularly used for amplification of LASV at the BNITM, and the two *Mastomys* cell lines. The median size of the progeny viruses did not significantly differ neither between the two virus strains nor between the different cell lines used and all released particles ranged in diameter from 80 to 102 nm. This observation was in accordance with observations from others, who found LASV particles being spherical and having a size from 70 to 150 nm [102]. The particles imaged during this experiment also mainly had a spherical shape with no outstanding alternations between the two virus strains or the different cell lines used for virus production.

Taken these results together, using MasKEC for *in vitro* infection experiments represents a suitable model for LASV infection studies. Additionally, the Kak428 strain was impaired in virus growth on these cells, but nevertheless, it was able to produce progeny virus particles, which was confirmed by EM.

6.2. Which impact do individual proteins have on the ability to establish persistent infection in *M. natalensis*?

Next, the question was raised, which impact the individual proteins of LASV have for the ability to establish prolonged infection in *M. natalensis* and thus to overcome the virus-host barrier for the prototypic heterologous LASV strain Kak428. For this, four chimeric viruses with an insertion of individual proteins of the heterologous Kak428 strain in the genetic background of the homologous Ba366 strain, namely GP, L, NP and Z chimeras, were successfully generated.

During the *in vitro* experiments to characterize the respective growth kinetics of the chimeras, all chimeric viruses were attenuated compared to the homologous Ba366 strain. Surprisingly, all chimeras reached the highest titers in Vero76 cells, which might be due to their deficiency in interferon synthesis [210]. In contrast, we found MasKEC to be highly sensitive to interferon treatment [198]. On Vero76 cells, both the NP as well as the Z chimera reached titers around 1×10^5 FFU/mL, but the growth of the NP chimera as well as the GP and L chimera were highly attenuated in the *Mastomys* cells. Only the Z chimera reached high titers in the MasEF on day four post infection. The observed impaired growth of the chimeras on the MasKEC, might be due poor cell viability of these cells, that was noted during this experiment. Further experiments to confirm or refute these finding need to be done to investigate the behaviors of the chimeric viruses in the MasKEC.

To compare the *in vitro* data with the growth kinetics in the animals, *in vivo* experiments with *M. natalensis* were performed. Here, the findings from the *in vitro* experiments could be confirmed. Infection patterns of the chimeric viruses, except for the Z chimera, resembled patterns observed with the Kak428 wt, with a brief transient infection followed by rapid virus clearance. The NP chimera was cleared even quicker than the Kak428 wt strain. The animals infected with the Z chimera stayed highly positive throughout the experiment with high infectious virus titers in most organs. This resembled the course of infection of the homologous Ba366 strain, showing that the exchange of the Ba366 Z with the Kak428 Z does not lead to quicker viral clearance or lower overall virus titers. Noteworthy, the animal group infected with the Z chimera had to be terminated prematurely. Therefore, it is impossible to draw conclusions for the later sampling time points at 3 and 4 w. p. i. and the potential establishment of persistent infection.

Nevertheless, we concluded from both experiments that the Z protein is of least importance for the observed virus-host barrier. The Z protein is mostly responsible for virus budding and serves as an important regulatory factor for the L protein [126-128]. The observations that exchanging the Z protein has little impact in the Ba366 strain is in accordance with the observations from the initial electron microscopy experiments which revealed that budding is taking place efficiently for the homologous and the heterologous virus and that the released virus particles showed no obvious alterations. In contrast, all other three viral proteins, namely the GP, NP and L seem to be highly important as inserting them into the Ba366 virus leads to an impaired virus growth *in vitro* and an accelerated viral clearance *in vivo*.

As previously described for many viruses, the entry process is usually the first barrier to overcome to infect new host species [161, 162]. One example is the adaptation of TAMV-FL towards using human hTFR1 by mutation of just one amino acid [165]. Previous studies on chimeric LCMV, which had its own GP replaced with LASV GP, found the exchange of GP led to persistent infections and resulted in an enhanced cell entry into dendritic cells [211, 212]. Especially the adaptation of the cytoplasmic tail of the LASV GP was relevant for the viral fitness including GP maturation and transport as well as virus assembly [211]. These examples highlight the importance of the LASV GP in overcoming the initial virus-host barrier and are in accordance with the findings for the LASV GP chimera. When the GP of Ba366 was replaced with the Kak428 GP, the infection of *M. natalensis* with this chimera was rapidly terminated and the virus was cleared from most organs within the first two weeks post infection.

Also, the immune evasion within infected cells is of major importance for a virus to get established in a new host species [163]. One major step is to circumvent the innate immune response, including the induction of interferon-stimulated genes (ISGs). For LASV, both the NP as well as the Z protein have been proven to facilitate blockage of the ISG responses [170, 171, 173, 175]. However, only the functions carried out by the Z protein seem to be efficient in the heterologous Kak428 strain during infection of *M. natalensis* as the exchange of this protein does not alter the outcome of *in vivo* infection experiments with the Z chimera. Nevertheless, we did not find evidence for the Kak428 strain to induce an overall stronger ISG response in previous experiments making this assumption unlikely [158].

Apart from the NP functions in immune evasion, together with the L protein it is part of the RNP complex, which is responsible for replication of the virus genome and transcription of viral genes [120]. Thus, impairment of the L and NP chimeras in retaining high virus titers over the course of the experiment might be due to their incompatibility between the two strains. To confirm this, a new chimeric virus in the genetic background of the homologous strain with both proteins, L and NP, exchanged with the heterologous Kak428 proteins might provide more insights.

Given all these points, the role of each protein on the virus-host barriers was narrowed down to the GP, L and NP proteins being most important.

6.3. Is *in vitro* adaptation of heterologous LASV strains possible to *M. natalensis* and do host-adaptive mutations occur?

Before the adaptation process, virus variants were obtained through limiting dilution assays, namely A11, C2 and E8. They were produced to get a more homogenous set of viruses, as it was very likely that the original virus stock of the Kak428 strain harbored viral quasispecies. The occurrence of viral quasispecies within animal samples has been shown to be very likely [213]. The variants showed different growth patterns, which confirmed the hypothesis that different quasispecies might have distinct replication profiles. Some of the virus variants were attenuated on all cell lines tested (A11 variant) but the C2 variant had a growth impairment specifically on *Mastomys*-derived cell lines.

During the adaptation process, relatively stable RNA copy numbers were observed, but infectious virus titers greatly varied over the different cell passages. For arenaviruses, the production of defective interfering particles (DIPs) occurs frequently, especially during

infection experiments with a high MOI [169, 214-216]. This might explain the variations seen for the infectious virus titers, as those DIPs compete for valuable resources needed for transcription and replication.

After the adaptation process, the virus titers reached of the virus variants before and after adaptation were compared with growth kinetics on MasKEC. As expected, no significant change in the virus titers was seen for the homologous Ba366 strain, as this strain was already growing well on MasKEC in the beginning of the experiment. However, all Kak428 variants showed a 100- and 1,000-fold increase in the median change of viral titers on day three post infection, indicating a successful adaptation to MasKEC.

To simplify subsequent NGS analysis of virus mutations, which might have occurred during the adaptation process, sub-variants of the adapted VP10 variants (again a mixture of different quasispecies) were generated and named A11-C3, A11-C4, A11-F6; C2-A4, C2-D4, C2-E5; and E8-B6, E8-D2, E8-G5. These sub-variants likewise showed an overall increased fold change in the virus titers as compared to the initial virus stocks. However, the changes were varying between the sub-variants and only the E8-D2 and E8-G5 sub-variants grew to higher titers than the parental VP0. The C2 sub-variant had titers comparable to the VP10 mixture and the A11 variants reached higher titers than the VP0, but lower titers than the VP10 mixture. This might be due to a random selection of only three virus sub-variants per VP10 variant and does not exclude the existence of virus variants growing even better than the VP10 mixture. These experiments however also illustrate that quasispecies with very different growth behaviors quickly emerge from a homogeneous virus stock during serial passaging.

Then, potential host-adaptive mutations induced by the adaptation process were identified by NGS. For this, at first samples from all passages of the adaptation experiments including the final VP10 variants were sequenced followed by a second attempt during which the VP10 sub-variants, which were generated from the VP10, were analyzed. Here, only major variants were considered during the analysis, meaning mutations that occurred with a frequency >10 %. We only found mutations occurring during the adaptation process in the Kak428 strain and none in the Ba366 control. This is not too surprising as the Ba366 strain originates from *Mastomys* and thus no or very little adaptation pressure was present on the MasKEC. It also shows however, that the rate on random mutations is not very high, suggesting that mutation that developed in the Kak428 strain are not random but rather emerge due to selection pressure.

Of interest when looking at the Kak428 mutations is their early occurrence. Most major mutations found in the dataset of the VP10 variants were identified at latest during VP6 and included mutations only in the nucleoprotein and L protein. The impact of these mutations was demonstrated in the growth kinetics mentioned above, which overall resulted in an accelerated growth behavior. This early occurrence of mutations in *in vitro* adaptation experiment has also been shown for other viruses such as Ebola virus and SARS-CoV-2 [217, 218]. For the SARS-CoV-2 passaging experiments, even mutations have been identified, which were directly linked to a host-switch and that might have implications for the safety classification of this pathogen [218, 219]. For Ebola virus, a massive accumulation of mutations in the L, GP and NP have been observed already after four passages on human or bat cell lines, leading to a replication advantage [220]. Importantly, for Puumala virus, few passages in Vero E6 cells already resulted in attenuated infection properties due to a mutation in the L and using Vero cells is no longer a standard method for the isolation of new hantaviruses based on this finding [221-223].

Interestingly, in our dataset, mutations in the glycoprotein were only found in the sub-variants of the VP10-adapted viruses, likely because they were only present as minor variants in the first NGS dataset. These GP mutations, however, might contribute to host-switching, as viral entry into the host cells is one of the major hurdles to overcome when viruses adapt to new hosts [161, 162]. The mutations identified in the LASV GP, were mapped to the annotated sequence of LASV Josiah GP. Two mutations (Ile4Met and Asn37Tyr or Asn37Ile) are located in the stable signal peptide, one in the GP1 (Asn145) and one in the GP2 subunit (Ala296Asp). The stable signal peptide (SSP) consists of the first 58 amino acids (aa) of the GPC complex in size and contains two hydrophobic, membrane-spanning regions (ranging from 18-32 aa and 41-54 aa) as well as a hairpin structure in-between. The SSP is unique in the sense that it is retained in the matured GPC after cleavage and has been shown to be important for GPC maturation and membrane fusion by interacting with the GP2 subunit for Junín virus [224-228]. The membrane fusion activity of SSP requires the first 33 aa [229]. This is the region in which the Ile4Met mutation is located, however, this particular isoleucine was not among the residues particularly involved in its myristylation. The asparagine mutation at position 37 to either tyrosine or isoleucine, was mapped to the hairpin-region of the SSP and has been shown for Junín virus to be associated with resistance to small molecule fusion inhibitors [228, 230]. Taken together, neither of the two mutations in the SPP have been described before to be

directly involved in the entry process. The GP1 subunit of the GPC is known as the receptor binding domain with the important residues for receptor binding being at the positions 141, 146, 147 and 150 [203]. Interestingly, the Asn145Asp mutation has been mapped in this region without being actively involved in binding to the receptor. However, this mutation could potentially influence the receptor binding ability. Experiments measuring the strength of the binding of Kak428 wt and of the Asn145Asp mutant to *Mastomys* αDG would be very interesting. Lastly, the GP2 subunit has been shown to be responsible for membrane fusion [231]. The Ala296Asp mutation identified in the GP2 is located in between the internal fusion loop and the heptad repeat 1 and could not be assigned any particular function [203]. The functional changes induced by the GP mutations were partly evaluated in functional assays (see 6.4), but they should be more closely examined, e. g. by entry assays with reversely engineered, recombinant viruses that only carry one mutation at a time.

After successful cell entry, viruses which are adapting to a new host need to be able to evade the immune system [161, 162]. For arenaviruses, the NP and Z proteins have been shown to facilitate immune evasion by different pathways [71]. As seen already during the experiments with chimeric viruses, for Kak428 the NP rather than the Z seems to have little contribution to the attenuation of Kak428 in *Mastomys* cells. These findings are consistent with the observation from NGS analysis after the adaptation experiments, as no mutations were found in Z, implying low pressure to adapt. Potential adaptive mutations in the NP however mapped to the exonuclease domain (ExoN) of the protein, which is of major importance for suppression of the innate immune response [170]. This region has a 3´-5´exonuclease activity which cleaves dsRNA to prevent recognition by innate immune sensors RIG-I and MDA-5 [168, 201]. Additionally, it blocks translocation of IRF-3 to directly block IFN production [170, 232]. The ExoN is located from 364 aa onwards in the C-terminal region of NP [201] and all four mutations identified, namely Lys424Arg, Ser473Leu, Gln523Glu and Leu569Met occur in this domain. While the Leu569Met mutation was mapped directly to the very end of the C-terminus, two of the mutations, namely Gln523Glu and Leu569Met, were found in flexible regions of the ExoN, whereas the latter was identified in a basic loop spanning the 514-526 aa and the first being part of the C-terminal arm between aa 549-570 [201]. The Gln523Glu mutation was mapped close to the active site, which has a DEEDh motif at the positions 389, 391, 466, 528 and 533. However, mutational studies of aa in a proximal position to aa 393 exemplarily showed that even residues in close proximity did not necessarily have an impact

on the catalytic activity [170]. Therefore, the effect of the identified mutations in the NP cannot be directly linked to structural changes in the ExoN. Nevertheless, the NP mutations should, in the next step, be evaluated regarding their ability to induce or interfere with the type I IFN system. For this, recombinant viruses carrying only one mutation at a time could be used during infection experiments. The production of type I interferons in the cells could be directly measured, e. g. with ELISAs [169] and the expression of ISGs could be followed by an already established RT-PCR assay [198]. Also, although the ExoN was for a long time believed not to be involved in viral genome replication and transcription, it was shown in 2011, that a defect in these processes, when residues in the ExoN were mutated [169]. Therefore, the examinations in replicon assays, as described in chapter 6.4 are essential to determine a potential influence of the NP mutations on transcription and replication as NP is required for these processes [201].

Interestingly, when amino acid alignments of the Kak428 GP and NP were compared to sequences obtained from homologous viruses, which were isolated from *M. natalensis* such as for e. g. the Ba366 strain, the MAD39 strain or several isolates from *Mastomys* trapped within household of LASV-infected individuals (named Z0947-SLE-2011 and Z0948-SLE-2011), all strains including the Kak428 strain had mostly the same initial amino acids at positions, which later harbored mutations during the adaptation experiments. This might be an indication of relatively conserved amino acids mutating randomly rather than towards *Mastomys*-specific sequences.

For the L protein, mutations were identified in all three domains of the protein with three mutations in the PA-like region, six mutations in the PB1-like region and three mutations occurring in the PB2-like region. The PA-like domain compromises of 1-711 aa and can further be divided subdomains [233]. The endonuclease region is located on the N-terminal part of the protein, which extends to the residue 197 and is important for cap-snatching and subsequently, initiation of transcription. During this understudied process, the endonuclease domain and C-terminal cap-binding domain, act together to generate mRNAs with host-derived nucleotides on their 5´ ends [202]. Besides the endonuclease region, a linker region (198-258 aa) is found, followed by the pyramid (320-464 aa) and pyramid-base (465-584 aa) regions as well as the core lobe (584-712 aa) region [233]. The Gly547Ser mutation was mapped to the pyramid-base region within close proximity to the RNA-binding region of the L protein. Here, the amino acid exchange occurred with a high frequency of 99 % and could

influence the electrostatic properties of this region as the original non-polar glycine was replaced with the polar serine. In contrast, the Phe589Leu was only found in 58 % of the dataset and resembled an exchange of amino acids with the same biochemical properties as both the phenylalanine as well as the leucine are non-polar amino acids. Additionally, the group of Lelke et al. found that exchanging the phenylalanine at this position to an alanine had no effect on replication and transcription efficiency [234]. Thus, the Phe589Leu mutation most likely does not strongly affect the affect the virus growth behavior. The last mutation in the PA-like region, namely Tyr655Asp, was identified in the core-lobe region of the L protein and was found even less frequently (19 %). This position is not involved in RNA-binding as the residue is located on the protein surface. Although the change from a polar amino acid to an acidic amino acid might influence the electrostatic properties of the protein, the importance of this mutation is unclear due to its occurrence with a low frequency.

The PB1-like region of the protein can be subdivided into the canonical fingers, palm, and thumb domains, which are conserved polymerase motifs [202]. Here, we identified all mutations to be on the surface of the protein. In more detail, the Asp898Val or Asp898Glu and the Val900Met or Val900Gly mutations as well as the His936Arg and Thr1055Ala mutations, were mapped to loop regions. Those regions might be subject to evolutional pressure as loops are known to be strongly exposed and thus easily recognized by the immune system [235]. The Ille913Val mutation, however, was not located on the surface of the protein, but not in a loop region. Interestingly, this mutation was among the few mutational changes observed during this study, that resembled a change towards the amino acid sequence obtained from *Mastomys*-derived samples. Here, an amino acid alignment with the Kak428 L protein sequence compared to the Ba366, MAD39 and other *Mastomys*-derived sequences revealed that the Ba366m as well as the MAD39 strain, have a valine in position 913. Taking this observation together with the high frequency of 98 % of the Ille913Val mutation, the evidence points towards a strong evolutionary advantage of this mutation. Moreover, there were mutational studies done by Lehmann et al., on residues close to two of the mutations identified during our experiments. The mutation of histidine at position 1051 to alanine led to a reduced catalytical activity of the L protein and abolished both the transcription as well as the transcription [236]. This indicates that the region in which the detected Thr1055Ala mutation lies, is very important for the catalytical activity of the L protein and further characterization of the Thr1055Ala mutation is needed to determine its individual

contribution. This is especially true, because exchanging the polar threonine with the non-polar alanine might alter the protein's electrostatic properties. In contrast, the experimental exchange of glutamine at position 1514 to alanine, which is close to the Gly1511Val mutation, did not influence the catalytical activity [234]. Also, the Gly1511Val mutation represents a change within amino acids of the same biochemical properties (both are non-polar). Taken together with the low frequency of occurrence of the Gly1511Val mutation of only 20 %, these results point towards a smaller impact of this mutation on the L protein functions and the virus ability to replicate within a new host.

Lastly, three mutations were mapped to the PB2-like region. The PB2-like region is organized very similar to the influenza virus polymerase and consists of a thumb-ring (1613-1731 aa), a lid (1731-1801 aa), a mid-link (18525-1904 aa) as well as a cap-binding (1905-2078 aa) and a 627-like domain (2101-2117 aa). Two of the mutations found during this study, namely Tyr1640Asn and Val1676Ala, mapped to the thumb-ring domain, which is together with the lid domain responsible for the strand separation during RNA synthesis [202, 237]. The latter mutation is located on the protein's surface and represents a rather negligible change because of the similar biochemical properties of the initial valine and the newly identified alanine. In contrast, the Tyr1640Asn mutation was mapped close to the RNA binding site, making it highly interesting. Although it only occurred with a frequency of 20 %, it was one of the mutations, that represented an amino acid exchange towards the *Mastomys*-derived sequences. Thus, the MAD39 as well as some other isolates had asparagine in this position already. Taken together with the observations from Lehmann et al., that exchanging the tyrosine at the position 1640 to alanine resulted in a reduced transcriptional and replicational activity [236], the mutation at this position might be highly relevant for the observed phenotype during growth kinetics with the adapted viruses. Additionally, one mutation (Cy2012Arg) was mapped to the 627-like domain, which interacts with the Z protein, resulting in the inhibition of RNA synthesis [202]. The Cys2012Arg mutation was mapped close to a manganese ion binding site. However, it is not one of the residues actively involved in the ion coordination. The effect of exchanging amino acids at the positions 2015 and 2017 was tested by Lehmann et al. but did not show any effect on transcription and replication [236].

In summary, we identified three mutations in the L protein (Gly547Ser, Thr1055Ala and Tyr1640Asn), which might be highly relevant for the observed adaptation of the Kak428 strain to *M. natalensis* cells. Nevertheless, a more detailed characterization of all L mutations is

needed and could for example be done by testing L proteins modified by site-directed mutagenesis in the replicon assay or by using reverse genetics to engineer the Kak428 strain to carry one of the L mutations in the full virus context and characterize its growth kinetics.

Taken together, we observed the appearance of several mutations in the GP, L and NP genes, during the adaptation to *Mastomys* cells, which might be of importance for host switching. However, up to this date changes in the noncoding regions have not been analyzed and those with regulatory functions might be highly relevant for host restriction. For LASV, the promotor, which consists of the first 19 nt of the genome, is extremely important for the regulation of transcription and replication [105] and the intergenic regions, which separate the two ambisense open reading frames on each segment, facilitate the termination of transcription [106, 107]. To evaluate the contribution of mutations, that might have occurred in these regions, further analyses are needed.

Finally, the growth behavior of the VP10-adapted variants was assessed in an *in vivo* experiment to determine the effects of the *in vitro* acquired mutations. Overall, the same organ tropism was noted for the adapted variants as seen for the Kak428 wt except for the eyes, which were not sampled during the initial experiment with the Kak428 wt strain. The prolonged viral presence in the eyes might be due to the eyes representing an immune privileged site. The eyes have a blood barrier and lack a direct lymphoid drainage, which makes them hard to reach for immune cells. Additionally, the presence of immunosuppressive molecules might negatively affect the activation of the immune system [238, 239]. These findings could explain the prolonged infection in the eyes with the adapted Kak428 variants, but reference data to determine the potential of the Kak428 wt to infect the eyes will still need to be generated. In general, prolonged infections of the eyes have also been observed for other viruses such as Ebola virus. In a case report, a patient was even found to harbor infectious virus in his eyes for up to nine weeks post clearance of viremia [240].

In contrast to the *in vitro* experiments, not all strains induced a longer infection in the animals. Especially the C2 VP10 adapted variant, which showed the strongest change in the virus titer with an increase of 1,000-fold was not able to induce stable virus titers over the course of the experiment. Additionally, virus was only found in the eyes, salivary gland and thymus. As the infection of the animals was done via the s. c. route, this might pose a hurdle for the virus to establish infection of this new host in the first place. Not only infection close to the injection site, but also infection of other organs, e.g. via the bloodstream, is needed for the virus to

productively spread throughout the whole body. Thus, the virus was unable to disseminate and cause systemic infection, e.g. due to strong activation of the immune system or impairment in virus replication. The Kak428 C2 VP10 variant might have acquired random or cell culture-specific mutations, rather than *Mastomys*-specific mutations. The A11 and E8 VP10 variants however, resembled more closely the Kak428 wt strain and even developed higher virus titers 1 and 2 w. p. i., respectively. The A11 VP10 variant was cleared faster from the animals than the E8 VP10 variant, which is in line with the trends seen in the *in vitro* experiments. Here, the A11 variant had with only 100-fold the least change of virus titer compared to the non-adapted, initial variants. Thus, the mutations identified especially in the E8V VP10 variant might be beneficial for the virus replication in *M. natalensis* as a new host for the Kak428 strain.

Taken together, we identified mutations in the GP, L and NP gene of the LASV strain Kak428, which were acquired during the adaptation process to *M. natalensis* and assessed the growth behavior of the adapted variants both *in vitro* as well as *in vivo.* However, their individual contribution to overcome the virus host barrier, needs to be further elucidated, e. g. in life-cycle modelling systems.

6.4. Which step of the virus life cycle restricts LASV from spillover into new host species?

So far, evidence has been collected that the LASV GP, L and NP to contribute to the virus-host barriers for the heterologous Kak428 strain to infect *M. natalensis*. To assess their contribution to each step of the virus life cycle to this restriction, surrogate models were used. Firstly, it was shown that the Kak428 GP is principally able to mediate entry into *M. natalensis* cells efficiently by using a recombinant, replication-competent VSV-pseudotyped system with LASV GP on its surface. Examining viral entry with a confocal, laser scanning microscope revealed successful entry facilitated by the Kak428 GP and the Josiah GP, which was used as a lineage-matched surrogate for the Ba366 strain. It is important to note here, that the Josiah strain represents a human isolate and is thus not an ideal surrogate for the homologous Ba366 strain, which has been isolated from *M. natalensis,* when looking at virus-host restrictions in rodent hosts. However, at that time, a pseudotyped VSV with the Ba366 GP was not readily available. Therefore, additional experiments were performed with full LASV under BSL-4 conditions. The results from those entry assays pointed in the same direction as seen in the

entry assays with the VSV-pseudotyped viruses. The entry of the Kak428 strain into Vero76 cells (which have been also used to determine virus titers prior to the experiment) was not impaired. However, the entry of the Kak428 strain in the MasKEC and MasEF was reduced by approximately 50 % compared to the homologous Ba366 strain. This global observation can be due to different factors: inefficient interactions of the Kak428 GP with the cell surface receptor αDG, problems during the internalization of the virus particles or the release from the endosomes [241]. To further evaluate, which of these steps is affected, binding and internalization assays are needed. Those usually involve a virus binding step on ice to synchronize the virus attachment, followed by a temperature shift to 37 °C. Over a time course of 2 h, the virus can be monitored during the different entry steps, e. g. via fluorescence microscopy staining. Due to the complicated nature of these experiments under BSL4 restrictions and a lack of readily available reagents that would allow e.g. the staining of *Mastomys* cell endosomes with antibodies, these assays are still to be established. Binding assays to quantify the binding of the Kak428 GPC to αDG and LAMP1 of *Mastomys* also would give valuable insights into potential impairment of cell entry.

As the adaptation experiments also revealed that mutations accumulate in the Kak428 GP, the entry assays were repeated with the non-adapted (VP0) viruses and their adapted counterparts (VP10). Interestingly, an increased foci size was observed after the adaptation, pointing towards a better cell-to-cell spread of the adapted variants [217]. Additionally, the entry efficiency of the adapted viruses into the MasKEC and MasEF was increased, while their entry into Vero76 became less efficient. This could be explained by potential fitness trade-offs, meaning a successful adaptation to the *Mastomys* cells might come along with fitness costs for entry into Vero76 cells. For viruses which successfully adapted to a new host, it is often seen, that infection of the original host (or, in this case, the cell lines used regularly for amplification) is getting worse [162]. However, up to now, we cannot trace back, which GP mutations have contributed to the improved entry efficiency. For this, it would be helpful, to engineer recombinant viruses with only one mutation on the GP at a time.

In addition to the adaptation experiments, replicon assays were performed to examine the virus replication and transcription more in detail. First, the influence of exchanged NP and L in a replicon assay was investigated. The Kak428 L was overall more active than the Ba366 L but introducing the Kak428 NP into the system almost completely abolished the activity. The Kak428L/Kak428 NP combination reached again baseline levels, indicating that the Kak428 L

might compensate for the weak activity of the NP. In the *in vitro* experiment with the L chimera we could however not observe any increased activity or replication rates, highlighting that the L and NP as co-factors might be well adapted to each other in the full virus context and changing only one of them will always result in reduced activity in more complicated systems. During the adaptation process, mutations were found in both the NP and L genes, but the experiments with the chimeras as well as the first set of replicon assays highlight the strong inhibition conferred by the NP. Therefore, the mutations identified in the NP after the adaptation process were introduced and mimicked their effect on transcription and replication in another set of replicon assays. Those NP mutations led to a slight increase in activity. However, their contribution was not significant. As there were several mutations also in the L protein and none of the virus variants only had one mutation, the next step would be to determine the effect of double mutants by testing different combinations of L and NP mutations. Those mutations could be compensatory [161, 162]. Moreover, the system used in this study represents an artificial system without the presence of natural host cell factors from *M. natalensis* as the assays were performed in BSR-T7/5 cells. In the next steps, a transfer into a *Mastomys*-based *in vitro* system would be highly beneficial. To further dissect the replication and transcription processes, Northern Blots could be used.

7. Summary and outlook

During this study, an *in vitro* system to model LASV in one of the main rodent hosts, *M. natalensis,* was developed and compared to *in vivo* experiments. After having validated the expression of the major receptor and the efficient release of progeny virus from the MasKEC and MasEF cells, the growth kinetics on these cells also resembled the *in vivo* observations made by [157].

By generating chimeric viruses with Kak428 proteins in the genetic background of the Ba366 strain and comparing the infection dynamics of cell culture and animal experiments, the model was further validated. Here, the generation and characterization of a chimeric virus with the NP and L proteins replaced at the same time would be a great opportunity to study the interplay of the NP and L further. It would be particularly interesting if this potential L/NP chimera could be rescued quicker, indicating less attenuation than the NP chimera, and replicating to higher titers *in vitro*, proofing the compensatory effects known for the interplay of LASV L and NP.

Next, the adaptation process of Kak428 to MasKEC was performed and resulted in increased virus titers as well as a total of 20 potential host-adaptive mutations that were identified by NGS. These mutations were identified in the GP, L and NP genes, and their potential influence on the growth behavior changes seen earlier was discussed by using amino acid alignments and 3D structure models. To this date, only the NP mutations were characterized further due to the observation of a greater contribution of the NP to the virus-host barrier, which was made during replicon assays with interchanged proteins between the homologous and heterologous strains. The characterization of the other mutations is still ongoing. To further investigate the L protein mutations, further replicon assays could be applied to narrow down the contribution of each mutation to replication and transcription. Ideally, these replicon assays could be established on *Mastomys* cells so that all host factors are present during the assay. Additionally, the effect of two or more mutations at the same time should be assessed as some mutations could be compensatory. As indicated by virus entry assays with VP10 adapted variants in comparison to the virus variants before adaptation, a more efficient entry was seen after the adaptation. However, to date, the effects of each GP mutation was not assessed individually. This can be either done in further entry assays after introducing the mutation in either reverse-engineered, recombinant LASV or with the previously used

pseudotyped system. After having assessed the contribution of the L and NP mutations in the replicon assay, the mutation identified to be highly beneficial could also be inserted into recombinant viruses. All in all, the *in vitro* adaptation reduced the use of several animals and provided valuable insights in the arising mutations, but further experiments are needed to assess which of them has the greatest importance for the observed virus-host barrier. Once these mutations are known, they could be implemented in sequencing-based surveillance systems for LASV and serve as an indicator for spillover into *M. natalensis,* and thus posing a risk for human infections with these recently identified strains.

8. Supplements

Supplementary Table 1: Scoring of animals and humane endpoint criteria.

Monitoring	**Score[1]**
A Bodyweight	
Compared to control group for juveniles	
Unchanged or increased	0
Reduction < 5 %	1
Reduction < 10 %	2
Reduction < 20 %	3
B General well being	
Smooth, glossy, close-lying coat; clean orifices	0
Dull, matted or ruffled coat, cloudy eyes	1
Orifices moist or clotted by secretions; abnormal posture; high muscle tone; dehydration	2
Cramps or Spasms; paralysis; raspy breathing; hypothermia	3
C Behavior	
Normal behavior (sleep, reaction to stimuli, curiosity, social behavior)	0
Abnormal behavior; impaired motor skills or hyperkinetics	1
Isolation; signs of pain; apathy; pronounced hyperkinetics or stereotypy; ataxia	2
Automutilation	3
D Experiment specific criteria	
No experiment specific symptoms are expected	
Evaluation and measures taken	**Total Score**
No burden	0
Minor burden: continue close monitoring (1x daily) including supportive measures (e. g. heat supply, special food therapy)	1
Medium burden: Animal is euthanized	2
High burden: not applicable, as animals are euthanized at medium burden	3

[1] Scores are assigned once if at least one criterion is fulfilled. If multiple criteria are fulfilled in the same category, only the highest possible score is assigned.

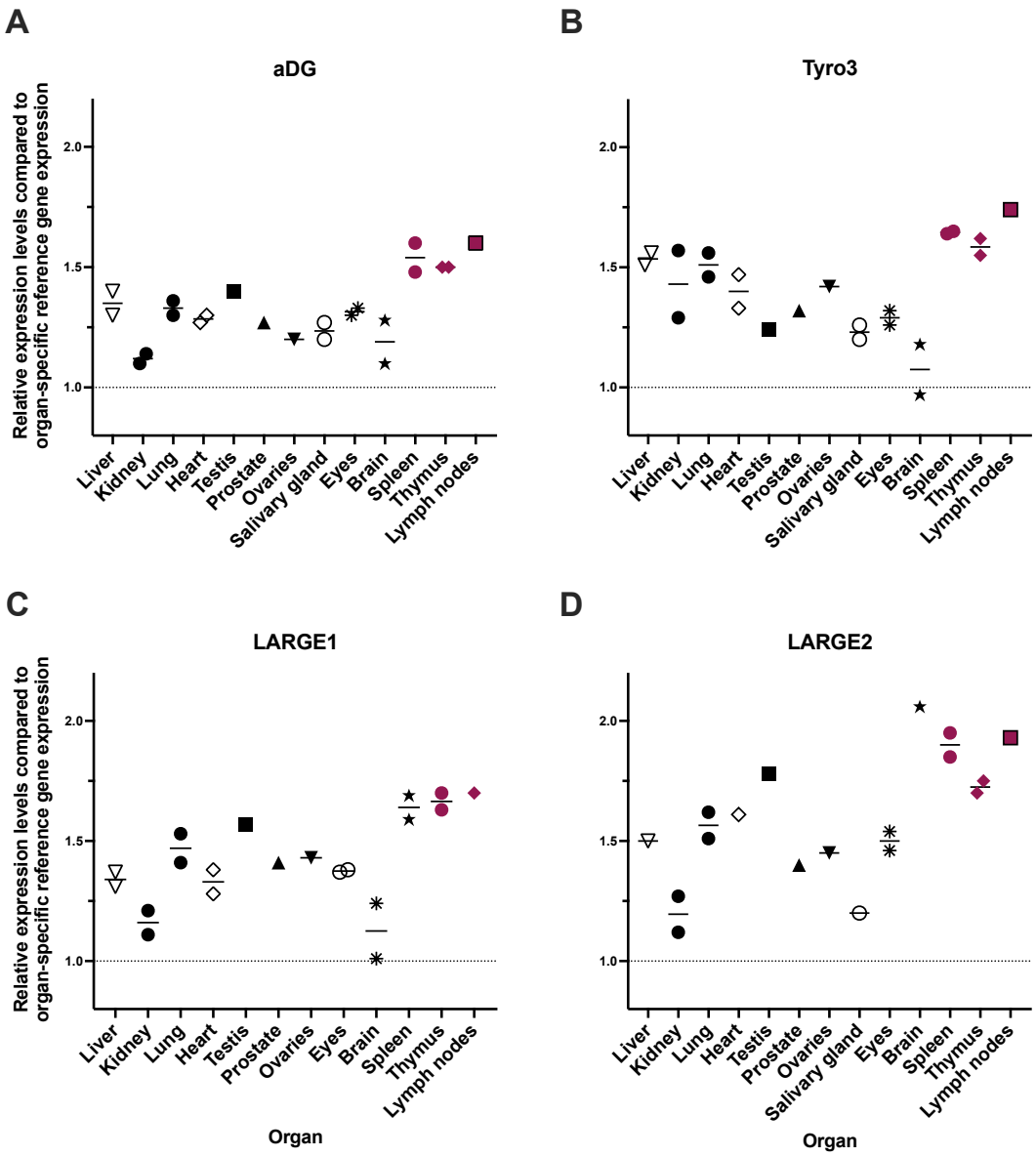

Supplementary Figure 1: Relative gene expression levels of LASV receptors in *M. natalensis* organs. **A** α-dystroglycan (αDG), **B** tyrosine-protein kinase receptor (Tyro3), **C** glycosyltransferase-like protein 1 (LARGE1) and **D** glycosyltransferase-like protein 2 (LARGE2) compared to organ-specific reference gene expression. Marked in red are immunogenic organs. The dashed line indicated the reference gene expression.

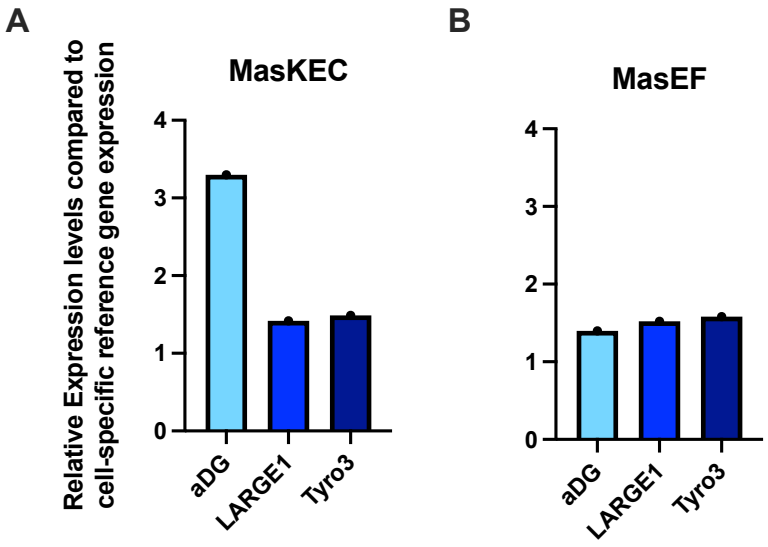

Supplementary Figure 2: Relative gene expression levels of LASV receptors in *Mastomys* cell lines. α-dystroglycan (αDG), glycosyltransferase-like protein 1 (LARGE1) and tyrosine-protein kinase receptor (Tyro3) compared to cell-specific reference gene expression in **A** *Mastomys* kidney epithelial cells (MasKEC) and **B** *Mastomys* embryonal fibroblasts (MasEF).

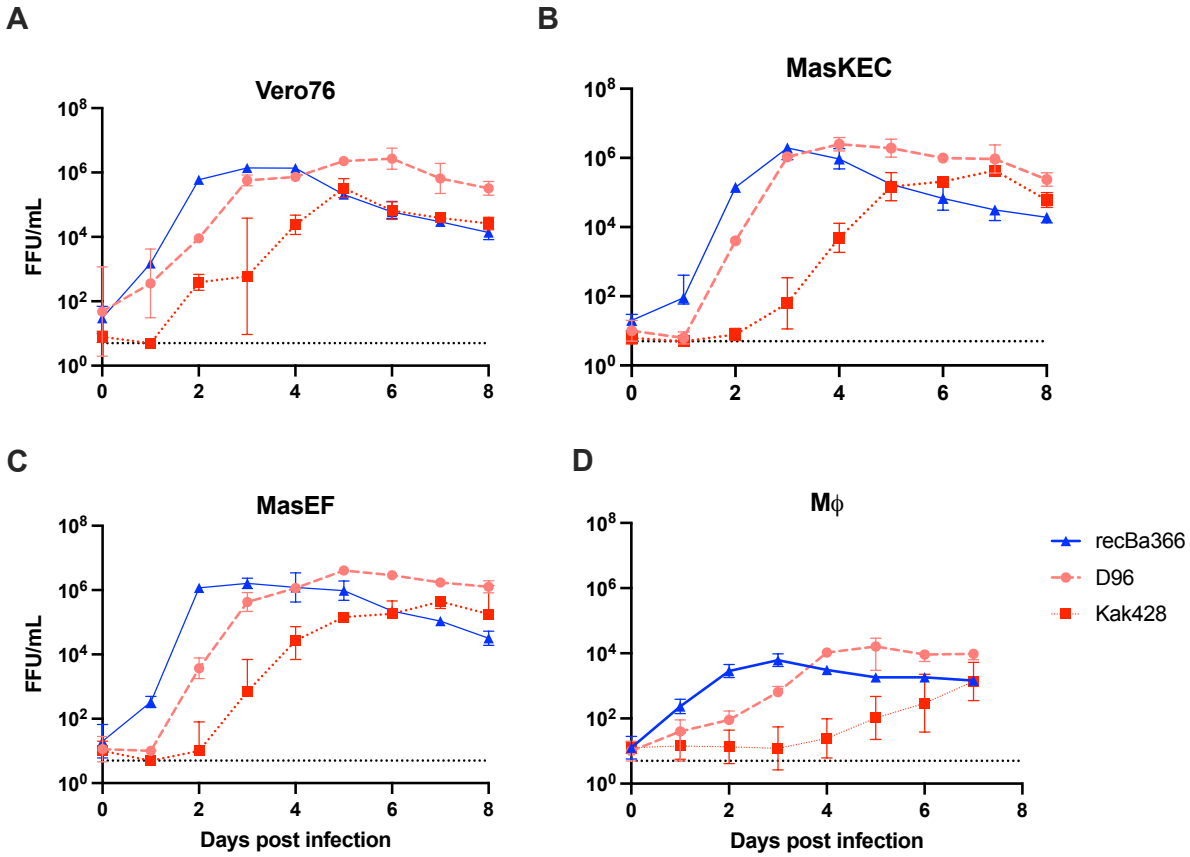

Supplementary Figure 3: Growth kinetics with homologous and heterologous LASV strains on different cell lines. Three different cells lines (**A** Vero76, **B** MasKEC and **C** MasEF and **D** MΦ) have been infected with a MOI of 0.01 for 8 days with either homologous (Ba366; blue triangles) or heterologous LASV strains (D96; pink circles, and Kak428; red rectangles). Virus supernatant was harvested on days 0, 1, 2, 3, 4, 5, 6, 7 and 8 post infection.

Viral titers in focus forming units per mL (FFU/mL) were determined by immunofocus assay. The dashed line indicates the limit of detection. Experiments were done with three technical replicates per experiment. Depicted are median titers with a 95 % confidence interval and standard deviation for the time points.

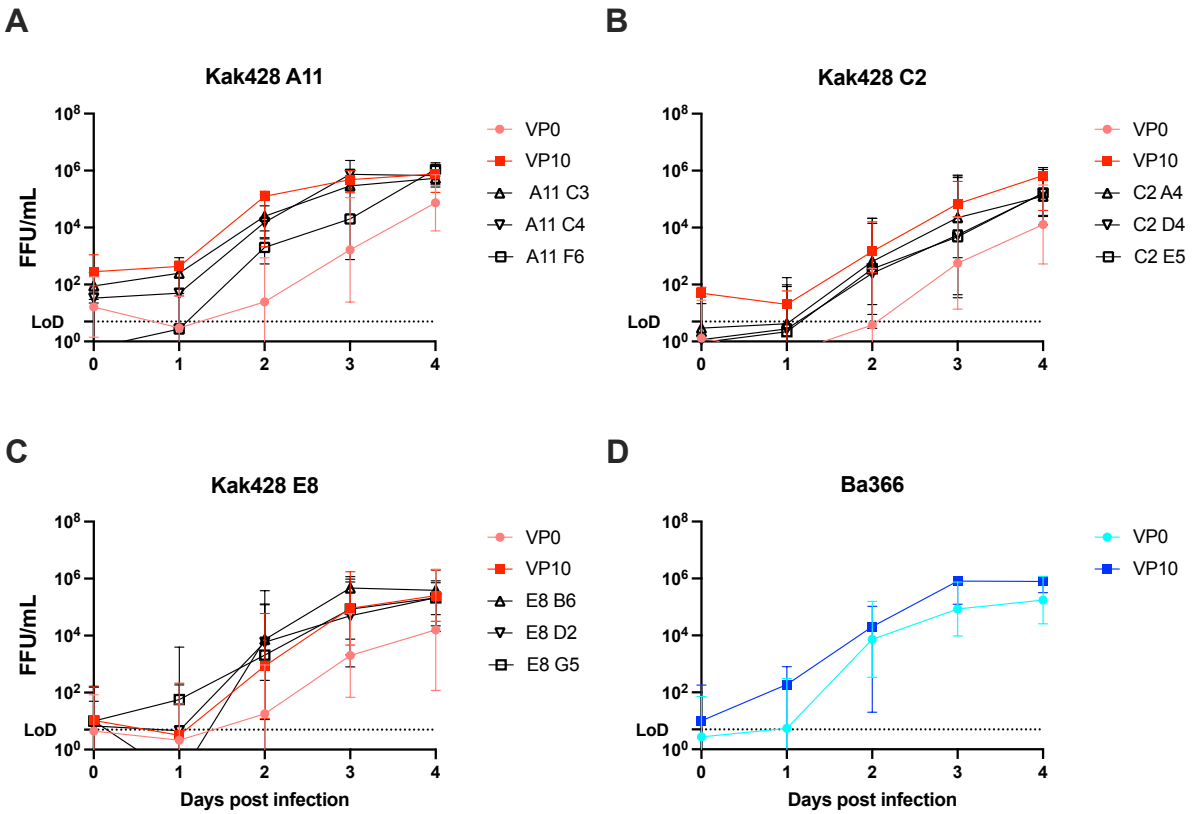

Supplementary Figure 4: Growth kinetics with homologous and heterologous LASV strains and its variants before and after adaptation on MasKEC including the sub-variants of VP10. MasKEC have been infected with a MOI of 0.01 for 4 days with either homologous (Ba366) or heterologous Kak428 LASV strain and its sub-variants. Virus supernatant was harvested on days 0, 1, 2, 3 and 4 post infection. Viral titers in focus forming units per mL (FFU/mL) were determined by immunofocus assay. The dashed line indicates the limit of detection (LoD). Experiments were done with three technical replicates per experiment. Depicted are median titers with a 95 % confidence interval and standard deviation for the time points.

Supplementary Table 2: Virus titers in liver, spleen, kidney, and gonads of *M. natalensis* following inoculation with the chimeras.

Group	Sampling period. (w. p. i.)	Liver			Spleen			Kidney			Gonads		
		positive/ tested[1]	FFU/g of Organ		positive/ tested[1]	FFU/g of Organ		positive/ tested[1]	FFU/g of Organ		positive/ tested[1]	FFU/g of Organ	
			Min	Max		Min	Max		Min	Max		Min	Max
GP Chimera	1	0/3	negative		1/3	2.78E+02		0/3	negative		n. t.	n. t.	n. t.
	2	0/3	negative		0/3	negative		0/3	negative		0/3	negative	
	3	0/2	negative		1/2	7.14E+02		0/2	negative		0/2	negative	
	4	0/2	negative		0/2	negative		0/2	negative		0/2	negative	
L Chimera	1	1/4	6.58E+01		1/4	2.63E+02		1/4	5.81E+01		2/3	2.17E+02	1.28E+04
	2	0/4	negative		0/4	negative		0/4	negative		0/4	negative	
	3	0/3	negative		0/3	negative		0/3	negative		0/3	negative	
	4	0/3	negative		0/3	negative		0/3	negative		0/3	negative	
NP Chimera	1	1/4	8.06E+01		4/4	1.85E+02	1.58E+03	1/4	7.25E+01		0/2	negative	
	2	0/4	negative		0/4	negative		0/4	negative		0/4	negative	
	3	0/3	negative		0/3	negative		0/3	negative		0/3	negative	
Z Chimera	1	4/4	1.34E+06	2.19E+07	4/4	4.08E+06	3.78E+07	4/4	1.67E+07	4.41E+07	n. t.	n. t.	n. t.
	2	4/5	5.24E+03	1.65E+05	5/5	3.36E+04	1.96E+06	5/5	1.45E+05	1.67E+07	4/4	2.57E+06	1.39E+08

Supplementary Table 3: Virus titers in heart, lung, brain, and salivary glands of *M. natalensis* following inoculation with Kak428 VP10 adapted LASV strains.

Group	Sampling period. (w. p. i.)	Heart			Lung			Brain			Salivary glands		
		positive/ tested[1]	FFU/g of Organ		positive/ tested[1]	FFU/g of Organ		positive/ tested[1]	FFU/g of Organ		positive/ tested[1]	FFU/g of Organ	
			Min	Max		Min	Max		Min	Max		Min	Max
GP Chimera	1	0/3	negative		0/3	negative		0/3	negative		0/3	negative	
	2	0/3	negative		1/3	1.56E+02	9.21E+03	1/3	2.67E+01		0/3	negative	
	3	0/2	negative		0/2	negative		0/2	negative		0/2	negative	
	4	0/2	negative		0/2	negative		0/2	negative		0/2	negative	
L Chimera	1	4/4	3.57E+02	2.14E+03	4/4	1.22E+03		1/4	1.93E+01		2/4	2.86E+02	2.03E+03
	2	1/4	8.62E+01		2/4	3.06E+02	7.41E+02	0/4	negative		0/4	negative	
	3	0/3	negative		0/3	negative		1/3	1.61E+01		0/3	negative	
	4	0/3	negative		0/3	negative		0/3	negative		0/3	negative	
NP Chimera	1	2/4	3.33E+02	4.84E+02	4/4	1.09E+02	2.63E+02	0/4	negative		1/4	1.43E+02	
	2	0/4	negative		0/4	negative		0/4	negative		0/4	negative	
	3	0/3	negative		0/3	negative		0/3	negative		n. t.	n. t.	n. t.
Z Chimera	1	4/4	7.44E+06	1.67E+07	4/4	4.75E+07	5.78E+08	4/4	7.47E+05	9.07E+06	3/3	1.08E+05	5.58E+06
	2	5/5	1.16E+05	7.84E+06	5/5	1.87E+06	1.89E+08	4/4	1.20E+07	9.47E+07	4/4	1.85E+02	1.64E+06

Supplementary Table 4: Virus titers in thymus and eyes of *M. natalensis* following inoculation with chimeric viruses.

Group	Sampling period (w.p.i.)	Thymus			Eyes		
		positive/tested[1]	FFU/g of Organ		positive/tested[1]	FFU/g of Organ	
			Min	Max		Min	Max
GP Chimera	1	0/3	negative		0/3	negative	
	2	0/3	negative		0/3	negative	
	3	n. t.	n. t.	n. t.	0/2	negative	
	4	n. t.	n. t.	n. t.	0/2	negative	
L Chimera	1	1/4	2.27E+02		n. t.	n. t.	n. t.
	2	0/4	negative		1/4	2.17E+02	
	3	0/3	negative		0/3	negative	
	4	0/3	negative		0/3	negative	
NP Chimera	1	0/4	negative		2/4	5.56E+02	1.67E+03
	2	0/4	negative		2/4	1.22E+02	2.94E+02
	3	n. t.	n. t.	n. t.	0/3	negative	
Z Chimera	1	3/3	1.60E+07	7.78E+07	3/3	1.13E+07	7.25E+07
	2	4/4	1.36E+05	5.53E+06	4/4	1.96E+06	3.98E+06

Supplementary Table 5: Genome coverage per virus passage and variant. All passages with a coverage <1000 have been marked in grey.

Passage	A11	C2	E8	recBa366
0	20837	288765	161698	160766
1	18	86	27	31
2	84	147	41	114550
3	45955	14386	1399	1877
4	99479	93824	14908	211585
5	176273	224432	42312	2377
6	6096	66174	73188	122302
7	5585	4575	5394	582
8	10803	49838	31492	16215
9	9562	10051	481	1039
10	10659	7	37043	14360

Supplementary Table 6: Genome coverage per virus passage of the Kak428 VP10 sub-variants.

	Sub-variants		
	A11		
	C3	**C4**	**F6**
Coverage	93263	104349	71609
	C2		
	A4	**D4**	**E5**
Coverage	n/a	75804	181557
	E8		
	B6	**D2**	**G5**
Coverage	352045	229049	2655402

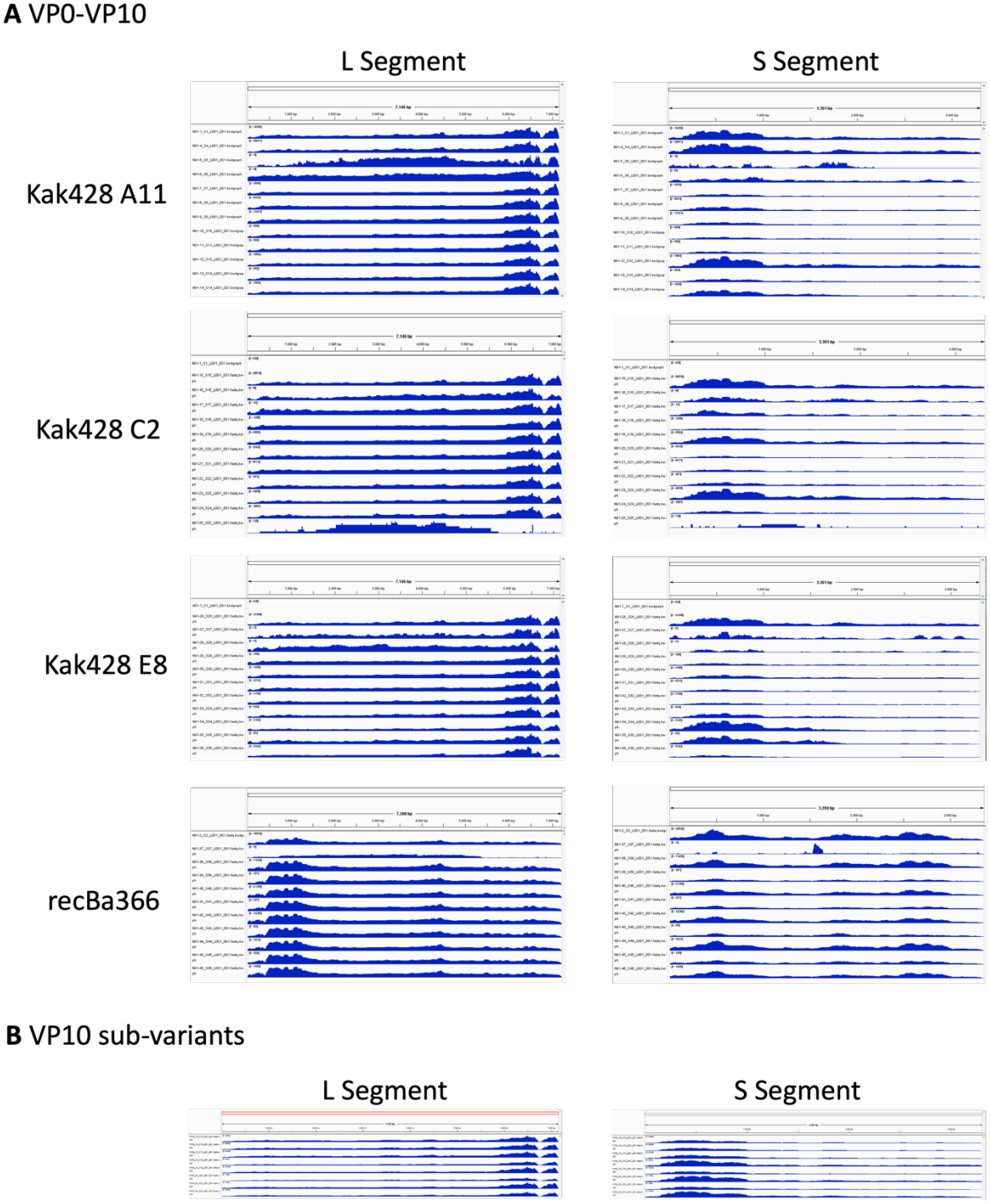

Supplementary Figure 5: Coverage plots of the sequenced variants. A Coverage plots of virus passages 0 to 10 of the variants Kak428 A11, C2 and E8 as well as Ba366. **B** Coverage plots of the VP10 sub-variants.

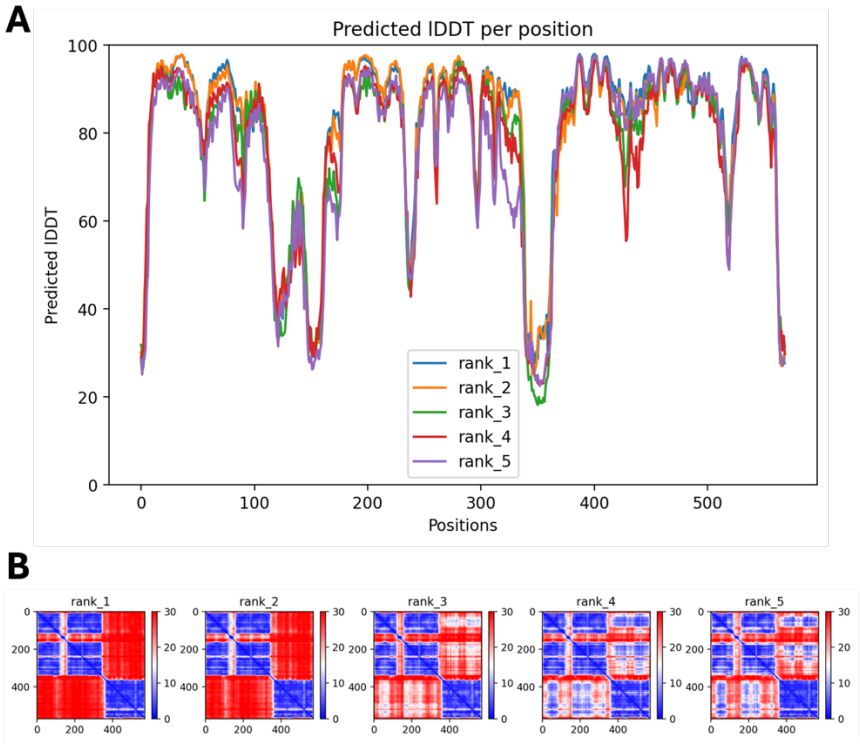

Supplementary Figure 6: Quality measures of the AlphaFold2 prediction for the Kak428 NP protein. A shows the predicted IDDT per position and **B** shows the predicted alignment error (PAE).

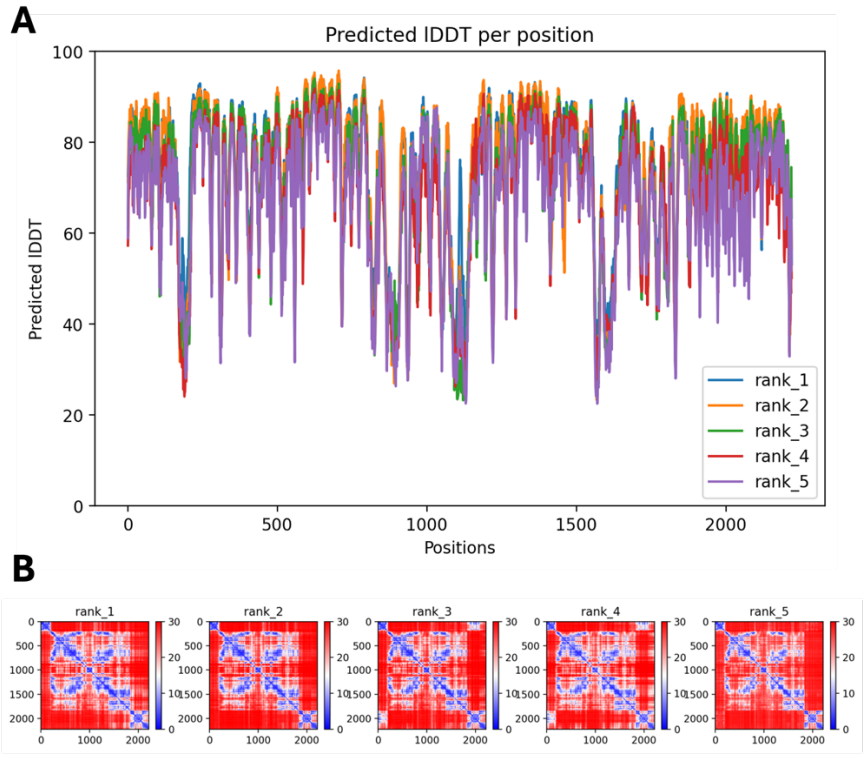

Supplementary Figure 7: Quality measures of the AlphaFold2 prediction for the Kak428 L protein. A shows the predicted IDDT per position and **B** shows the predicted alignment error (PAE).

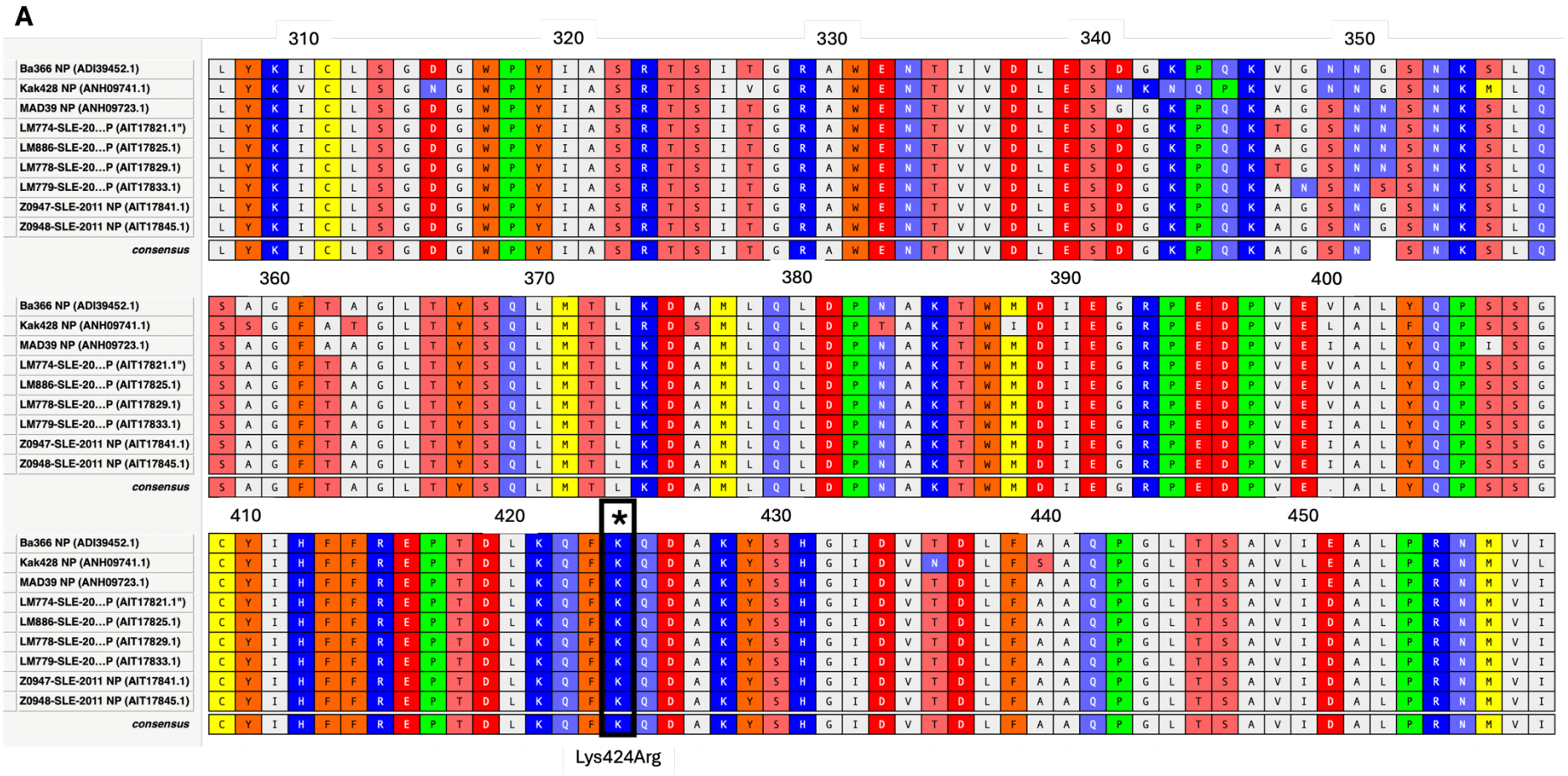
A
310
320
330
340
350
Ba366 NP (ADI39452.1)
Kak428 NP (ANH09741.1)
MAD39 NP (ANH09723.1)
LM774-SLE-20...P (AIT17821.1")
LM886-SLE-20...P (AIT17825.1)
LM778-SLE-20...P (AIT17829.1)
LM779-SLE-20...P (AIT17833.1)
Z0947-SLE-2011 NP (AIT17841.1)
Z0948-SLE-2011 NP (AIT17845.1)
consensus
360
370
380
390
400
410
420
430
440
450
Lys424Arg

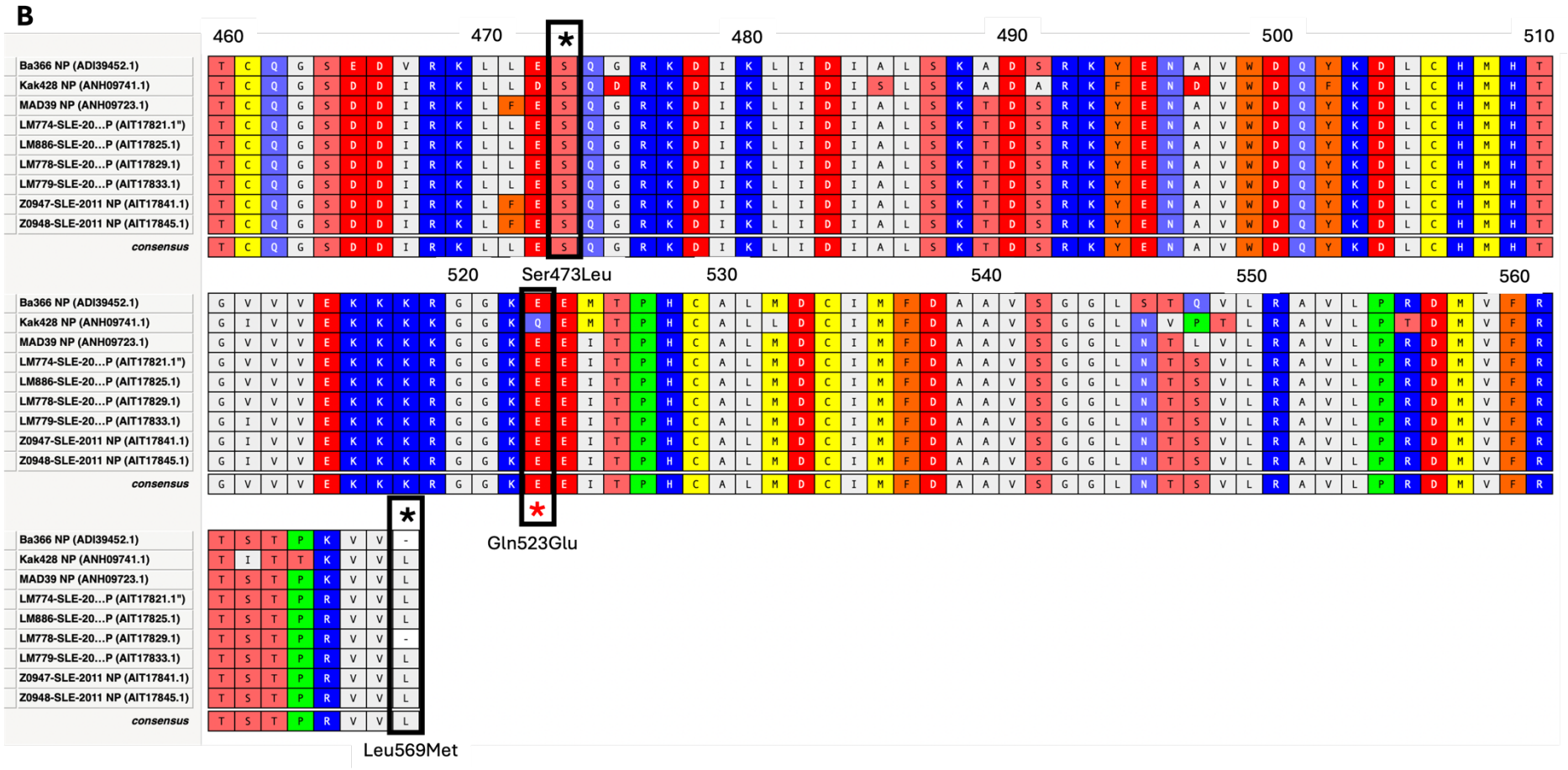

Supplementary Figure 8: Amino acid alignment of the Kak428 NP in comparison with different *Mastomys*-derived NP sequences. A Amino acid sequences from 307 aa – 459 aa, **B** 460 aa – 569 aa. The Kak428 and Ba366 NP sequences were aligned to different *Mastomys*-derived NP sequences in MacVector by using the Clustal W algorithm. Mutations identified in our NGS dataset were marked with asterisks. Black asterisks indicate regions with consensus sequences and red asterisks mark regions in which the Kak428 NP has a different amino acid than the other isolates.

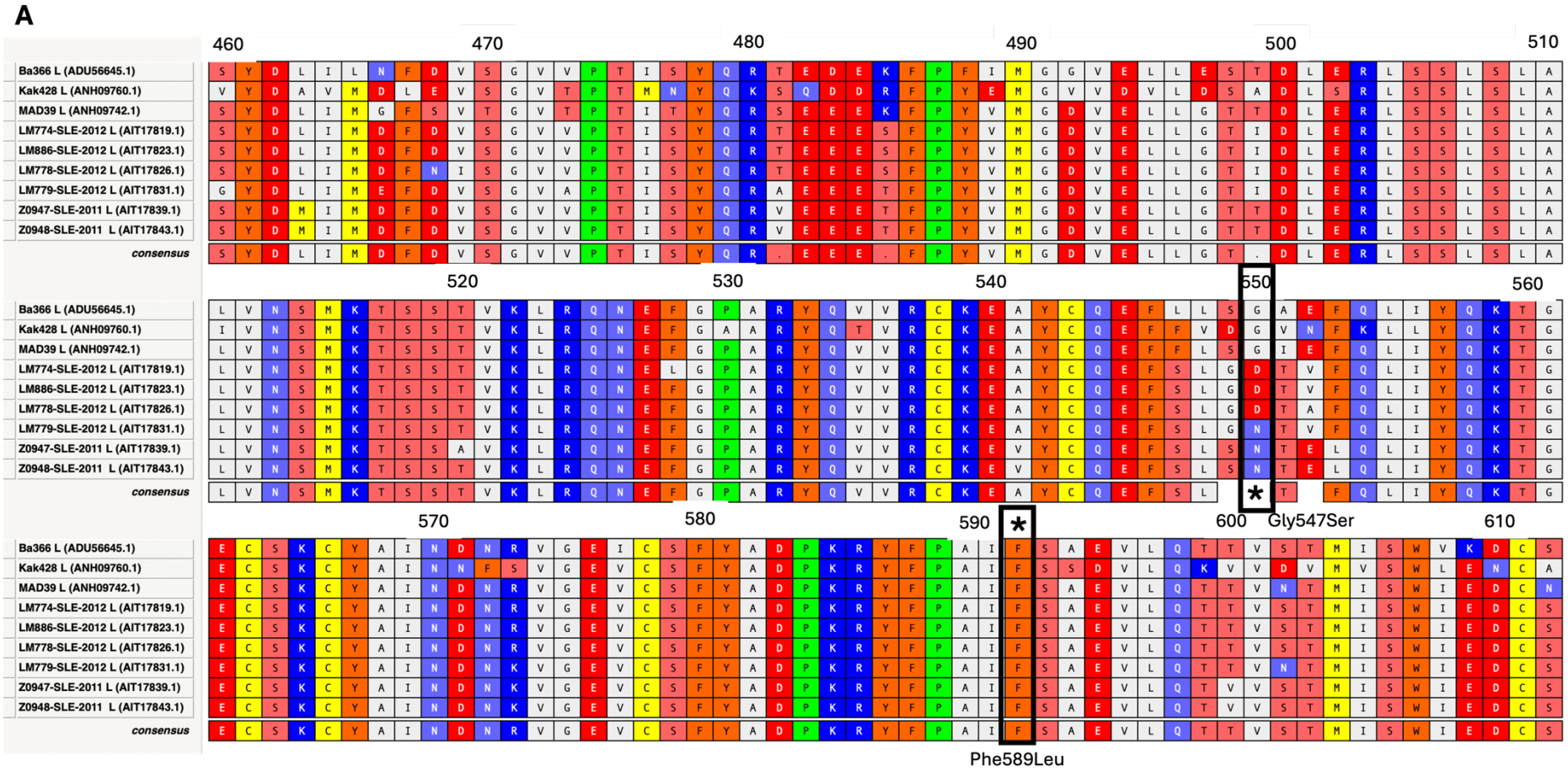
A
460
470
480
490
500
510
Ba366 L (ADU56645.1)
Kak428 L (ANH09760.1)
MAD39 L (ANH09742.1)
LM774-SLE-2012 L (AIT17819.1)
LM886-SLE-2012 L (AIT17823.1)
LM778-SLE-2012 L (AIT17826.1)
LM779-SLE-2012 L (AIT17831.1)
Z0947-SLE-2011 L (AIT17839.1)
Z0948-SLE-2011 L (AIT17843.1)
consensus
520
530
540
550
560
570
580
590
600
610
Gly547Ser
Phe589Leu

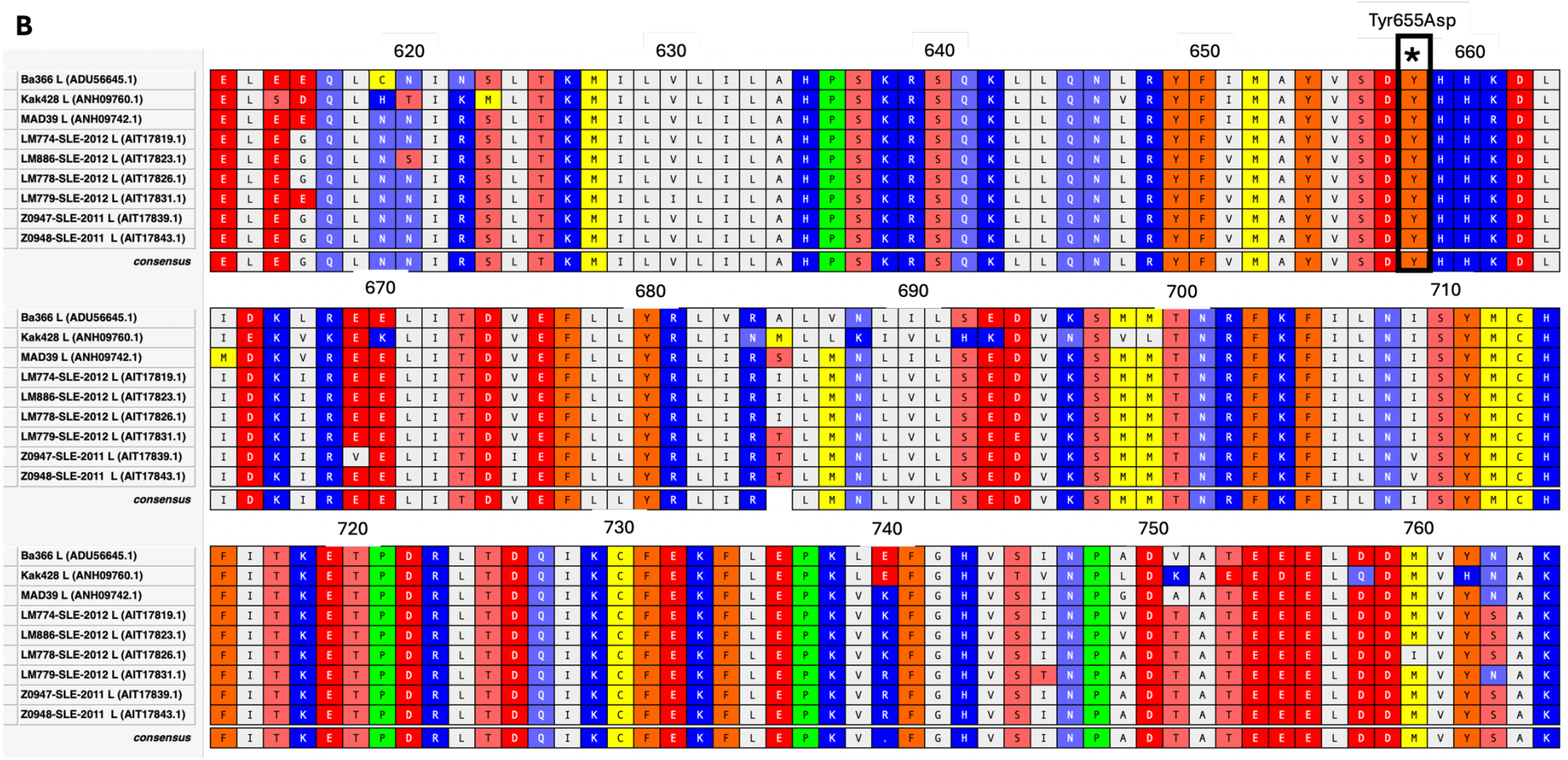
B
Tyr655Asp
620
630
640
650
660
670
680
690
700
710
720
730
740
750
760
Ba366 L (ADU56645.1)
Kak428 L (ANH09760.1)
MAD39 L (ANH09742.1)
LM774-SLE-2012 L (AIT17819.1)
LM886-SLE-2012 L (AIT17823.1)
LM778-SLE-2012 L (AIT17826.1)
LM779-SLE-2012 L (AIT17831.1)
Z0947-SLE-2011 L (AIT17839.1)
Z0948-SLE-2011 L (AIT17843.1)
consensus

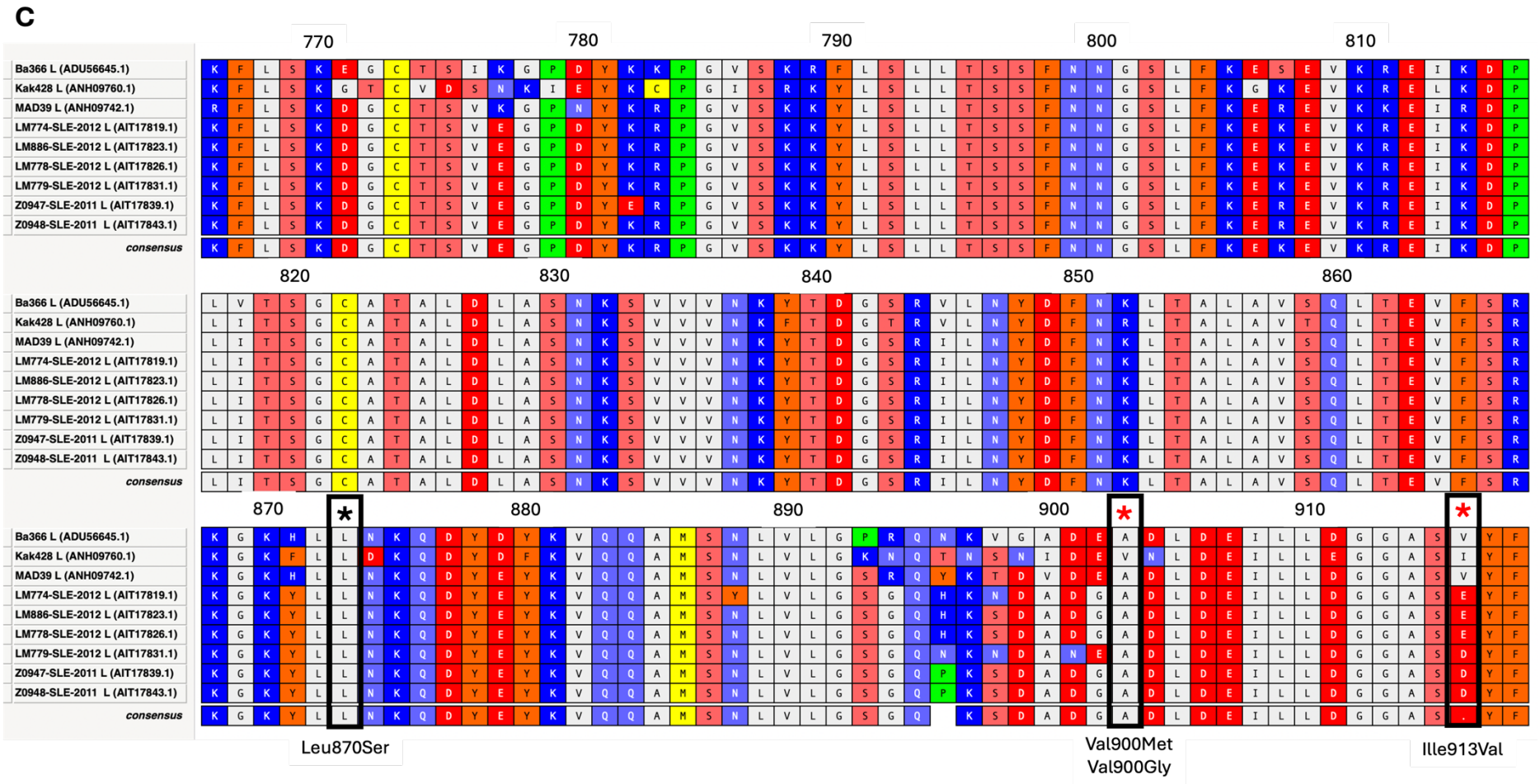
C
770
780
790
800
810
Ba366 L (ADU56645.1)
Kak428 L (ANH09760.1)
MAD39 L (ANH09742.1)
LM774-SLE-2012 L (AIT17819.1)
LM886-SLE-2012 L (AIT17823.1)
LM778-SLE-2012 L (AIT17826.1)
LM779-SLE-2012 L (AIT17831.1)
Z0947-SLE-2011 L (AIT17839.1)
Z0948-SLE-2011 L (AIT17843.1)
consensus
820
830
840
850
860
870
880
890
900
910
Leu870Ser
Val900Met
Val900Gly
Ille913Val

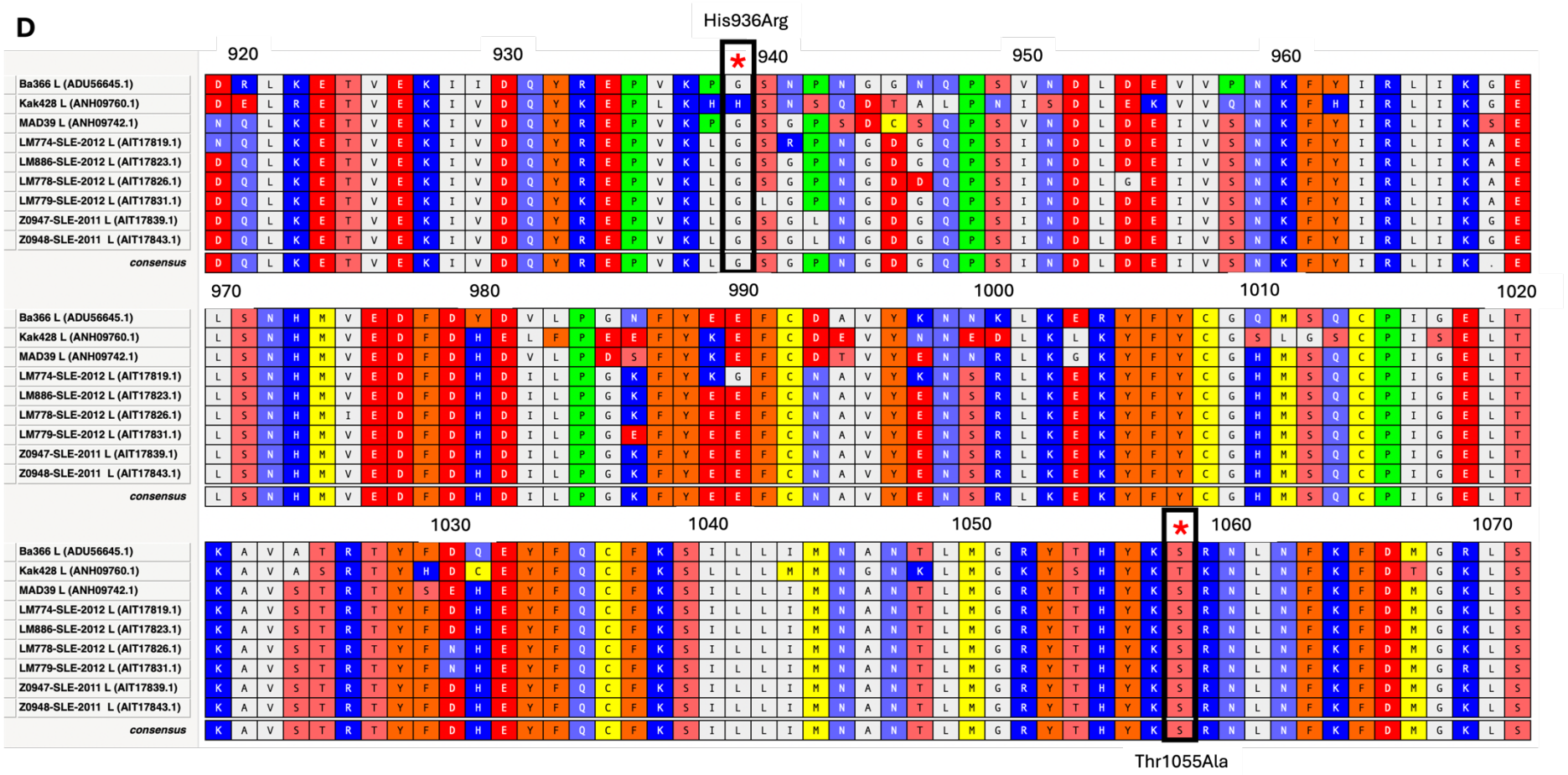
D
His936Arg
920
930
940
950
960
970
980
990
1000
1010
1020
1030
1040
1050
1060
1070
Ba366 L (ADU56645.1)
Kak428 L (ANH09760.1)
MAD39 L (ANH09742.1)
LM774-SLE-2012 L (AIT17819.1)
LM886-SLE-2012 L (AIT17823.1)
LM778-SLE-2012 L (AIT17826.1)
LM779-SLE-2012 L (AIT17831.1)
Z0947-SLE-2011 L (AIT17839.1)
Z0948-SLE-2011 L (AIT17843.1)
consensus
Thr1055Ala

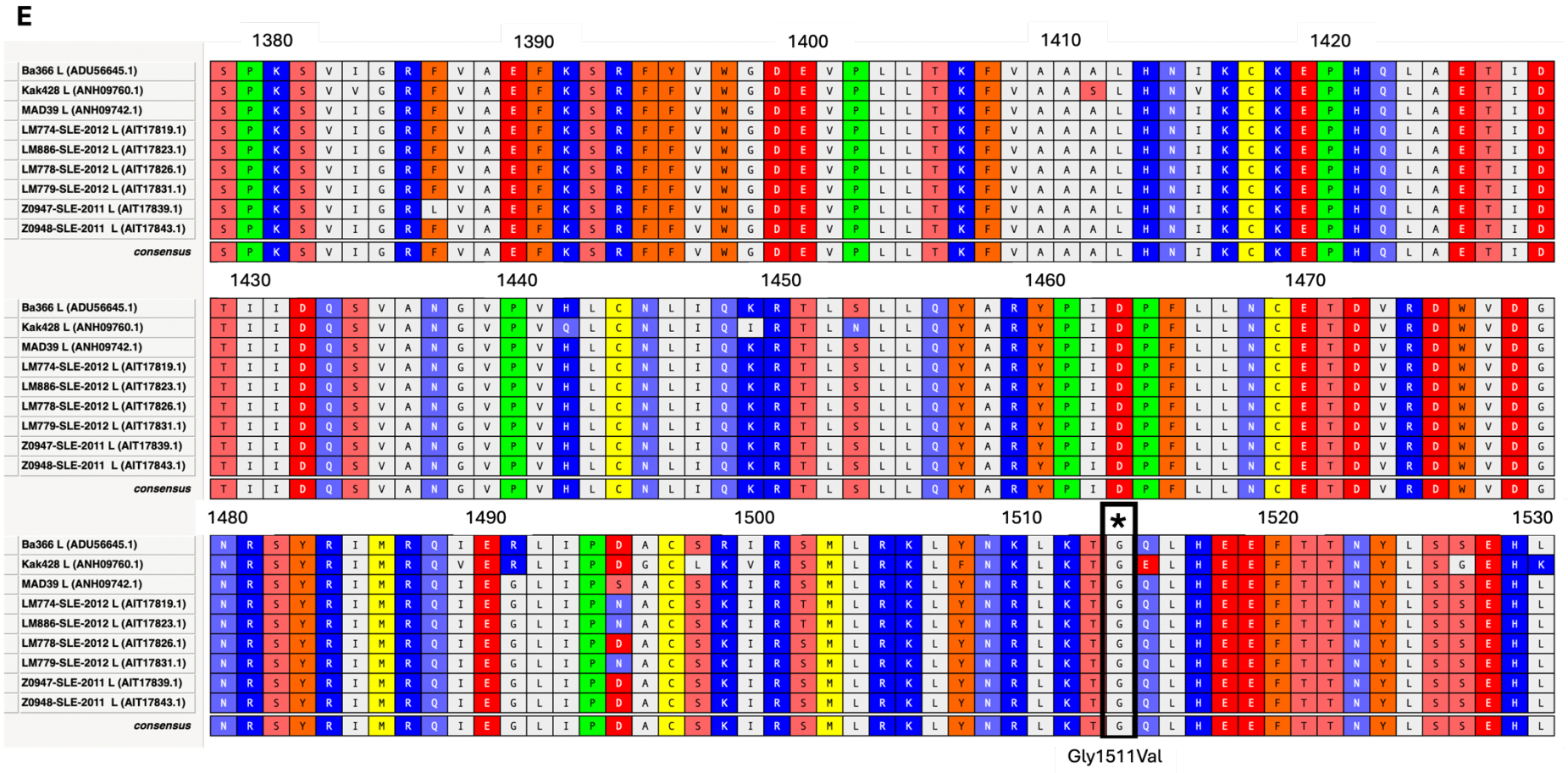
E
1380
1390
1400
1410
1420
Ba366 L (ADU56645.1)
Kak428 L (ANH09760.1)
MAD39 L (ANH09742.1)
LM774-SLE-2012 L (AIT17819.1)
LM886-SLE-2012 L (AIT17823.1)
LM778-SLE-2012 L (AIT17826.1)
LM779-SLE-2012 L (AIT17831.1)
Z0947-SLE-2011 L (AIT17839.1)
Z0948-SLE-2011 L (AIT17843.1)
consensus
1430
1440
1450
1460
1470
1480
1490
1500
1510
1520
1530
*
Gly1511Val

F

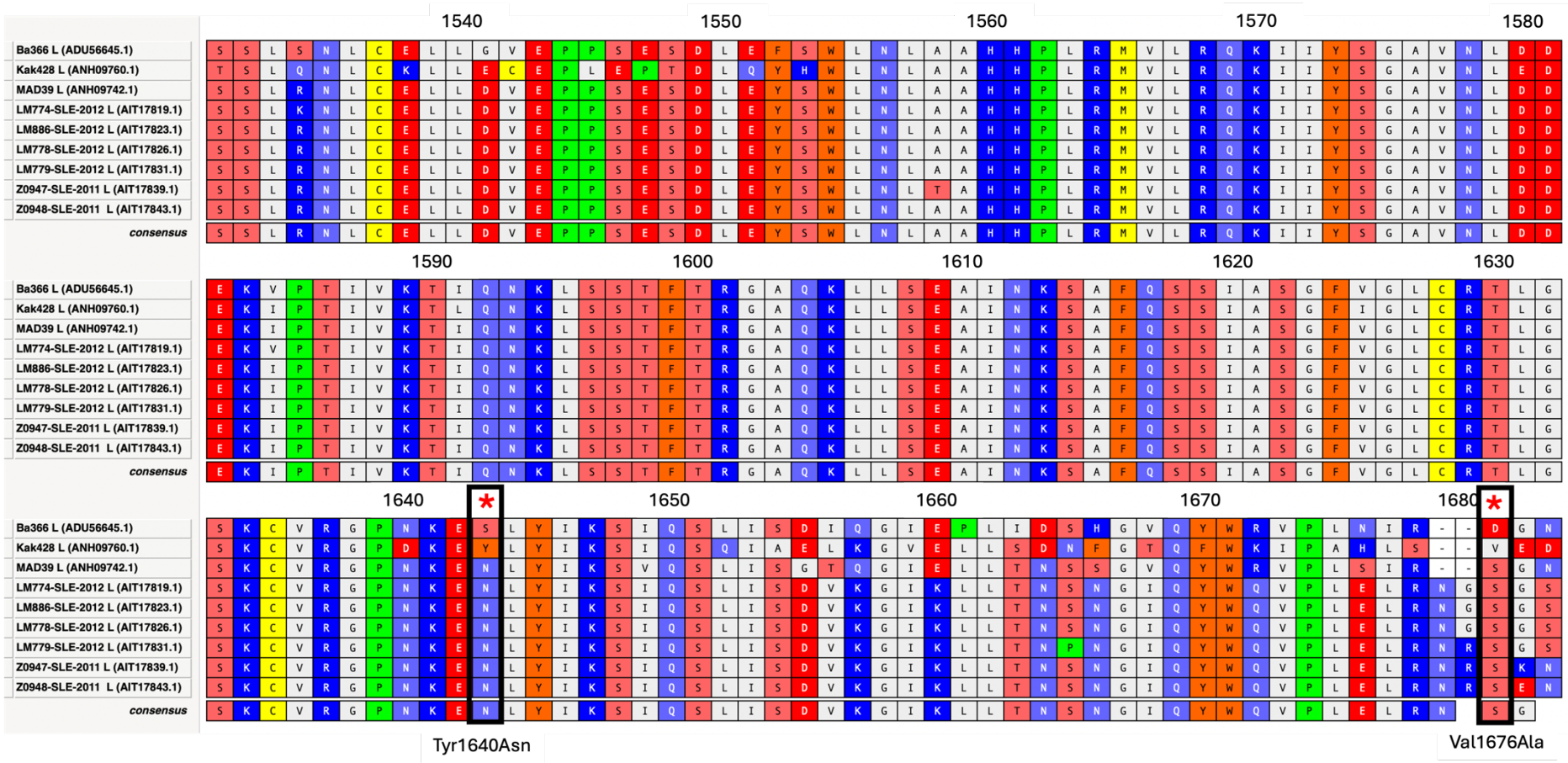
1540
1550
1560
1570
1580
Ba366 L (ADU56645.1)
Kak428 L (ANH09760.1)
MAD39 L (ANH09742.1)
LM774-SLE-2012 L (AIT17819.1)
LM886-SLE-2012 L (AIT17823.1)
LM778-SLE-2012 L (AIT17826.1)
LM779-SLE-2012 L (AIT17831.1)
Z0947-SLE-2011 L (AIT17839.1)
Z0948-SLE-2011 L (AIT17843.1)
consensus
1590
1600
1610
1620
1630
1640
1650
1660
1670
1680
Tyr1640Asn
Val1676Ala

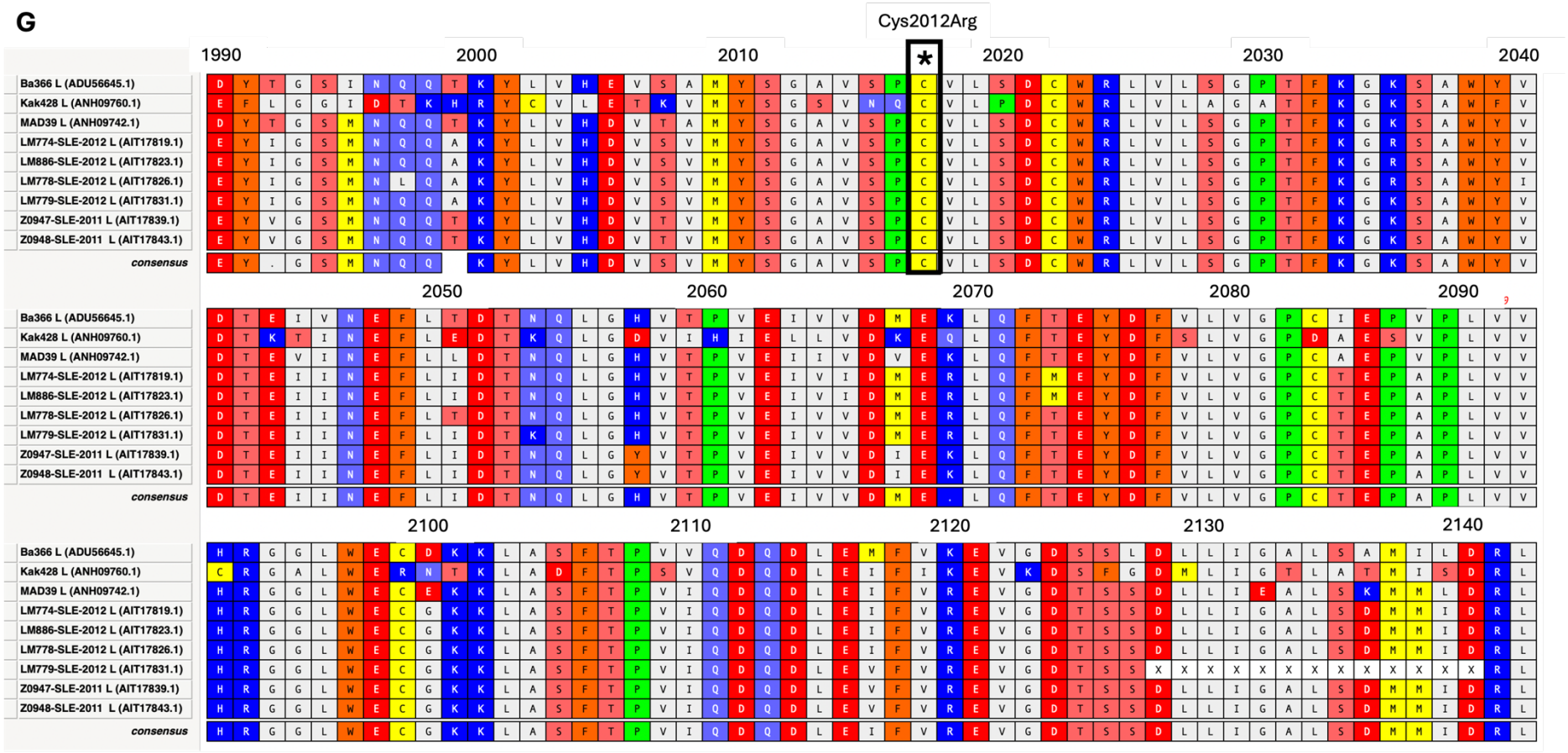

Supplementary Figure 9: Amino acid alignment of the Kak428 L in comparison with different *Mastomys*-derived L sequences.A Amino acid sequences from 460 – 4612 aa, **B** 766 – 918 aa **C** 919 – 1071 aa, **D** 1072- 1224 aa, **E** 1378 – 1530 aa, **F** 1531 -1683 aa, **G** 1990 – 2142 aa. The Kak428 and Ba366 GP sequences were aligned to different *Mastomys*-derived GP sequences in MacVector by using the Clustal W algorithm. Mutations identified in our NGS dataset were marked with asterisks. Black asterisks indicate region with consensus sequences and red asterisks mark regions in which the Kak428 NP has a different amino acid than the other isolates. Please not here, that the amoni acid positions described in te text do not match exactly with the position marked in this alignment, as the Clustal W algorithm also inserted gaps in the sequences.

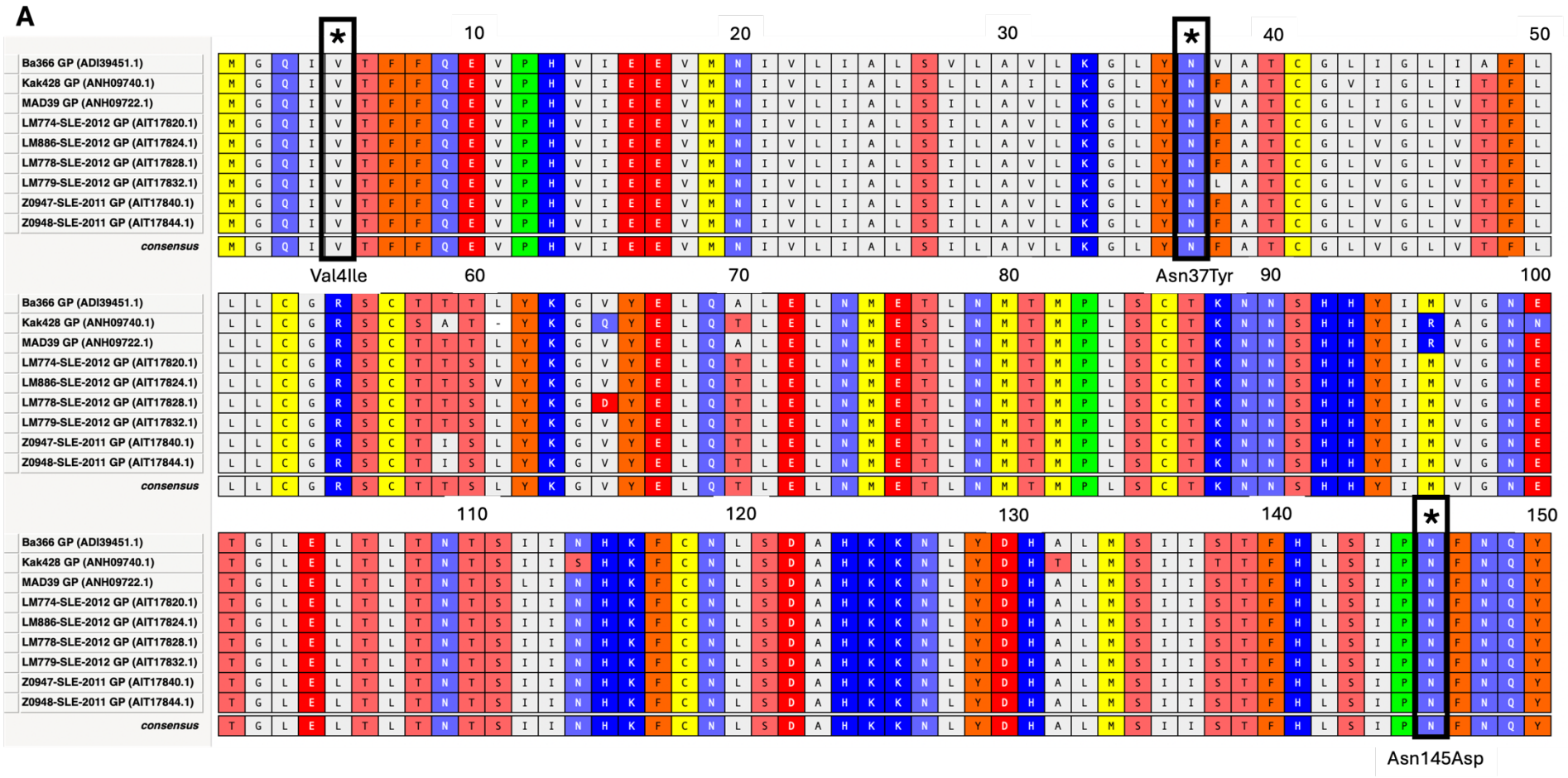
A
Ba366 GP (ADI39451.1)
Kak428 GP (ANH09740.1)
MAD39 GP (ANH09722.1)
LM774-SLE-2012 GP (AIT17820.1)
LM886-SLE-2012 GP (AIT17824.1)
LM778-SLE-2012 GP (AIT17828.1)
LM779-SLE-2012 GP (AIT17832.1)
Z0947-SLE-2011 GP (AIT17840.1)
Z0948-SLE-2011 GP (AIT17844.1)
consensus
Val4Ile
Asn37Tyr
Asn145Asp

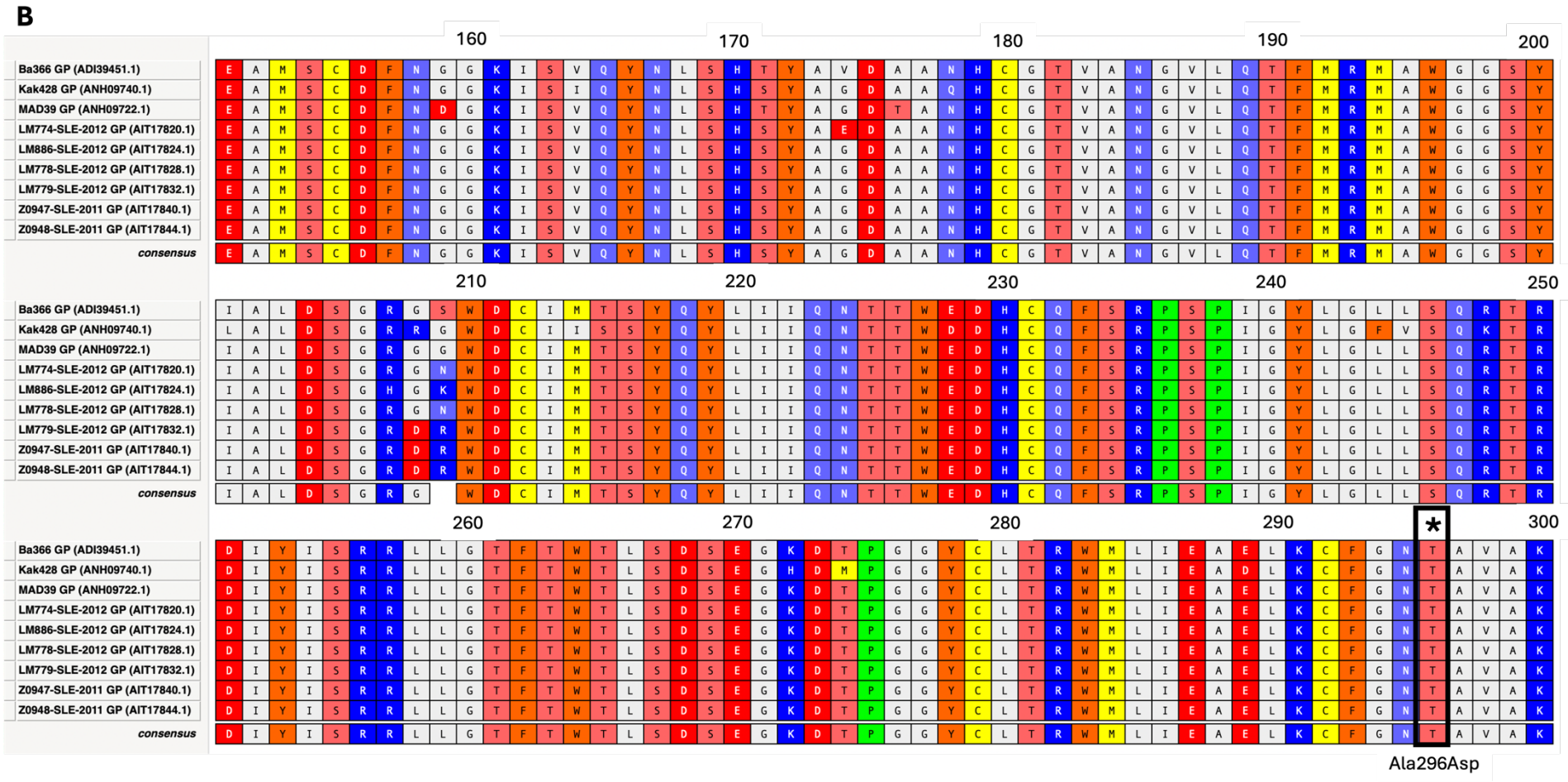

Supplementary Figure 10: Amino acid alignment of the Kak428 GP in comparison with different *Mastomys*-derived GP sequences. A Amino acid sequences from 1 aa – 150 aa, **B** 151 aa – 300 aa The Kak428 and Ba366 GP sequences were aligned to different *Mastomys*-derived GP sequences in MacVector by using the Clustal W algorithm. Mutations identified in our NGS dataset were marked with asterisks. Black asterisks indicate region with consensus sequences.

Supplementary Table 7: Virus titers in liver, spleen, kidney, and gonads of *M. natalensis* following inoculation with Kak428 VP10 adapted LASV strains.

Group	Sampling period. (w. p. i.)	Liver			Spleen			Kidney			Gonads		
		positive/ tested[1]	FFU/g of Organ		positive/ tested[1]	FFU/g of Organ		positive/ tested[1]	FFU/g of Organ		positive/ tested[1]	FFU/g of Organ	
			Min	Max		Min	Max		Min	Max		Min	Max
Kak428 A11	1	0/2	negative	negative	1/2	1.25E+03		1/2	8.50E+01		2/2	1.50E+01	5.00E+01
	2	0/2	negative	negative	0/2	negative	negative	0/2	negative	negative	0/2	negative	negative
	3	0/2	negative	negative	0/2	negative	negative	0/2	negative	negative	0/2	negative	negative
	4	0/2	negative	negative	0/2	negative	negative	0/2	negative	negative	0/2	negative	negative
Kak428 C2	1	0/3	negative	negative	0/3	negative	negative	0/3	negative	negative	0/3	negative	negative
	2	0/3	negative	negative	0/3	negative	negative	0/3	negative	negative	0/3	negative	negative
	3	0/3	negative	negative	0/3	negative	negative	0/3	negative	negative	0/3	negative	negative
	4	0/4	negative	negative	0/4	negative	negative	0/4	negative	negative	0/4	negative	negative
Kak428 E8	1	3/3	4.35E+01	9.77E+02	3/3	5.00E+02	1.83E+04	2/3	3.51E+02	1.63E+03	n. t.	n. t.	n. t.
	2	0/3	negative		0/3	negative		0/3	negative		0/3	negative	
	3	0/2	negative		0/2	negative		0/2	negative		0/2	negative	
	4	0/2	negative		0/2	negative		0/2	negative		0/2	negative	

[1] The number of positive organs versus the total number of tested organs is shown.

Supplementary Table 8: Virus titers in heart, lung, brain, and salivary glands of *M. natalensis* following inoculation with Kak428 VP10 adapted LASV strains.

Group	Sampling period (w. p. i.)	Heart			Lung			Brain			Salivary glands		
		positive/ tested[1]	FFU/g of Organ		positive/ tested[1]	FFU/g of Organ		positive/ tested[1]	FFU/g of Organ		positive/ tested[1]	FFU/g of Organ	
			Min	Max		Min	Max		Min	Max		Min	Max
Kak428 A11	1	2/2	2.50E+02	2.60E+02	2/2	3.15E+02	5.50E+04	2/2	5.00E+00	1.50E+01	2/2	1.95E+02	1.15E+02
	2	0/2	negative	negative	0/2	negative	negative	0/2	negative	negative	0/2	negative	negative
	3	0/2	negative	negative	0/2	negative	negative	0/2	negative	negative	0/2	negative	negative
	4	0/2	negative	negative	0/2	negative	negative	1/2	1.10E+03		0/2	negative	negative
Kak428 C2	1	0/3	negative	negative	0/3	negative	negative	0/3	negative	negative	2/3	5.00E+00	1.50E+01
	2	0/3	negative	negative	0/3	negative	negative	0/3	negative	negative	0/3	negative	negative
	3	0/3	negative	negative	0/3	negative	negative	0/3	negative	negative	0/3	negative	negative
	4	0/4	negative	negative	0/4	negative	negative	0/4	negative	negative	0/4	negative	negative
Kak428 E8	1	3/3	3.43E+04	2.45E+05	3/3	5.13E+03	3.13E+05	2/3	5.62E+01	3.48E+03	2/3	8.77E+01	2.25E+03
	2	1/3	5.88E+01		3/3	2.40E+03	5.11E+03	1/3	1.19E+03		0/3	negative	
	3	0/2	negative		0/2	negative		0/2	negative		1/2	1.53E+02	
	4	0/2	negative		0/2	negative		0/2	negative		0/2	negative	

[1] The number of positive organs versus the total number of tested organs is shown.

Supplementary Table 9: Virus titers in thymus and eyes of *M. natalensis* following inoculation with Kak428 VP10 adapted LASV strains.

Group	Sampling period (w.p.i.)	Thymus			Eyes		
		positive/tested[1]	FFU/g of Organ		positive/tested[1]	FFU/g of Organ	
			Min	Max		Min	Max
Kak428 A11	1	2/2	1.00E+01	4.00E+01	2/2	3.15E+02	4.45E+03
	2	0/2	negative	negative	1/2	5.00E+00	
	3	0/2	negative	negative	1/2	5.98E+03	
	4	0/2	negative	negative	2/2	3.57E+05	8.14E+05
Kak428 C2	1	1/3	5.00E+00		2/3	1.00E+01	2.50E+01
	2	1/3	5.00E+00		0/3	negative	negative
	3	0/3	negative	negative	0/3	negative	negative
	4	0/4	negative	negative	0/4	negative	negative
Kak428 E8	1	3/3	3.33E+02	6.88E+03	3/3	3.65E+03	3.89E+05
	2	0/3	negative		2/3	2.94E+03	4.39E+03
	3	n. t.	n. t.	n. t.	2/2	2,05E+04	1,39E+05
	4	0/2	negative		1/2	2.38E+02	.

[1] The number of positive organs versus the total number of tested organs is shown.

Supplementary Table 10: Overview of support during experiments

Experiment type	Own contribution	Contribution from others	Name of helping person
qPCR for LASV receptor expression	Testing and performing the assay on *Mastomys* samples	Primer (Tyro3) design	Thomas Strecker & Helena Müller-Kräuter (Philipps University Marburg)
Transmission electron microscopy	Infection experiments and data analysis	Fixation, staining and imaging	Katharina Höhn (BNITM EM core facility)
Cloning of plasmids for LASV chimeras	Cloning	Cloning assistance	Stephanie Wurr & Lukas Jungblut (BNITM)
Animal experiments (chimeras and adapted viruses)	Sample preparation and processing, titrations and data analysis	Infections, scoring, euthanasia, support with data analysis	Chris Hoffmann, Lisa Oestereich, Ludmilla Unrau (BNITM)
Next Generation Sequencing of adapted viruses	Infection experiments, inactivation, RNA isolation	Library preparation and Illumina Sequencing, Genome Assembly	Daniel Cadar (BNITM NGS core facility)
NGS Data analysis	Data analysis	Setting up the analysis workflow	Rui da Costa and Trøels Scheel (University of Copenhagen)
AlphaFold and protein modelling	Provided sequences and performed analysis	Modelling L protein with AlphaFold and displaying NP, GP and L models in Pymol	Timothy Soh, Maria Rosenthal, Harry Williams & Lennart Sänger (BNITM/CSSB)
Immunofluorescence with pseudotyped VSV	Infection experiments, data analysis	Infection experiments, planning	Sarah Müller-Aguirre, Anna-Lena Rupp & Thomas Strecker (Philipps University Marburg)
Entry assays	Performing the assays	Assay establishment	Helena Müller-Kräuter (Philipps University Marburg)

Replicon assays to characterize the NP mutations	Assay design and data analysis	Cloning of mutations and performing the replicon assays	Chloé Madras (ESTBB) & Anna-Lena Rupp (Philipps University Marburg)

9. List of abbreviations

aa	Amino acids
αDG	α-dystroglycan
AIV	Avian influenza virus
ANP32A	Acidic nuclear phosphoprotein 32 family member
APOBEC	Apolipoprotein B mRNA editing enzyme, catalytic polypeptide
BNITM	Bernhard Nocht Institute for Tropical Medicine
BSL-4	Biosafety laboratory level 4
CAT	chloramphenicol acetyltransferase
d. p. i.	Days post infection
DC-SIGN	Dendritic cell-specific intercellular adhesion molecule -3 grabbing
DIP	Defective interfering particle
DNA	Desoxyribonucleic acid
EBS-LASV	Emergent BioSolutions LASV vaccine candidate
ELISA	Enzyme-linked immunosorbent assay
ESCRT	Endosomal sorting complexes required for transport
ExoN	Exonuclease
FDA	Food and drug administration
FELASA	Federation of European Laboratory Animal Science Associations
G	Glycoprotein
GAIV	Gairo virus
Gal	Galactose
GISN	Global Influenza Surveillance Network
GISRS	Global Influenza Surveillance and Response System
GlcNAc	Glucosamine
GMEM	Glasgow's Minimum Essential Medium
GP	Glycoprotein
GP1	Glycoprotein subunit 1
GP2	Glycoprotein subunit 2
GPC	Glycoprotein precursor complex
H. pamfi	*Hylomyscus pamfi*

HA	Hemagglutinin
HIV	Human immunodeficiency virus
hTFR1	the human transferrin receptor 1
IAV	Influenza A virus
IDT	Integrated DNA Technologies
IFN	Interferon
IFN-γ	Interferon-γ
IgG	Immunglobulin G
IgM	Immunglobulin M
IRF3	Interferon-regulatory factor 3
ISG	Interferon-stimulated gene
IUCN	International Union for Conservation of Nature
L	L protein
L Segment	Large Segment
LAMP1	Lysosomal-associated membrane protein 1
LARGE	Like-acetylglucosaminyltransferase
LF	Lassa fever
LASV	Lassa virus
MAD39	LASV Madina strain
MasEF	*Mastomys* embryonal fibroblasts
MasKEC	*Mastomys* kidney epithelial cells
M-CSF	Macrophage colony- stimulating factor
M. natalensis	*Mastomys natalensis*
MDA5	Melanoma differentiation-associated protein 5
MG	Mini genome
MOBV	Mobala virus
MOI	Multiplicity of infection
MOPV	Mopeia virus
MORV	Morogoro virus
mRNA	Messenger RNA
MV	Measles virus
Mθ	Bone marrow-derived macrophages

N	Number
NA	Neuraminidase
Neu5Ac	N-acetylneuraminic acid
NGS	Next Generation Sequencing
NP	Nucleoprotein
ns	non-significant
NS1	Non-structural protein 1
PA	Polymerase acidic
PCR	Polymerase chain reaction
PAE	Predicted alignment error
PB	Polymerase basic
RIG-I	Retinoic acid-inducible gene I
RKI	Robert Koch Institute
RLU	Relative light units
RNA	Ribonucleic acid
RNP	Ribonucleoprotein complex
RT-PCR	Reverse transcription polymerase chain reaction
S Segement	Small Segment
SIA	Sialic acid
SKI-1/S1P	Subtilase/kexin isozyme-1
Spase	Cellular signal peptidase
SSP	Stable signal peptide
STD	Standard deviation
T7	Bacteriophage *T7*
TAM	Tyro3/Axl/Mer
TAMV-FL	Tamiami mammarenavirus
TEM	Transmission electron microscopy
TMB	3,3’,5,5’-Tetramethylbenzidine
TNF-α	Tumor necrosis factor-α
TRIM5α	Tripartite motif-containing protein 5
VLP	Virus-like particle
VP	Virus passage

vRNA	Viral RNA
VSV	Vesicular stomatitis virus
WHO	World Health Organization
Z	matrix protein Z

10. List of figures

11. List of tables

12. List of supplementary figures

13. List of supplementary tables

14. Bibliography

[1] A. J. Basinski *et al.*, "Bridging the gap: Using reservoir ecology and human serosurveys to estimate Lassa virus spillover in West Africa," *PLoS Comput Biol,* vol. 17, no. 3, p. e1008811, Mar 2021, doi: 10.1371/journal.pcbi.1008811.

[2] M. D. Bajani *et al.*, "A survey for antibodies to Lassa virus among health workers in Nigeria," *Trans R Soc Trop Med Hyg,* vol. 91, no. 4, pp. 379-81, Jul-Aug 1997, doi: 10.1016/s0035-9203(97)90247-9.

[3] D. E. Carey *et al.*, "Lassa fever. Epidemiological aspects of the 1970 epidemic, Jos, Nigeria," *Trans R Soc Trop Med Hyg,* vol. 66, no. 3, pp. 402-8, 1972, doi: 10.1016/0035-9203(72)90271-4.

[4] O. Tomori, A. Fabiyi, A. Sorungbe, A. Smith, and J. B. McCormick, "Viral hemorrhagic fever antibodies in Nigerian populations," *Am J Trop Med Hyg,* vol. 38, no. 2, pp. 407-10, Mar 1988, doi: 10.4269/ajtmh.1988.38.407.

[5] H. A. White, "Lassa fever. A study of 23 hospital cases," *Trans R Soc Trop Med Hyg,* vol. 66, no. 3, pp. 390-401, 1972, doi: 10.1016/0035-9203(72)90269-6.

[6] J. M. Troup, H. A. White, A. L. Fom, and D. E. Carey, "An outbreak of Lassa fever on the Jos plateau, Nigeria, in January-February 1970. A preliminary report," *Am J Trop Med Hyg,* vol. 19, no. 4, pp. 695-6, Jul 1970, doi: 10.4269/ajtmh.1970.19.695.

[7] D. G. Bausch *et al.*, "Lassa fever in Guinea: I. Epidemiology of human disease and clinical observations," *Vector Borne Zoonotic Dis,* vol. 1, no. 4, pp. 269-81, Winter 2001, doi: 10.1089/15303660160025903.

[8] I. S. Lukashevich, J. C. Clegg, and K. Sidibe, "Lassa virus activity in Guinea: distribution of human antiviral antibody defined using enzyme-linked immunosorbent assay with recombinant antigen," *J Med Virol,* vol. 40, no. 3, pp. 210-7, Jul 1993, doi: 10.1002/jmv.1890400308.

[9] J. Ter Meulen *et al.*, "Hunting of peridomestic rodents and consumption of their meat as possible risk factors for rodent-to-human transmission of Lassa virus in the Republic of Guinea," *Am J Trop Med Hyg,* vol. 55, no. 6, pp. 661-6, Dec 1996, doi: 10.4269/ajtmh.1996.55.661.

[10] J. Ter Meulen *et al.*, "Detection of Lassa virus antinucleoprotein immunoglobulin G (IgG) and IgM antibodies by a simple recombinant immunoblot assay for field use," *J Clin Microbiol,* vol. 36, no. 11, pp. 3143-8, Nov 1998, doi: 10.1128/JCM.36.11.3143-3148.1998.

[11] J. B. McCormick, P. A. Webb, J. W. Krebs, K. M. Johnson, and E. S. Smith, "A prospective study of the epidemiology and ecology of Lassa fever," *J Infect Dis,* vol. 155, no. 3, pp. 437-44, Mar 1987, doi: 10.1093/infdis/155.3.437.

[12] D. W. Fraser, C. C. Campbell, T. P. Monath, P. A. Goff, and M. B. Gregg, "Lassa fever in the Eastern Province of Sierra Leone, 1970-1972. I. Epidemiologic studies," *Am J Trop Med Hyg,* vol. 23, no. 6, pp. 1131-9, Nov 1974, doi: 10.4269/ajtmh.1974.23.1131.

[13] O. B. Salu *et al.*, "Molecular confirmation and phylogeny of Lassa fever virus in Benin Republic 2014-2016," *Afr J Lab Med,* vol. 8, no. 1, p. 803, 2019, doi: 10.4102/ajlm.v8i1.803.

[14] A. Yadouleton *et al.*, "Lassa fever in Benin: description of the 2014 and 2016 epidemics and genetic characterization of a new Lassa virus," *Emerg Microbes Infect,* vol. 9, no. 1, pp. 1761-1770, Dec 2020, doi: 10.1080/22221751.2020.1796528.

[15] J. D. Frame, P. B. Jahrling, J. E. Yalley-Ogunro, and M. H. Monson, "Endemic Lassa fever in Liberia. II. Serological and virological findings in hospital patients," *Trans R Soc Trop Med Hyg,* vol. 78, no. 5, pp. 656-60, 1984, doi: 10.1016/0035-9203(84)90232-3.

[16] J. D. Frame, J. E. Yalley-Ogunro, and A. P. Hanson, "Endemic Lassa fever in Liberia. V. Distribution of Lassa virus activity in Liberia: hospital staff surveys," *Trans R Soc Trop Med Hyg,* vol. 78, no. 6, pp. 761-3, 1984, doi: 10.1016/0035-9203(84)90012-9.

[17] T. P. Monath *et al.*, "A hospital epidemic of Lassa fever in Zorzor, Liberia, March-April 1972," *Am J Trop Med Hyg,* vol. 22, no. 6, pp. 773-9, Nov 1973, doi: 10.4269/ajtmh.1973.22.773.

[18] P. E. Mertens, R. Patton, J. J. Baum, and T. P. Monath, "Clinical presentation of Lassa fever cases during the hospital epidemic at Zorzor, Liberia, March-April 1972," *Am J Trop Med Hyg,* vol. 22, no. 6, pp. 780-4, Nov 1973, doi: 10.4269/ajtmh.1973.22.780.

[19] M. H. Monson, J. D. Frame, P. B. Jahrling, and K. Alexander, "Endemic Lassa fever in Liberia. I. Clinical and epidemiological aspects at Curran Lutheran Hospital, Zorzor, Liberia," *Trans R Soc Trop Med Hyg,* vol. 78, no. 4, pp. 549-53, 1984, doi: 10.1016/0035-9203(84)90082-8.

[20] J. E. Yalley-Ogunro, J. D. Frame, and A. P. Hanson, "Endemic Lassa fever in Liberia. VI. Village serological surveys for evidence of Lassa virus activity in Lofa County, Liberia," *Trans R Soc Trop Med Hyg,* vol. 78, no. 6, pp. 764-70, 1984, doi: 10.1016/0035-9203(84)90013-0.

[21] M. Mateo *et al.*, "Fatal Case of Lassa Fever, Bangolo District, Cote d'Ivoire, 2015," *Emerg Infect Dis,* vol. 25, no. 9, pp. 1753-1756, Sep 2019, doi: 10.3201/eid2509.190239.

[22] J. T. Manning, N. Forrester, and S. Paessler, "Lassa virus isolates from Mali and the Ivory Coast represent an emerging fifth lineage," *Front Microbiol,* vol. 6, p. 1037, 2015, doi: 10.3389/fmicb.2015.01037.

[23] S. L. M. Whitmer *et al.*, "New Lineage of Lassa Virus, Togo, 2016," *Emerg Infect Dis,* vol. 24, no. 3, pp. 599-602, Mar 2018, doi: 10.3201/eid2403.171905.

[24] A. A. Patassi *et al.*, "Emergence of Lassa Fever Disease in Northern Togo: Report of Two Cases in Oti District in 2016," *Case Rep Infect Dis,* vol. 2017, p. 8242313, 2017, doi: 10.1155/2017/8242313.

[25] J. Q. McKendrick, W. S. D. Tennant, and M. J. Tildesley, "Modelling seasonality of Lassa fever incidences and vector dynamics in Nigeria," *PLoS Negl Trop Dis,* vol. 17, no. 11, p. e0011543, Nov 2023, doi: 10.1371/journal.pntd.0011543.
[26] T. P. Monath, V. F. Newhouse, G. E. Kemp, H. W. Setzer, and A. Cacciapuoti, "Lassa virus isolation from Mastomys natalensis rodents during an epidemic in Sierra Leone," *Science,* vol. 185, no. 4147, pp. 263-5, Jul 19 1974, doi: 10.1126/science.185.4147.263.
[27] D. H. Walker, H. Wulff, J. V. Lange, and F. A. Murphy, "Comparative pathology of Lassa virus infection in monkeys, guinea-pigs, and Mastomys natalensis," *Bull World Health Organ,* vol. 52, no. 4-6, pp. 523-34, 1975. [Online]. Available: https://www.ncbi.nlm.nih.gov/pubmed/821625.
[28] S. P. Fisher-Hoch *et al.*, "Review of cases of nosocomial Lassa fever in Nigeria: the high price of poor medical practice," *BMJ,* vol. 311, no. 7009, pp. 857-9, Sep 30 1995, doi: 10.1136/bmj.311.7009.857.
[29] S. Gunther and O. Lenz, "Lassa virus," *Crit Rev Clin Lab Sci,* vol. 41, no. 4, pp. 339-90, 2004, doi: 10.1080/10408360490497456.
[30] S. Gunther *et al.*, "Imported lassa fever in Germany: molecular characterization of a new lassa virus strain," *Emerg Infect Dis,* vol. 6, no. 5, pp. 466-76, Sep-Oct 2000, doi: 10.3201/eid0605.000504.
[31] C. Lehmann *et al.*, "Control measures following a case of imported Lassa fever from Togo, North Rhine Westphalia, Germany, 2016," *Euro Surveill,* vol. 22, no. 39, Sep 2017, doi: 10.2807/1560-7917.ES.2017.22.39.17-00088.
[32] R. F. Garry, "Lassa fever - the road ahead," *Nat Rev Microbiol,* vol. 21, no. 2, pp. 87-96, Feb 2023, doi: 10.1038/s41579-022-00789-8.
[33] T. Wolf, R. Ellwanger, U. Goetsch, N. Wetzstein, and R. Gottschalk, "Fifty years of imported Lassa fever: a systematic review of primary and secondary cases," *J Travel Med,* vol. 27, no. 4, Jul 14 2020, doi: 10.1093/jtm/taaa035.
[34] A. Duvignaud *et al.*, "Lassa fever outcomes and prognostic factors in Nigeria (LASCOPE): a prospective cohort study," *Lancet Glob Health,* vol. 9, no. 4, pp. e469-e478, Apr 2021, doi: 10.1016/S2214-109X(20)30518-0.
[35] J. G. Shaffer *et al.*, "Lassa fever in post-conflict sierra leone," *PLoS Negl Trop Dis,* vol. 8, no. 3, p. e2748, Mar 2014, doi: 10.1371/journal.pntd.0002748.
[36] J. Strampe *et al.*, "Factors associated with progression to death in patients with Lassa fever in Nigeria: an observational study," *Lancet Infect Dis,* vol. 21, no. 6, pp. 876-886, Jun 2021, doi: 10.1016/S1473-3099(20)30737-4.
[37] D. Simons, "Lassa fever cases suffer from severe underreporting based on reported fatalities," *Int Health,* vol. 15, no. 5, pp. 608-610, Sep 1 2023, doi: 10.1093/inthealth/ihac076.
[38] N. D. Kayem *et al.*, "Lassa fever in pregnancy: a systematic review and meta-analysis," *Trans R Soc Trop Med Hyg,* vol. 114, no. 5, pp. 385-396, May 7 2020, doi: 10.1093/trstmh/traa011.
[39] S. Okogbenin *et al.*, "Retrospective Cohort Study of Lassa Fever in Pregnancy, Southern Nigeria," *Emerg Infect Dis,* vol. 25, no. 8, pp. 1494-500, Aug 2019, doi: 10.3201/eid2508.181299.
[40] M. E. Price, S. P. Fisher-Hoch, R. B. Craven, and J. B. McCormick, "A prospective study of maternal and fetal outcome in acute Lassa fever infection during pregnancy," *BMJ,* vol. 297, no. 6648, pp. 584-7, Sep 3 1988, doi: 10.1136/bmj.297.6648.584.
[41] V. Raabe, A. K. Mehta, J. D. Evans, T. Science Working Group of the National Emerging Special Pathogens, and N. Education Center Special Pathogens Research, "Lassa Virus Infection: a Summary for Clinicians," *Int J Infect Dis,* vol. 119, pp. 187-200, Jun 2022, doi: 10.1016/j.ijid.2022.04.004.
[42] J. K. Richmond and D. J. Baglole, "Lassa fever: epidemiology, clinical features, and social consequences," *BMJ,* vol. 327, no. 7426, pp. 1271-5, Nov 29 2003, doi: 10.1136/bmj.327.7426.1271.
[43] N. C. f. D. Control, "National Guidelines for Lassa Fever Case Management," 2018.
[44] P. Okokhere *et al.*, "Clinical and laboratory predictors of Lassa fever outcome in a dedicated treatment facility in Nigeria: a retrospective, observational cohort study," *Lancet Infect Dis,* vol. 18, no. 6, pp. 684-695, Jun 2018, doi: 10.1016/S1473-3099(18)30121-X.
[45] A. E. Adetunji *et al.*, "Acute kidney injury and mortality in pediatric Lassa fever versus question of access to dialysis," *Int J Infect Dis,* vol. 103, pp. 124-131, Feb 2021, doi: 10.1016/j.ijid.2020.11.006.
[46] E. J. Mateer, C. Huang, N. Y. Shehu, and S. Paessler, "Lassa fever-induced sensorineural hearing loss: A neglected public health and social burden," *PLoS Negl Trop Dis,* vol. 12, no. 2, p. e0006187, Feb 2018, doi: 10.1371/journal.pntd.0006187.
[47] L. P. Rybak, "Deafness associated with Lassa fever," *JAMA,* vol. 264, no. 16, p. 2119, Oct 24-31 1990. [Online]. Available: https://www.ncbi.nlm.nih.gov/pubmed/2214082.
[48] S. C. Ficenec *et al.*, "Lassa Fever Induced Hearing Loss: The Neglected Disability of Hemorrhagic Fever," *Int J Infect Dis,* vol. 100, pp. 82-87, Nov 2020, doi: 10.1016/j.ijid.2020.08.021.
[49] D. Cummins *et al.*, "Acute sensorineural deafness in Lassa fever," *JAMA,* vol. 264, no. 16, pp. 2093-6, Oct 24-31 1990. [Online]. Available: https://www.ncbi.nlm.nih.gov/pubmed/2214077.
[50] T. S. Ibekwe *et al.*, "Early-onset sensorineural hearing loss in Lassa fever," *Eur Arch Otorhinolaryngol,* vol. 268, no. 2, pp. 197-201, Feb 2011, doi: 10.1007/s00405-010-1370-4.
[51] E. L. Hamblion *et al.*, "The challenges of detecting and responding to a Lassa fever outbreak in an Ebola-affected setting," *Int J Infect Dis,* vol. 66, pp. 65-73, Jan 2018, doi: 10.1016/j.ijid.2017.11.007.

[52] C. Drosten *et al.*, "Rapid detection and quantification of RNA of Ebola and Marburg viruses, Lassa virus, Crimean-Congo hemorrhagic fever virus, Rift Valley fever virus, dengue virus, and yellow fever virus by real-time reverse transcription-PCR," *J Clin Microbiol,* vol. 40, no. 7, pp. 2323-30, Jul 2002, doi: 10.1128/JCM.40.7.2323-2330.2002.

[53] N. F. Takah, P. Brangel, P. Shrestha, and R. Peeling, "Sensitivity and specificity of diagnostic tests for Lassa fever: a systematic review," *BMC Infect Dis,* vol. 19, no. 1, p. 647, Jul 19 2019, doi: 10.1186/s12879-019-4242-6.

[54] S. G. Trappier, A. L. Conaty, B. B. Farrar, D. D. Auperin, J. B. McCormick, and S. P. Fisher-Hoch, "Evaluation of the polymerase chain reaction for diagnosis of Lassa virus infection," *Am J Trop Med Hyg,* vol. 49, no. 2, pp. 214-21, Aug 1993, doi: 10.4269/ajtmh.1993.49.214.

[55] X. L. Luo *et al.*, "Comparative Evaluation of Standard RT-PCR Assays and Commercial Real-Time RT-PCR Kits for Detection of Lassa Virus," *Microbiol Spectr,* vol. 11, no. 2, p. e0501122, Mar 28 2023, doi: 10.1128/spectrum.05011-22.

[56] V. G. Dedkov *et al.*, "Development and Evaluation of a One-Step Quantitative RT-PCR Assay for Detection of Lassa Virus," *J Virol Methods,* vol. 271, p. 113674, Sep 2019, doi: 10.1016/j.jviromet.2019.113674.

[57] D. A. Asogun *et al.*, "Molecular diagnostics for lassa fever at Irrua specialist teaching hospital, Nigeria: lessons learnt from two years of laboratory operation," *PLoS Negl Trop Dis,* vol. 6, no. 9, p. e1839, 2012, doi: 10.1371/journal.pntd.0001839.

[58] L. E. Kafetzopoulou *et al.*, "Metagenomic sequencing at the epicenter of the Nigeria 2018 Lassa fever outbreak," *Science,* vol. 363, no. 6422, pp. 74-77, Jan 4 2019, doi: 10.1126/science.aau9343.

[59] K. J. Siddle *et al.*, "Genomic Analysis of Lassa Virus during an Increase in Cases in Nigeria in 2018," *N Engl J Med,* vol. 379, no. 18, pp. 1745-1753, Nov 1 2018, doi: 10.1056/NEJMoa1804498.

[60] J. U. Oguzie *et al.*, "Metagenomic surveillance uncovers diverse and novel viral taxa in febrile patients from Nigeria," *Nat Commun,* vol. 14, no. 1, p. 4693, Aug 4 2023, doi: 10.1038/s41467-023-40247-4.

[61] M. L. Boisen *et al.*, "Field validation of recombinant antigen immunoassays for diagnosis of Lassa fever," *Sci Rep,* vol. 8, no. 1, p. 5939, Apr 12 2018, doi: 10.1038/s41598-018-24246-w.

[62] M. L. Boisen *et al.*, "Field evaluation of a Pan-Lassa rapid diagnostic test during the 2018 Nigerian Lassa fever outbreak," *Sci Rep,* vol. 10, no. 1, p. 8724, May 26 2020, doi: 10.1038/s41598-020-65736-0.

[63] D. G. Bausch *et al.*, "Diagnosis and clinical virology of Lassa fever as evaluated by enzyme-linked immunosorbent assay, indirect fluorescent-antibody test, and virus isolation," *J Clin Microbiol,* vol. 38, no. 7, pp. 2670-7, Jul 2000, doi: 10.1128/JCM.38.7.2670-2677.2000.

[64] M. Gabriel *et al.*, "Development and evaluation of antibody-capture immunoassays for detection of Lassa virus nucleoprotein-specific immunoglobulin M and G," *PLoS Negl Trop Dis,* vol. 12, no. 3, p. e0006361, Mar 2018, doi: 10.1371/journal.pntd.0006361.

[65] H. J. Hallam *et al.*, "Baseline mapping of Lassa fever virology, epidemiology and vaccine research and development," *NPJ Vaccines,* vol. 3, p. 11, 2018, doi: 10.1038/s41541-018-0049-5.

[66] D. Y. Meunier, J. B. McCormick, A. J. Georges, M. C. Georges, and J. P. Gonzalez, "Comparison of Lassa, Mobala, and Ippy virus reactions by immunofluorescence test," *Lancet,* vol. 1, no. 8433, pp. 873-4, Apr 13 1985, doi: 10.1016/s0140-6736(85)92233-0.

[67] T. Briese *et al.*, "Genetic detection and characterization of Lujo virus, a new hemorrhagic fever-associated arenavirus from southern Africa," *PLoS Pathog,* vol. 5, no. 5, p. e1000455, May 2009, doi: 10.1371/journal.ppat.1000455.

[68] A. N. Happi, C. T. Happi, and R. J. Schoepp, "Lassa fever diagnostics: past, present, and future," *Curr Opin Virol,* vol. 37, pp. 132-138, Aug 2019, doi: 10.1016/j.coviro.2019.08.002.

[69] S. Mahanty, K. Hutchinson, S. Agarwal, M. McRae, P. E. Rollin, and B. Pulendran, "Cutting edge: impairment of dendritic cells and adaptive immunity by Ebola and Lassa viruses," *J Immunol,* vol. 170, no. 6, pp. 2797-801, Mar 15 2003, doi: 10.4049/jimmunol.170.6.2797.

[70] I. S. Lukashevich *et al.*, "Lassa and Mopeia virus replication in human monocytes/macrophages and in endothelial cells: different effects on IL-8 and TNF-alpha gene expression," *J Med Virol,* vol. 59, no. 4, pp. 552-60, Dec 1999. [Online]. Available: https://www.ncbi.nlm.nih.gov/pubmed/10534741.

[71] H. Murphy and H. Ly, "Understanding Immune Responses to Lassa Virus Infection and to Its Candidate Vaccines," *Vaccines (Basel),* vol. 10, no. 10, Oct 6 2022, doi: 10.3390/vaccines10101668.

[72] S. Baize *et al.*, "Early and strong immune responses are associated with control of viral replication and recovery in lassa virus-infected cynomolgus monkeys," *J Virol,* vol. 83, no. 11, pp. 5890-903, Jun 2009, doi: 10.1128/JVI.01948-08.

[73] H. Schmitz *et al.*, "Monitoring of clinical and laboratory data in two cases of imported Lassa fever," *Microbes Infect,* vol. 4, no. 1, pp. 43-50, Jan 2002, doi: 10.1016/s1286-4579(01)01508-8.

[74] N. Baillet *et al.*, "Systemic viral spreading and defective host responses are associated with fatal Lassa fever in macaques," *Commun Biol,* vol. 4, no. 1, p. 27, Jan 4 2021, doi: 10.1038/s42003-020-01543-7.

[75] M. Mateo *et al.*, "Pathogenesis of recent Lassa virus isolates from lineages II and VII in cynomolgus monkeys," *Virulence,* vol. 13, no. 1, pp. 654-669, Dec 2022, doi: 10.1080/21505594.2022.2060170.

[76] L. Flatz *et al.*, "T cell-dependence of Lassa fever pathogenesis," *PLoS Pathog,* vol. 6, no. 3, p. e1000836, Mar 26 2010, doi: 10.1371/journal.ppat.1000836.

[77] S. Gunther *et al.*, "Antibodies to Lassa virus Z protein and nucleoprotein co-occur in human sera from Lassa fever endemic regions," *Med Microbiol Immunol,* vol. 189, no. 4, pp. 225-9, Sep 2001, doi: 10.1007/s004300100061.

[78] J. ter Meulen *et al.*, "Characterization of human CD4(+) T-cell clones recognizing conserved and variable epitopes of the Lassa virus nucleoprotein," *J Virol,* vol. 74, no. 5, pp. 2186-92, Mar 2000, doi: 10.1128/jvi.74.5.2186-2192.2000.

[79] N. E. Yun and D. H. Walker, "Pathogenesis of Lassa fever," *Viruses,* vol. 4, no. 10, pp. 2031-48, Oct 9 2012, doi: 10.3390/v4102031.

[80] A. Thielebein *et al.*, "Virus persistence after recovery from acute Lassa fever in Nigeria: a 2-year interim analysis of a prospective longitudinal cohort study," *Lancet Microbe,* vol. 3, no. 1, pp. e32-e40, Jan 2022, doi: 10.1016/S2666-5247(21)00178-6.

[81] B. G. Schindell, A. L. Webb, and J. Kindrachuk, "Persistence and Sexual Transmission of Filoviruses," *Viruses,* vol. 10, no. 12, Dec 2 2018, doi: 10.3390/v10120683.

[82] K. Manothummetha *et al.*, "Ribavirin treatment for respiratory syncytial virus infection in patients with haematologic malignancy and haematopoietic stem cell transplant recipients: a systematic review and meta-analysis," *Clin Microbiol Infect,* vol. 29, no. 10, pp. 1272-1279, Oct 2023, doi: 10.1016/j.cmi.2023.04.021.

[83] J. Paeshuyse, K. Dallmeier, and J. Neyts, "Ribavirin for the treatment of chronic hepatitis C virus infection: a review of the proposed mechanisms of action," *Curr Opin Virol,* vol. 1, no. 6, pp. 590-8, Dec 2011, doi: 10.1016/j.coviro.2011.10.030.

[84] A. P. Salam *et al.*, "Ribavirin for treating Lassa fever: A systematic review of pre-clinical studies and implications for human dosing," *PLoS Negl Trop Dis,* vol. 16, no. 3, p. e0010289, Mar 2022, doi: 10.1371/journal.pntd.0010289.

[85] B. N. I. f. T. Medicine. "Pharmacokinetics, Tolerability and Safety of Favipiravir Compared to Ribavirin for the Treatment of Lassa Fever (SAFARI) " https://ichgcp.net/clinical-trials-registry/NCT04907682 (accessed.

[86] R. W. Cross *et al.*, "Treatment of Lassa virus infection in outbred guinea pigs with first-in-class human monoclonal antibodies," *Antiviral Res,* vol. 133, pp. 218-222, Sep 2016, doi: 10.1016/j.antiviral.2016.08.012.

[87] R. W. Cross *et al.*, "A human monoclonal antibody combination rescues nonhuman primates from advanced disease caused by the major lineages of Lassa virus," *Proc Natl Acad Sci U S A,* vol. 120, no. 34, p. e2304876120, Aug 22 2023, doi: 10.1073/pnas.2304876120.

[88] C. E. Mire *et al.*, "Human-monoclonal-antibody therapy protects nonhuman primates against advanced Lassa fever," *Nat Med,* vol. 23, no. 10, pp. 1146-1149, Oct 2017, doi: 10.1038/nm.4396.

[89] T. Takenaga *et al.*, "CP100356 Hydrochloride, a P-Glycoprotein Inhibitor, Inhibits Lassa Virus Entry: Implication of a Candidate Pan-Mammarenavirus Entry Inhibitor," *Viruses,* vol. 13, no. 9, Sep 3 2021, doi: 10.3390/v13091763.

[90] G. Sulis, A. Peebles, and N. E. Basta, "Lassa fever vaccine candidates: A scoping review of vaccine clinical trials," *Trop Med Int Health,* vol. 28, no. 6, pp. 420-431, Jun 2023, doi: 10.1111/tmi.13876.

[91] R. Tschismarov *et al.*, "Immunogenicity, safety, and tolerability of a recombinant measles-vectored Lassa fever vaccine: a randomised, placebo-controlled, first-in-human trial," *Lancet,* vol. 401, no. 10384, pp. 1267-1276, Apr 15 2023, doi: 10.1016/S0140-6736(23)00048-X.

[92] R. W. Cross *et al.*, "A recombinant VSV-vectored vaccine rapidly protects nonhuman primates against heterologous lethal Lassa fever," *Cell Rep,* vol. 40, no. 3, p. 111094, Jul 19 2022, doi: 10.1016/j.celrep.2022.111094.

[93] G. Akintunde, "EBS-LASV, a dual-attenuated rVSV-vectored vaccine candidate for Lassa fever," 2022. [Online]. Available: https://cdn.who.int/media/docs/default-source/blue-print/day1_session2_6_gideon-akintunde_lassa-vaccine-meeting_nigeria.pdf?sfvrsn=8d808d6f_3. [Online]. Available: https://cdn.who.int/media/docs/default-source/blue-print/day1_session2_6_gideon-akintunde_lassa-vaccine-meeting_nigeria.pdf?sfvrsn=8d808d6f_3

[94] M. Mateo *et al.*, "Rapid protection induced by a single-shot Lassa vaccine in male cynomolgus monkeys," *Nat Commun,* vol. 14, no. 1, p. 1352, Mar 11 2023, doi: 10.1038/s41467-023-37050-6.

[95] B. Malkin E, L,; Kieh M,; Fitz Patrick D, ; Diemert D,; Mutua G,; Philiponis V,; Zaric M,; Hunt D,; Barin B,; Engelbrecht M,; Malherbe M,; Walker K,; Lehrman J,; Fast P,; Parks C,; Gupta SB "First Safety & Immunogenicity Data from a FIH, Placebo-controlled, Dose-escalation Trial of a Recombinant Vesicular Stomatitis Virus-based Lassa Fever Vaccine in Healthy Adults," presented at the ASTMH 72nd Annual Meeting Chicago, 2023. [Online]. Available: https://www.iavi.org/wp-content/uploads/2023/11/C102_ASTMH_Poster_Chicago2023.pdf.

[96] I. A. V. Initiative. "A Lassa Fever Vaccine Trial in Adults and Children Residing in West Africa." https://classic.clinicaltrials.gov/ct2/show/NCT05868733 (accessed.

[97] J. Marien *et al.*, "Evaluation of rodent control to fight Lassa fever based on field data and mathematical modelling," *Emerg Microbes Infect,* vol. 8, no. 1, pp. 640-649, 2019, doi: 10.1080/22221751.2019.1605846.

[98] A. Mari Saez *et al.*, "Rodent control to fight Lassa fever: Evaluation and lessons learned from a 4-year study in Upper Guinea," *PLoS Negl Trop Dis,* vol. 12, no. 11, p. e0006829, Nov 2018, doi: 10.1371/journal.pntd.0006829.

[99] G. Reuter, A. Boros, K. Takats, R. Matics, and P. Pankovics, "A novel mammarenavirus (family Arenaviridae) in hedgehogs (Erinaceus roumanicus) in Europe," *Arch Virol,* vol. 168, no. 7, p. 174, Jun 8 2023, doi: 10.1007/s00705-023-05804-8.

[100] B. Flannery, M. Cain, and H. Ly, "Recent Discoveries of Novel Mammarenaviruses Infecting Humans and Other Mammals in Asia and Southeast Asia," *Virulence,* vol. 14, no. 1, p. 2231392, Dec 2023, doi: 10.1080/21505594.2023.2231392.

[101] N. Sarute and S. R. Ross, "New World Arenavirus Biology," *Annu Rev Virol,* vol. 4, no. 1, pp. 141-158, Sep 29 2017, doi: 10.1146/annurev-virology-101416-042001.

[102] O. Ogbu, "Viruses: Lassa Fever Virus," *Enceclopedia of Food Safety,* vol. 2, pp. 208-213, 2014, doi: doi.org/10.1016/B978-0-12-378612-8.00128-1.

[103] D. D. Auperin, V. Romanowski, M. Galinski, and D. H. Bishop, "Sequencing studies of pichinde arenavirus S RNA indicate a novel coding strategy, an ambisense viral S RNA," *J Virol,* vol. 52, no. 3, pp. 897-904, Dec 1984, doi: 10.1128/JVI.52.3.897-904.1984.

[104] M. Perez and J. C. de la Torre, "Characterization of the genomic promoter of the prototypic arenavirus lymphocytic choriomeningitis virus," *J Virol,* vol. 77, no. 2, pp. 1184-94, Jan 2003, doi: 10.1128/jvi.77.2.1184-1194.2003.

[105] M. Hass, M. Westerkofsky, S. Muller, B. Becker-Ziaja, C. Busch, and S. Gunther, "Mutational analysis of the lassa virus promoter," *J Virol,* vol. 80, no. 24, pp. 12414-9, Dec 2006, doi: 10.1128/JVI.01374-06.

[106] D. D. Pinschewer, M. Perez, and J. C. de la Torre, "Dual role of the lymphocytic choriomeningitis virus intergenic region in transcription termination and virus propagation," *J Virol,* vol. 79, no. 7, pp. 4519-26, Apr 2005, doi: 10.1128/JVI.79.7.4519-4526.2005.

[107] N. Lopez and M. T. Franze-Fernandez, "A single stem-loop structure in Tacaribe arenavirus intergenic region is essential for transcription termination but is not required for a correct initiation of transcription and replication," *Virus Res,* vol. 124, no. 1-2, pp. 237-44, Mar 2007, doi: 10.1016/j.virusres.2006.10.007.

[108] W. Cao *et al.*, "Identification of alpha-dystroglycan as a receptor for lymphocytic choriomeningitis virus and Lassa fever virus," *Science,* vol. 282, no. 5396, pp. 2079-81, Dec 11 1998, doi: 10.1126/science.282.5396.2079.

[109] J. M. Rojek, C. F. Spiropoulou, K. P. Campbell, and S. Kunz, "Old World and clade C New World arenaviruses mimic the molecular mechanism of receptor recognition used by alpha-dystroglycan's host-derived ligands," *J Virol,* vol. 81, no. 11, pp. 5685-95, Jun 2007, doi: 10.1128/JVI.02574-06.

[110] K. H. Holt, R. H. Crosbie, D. P. Venzke, and K. P. Campbell, "Biosynthesis of dystroglycan: processing of a precursor propeptide," *FEBS Lett,* vol. 468, no. 1, pp. 79-83, Feb 18 2000, doi: 10.1016/s0014-5793(00)01195-9.

[111] R. Barresi and K. P. Campbell, "Dystroglycan: from biosynthesis to pathogenesis of human disease," *J Cell Sci,* vol. 119, no. Pt 2, pp. 199-207, Jan 15 2006, doi: 10.1242/jcs.02814.

[112] S. Kunz *et al.*, "Posttranslational modification of alpha-dystroglycan, the cellular receptor for arenaviruses, by the glycosyltransferase LARGE is critical for virus binding," *J Virol,* vol. 79, no. 22, pp. 14282-96, Nov 2005, doi: 10.1128/JVI.79.22.14282-14296.2005.

[113] R. B. Brouillette *et al.*, "TIM-1 Mediates Dystroglycan-Independent Entry of Lassa Virus," *J Virol,* vol. 92, no. 16, Aug 15 2018, doi: 10.1128/JVI.00093-18.

[114] C. Fedeli *et al.*, "Axl Can Serve as Entry Factor for Lassa Virus Depending on the Functional Glycosylation of Dystroglycan," *J Virol,* vol. 92, no. 5, Mar 1 2018, doi: 10.1128/JVI.01613-17.

[115] M. Shimojima, U. Stroher, H. Ebihara, H. Feldmann, and Y. Kawaoka, "Identification of cell surface molecules involved in dystroglycan-independent Lassa virus cell entry," *J Virol,* vol. 86, no. 4, pp. 2067-78, Feb 2012, doi: 10.1128/JVI.06451-11.

[116] A. R. Goncalves, M. L. Moraz, A. Pasquato, A. Helenius, P. Y. Lozach, and S. Kunz, "Role of DC-SIGN in Lassa virus entry into human dendritic cells," *J Virol,* vol. 87, no. 21, pp. 11504-15, Nov 2013, doi: 10.1128/JVI.01893-13.

[117] J. Oppliger, G. Torriani, A. Herrador, and S. Kunz, "Lassa Virus Cell Entry via Dystroglycan Involves an Unusual Pathway of Macropinocytosis," *J Virol,* vol. 90, no. 14, pp. 6412-6429, Jul 15 2016, doi: 10.1128/JVI.00257-16.

[118] H. Cohen-Dvashi, N. Cohen, H. Israeli, and R. Diskin, "Molecular Mechanism for LAMP1 Recognition by Lassa Virus," *J Virol,* vol. 89, no. 15, pp. 7584-92, Aug 2015, doi: 10.1128/JVI.00651-15.

[119] H. Cohen-Dvashi, H. Israeli, O. Shani, A. Katz, and R. Diskin, "Role of LAMP1 Binding and pH Sensing by the Spike Complex of Lassa Virus," *J Virol,* vol. 90, no. 22, pp. 10329-10338, Nov 15 2016, doi: 10.1128/JVI.01624-16.

[120] L. Sanger *et al.*, "RNA to Rule Them All: Critical Steps in Lassa Virus Ribonucleoparticle Assembly and Recruitment," *J Am Chem Soc,* vol. 145, no. 51, pp. 27958-27974, Dec 27 2023, doi: 10.1021/jacs.3c07325.

[121] D. Vogel, M. Rosenthal, N. Gogrefe, S. Reindl, and S. Gunther, "Biochemical characterization of the Lassa virus L protein," *J Biol Chem,* vol. 294, no. 20, pp. 8088-8100, May 17 2019, doi: 10.1074/jbc.RA118.006973.

[122] B. J. Meyer and P. J. Southern, "Concurrent sequence analysis of 5' and 3' RNA termini by intramolecular circularization reveals 5' nontemplated bases and 3' terminal heterogeneity for lymphocytic choriomeningitis virus mRNAs," *J Virol,* vol. 67, no. 5, pp. 2621-7, May 1993, doi: 10.1128/JVI.67.5.2621-2627.1993.

[123] D. J. Burri, G. Pasqual, C. Rochat, N. G. Seidah, A. Pasquato, and S. Kunz, "Molecular characterization of the processing of arenavirus envelope glycoprotein precursors by subtilisin kexin isozyme-1/site-1 protease," *J Virol,* vol. 86, no. 9, pp. 4935-46, May 2012, doi: 10.1128/JVI.00024-12.

[124] R. Eichler, O. Lenz, T. Strecker, and W. Garten, "Signal peptide of Lassa virus glycoprotein GP-C exhibits an unusual length," *FEBS Lett,* vol. 538, no. 1-3, pp. 203-6, Mar 13 2003, doi: 10.1016/s0014-5793(03)00160-1.

[125] O. Lenz, J. ter Meulen, H. D. Klenk, N. G. Seidah, and W. Garten, "The Lassa virus glycoprotein precursor GP-C is proteolytically processed by subtilase SKI-1/S1P," *Proc Natl Acad Sci U S A,* vol. 98, no. 22, pp. 12701-5, Oct 23 2001, doi: 10.1073/pnas.221447598.

[126] T. I. Cornu and J. C. de la Torre, "RING finger Z protein of lymphocytic choriomeningitis virus (LCMV) inhibits transcription and RNA replication of an LCMV S-segment minigenome," *J Virol,* vol. 75, no. 19, pp. 9415-26, Oct 2001, doi: 10.1128/JVI.75.19.9415-9426.2001.

[127] R. Jacamo, N. Lopez, M. Wilda, and M. T. Franze-Fernandez, "Tacaribe virus Z protein interacts with the L polymerase protein to inhibit viral RNA synthesis," *J Virol,* vol. 77, no. 19, pp. 10383-93, Oct 2003, doi: 10.1128/jvi.77.19.10383-10393.2003.

[128] M. S. Salvato, K. J. Schweighofer, J. Burns, and E. M. Shimomaye, "Biochemical and immunological evidence that the 11 kDa zinc-binding protein of lymphocytic choriomeningitis virus is a structural component of the virus," *Virus Res,* vol. 22, no. 3, pp. 185-98, Mar 1992, doi: 10.1016/0168-1702(92)90050-j.

[129] R. F. Garry, "50 Years of Lassa Fever Research," *Curr Top Microbiol Immunol,* vol. 440, pp. 1-22, 2023, doi: 10.1007/82_2020_214.
[130] S. Urata and J. Yasuda, "Molecular mechanism of arenavirus assembly and budding," *Viruses,* vol. 4, no. 10, pp. 2049-79, Oct 10 2012, doi: 10.3390/v4102049.
[131] M. Perez, D. L. Greenwald, and J. C. de la Torre, "Myristoylation of the RING finger Z protein is essential for arenavirus budding," *J Virol,* vol. 78, no. 20, pp. 11443-8, Oct 2004, doi: 10.1128/JVI.78.20.11443-11448.2004.
[132] C. M. Ziegler *et al.*, "The Lymphocytic Choriomeningitis Virus Matrix Protein PPXY Late Domain Drives the Production of Defective Interfering Particles," *PLoS Pathog,* vol. 12, no. 3, p. e1005501, Mar 2016, doi: 10.1371/journal.ppat.1005501.
[133] M. Garbutt *et al.*, "Properties of replication-competent vesicular stomatitis virus vectors expressing glycoproteins of filoviruses and arenaviruses," *J Virol,* vol. 78, no. 10, pp. 5458-65, May 2004, doi: 10.1128/jvi.78.10.5458-5465.2004.
[134] M. A. Whitt, "Generation of VSV pseudotypes using recombinant DeltaG-VSV for studies on virus entry, identification of entry inhibitors, and immune responses to vaccines," *J Virol Methods,* vol. 169, no. 2, pp. 365-74, Nov 2010, doi: 10.1016/j.jviromet.2010.08.006.
[135] M. Hass, U. Golnitz, S. Muller, B. Becker-Ziaja, and S. Gunther, "Replicon system for Lassa virus," *J Virol,* vol. 78, no. 24, pp. 13793-803, Dec 2004, doi: 10.1128/JVI.78.24.13793-13803.2004.
[136] T. Strecker *et al.*, "Lassa virus Z protein is a matrix protein and sufficient for the release of virus-like particles [corrected]," *J Virol,* vol. 77, no. 19, pp. 10700-5, Oct 2003, doi: 10.1128/jvi.77.19.10700-10705.2003.
[137] F. I. Ibukun, "Inter-Lineage Variation of Lassa Virus Glycoprotein Epitopes: A Challenge to Lassa Virus Vaccine Development," *Viruses,* vol. 12, no. 4, Mar 31 2020, doi: 10.3390/v12040386.
[138] K. G. Andersen *et al.*, "Clinical Sequencing Uncovers Origins and Evolution of Lassa Virus," *Cell,* vol. 162, no. 4, pp. 738-50, Aug 13 2015, doi: 10.1016/j.cell.2015.07.020.
[139] A. H. Demby *et al.*, "Lassa fever in Guinea: II. Distribution and prevalence of Lassa virus infection in small mammals," *Vector Borne Zoonotic Dis,* vol. 1, no. 4, pp. 283-97, Winter 2001, doi: 10.1089/15303660160025912.
[140] R. A. Keenlyside, J. B. McCormick, P. A. Webb, E. Smith, L. Elliott, and K. M. Johnson, "Case-control study of Mastomys natalensis and humans in Lassa virus-infected households in Sierra Leone," *Am J Trop Med Hyg,* vol. 32, no. 4, pp. 829-37, Jul 1983, doi: 10.4269/ajtmh.1983.32.829.
[141] L. Granjon, "Mastomys natalensis. The IUCN Red List of Threatened Species 2016," 2017.
[142] A. Olayemi and E. Fichet-Calvet, "Systematics, Ecology, and Host Switching: Attributes Affecting Emergence of the Lassa Virus in Rodents across Western Africa," *Viruses,* vol. 12, no. 3, Mar 14 2020, doi: 10.3390/v12030312.
[143] S. Gryseels, S. J. Baird, B. Borremans, R. Makundi, H. Leirs, and J. Gouy de Bellocq, "When Viruses Don't Go Viral: The Importance of Host Phylogeographic Structure in the Spatial Spread of Arenaviruses," *PLoS Pathog,* vol. 13, no. 1, p. e1006073, Jan 2017, doi: 10.1371/journal.ppat.1006073.
[144] A. Olayemi *et al.*, "Arenavirus Diversity and Phylogeography of Mastomys natalensis Rodents, Nigeria," *Emerg Infect Dis,* vol. 22, no. 4, pp. 694-7, Apr 2016, doi: 10.3201/eid2204.150155.
[145] A. Olayemi *et al.*, "New Hosts of The Lassa Virus," *Sci Rep,* vol. 6, p. 25280, May 3 2016, doi: 10.1038/srep25280.
[146] B. Borremans *et al.*, "Shedding dynamics of Morogoro virus, an African arenavirus closely related to Lassa virus, in its natural reservoir host Mastomys natalensis," *Sci Rep,* vol. 5, p. 10445, May 29 2015, doi: 10.1038/srep10445.
[147] S. Gunther *et al.*, "Mopeia virus-related arenavirus in natal multimammate mice, Morogoro, Tanzania," *Emerg Infect Dis,* vol. 15, no. 12, pp. 2008-12, Dec 2009, doi: 10.3201/eid1512.090864.
[148] H. Wulff, B. M. McIntosh, D. B. Hamner, and K. M. Johnson, "Isolation of an arenavirus closely related to Lassa virus from Mastomys natalensis in south-east Africa," *Bull World Health Organ,* vol. 55, no. 4, pp. 441-4, 1977. [Online]. Available: https://www.ncbi.nlm.nih.gov/pubmed/304387.
[149] J. Goyens, J. Reijniers, B. Borremans, and H. Leirs, "Density thresholds for Mopeia virus invasion and persistence in its host Mastomys natalensis," *J Theor Biol,* vol. 317, pp. 55-61, Jan 21 2013, doi: 10.1016/j.jtbi.2012.09.039.
[150] D. Safronetz *et al.*, "Establishment of a Genetically Confirmed Breeding Colony of Mastomys natalensis from Wild-Caught Founders from West Africa," *Viruses,* vol. 13, no. 4, Mar 31 2021, doi: 10.3390/v13040590.
[151] D. M. Wozniak, N. Kirchoff, K. Hansen-Kant, N. Sogoba, D. Safronetz, and J. Prescott, "Hematology and Clinical Chemistry Reference Ranges for Laboratory-Bred Natal Multimammate Mice (Mastomys natalensis)," *Viruses,* vol. 13, no. 2, Jan 27 2021, doi: 10.3390/v13020187.
[152] D. M. Wozniak *et al.*, "Inoculation route-dependent Lassa virus dissemination and shedding dynamics in the natural reservoir - Mastomys natalensis," *Emerg Microbes Infect,* vol. 10, no. 1, pp. 2313-2325, Dec 2021, doi: 10.1080/22221751.2021.2008773.
[153] D. Safronetz *et al.*, "Temporal analysis of Lassa virus infection and transmission in experimentally infected Mastomys natalensis," *PNAS Nexus,* vol. 1, no. 3, p. pgac114, Jul 2022, doi: 10.1093/pnasnexus/pgac114.
[154] E. Fichet-Calvet, E. Lecompte, L. Koivogui, S. Daffis, and J. ter Meulen, "Reproductive characteristics of Mastomys natalensis and Lassa virus prevalence in Guinea, West Africa," *Vector Borne Zoonotic Dis,* vol. 8, no. 1, pp. 41-8, Spring 2008, doi: 10.1089/vbz.2007.0118.
[155] C. Hoffmann *et al.*, "Experimental Morogoro Virus Infection in Its Natural Host, Mastomys natalensis," *Viruses,* vol. 13, no. 5, May 7 2021, doi: 10.3390/v13050851.
[156] C. Hoffmann *et al.*, "Lassa virus persistence with high viral titers following experimental infection in its natural reservoir host, Mastomys natalensis," Preprint (Version 1) 04.04.2024 2024, doi: doi.org/10.21203/rs.3.rs-4157727/v1.

[157] C. Hoffmann, "The immunology and virology of Lassa virus in its natural host, Mastomys natalensis," Dr. rer. nat., University of Bremen, 2022.
[158] N. M. Burckhardt, "Establishment of RT-PCR Assays for the Analysis of the Virus-Induced Immune Response in Mastomys natalensis," Master of Science, Department of Chemistry, University of Hamburg, 2020.
[159] A. J. Meadows, N. Stephenson, N. K. Madhav, and B. Oppenheim, "Historical trends demonstrate a pattern of increasingly frequent and severe spillover events of high-consequence zoonotic viruses," *BMJ Glob Health,* vol. 8, no. 11, Nov 2023, doi: 10.1136/bmjgh-2023-012026.
[160] C. J. Carlson *et al.*, "Climate change increases cross-species viral transmission risk," *Nature,* vol. 607, no. 7919, pp. 555-562, Jul 2022, doi: 10.1038/s41586-022-04788-w.
[161] B. Escudero-Perez, A. Lalande, C. Mathieu, and P. Lawrence, "Host-Pathogen Interactions Influencing Zoonotic Spillover Potential and Transmission in Humans," *Viruses,* vol. 15, no. 3, Feb 22 2023, doi: 10.3390/v15030599.
[162] C. R. Parrish *et al.*, "Cross-species virus transmission and the emergence of new epidemic diseases," *Microbiol Mol Biol Rev,* vol. 72, no. 3, pp. 457-70, Sep 2008, doi: 10.1128/MMBR.00004-08.
[163] G. F. Albery *et al.*, "The science of the host-virus network," *Nat Microbiol,* vol. 6, no. 12, pp. 1483-1492, Dec 2021, doi: 10.1038/s41564-021-00999-5.
[164] S. R. Radoshitzky *et al.*, "Machupo virus glycoprotein determinants for human transferrin receptor 1 binding and cell entry," *PLoS One,* vol. 6, no. 7, p. e21398, 2011, doi: 10.1371/journal.pone.0021398.
[165] H. Moreno *et al.*, "A novel circulating tamiami mammarenavirus shows potential for zoonotic spillover," *PLoS Negl Trop Dis,* vol. 14, no. 12, p. e0009004, Dec 2020, doi: 10.1371/journal.pntd.0009004.
[166] E. de Vries, Du, W., Guo, H., de Haan, C. A. M., "Influenza A Virus Hemagglutinin–Neuraminidase–Receptor Balance- Preserving Virus Motility," *Trends in Microbiology,* vol. 28, no. 1, pp. 57-67, 2020.
[167] L. Byrd-Leotis, R. D. Cummings, and D. A. Steinhauer, "The Interplay between the Host Receptor and Influenza Virus Hemagglutinin and Neuraminidase," *Int J Mol Sci,* vol. 18, no. 7, Jul 17 2017, doi: 10.3390/ijms18071541.
[168] S. Reynard, M. Russier, A. Fizet, X. Carnec, and S. Baize, "Exonuclease domain of the Lassa virus nucleoprotein is critical to avoid RIG-I signaling and to inhibit the innate immune response," *J Virol,* vol. 88, no. 23, pp. 13923-7, Dec 2014, doi: 10.1128/JVI.01923-14.
[169] X. Carnec *et al.*, "Lassa virus nucleoprotein mutants generated by reverse genetics induce a robust type I interferon response in human dendritic cells and macrophages," *J Virol,* vol. 85, no. 22, pp. 12093-7, Nov 2011, doi: 10.1128/JVI.00429-11.
[170] K. M. Hastie, C. R. Kimberlin, M. A. Zandonatti, I. J. MacRae, and E. O. Saphire, "Structure of the Lassa virus nucleoprotein reveals a dsRNA-specific 3' to 5' exonuclease activity essential for immune suppression," *Proc Natl Acad Sci U S A,* vol. 108, no. 6, pp. 2396-401, Feb 8 2011, doi: 10.1073/pnas.1016404108.
[171] X. Qi *et al.*, "Cap binding and immune evasion revealed by Lassa nucleoprotein structure," *Nature,* vol. 468, no. 7325, pp. 779-83, Dec 9 2010, doi: 10.1038/nature09605.
[172] B. Meyer and A. Groseth, "Apoptosis during arenavirus infection: mechanisms and evasion strategies," *Microbes Infect,* vol. 20, no. 2, pp. 65-80, Feb 2018, doi: 10.1016/j.micinf.2017.10.002.
[173] L. Fan, T. Briese, and W. I. Lipkin, "Z proteins of New World arenaviruses bind RIG-I and interfere with type I interferon induction," *J Virol,* vol. 84, no. 4, pp. 1785-91, Feb 2010, doi: 10.1128/JVI.01362-09.
[174] R. J. Stott, T. Strecker, and T. L. Foster, "Distinct Molecular Mechanisms of Host Immune Response Modulation by Arenavirus NP and Z Proteins," *Viruses,* vol. 12, no. 7, Jul 21 2020, doi: 10.3390/v12070784.
[175] J. Xing, H. Ly, and Y. Liang, "The Z proteins of pathogenic but not nonpathogenic arenaviruses inhibit RIG-I-like receptor-dependent interferon production," *J Virol,* vol. 89, no. 5, pp. 2944-55, Mar 2015, doi: 10.1128/JVI.03349-14.
[176] E. Staller, Sheppard, C. M., Neasham, P. J., Mistry, B., Peacock, T. P., Goldhill, D. H., Long, J. S., Barclay W. S., "ANP32 Proteins Are Essential for Influenza Virus Replication in Human Cells," *Journal of Virology,* vol. 93, no. 17, pp. e00217-19, 2019, doi: 10.1128/JVI.00217-19.
.
[177] B. E. Nilsson-Payent, tenOever, B. R., te Velthuis, A. J. W., "The Host Factor ANP32 is required for Influenza A virus vRNA and cRNA synthesis," *Journal of Virology,* vol. 96, no. 4, pp. e02092-21, 2022.
[178] E. Domingo, Holland, J. J. , "RNA virus mutations and fitness for survival," *Annu. Rev. Microbiol.,* vol. 51, pp. 151-178, 1997.
[179] D. Coulibaly-N'Golo *et al.*, "Novel arenavirus sequences in Hylomyscus sp. and Mus (Nannomys) setulosus from Cote d'Ivoire: implications for evolution of arenaviruses in Africa," *PLoS One,* vol. 6, no. 6, p. e20893, 2011, doi: 10.1371/journal.pone.0020893.
[180] E. Visher *et al.*, "The three Ts of virulence evolution during zoonotic emergence," *Proc Biol Sci,* vol. 288, no. 1956, p. 20210900, Aug 11 2021, doi: 10.1098/rspb.2021.0900.
[181] P. K. Tosh, R. M. Jacobson, and G. A. Poland, "Influenza vaccines: from surveillance through production to protection," *Mayo Clin Proc,* vol. 85, no. 3, pp. 257-73, Mar 2010, doi: 10.4065/mcp.2009.0615.
[182] C. Duan, C. Li, R. Ren, W. Bai, and L. Zhou, "An overview of avian influenza surveillance strategies and modes," *Science in One Health,* vol. 2, 2023, doi: 10.1016/j.soh.2023.100043.
[183] S. T. Ali and B. J. Cowling, "Influenza Virus: Tracking, Predicting, and Forecasting," *Annu Rev Public Health,* vol. 42, pp. 43-57, Apr 1 2021, doi: 10.1146/annurev-publhealth-010720-021049.
[184] K. R. Short *et al.*, "One health, multiple challenges: The inter-species transmission of influenza A virus," *One Health,* vol. 1, pp. 1-13, Dec 1 2015, doi: 10.1016/j.onehlt.2015.03.001.

[185] G. N. Rogers and J. C. Paulson, "Receptor determinants of human and animal influenza virus isolates: differences in receptor specificity of the H3 hemagglutinin based on species of origin," *Virology,* vol. 127, no. 2, pp. 361-73, Jun 1983, doi: 10.1016/0042-6822(83)90150-2.

[186] A. Mehle, V. G. Dugan, J. K. Taubenberger, and J. A. Doudna, "Reassortment and mutation of the avian influenza virus polymerase PA subunit overcome species barriers," *J Virol,* vol. 86, no. 3, pp. 1750-7, Feb 2012, doi: 10.1128/JVI.06203-11.

[187] L. B. Arruda *et al.*, "The niche of One Health approaches in Lassa fever surveillance and control," *Ann Clin Microbiol Antimicrob,* vol. 20, no. 1, p. 29, Apr 24 2021, doi: 10.1186/s12941-021-00431-0.

[188] W. H. Organization, "Lassa Fever Research and Development (R&D) Roadmap," 2019. [Online]. Available: https://cdn.who.int/media/docs/default-source/blue-print/lassafever_rdblueprint_roadmap_advanceddraftjan2019.pdf?sfvrsn=dc00b058_3&download=true.

[189] H. Soubrier *et al.*, "Detection of Lassa Virus-Reactive IgG Antibodies in Wild Rodents: Validation of a Capture Enzyme-Linked Immunological Assay," *Viruses,* vol. 14, no. 5, May 7 2022, doi: 10.3390/v14050993.

[190] U. Bangura, "Molecular Epidemiology of Lassa virus in the Mano River Union area, West Africa," University of Hamburg, 2022.

[191] A. R. Smither *et al.*, "Novel Tools for Lassa Virus Surveillance in Peri-domestic Rodents," *medRxiv,* Mar 20 2023, doi: 10.1101/2023.03.17.23287380.

[192] U. Bangura *et al.*, "Lassa Virus Circulation in Small Mammal Populations in Bo District, Sierra Leone," *Biology (Basel),* vol. 10, no. 1, Jan 5 2021, doi: 10.3390/biology10010028.

[193] E. Fichet-Calvet *et al.*, "Spatial and temporal evolution of Lassa virus in the natural host population in Upper Guinea," *Sci Rep,* vol. 6, p. 21977, Feb 25 2016, doi: 10.1038/srep21977.

[194] J. Marien, G. Lo Iacono, T. Rieger, N. Magassouba, S. Gunther, and E. Fichet-Calvet, "Households as hotspots of Lassa fever? Assessing the spatial distribution of Lassa virus-infected rodents in rural villages of Guinea," *Emerg Microbes Infect,* vol. 9, no. 1, pp. 1055-1064, Dec 2020, doi: 10.1080/22221751.2020.1766381.

[195] J. G. Victoria, Kapoor, A., Dupuis, K., Schnurr, D. P., Delwart, E. L., "Rapid Identification of Known and New RNA Viruses from Animal Tissues," *PLOS Pathogen,* 2008, doi: doi.org/10.1371/journal.ppat.1000163.

[196] A. Roldao, R. Oliveira, M. J. Carrondo, and P. M. Alves, "Error assessment in recombinant baculovirus titration: evaluation of different methods," *J Virol Methods,* vol. 159, no. 1, pp. 69-80, Jul 2009, doi: 10.1016/j.jviromet.2009.03.007.

[197] A. Tayeh, C. Tatard, S. Kako-Ouraga, J. M. Duplantier, and G. Dobigny, "Rodent host cell/Lassa virus interactions: evolution and expression of alpha-Dystroglycan, LARGE-1 and LARGE-2 genes, with special emphasis on the Mastomys genus," *Infect Genet Evol,* vol. 10, no. 8, pp. 1262-70, Dec 2010, doi: 10.1016/j.meegid.2010.07.018.

[198] N. M. Brinkmann *et al.*, "Understanding Host-Virus Interactions: Assessment of Innate Immune Responses in Mastomys natalensis Cells after Arenavirus Infection," *Viruses,* vol. 14, no. 9, Sep 8 2022, doi: 10.3390/v14091986.

[199] M. W. Pfaffl, *Relative Quantification*. Taylor & Francis Group, 2006.

[200] M. Kanagawa *et al.*, "Molecular recognition by LARGE is essential for expression of functional dystroglycan," *Cell,* vol. 117, no. 7, pp. 953-64, Jun 25 2004, doi: 10.1016/j.cell.2004.06.003.

[201] N. Papageorgiou *et al.*, "Brothers in Arms: Structure, Assembly and Function of Arenaviridae Nucleoprotein," *Viruses,* vol. 12, no. 7, Jul 17 2020, doi: 10.3390/v12070772.

[202] T. Kouba *et al.*, "Conformational changes in Lassa virus L protein associated with promoter binding and RNA synthesis activity," *Nat Commun,* vol. 12, no. 1, p. 7018, Dec 2 2021, doi: 10.1038/s41467-021-27305-5.

[203] H. N. Pennington and J. Lee, "Lassa virus glycoprotein complex review: insights into its unique fusion machinery," *Biosci Rep,* vol. 42, no. 2, Feb 25 2022, doi: 10.1042/BSR20211930.

[204] H. R. Perrett *et al.*, "Structural conservation of Lassa virus glycoproteins and recognition by neutralizing antibodies," *Cell Rep,* vol. 42, no. 5, p. 112524, May 30 2023, doi: 10.1016/j.celrep.2023.112524.

[205] P. K. Grewal, J. M. McLaughlan, C. J. Moore, C. A. Browning, and J. E. Hewitt, "Characterization of the LARGE family of putative glycosyltransferases associated with dystroglycanopathies," *Glycobiology,* vol. 15, no. 10, pp. 912-23, Oct 2005, doi: 10.1093/glycob/cwi094.

[206] K. Fujimura *et al.*, "LARGE2 facilitates the maturation of alpha-dystroglycan more effectively than LARGE," *Biochem Biophys Res Commun,* vol. 329, no. 3, pp. 1162-71, Apr 15 2005, doi: 10.1016/j.bbrc.2005.02.082.

[207] M. Brockington *et al.*, "Localization and functional analysis of the LARGE family of glycosyltransferases: significance for muscular dystrophy," *Hum Mol Genet,* vol. 14, no. 5, pp. 657-65, Mar 1 2005, doi: 10.1093/hmg/ddi062.

[208] L. M. Crosby *et al.*, "Transformation of SV40-immortalized human uroepithelial cells by 3-methylcholanthrene increases IFN- and Large T Antigen-induced transcripts," *Cancer Cell Int,* vol. 10, p. 4, Feb 23 2010, doi: 10.1186/1475-2867-10-4.

[209] S. Baize, J. Kaplon, C. Faure, D. Pannetier, M. C. Georges-Courbot, and V. Deubel, "Lassa virus infection of human dendritic cells and macrophages is productive but fails to activate cells," *J Immunol,* vol. 172, no. 5, pp. 2861-9, Mar 1 2004, doi: 10.4049/jimmunol.172.5.2861.

[210] J. M. Emeny and M. J. Morgan, "Regulation of the interferon system: evidence that Vero cells have a genetic defect in interferon production," *J Gen Virol,* vol. 43, no. 1, pp. 247-52, Apr 1979, doi: 10.1099/0022-1317-43-1-247.

[211] R. Sommerstein *et al.*, "Evolution of recombinant lymphocytic choriomeningitis virus/Lassa virus in vivo highlights the importance of the GPC cytosolic tail in viral fitness," *J Virol,* vol. 88, no. 15, pp. 8340-8, Aug 2014, doi: 10.1128/JVI.00236-14.

[212] A. M. Lee, J. Cruite, M. J. Welch, B. Sullivan, and M. B. Oldstone, "Pathogenesis of Lassa fever virus infection: I. Susceptibility of mice to recombinant Lassa Gp/LCMV chimeric virus," *Virology,* vol. 442, no. 2, pp. 114-21, Aug 1 2013, doi: 10.1016/j.virol.2013.04.010.

[213] J. C. Zapata and M. S. Salvato, "Arenavirus variations due to host-specific adaptation," *Viruses,* vol. 5, no. 1, pp. 241-78, Jan 17 2013, doi: 10.3390/v5010241.

[214] F. J. Dutko and C. J. Pfau, "Arenavirus defective interfering particles mask the cell-killing potential of standard virus," *J Gen Virol,* vol. 38, no. 2, pp. 195-208, Feb 1978, doi: 10.1099/0022-1317-38-2-195.

[215] R. A. Lazzarini, J. D. Keene, and M. Schubert, "The origins of defective interfering particles of the negative-strand RNA viruses," *Cell,* vol. 26, no. 2 Pt 2, pp. 145-54, Oct 1981, doi: 10.1016/0092-8674(81)90298-1.

[216] R. M. Welsh, C. M. O'Connell, and C. J. Pfau, "Properties of defective lymphocytic choriomeningitis virus," *J Gen Virol,* vol. 17, no. 3, pp. 355-9, Dec 1972, doi: 10.1099/0022-1317-17-3-355.

[217] Z. J. Whitfield *et al.*, "Species-Specific Evolution of Ebola Virus during Replication in Human and Bat Cells," *Cell Rep,* vol. 32, no. 7, p. 108028, Aug 18 2020, doi: 10.1016/j.celrep.2020.108028.

[218] S. T. Sonnleitner *et al.*, "The mutational dynamics of the SARS-CoV-2 virus in serial passages in vitro," *Virol Sin,* vol. 37, no. 2, pp. 198-207, Apr 2022, doi: 10.1016/j.virs.2022.01.029.

[219] H. Chung, J. Y. Noh, B. S. Koo, J. J. Hong, and H. K. Kim, "SARS-CoV-2 mutations acquired during serial passage in human cell lines are consistent with several of those found in recent natural SARS-CoV-2 variants," *Comput Struct Biotechnol J,* vol. 20, pp. 1925-1934, 2022, doi: 10.1016/j.csbj.2022.04.022.

[220] G. Wong *et al.*, "Naturally Occurring Single Mutations in Ebola Virus Observably Impact Infectivity," *J Virol,* vol. 93, no. 1, Jan 1 2019, doi: 10.1128/JVI.01098-18.

[221] K. Nemirov, A. Lundkvist, A. Vaheri, and A. Plyusnin, "Adaptation of Puumala hantavirus to cell culture is associated with point mutations in the coding region of the L segment and in the noncoding regions of the S segment," *J Virol,* vol. 77, no. 16, pp. 8793-800, Aug 2003, doi: 10.1128/jvi.77.16.8793-8800.2003.

[222] A. Lundkvist, Y. Cheng, K. B. Sjolander, B. Niklasson, A. Vaheri, and A. Plyusnin, "Cell culture adaptation of Puumala hantavirus changes the infectivity for its natural reservoir, Clethrionomys glareolus, and leads to accumulation of mutants with altered genomic RNA S segment," *J Virol,* vol. 71, no. 12, pp. 9515-23, Dec 1997, doi: 10.1128/JVI.71.12.9515-9523.1997.

[223] T. Strandin *et al.*, "Orthohantavirus Isolated in Reservoir Host Cells Displays Minimal Genetic Changes and Retains Wild-Type Infection Properties," *Viruses,* vol. 12, no. 4, Apr 17 2020, doi: 10.3390/v12040457.

[224] S. S. Agnihothram, J. York, and J. H. Nunberg, "Role of the stable signal peptide and cytoplasmic domain of G2 in regulating intracellular transport of the Junin virus envelope glycoprotein complex," *J Virol,* vol. 80, no. 11, pp. 5189-98, Jun 2006, doi: 10.1128/JVI.00208-06.

[225] J. York and J. H. Nunberg, "Role of the stable signal peptide of Junin arenavirus envelope glycoprotein in pH-dependent membrane fusion," *J Virol,* vol. 80, no. 15, pp. 7775-80, Aug 2006, doi: 10.1128/JVI.00642-06.

[226] S. S. Agnihothram, J. York, M. Trahey, and J. H. Nunberg, "Bitopic membrane topology of the stable signal peptide in the tripartite Junin virus GP-C envelope glycoprotein complex," *J Virol,* vol. 81, no. 8, pp. 4331-7, Apr 2007, doi: 10.1128/JVI.02779-06.

[227] J. York, V. Romanowski, M. Lu, and J. H. Nunberg, "The signal peptide of the Junin arenavirus envelope glycoprotein is myristoylated and forms an essential subunit of the mature G1-G2 complex," *J Virol,* vol. 78, no. 19, pp. 10783-92, Oct 2004, doi: 10.1128/JVI.78.19.10783-10792.2004.

[228] S. Shankar, L. R. Whitby, H. E. Casquilho-Gray, J. York, D. L. Boger, and J. H. Nunberg, "Small-Molecule Fusion Inhibitors Bind the pH-Sensing Stable Signal Peptide-GP2 Subunit Interface of the Lassa Virus Envelope Glycoprotein," *J Virol,* vol. 90, no. 15, pp. 6799-807, Aug 1 2016, doi: 10.1128/JVI.00597-16.

[229] E. L. Messina, J. York, and J. H. Nunberg, "Dissection of the role of the stable signal peptide of the arenavirus envelope glycoprotein in membrane fusion," *J Virol,* vol. 86, no. 11, pp. 6138-45, Jun 2012, doi: 10.1128/JVI.07241-11.

[230] J. York, D. Dai, S. M. Amberg, and J. H. Nunberg, "pH-induced activation of arenavirus membrane fusion is antagonized by small-molecule inhibitors," *J Virol,* vol. 82, no. 21, pp. 10932-9, Nov 2008, doi: 10.1128/JVI.01140-08.

[231] M. Katz *et al.*, "Structure and receptor recognition by the Lassa virus spike complex," *Nature,* vol. 603, no. 7899, pp. 174-179, Mar 2022, doi: 10.1038/s41586-022-04429-2.

[232] L. Martinez-Sobrido, E. I. Zuniga, D. Rosario, A. Garcia-Sastre, and J. C. de la Torre, "Inhibition of the type I interferon response by the nucleoprotein of the prototypic arenavirus lymphocytic choriomeningitis virus," *J Virol,* vol. 80, no. 18, pp. 9192-9, Sep 2006, doi: 10.1128/JVI.00555-06.

[233] H. Malet, H. M. Williams, S. Cusack, and M. Rosenthal, "The mechanism of genome replication and transcription in bunyaviruses," *PLoS Pathog,* vol. 19, no. 1, p. e1011060, Jan 2023, doi: 10.1371/journal.ppat.1011060.

[234] M. Lelke, L. Brunotte, C. Busch, and S. Gunther, "An N-terminal region of Lassa virus L protein plays a critical role in transcription but not replication of the virus genome," *J Virol,* vol. 84, no. 4, pp. 1934-44, Feb 2010, doi: 10.1128/JVI.01657-09.

[235] E. Baranowski, C. M. Ruiz-Jarabo, N. Pariente, N. Verdaguer, and E. Domingo, "Evolution of cell recognition by viruses: a source of biological novelty with medical implications," *Adv Virus Res,* vol. 62, pp. 19-111, 2003, doi: 10.1016/s0065-3527(03)62002-6.

[236] M. Lehmann, M. Pahlmann, H. Jerome, C. Busch, M. Lelke, and S. Gunther, "Role of the C terminus of Lassa virus L protein in viral mRNA synthesis," *J Virol,* vol. 88, no. 15, pp. 8713-7, Aug 2014, doi: 10.1128/JVI.00652-14.

[237] T. Kouba, P. Drncova, and S. Cusack, "Structural snapshots of actively transcribing influenza polymerase," *Nat Struct Mol Biol,* vol. 26, no. 6, pp. 460-470, Jun 2019, doi: 10.1038/s41594-019-0232-z.

[238] J. V. M. Forrester, C.; Kuffova, L. , "Immune Privilege Furnishes a Niche for Latent Infection," *Sec. Inflammatory Eye Diseases* vol. 2, 2022, doi: 10.3389/fopht.2022.869046

[239] A. W. Taylor, "Ocular immune privilege," *Eye (Lond),* vol. 23, no. 10, pp. 1885-9, Oct 2009, doi: 10.1038/eye.2008.382.

[240] J. B. Varkey *et al.*, "Persistence of Ebola Virus in Ocular Fluid during Convalescence," *N Engl J Med,* vol. 372, no. 25, pp. 2423-7, Jun 18 2015, doi: 10.1056/NEJMoa1500306.

[241] D. S. Dimitrov, "Virus entry: molecular mechanisms and biomedical applications," *Nat Rev Microbiol,* vol. 2, no. 2, pp. 109-22, Feb 2004, doi: 10.1038/nrmicro817.

15. List of publications

Brinkmann N. M., Hoffmann C., Wurr S., *et al*. Understanding Host-Virus Interactions: Assessment of Innate Immune Responses in *Mastomys natalensis* Cells after Arenavirus Infection. Viruses. 2022 Sep;14(9):1986. DOI: 10.3390/v14091986.

Beal, J., Farny, N. G., Haddock-Angelli, T., […], **Burckhardt, N**., […] Workman, C. T.: Robust estimation of bacterial cell count from optical density. Commun Biol 3, 512 (2020). DOI: 10.1038/s42003-020-01127-5

Wedemeyer, D., Kartheiser, A., Kähler, N. P., **Burckhardt, N.**, […], Hoffmeister, J.: Animal Luring Device. Submitted as international patent (No: WO/2020/049118, Publication date: 12.03.2020).

16. Declaration on oath - Eidesstattliche Versicherung

I hereby declare, on oath, that I have written the present dissertation by my own and have not used other than the acknowledged resources and aids.

Hiermit erkläre ich an Eides statt, dass ich die vorliegende Dissertationsschrift selbst verfasst und keine anderen als die angegebenen Quellen und Hilfsmittel benutzt habe.

Hamburg, den 16.05.2024

Ich versichere, dass dieses gebundene Exemplar der Dissertation und das in elektronischer Form eingereichte Dissertationsexemplar (über den Docata-Upload) und das bei der Fakultät (zuständiges Studienbüro bzw. Promotionsbüro Physik) zur Archivierung eingereichte gedruckte gebundene Exemplar der Dissertationsschrift identisch sind.

I, the undersigned, declare that this bound copy of the dissertation and the dissertation submitted in electronic form (via the Docata upload) and the printed bound copy of the dissertation submitted to the faculty (responsible Academic Office or the Doctoral Office Physics) for archiving are identical.

Hamburg, den 16.05.2024

17. Acknowledgements

Firstly, I want to express my gratitude for the Jürgen Manchot Foundation for providing funding for the first three years of my PhD. I would like to thank Prof. Dr. Jonas Schmidt-Chanasit for assessing my dissertation. Likewise, I would like to express my deep gratitude to Prof. Dr. Stephan Günther for making my comeback to the BNITM possible and allowing me to finalize my dissertation.

To Lisa, I want to say how much I appreciate your scientific support and guidance also in the more challenging times. Most likely, I would not have completed my PhD without you and your encouraging attitude. Thank you very much for supporting me and being such an inspiring mentor for such a long time.

Thank you very much Elly, for taking care of training me in the BSL-4 and not losing patience, especially at the beginning of my training. I would also like to thank Steffi and Lukas, for their patient experimental and mental support during cloning various constructs. Thank you Sabrina and Lars for helping me with all the titration plates. Special thanks also goes to the group of Dr. Thomas Strecker in Marburg including all lab members who enabled me to visit his lab during a lab rotation in 2023. Especially, I want to thank Sarah for teaching me confocal laser scanning microscopy, Birthe for taking care of me and my budding assays, as well as Helena for your ideas regarding the qPCR assay. Additionally, I would like to thank my interns, Chloé and Anna-Lena for contributing to my project and supporting me with experiments. Thank you, Lilly for all your advice and thank you Chris for listening to my thoughts and supplying me with chocolate cupcakes, when it was needed at most. Of course, my gratitude also goes to the whole Merlin team, the department of virology, the animal facility as well as my fellow PhD students in the BNITM graduate school. I enjoyed working with you a lot and I am grateful for all the mind-opening discussions.

At last, I would like to thank my husband Maximilian, for always being at my side and keeping my back the last eleven years. Without your support and encouragement, I would

for sure not be where I am today. Thank you especially for keeping me sane and providing any needed me(n)tal support.